THIOL SIGNALLING IN SKELETAL MUSCLE AGEING

Neil T Smith

Thesis submitted in accordance with the requirements of the University of Liverpool for the degree of Doctor in Philosophy

February 2018

Abstract

An age-related loss of muscle mass is associated with increased frailty in the elderly. The effect is felt at both a national scale, with an increased budgetary demand for health services directed towards the ageing population, and by the individual where reduced mobility significantly reduces their quality of life. It is unclear whether all skeletal muscle types are affected in the same manner. This thesis considered how thiol signalling, facilitated through reactive thiol groups on cysteine amino acids, may affect skeletal muscle ageing as it is crucial for normal intracellular function. Several studies have identified reactive oxygen species (ROS) as crucial signalling molecules in healthy muscle and various proteins can detect and respond to changes in their concentration. The cysteines are evolutionarily conserved in functionally important locations and have a direct impact on protein function, affecting either its active site or conformation. In healthy muscle, proteins can quickly and efficiently respond to changes in ROS concentrations via this mechanism whereas in aged muscle these responses appear to be impaired.

The quadriceps and soleus muscles were selected because of their differing primary metabolic pathways and physiology, reflecting fast and slow twitch muscle respectively. This enabled determination of age related changes to the redox proteome between two different skeletal muscles. They are hypothesised to age differently and to determine this, adult (12 months) and old (24 months) tissue were subjected to a deep proteomics investigation, elucidating changes to the global proteome of ageing mouse muscle as well as using differential labelling of reduced and reversibly oxidised cysteine residues to identify redox-susceptible locations on individual proteins. Prior to this a proteomics study had not analysed changes to the redox proteome between two skeletal muscle tissues before.

Analysis of the quadriceps label free results identified changes to redox protein abundance such as a significant increase in Protein Disulphide Isomerase, crucial to disulphide bond formation and breakage. HSC70, important for protein folding, was significantly decreased with age. Differential labelling of specific cysteine residues demonstrated Cys46 increased in its reduced form with age in PARK7. Furthermore, many changes observed in the label free analysis highlighted cytoskeletal proteins as those primarily affected.

The soleus label free results demonstrated significant decreases in abundance of a number of mitochondrial proteins involved in the electron transport chain such as NAD(P)H dehydrogenase and ATP Synthase. One example of differential labelling highlighted ATP Synthase Cys101 as becoming increasingly reduced with age. This increase in a reduced redox state of cysteines was observed across a range of other mitochondrial proteins, possibly indicating a negative impact on energy metabolism in the soleus with age.

A successful preliminary study considered the effect of stretching C2C12 mouse skeletal muscle cells *in vitro*. A protocol for testing the effect of mechanical stretching on C2C12 cells was optimised with a future goal of producing replicable *in vitro* proteomics data and thereby reducing the requirement for animal tissue.

The studies in this thesis identified various redox proteome changes in quadriceps and soleus muscle with age. This data will provide a basis for a targeted analysis of musculoskeletal proteins with a view to a better understanding of musculoskeletal ageing and its impact via the proteome.

Doctor of Philosophy Declaration

I hereby declare that this dissertation is a record of work carried out in the Institute of Ageing and Chronic Disease at the University of Liverpool during the period from September 2013 to June 2016. The dissertation is original in content except where otherwise indicated.

February 2018

……..

Neil T. Smith

Acknowledgements

Many warm thanks to my primary supervisor Dr Brian McDonagh for his support and guidance throughout the PhD and write up. I am indebted to him for the opportunity and the experience. Many thanks to Professor Malcolm J Jackson as my secondary supervisor for his help and advice throughout my three years and during the thesis writeup. Thanks to Dr. Aphrodite Vasilaki as my secondary supervisor for her advice throughout the three years.

Thanks to the Biotechnical and Biological Sciences Research Council Doctoral Training Programme for their financial support and to the Institute of Ageing and Chronic Disease for providing the equipment, reagents and space for my work.

I would like to extend my thanks to all who have helped and supported me throughout my time in IACD. To Dr Gareth Nye, many thanks for the provision of quadriceps and soleus muscle and for his friendship, advice and good chats throughout the three years. Miss Niamh Horton and Dr Ian Li for their wonderful offerings of help, perspective and laughs, sometimes all at once! Heartfelt thanks to Mr Stephen Beard whose love and support during the write up and beyond has been immeasurable. Warm thanks to Dr Hannah Barrow for the friendship and encouragement at the start of this journey. Finally, Mr G. Roebuck. I am forever grateful for his inspiration and encouragement at school, where this adventure began.

"I asked the question for the best reason possible, for the only reason, indeed, that excuses anyone for asking any question - simple curiosity." Oscar Wilde, The Picture of Dorian Gray

Dedication

This work is dedicated to my family: Mr Jeremy Smith, Mrs Moira Smith and Miss Gillian Smith. Thanks to their unwavering support, no challenge is insurmountable.

LIST OF ABBREVIATIONS:

ALDH	Aldehyde dehydrogenase (mitochondrial)
ALDOA	Fructose bisphosphate aldolase A
AMPK	Adenosine monophosphate kinase
CASQ1	Calsequestrin 1
ENO1	α-Enolase
ENO3	β-Enolase
GAPDH / G3p	Glyceraldehyde 3-Phosphate Dehydrogenase
GPX1	Glutathione peroxidase 1
GRP78	78 kDa Glucose-regulated protein
GSH	Glutathione
GSSG	Glutathione (reduced)
GST-k/GST-μ/GST-π	Glutathione S-Transferase κ / μ / π
HS71A/HSPA1A	Heat shock 70 kDa protein
H_2O_2	Hydrogen peroxide
MYH	Myosin heavy chain
MYL	Myosin light chain
NAD	Nicotinamide adenine dinucleotide
NADP	Nicotinamide adenine dinucleotide phosphate
NAD(P)H	Nicotinamide adenine dinucleotide phosphate (reduced)
NO	Nitric oxide
NOS	Nitric oxide synthase
NOX	NAD(P)H oxidase
P70S6K	Ribosomal protein s6-kinase β 1
PARK7	Parkinson disease protein 7
PDI/PDIA1/P4HB	Protein disulphide isomerase
PRDX	Peroxiredoxin
PYGM	Glycogen Phosphorylase
RNS	Reactive Nitrogen Species
ROS	Reactive Oxygen Species
SIRT1	Succinate Dehydrogenases
SOD1/Cu-Zn SOD	Superoxide Dismutase 1
SOD2/Mn-SOD	Superoxide Dismutase 2
SRXN	Sulfiredoxin
TBS	Tris-Buffered Saline
TXN	Thioredoxin
TXNIP	Thioredoxin Interacting Protein
TXNR	Thioredoxin Reductase

Publications

Results from this study were published in:

Journal of Proteomics "Redox responses are preserved across muscle fibres with differential susceptibility to aging" (Neil T. Smith *et al.*, 2018, https://doi.org/10.1016/j.jprot.2018.02.015).

This work was presented at the following scientific meeting:

SFRR-Europe 2016; Budapest, Hungary under the title "Redox proteomics of mouse skeletal muscle ageing".

TABLE OF CONTENTS

LIST OF FIGURES:

LIST OF TABLES:

CHAPTER 1

INTRODUCTION

1.1 Physiology of Skeletal Muscle

Skeletal muscle is crucial for movement and in humans makes up about 40% of the total body mass (Janssen et al., 2000). Striated skeletal muscle is so called because of the repeating contractile units first observed under the microscope by van Leeuwenhoek in the 1670s (Salmons, 2017). The apparent striations are caused by the I and A bands within the sarcomere which enable the muscle to contract. A highly adaptable organ, it retains a plasticity enabling adaptation to changing physiological conditions throughout an organisms' lifespan (Zierath and Hawley, 2004). Innervation by a motor nerve causes depolarization of the myofibres leading to a contraction of the muscle and the force generated is transferred to the skeletal system via tendons that link muscle to bone. Muscles are often arranged in opposing pairs to enable controlled movement of limbs via regular contraction and relaxation. In addition to locomotion, muscle groups involved in posture control undergo semi-permanent contraction and each muscle's primary function is reflected by their fibre type (Barclay et al., 1993). There are two general categories of fibre type which are based on the Myosin Heavy Chain (MHC) content of the cells. In mice, slow twitch or type I muscles, such as the soleus, produce energy via oxidative phosphorylation. In contrast, fast twitch type II muscles, such as the quadriceps, produce energy via glycolysis.

Skeletal muscle originates with precursor stem cells called satellite cells. These are produced throughout the lifetime of the organism and after production are located between the basal lamina and the sarcolemma (Garcia et al., 2017). The cells are mitotically quiescent until activated via injury or growth stimuli which causes them to enter the cell cycle and proliferate before exiting to either differentiate, forming new myocytes and subsequently new muscle, or they form more satellite cells to enable future regeneration of the muscle (Motohashi and Asakura, 2012, Dumont et al., 2015). Differentiation of the myocytes causes them to combine forming multinucleated myotubes that stretch longitudinally forming myofibres (Sherwood et

al., 2004). The basic unit of a muscle fibre is the sarcomere which refers to the actin and myosin cross bridges as a single contractile unit (Vasilaki et al., 2017). Intracellularly, they contain a range of components with specialised terms related to the muscle function. The equivalent of the cytoplasm is referred to as sarcoplasm and contains an abundance of myosin and actin fibres for contraction, titin for elasticity of the cell and glycogen as a ready source of energy for contraction (Bohnert et al., 2018, Linsley et al., 2017). A sarcoplasmic reticulum surrounds the myofibrils. Activation of ryanodine receptors, specifically dihydropyridine receptors in the case of skeletal muscle, control the release of calcium (Ca^{2+}) from the sarcoplasmic reticulum. This causes the cell to depolarise and inducing a contraction by removing the tropomyosin from its inhibitory location on an actin fibre (Bohnert et al., 2018, Linsley et al., 2017, Santulli and Marks, 2015). Action potential frequency induced via motor neuron innervation controls the extent of skeletal muscle contractions (Vasilaki et al., 2017). Where single twitches are induced, only a small amount of force is generated. However, higher frequencies of action potentials produce a cumulative effect on the muscle, increasing tension and leading to muscle contraction. Innervation of a motor neuron at neuromuscular junctions causes the release of acetylcholine (ACh) into the pre-synaptic cleft resulting in stimulation of acetylcholine receptors on the myofibres. This action potential is translated through the plasma membrane and via transverse (T) tubules into the fibre's sarcoplasm, causing the release of calcium (Ca^{2+}) from the sarcoplasmic reticulum causing the cell to depolarise and inducing a contraction by removing the tropomyosin from its inhibitory location on an actin fibre (Linsley et al., 2017). The location of tropomyosin is controlled by the troponin complex (Campbell and Reece, 2005). Meanwhile magnesium (Mg^{2+}) causes the myosin head to convert ATP (Adenosine triphosphate) to ADP (Adenosine diphosphate) with the release of an inorganic Phosphate molecule (P*i*). The myosin head then releases the ADP and binds new ATP causing it to return to its initial state. At the same time, calcium ions are released by the Troponin. If the Calcium

concentration is high enough, the cycle repeats allowing the contraction to continue, if not then contraction stops (Campbell and Reece, 2005). This general mechanism is true of all muscle fibres and it is in addition to these contractions that reactive oxygen species (ROS) appear to be generated as cellular demand for energy increases (Goljanek-Whysall et al., 2016, Campbell and Reece, 2005, Devasagayam et al., 2004).

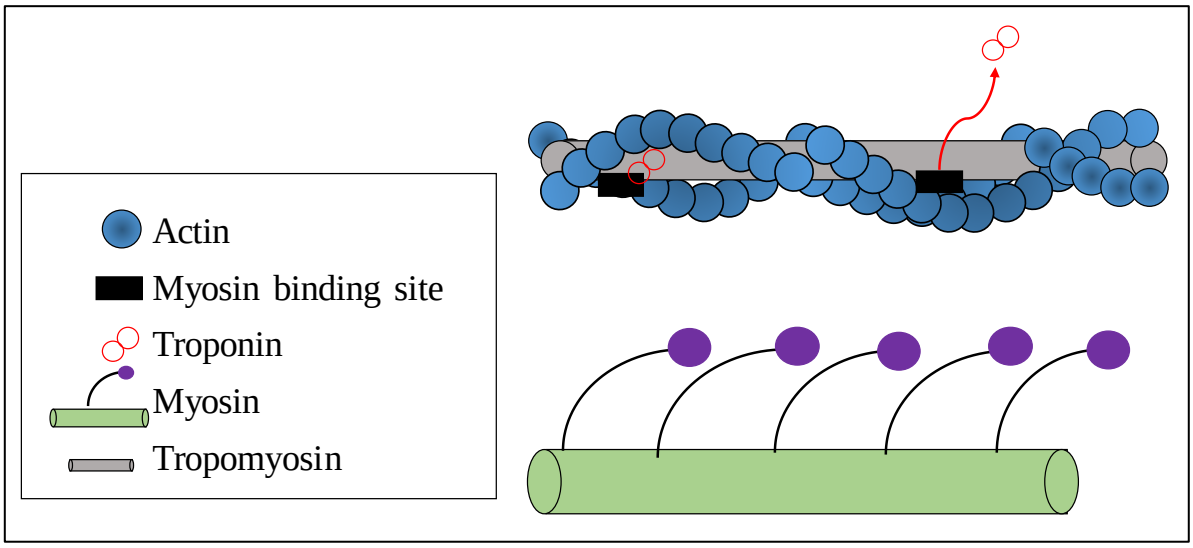

Figure 1.1.1 Actin-myosin binding. At rest the black binding site for the myosin head is blocked by the red double-ringed troponin but initiation via an increase in intracellular calcium leads to the dissociation of troponin (indicated with the red arrow) enabling attachment of the purple myosin heads to the actin binding site. Adapted from (Huxley and Niedergerke, 1954, Huxley and Hanson, 1954).

The current understanding of skeletal muscle contractions is based on the cross-bridge theory (Huxley and Niedergerke, 1954, Huxley and Hanson, 1954). Each muscle cell contains a single neuromuscular junction however, one motor neuron can have multiple branches attaching to several muscle fibres, together termed the motor unit. These muscle fibre bundles are then packaged together forming fascicles. When innervation occurs, the action potential is spread across whole fascicles causing large scale contraction and movement as previously described. At the intracellular level, within myotubes, are myofibrils that contain the sarcomeric filaments (Huxley and Niedergerke, 1954, Huxley and Hanson, 1954). It is these

sarcomeres that contain interlocking fibres of thin filaments (I bands) which contain actin and thick filaments (Z discs) which contain myosin heads enabling contraction as defined in figure 1.1.1 (Campbell and Reece, 2005). The interlocking units within the sarcomere are shown in figure 1.1.2 and demonstrate the different bands and indicates how each of the individual units combine to form a contracting mechanism (Spudich and Watt, 1971).

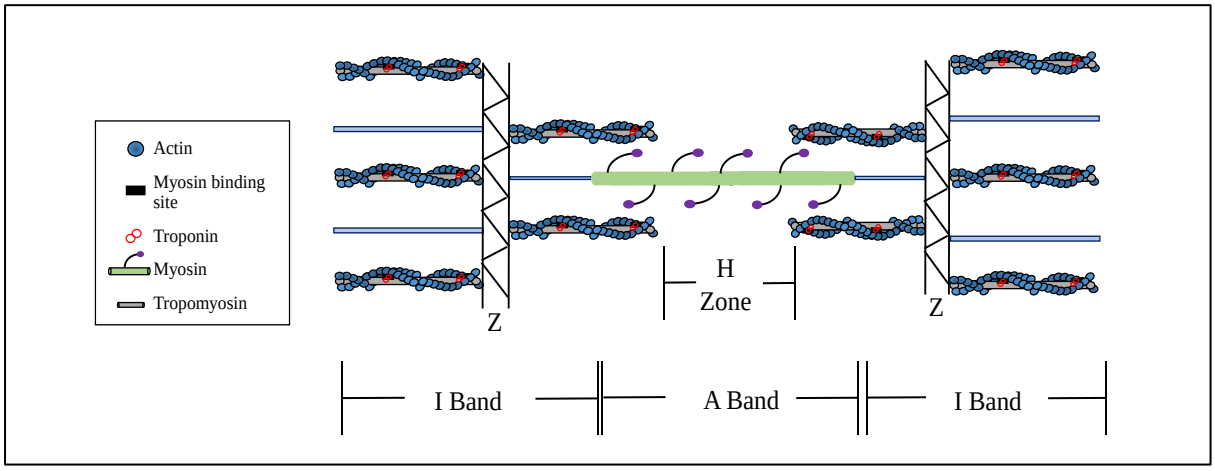

Figure 1.1.2 The sarcomere with a central myosin fibre in green and the outer actin filaments. The I and A bands, H zone and Z discs refer to the histological markers of appearance for skeletal muscle fibre giving its striated appearance. Contraction causes a narrowing of the H zone as the Z discs move towards each other, pulled in by the cross-bridge action of the myosin heads on the actin filaments.

1.2 Energy Metabolism

Energy metabolism in skeletal muscle falls into one of two categories: aerobic or anaerobic metabolism (Westerblad et al., 2010). The former utilises oxidative phosphorylation whereas the latter uses glycolysis. To this end, oxidative phosphorylation is a more sustained form of metabolism than glycolysis. Muscles offer a high level of plasticity throughout life and this is reflected in the ability to change constituent fibre types to suit long term demands of the muscle.

Some early skeletal muscle studies reflected this with the notable work of Salmons demonstrating a change in twitch intensity led to changes in muscle fibre type composition

(Salmons, 2017, Salmons and Sreter, 1976). Further detailed work led to understanding muscle in terms of its fibre type which today are defined as: slow twitch, oxidative fibres Type β/I, α, I/IIA, through to slow-medium (aka fast oxidative-glycolytic fibres) twitch type IIA, IIA/IIX, IIX, IIX/IIB and the fast glycolytic fibres type IIB and IIM as the major adult forms based on myosin heavy chain content (Schiaffino and Reggiani, 2011, Sciote and Morris, 2000). There are also extra-ocular, embryonic and neonatal forms of MHC which are beyond the scope of this thesis (Sciote and Morris, 2000).

Energy is most simply described as 'the capacity to do work' (Atkins and De Paula, 2010). Within a biological setting it is fundamental for all organic processes, sustaining life. Skeletal muscle has a number of ways it generates the energy required for contractions, each of which depend upon the muscle and its fibre type composition. Adenosine triphosphate (ATP) is the main energy currency and is a coenzyme required to enable the majority of biochemical reactions to take place (Itoh et al., 2004, Imamura et al., 2009).

The anaerobic metabolic pathways include Phosphocreatine breakdown via Creatine kinase leading to the production of Creatine and ATP (Westerblad et al., 2010, Imamura et al., 2009). However, an alternative route metabolises Glycogen into lactate and hydrogen ions via Glycogen phosphorylase causing the well-known painful build-up of lactic acid within muscle and a reduction in function. The reverse mechanism requires a different enzyme: Glycogen synthase, causing the two directions to be independently controllable. Both glycogen enzymes rely on phosphorylation for control of their activity (Westerblad et al., 2010, Roach, 2002).

Aerobic metabolism includes the degradation of triglycerides that are stored within skeletal muscle or adipose tissue. The hydrolysis of these triglycerides produces fatty acids that are a crucial energy source during exercise as they are involved in the production of the coenzymes NADH and $FADH_2$ which are then utilised in oxidative phosphorylation (Watt and Cheng, 2017, Achten et al., 2002). One key mechanism that is still not fully understood is

glucose uptake. Although AMP-dependent protein kinase (AMPK) has been implicated to a limited extent, it appears to perform a signalling role rather than to have a direct involvement. AMPK is involved in cellular energy metabolism control such as fatty acid and cholesterol synthesis and is activated by low levels of ATP or high levels of AMP/ADP. This follows a demonstration that reactive oxygen species induce glucose uptake during contractions, as signalled, by AMPK (Westerblad et al., 2010, Hardie and Sakamoto, 2006, Sandstrom et al., 2006, O'Neill, 2013).

Quadriceps are predominantly fast twitch muscles and therefore primarily produce energy via glycolysis (Saey et al., 2011). The process is initiated with the phosphorylation of glucose via Hexokinase to Glucose 6-phosphate following its active transport into the cell. This chemically destabilises it prior to the conversion by Phosphoglucomutase isomerase into Fructose 6-phosphate. Phosphofructokinase then converts Fructose 6-phosphate into Fructose 1,6-bisphosphate. At this point Aldolase produces two interchangeable three carbon molecules: Glyceraldehyde 3-phosphate (G3P) and Dihydroxyacetone phosphate. Triosephosphate isomerase can interchange these molecules with G3P continuing through to the final stage of glycolysis. The thermodynamics of the reaction ensures the process sees G3P as the primary successor to continue the reaction with the production of two ATP molecules. G3P dehydrogenase phosphorylates the aldehyde group of Glyceraldehyde 3-phosphate converting it to 1,3 Bisphosphoglycerate and in doing so also reduces the oxidised form of Nicotinamide adenine dinucleotide (NAD^+) to the reduced form of Nicotinamide adenine dinucleotide (NADH). Phosphoglycerate kinase removes this phosphate group leaving 3-Phosphoglycerate and in doing so the detached phosphate ion is added to a molecule of Adenosine diphosphate (ADP) producing Adenosine triphosphate (ATP). The phosphate group is subsequently moved by Phosphoglycerate mutase producing 2-Phosphoglycerate. Enolase removes this phosphate group via a condensation reaction, releasing water, and producing Phosphoenolpyruvate.

Finally, this is converted to Pyruvate by Pyruvate kinase which moves the phosphate group onto ADP producing ATP. At this stage Pyruvate has a number of potential fates as Lactate dehydrogenase can reversibly convert Pyruvate to Lactate or a reaction with NAD^+ and Co-enzyme A (CoA) leads to the production of Acetyl-Co-enzyme A (Acetyl CoA), Carbon dioxide (CO_2) and NADH. Notably, if the muscle produces lactate at a high rate (faster than it can be broken down) for example through sprinting, its concentration increases leading to the slowing of the energy production mechanism (Berg et al., 2002).

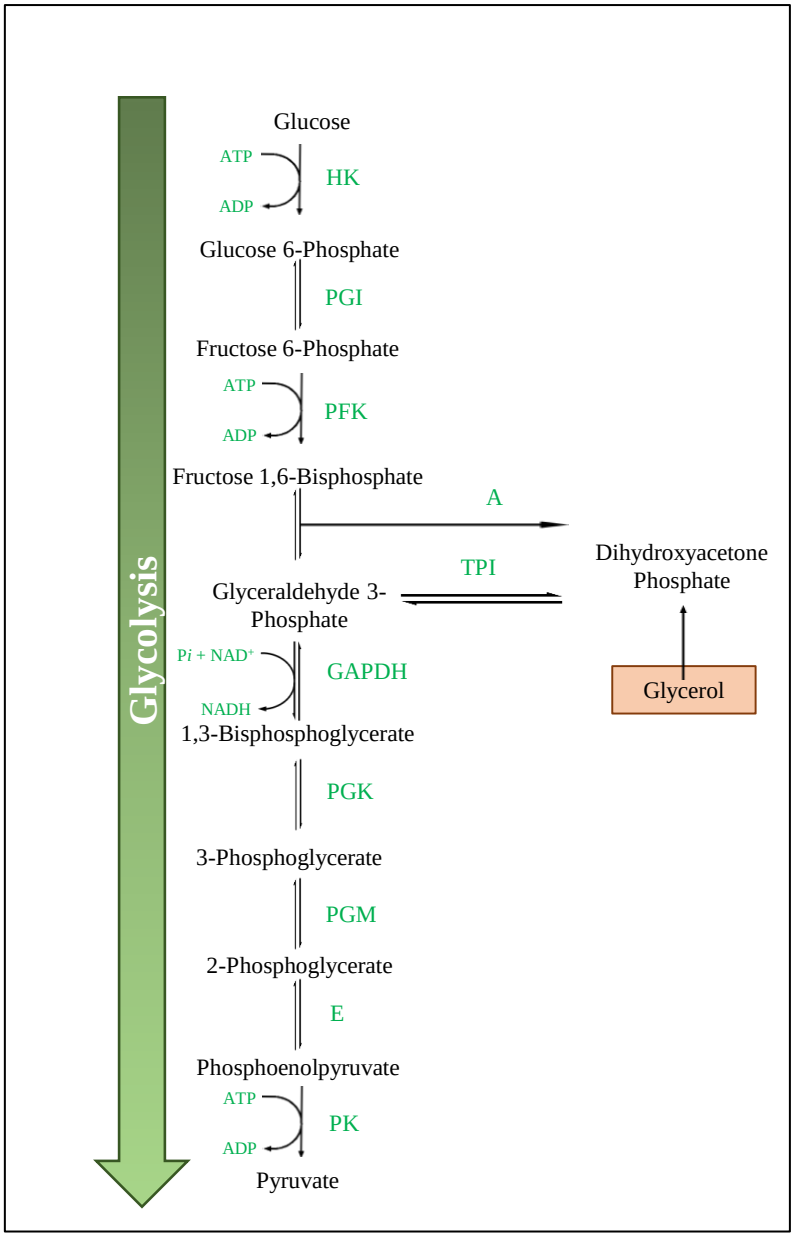

Figure 1.2.1 The glycolysis energy production pathway in skeletal muscle, which is predominant in the quadriceps. Enzymes are abbreviated and those common to glycolysis are highlighted in green along with the associated energy production from ATP. Glycolysis abbreviations: HK (Hexosekinase), PGI (Phosphoglucose isomerase), PFK (Phosphofructokinase), A (Aldolase), TPI (Triosephosphate isomerase), GAPDH (Glyceraldehyde 3-phosphate dehydrogenase), PGK (Phosphoglycerate kinase), PGM (Phosphoglycerate mutase), E (Enolase), PK (Pyruvate kinase), ATP (Adenosine triphosphate), ADP (Adenosine diphosphate), NADH (Reduced nicotinamide dinucleotide), NAD^+ (Oxidised nicotinamide dinucleotide) (adapted from (Berg et al., 2002)).

The soleus, on the other hand, predominantly uses oxidative phosphorylation via the electron transport chain for energy production and these processes occur in the mitochondria.

In discussing oxidative phosphorylation consideration must first be given to the citric acid cycle (abbreviated to TCA cycle, see figure 1.2.2) as it takes the Pyruvate produced by glycolysis and converts it to Acetyl CoA via a poly-enzyme complex which includes Transacetylase, Pyruvate dehydrogenase and Dihydrolipoyl dehydrogenase (Krebs and Holzach, 1952, Mitchell, 1961, Kalckar, 1974, Friedkin and Lehninger, 1949, Kalckar, 1991).

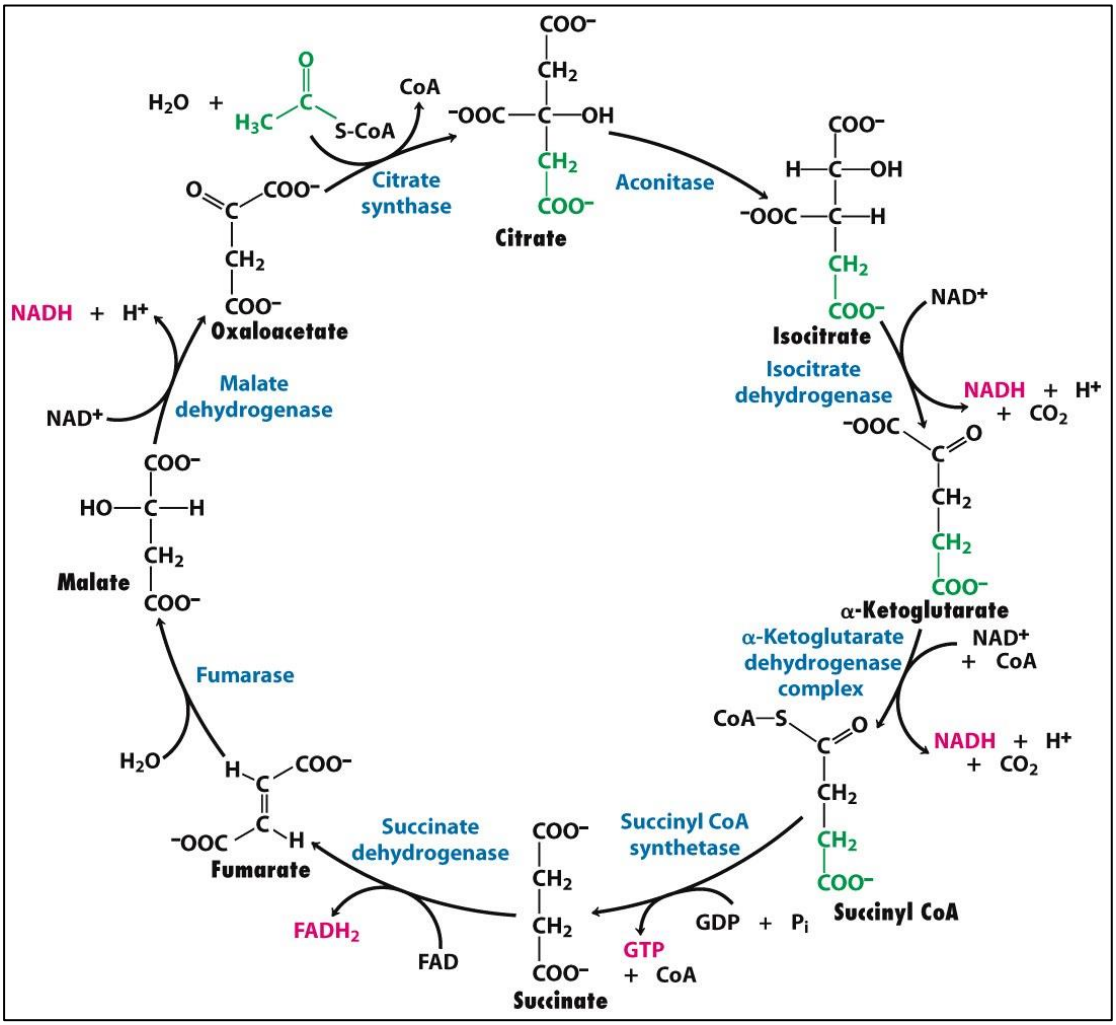

Figure 1.2.2 A citric acid cycle diagram representing the core of mitochondrial energy production.

Over several steps carbon dioxide is released, NAD^+ is reduced to NADH during which an acetate molecule is produced and finally Co-enzyme A is added. Then citrate is produced from Oxaloacetate and Acetyl Co-A via citrate synthase, requiring water. Aconitase converts

Citrate to *cis*-Aconitate, releasing water and then on to *D*-Isocitrate, again requiring water for the reaction. Isocitrate dehydrogenase produces α-Ketoglutarate whilst reducing NAD^+ to NADH and releasing a Hydrogen ion (H^+) before α-ketoglutarate dehydrogenase converts this to Succinyl-Co-enzyme A. This involves the reduction of NAD^+ to NADH, the release of H^+ and CO_2. Succinyl Co-enzyme A synthetase utilises GDP and P*i* producing Co-enzyme A-SH and GTP while also producing Succinate. The conversion of GTP to GDP, powering this reaction also leads to the production of ATP from ADP. Succinate dehydrogenase converts Succinate to Fumarate. This mechanism also converts Ubiquinone (Q) to Ubiquinol (QH_2) while requiring Flavin adenine dinucleotide (FAD) which is reduced to $FADH_2$. Fumarase converts Fumarate to *L*-Malate requiring water. *L*-Malate then gets converted to Oxaloacetate by Malate dehydrogenase whilst also reducing NAD^+ to NADH and producing one H^+. Finally, the cycle is back at the start where Oxaloacetate is joined with Acetyl Co-enzyme A and with water produce Citrate and Acetyl Co-enzyme A-SH via Citrate synthase and so the process repeats itself. In summary the TCA cycle produces three molecules of NADH, three Hydrogen ions, a molecule of Ubiquinol, a molecule of GTP, two molecules of CO_2 and one molecule of Co-enzyme A-SH (Berg et al., 2002).

At this point chemiosmosis links the electron transport chain to oxidative phosphorylation. Chemiosmosis is the use of a proton gradient, in this case across the mitochondrial membrane to move energy from redox reactions to cellular work (Berg et al., 2002).

Oxidative phosphorylation is so called due to the loss of electrons during this process and the production of ATP as the final stage which uses the proton gradient. The process requires NADH-Q oxidoreductase (Complex I), Q-cytochrome *c* oxidoreductase (Complex III) and cytochrome *c* oxidase (Complex IV) for electron transport. Also involved is Succinate-Q-Reductase (Complex II) however this is not involved in proton transport. Electron transport

between NADH-Q oxidoreductase and Q-cytochrome *c* oxidoreductase is carried out by Ubiquinone (Q) which easily disseminates within the inner mitochondrial membrane. Then cytochrome *c* transports electrons between Q-cytochrome *c* oxidoreductase and Cytochrome *c* oxidase, the final enzyme reducing Oxygen (O_2) to water (Berg et al., 2002). As the electron transport chain causes a proton gradient via the production of water from oxygen this leads to the emission of H^+ from the mitochondrial matrix producing a gradient that drives ATP synthase and therefore the production of ATP (Berg et al., 2002, Kalckar, 1991).

In summary, aerobic respiration of glucose leads to the production of 36 molecules of ATP. 2 ATP molecules are produced via glycolysis, 2 via the tricarboxylic acid cycle and 32 via the electron transport chain.

1.3 Reactive Oxygen Species in Skeletal Muscle

The term reactive oxygen species (ROS) refers to reactive oxygen-containing molecules (Devasagayam et al., 2004). Initially they were thought to be predominantly negative in their actions due to their reactivity with other intracellular proteins (Davies et al., 1982, Murphy and Kehrer, 1986). Following thirty years of study and the initial observation that contracting skeletal muscle produces an increase in ROS, they are now understood to be crucial signalling molecules (Jackson, 2016a, Nagahisa et al., 2016, Nathan and Cunningham-Bussel, 2013). Indeed, they are required for the normal function of skeletal muscle and the removal of ROS or the proteins involved in their control have demonstrated negative effects on muscle function such as increased oxidative damage and neurodegeneration as observed in SOD1 knockout mice (Smith and Reid, 2006, Radak et al., 2001, Sakellariou et al., 2018).

A redox reaction is one that involves a simultaneous and usually reversible chemical reaction between two compounds where one is reduced whilst the other is simultaneously oxidised. Reduction is defined as the loss of oxygen, the gain of hydrogen and the gain of electrons. Oxidation is the reverse and defined as the gain of oxygen and the loss of hydrogen

and electrons (Powers and Jackson, 2008). This provides a reversible mechanism by which fast and efficient signalling can occur between molecules within the cell. Furthermore, this enables the cell to respond to changes in ROS concentrations and induce a response. This redox flexibility is facilitated on the molecular scale by the amino acid Cysteine due to its evolutionary conservation and via its ability to form and break disulphide bonds.

Skeletal muscle generates superoxide or Nitric oxide (NO) as part of normal function (Jackson et al., 2007, Barbieri and Sestili, 2012). ROS generation occurs via a range of mechanisms however their source is still unclear. Although previously believed to be electron transport chain leakage recent studies now suggest a cytosolic origin (Jackson et al., 2007, Di Meo and Venditti, 2001, Kozlov et al., 2005, Goljanek-Whysall et al., 2016).

Free Radicals and Reactive Oxygen Species

The superoxide free radical ($O_2^{\cdot -}$) is produced via a number of reactions resulting from the partial reduction of oxygen, most notably from the electron transport chain (Powers et al., 2011). The negative charge makes it impermeable to the cell membrane however it has been suggested that further reactions can lead to the addition of a proton, producing a Hydroperoxyl radical ($HO_2^{\cdot}$) which can transfer across membranes. This molecule has a longer half-life allowing it to diffuse throughout the cell. It can also remove metal ions from the active sites of enzymes containing Iron-Sulphur or [Fe-S] clusters. This liberated Iron may then act to produce Hydroxyl free radicals via the Fenton reaction (Powers et al., 2011, Salvador et al., 2001, Liochev and Fridovich, 1999, McArdle et al., 2001).

Hydrogen peroxide (H_2O_2) is produced by the combination of a superoxide radical and water by one of three isoforms of Superoxide dismutase. They differ depending on their location (Batinic-Haberle et al., 2015) with the cytosolic Cu-Zn-Superoxide dismutase (SOD1), mitochondrial Mn-Superoxide dismutase (SOD2) and the extracellular Cu-Zn Superoxide Dismutase (SOD3). H_2O_2 is a relatively long lasting ROS molecule due to its

stability compared to free radicals which may provide a greater benefit in terms of signalling, but also a potentially greater threat in terms of damage to other proteins (Powers et al., 2011).

The hydroxyl radical ($^{\cdot}OH$) can be formed following incomplete breakdown of H_2O_2 via the Fenton reaction where oxidation of H_2O_2 by Fe^{2+} leads to $^{\cdot}OH$ production. A highly reactive molecule, this also makes them short lived as they react with whatever they meet and can be highly damaging to cells and their processes (Salvador et al., 2001, Powers et al., 2011).

Singlet oxygen ($^1O_2$) is not a radical but Oxygen with its valence electrons in an excited state. It has two energy states, one is an excited state described as $1\Delta gO_2$ and a second more highly excited state described as $2\Sigma gO_2$. The second excitation state has a higher reactivity than the first. Like the hydroxyl radical, singlet oxygen is very highly reactive and reacts with whatever it contacts due to a lack of spin restriction. This high reactivity also gives it a short half-life (Powers et al., 2011).

NAD(P)H oxidases (NOX) have been identified as a major source of ROS within skeletal muscle. Several isoforms of NOX enzymes have been identified and all require additional proteins for activation with the exception of NOX5 which produces homodimers (Brandes et al., 2014). The proteins and mechanisms required for functionality are not completely understood however for NOX1, NOX2 and NOX4, p22phox is required for assembly at the plasma membrane, followed by the requirement of p47phox for binding NOX1/NOX2 to the plasma membrane. In addition to this, DUOX1/2 and NOX5 homodimers require intracellular calcium for activation via EF hand proteins (Bedard and Krause, 2007). Furthermore, the enzymes require the GTPases RAC1/2 for either non-myeloid cells or leukocytes, respectively to control the protein-protein interactions described previously (Martyn et al., 2005). NOX1, NOX2 and NOX5 all produce superoxide radicals via the oxidation of NADPH while it is currently thought NOX4 produces Hydrogen peroxide along with DUOX1 and DUOX2. Within skeletal muscle NOX1, NOX2 and NOX4 have been

identified in muscle cell cultures and shown to co-precipitate with Protein disulphide isomerase, indicating their potential importance in a redox-sensitive protein chaperone mechanism (Ferreira and Laitano, 2016, Janiszewski et al., 2005). In relation to skeletal muscle, NOX5 contains an intracellular domain bound with calcium (Vendrov et al., 2015, Sakellariou et al., 2014, Paulsen and Carroll, 2013) and NOX2 has been identified as a source of skeletal muscle ROS (Espinosa et al., 2016). It should be noted that NOX3 is primarily expressed in foetal tissues and therefore not discussed here (Cheng et al., 2001). NOX4 appears to be located in the nucleus, thereby regulating gene expression via changes in ROS concentration within the nucleus (Kuroda et al., 2005).

Reactive Nitrogen Species

Reactive nitrogen species (RNS) which are produced via the enzymatic reactions of nitric oxide synthases (NOS). This leads to the generation of the nitric oxide free radical ($NO^{\cdot}$), nitric oxide (NO) molecule or the strong oxidising agent Peroxinitrite ion ($ONOO^{-}$) (Halliwell, 1994). $NO^{\cdot}$ is synthesised from L-arginine by NOS enzymes and is required for healthy muscle function. Sustained concentrations of $NO^{\cdot}$ can lead to reactions with $O_2^{\cdot -}$ producing the Peroxinitrite ion ($ONOO^{-}$) (Allen and Tresini, 2000, Collins et al., 2012, D'Autreaux and Toledano, 2007). The reactive properties of RNS can cause nitration of proteins, deplete thiol groups and damage DNA (Powers et al., 2011, Jackson, 2016b).

Nitric oxide synthases occur in three forms, all of which are found in skeletal muscle: NOS1 or neuronal NOS (nNOS) is located throughout a range of cell types while NOS2 (or iNOS) is inducible via inflammation and NOS3 (or eNOS) occurs in the endothelium (Oliveira-Paula et al., 2014, Stamler and Meissner, 2001). Of particular interest in skeletal muscle research is nNOS because during skeletal muscle contractions the NO concentration increases and leads to an increase in RNS however their reactivity suggests a localised reaction rather than diffusing throughout the cytoplasm (Silveira et al., 2003, Poole, 2015). Furthermore,

NOS1 and NOS3 have been shown to include a calmodulin binding site thereby linking them directly to skeletal muscle contractions and homeostatic mechanisms (Stamler and Meissner, 2001, De Palma et al., 2014).

Lipoxygenases

An alternative source of ROS is Lipoxygenases. Phospholipase A2 (PLA2) produces Arachidonic acid which, following secretion, becomes a superoxide precursor for lipoxygenase enzymes (Zuo et al., 2004). Alternatively, PLA2 can induce ROS production within the mitochondria, cytosol or release into the extracellular space (Powers and Jackson, 2008, Zuo et al., 2004, Woo et al., 2000). Another method is via the stimulation of NOXs leading to an overall increase in mitochondrial and cytosolic superoxide production and release into the extracellular space (Barbieri and Sestili, 2012, Brash, 1999).

1.4 The Importance of Cysteine in Redox Signalling

Cysteine is an amino acid encoded by UGU and UGC codons. Cysteine residues are among the least conserved amino acids, except for where they occur at active sites of proteins when they become one of the most highly conserved residues (Marino and Gladyshev, 2012). Cysteine has a functionally important thiol group which can be rapidly oxidised or reduced thereby forming disulphide bridges with other thiols. It usually undergoes nucleophilic reactions as determined by its pK_a of 8.3 meaning its intracellular 'reactive' state is in the form of a thiolate at physiological pK_a. However this value is related to the local environment's pH which can therefore impact cysteine reactivity (Paulsen and Carroll, 2013). It is also important to note that a low pK_a doesn't necessarily determine whether the reactive cysteine has increased oxidant sensitivity (Roos et al., 2013). The surrounding microenvironment has a major impact, as demonstrated by peroxiredoxins, upon cysteine activation where peroxide substrate and the transition state combine to enable an efficient nucleophilic substitution reaction (Le Moal et al., 2017).

Redox Signalling in Skeletal Muscle

Cysteine can undergo a range of modifications, many of which are reversible. This enables them to rapidly reflect changes to the intracellular oxidation state. In skeletal muscle this may include changes to ROS concentrations due to muscle contractions (Le Moal et al., 2017). However, a sustained increase in ROS concentration over time can lead to irreversible modifications (see figure 1.3.2.1) (Chung et al., 2013). Disulphide bridges (-S-S-) between thiol groups can temporarily affect protein function by changing their conformation thereby impacting the active site or metal ion binding mechanism. High concentrations of ROS such as H_2O_2 can produce sulphenic groups (-SOH) as an intermediate to disulphide bridges. Though it should be noted that in the thiolate form, cysteine will readily form -SOH without H_2O_2. Further reactions via sustained ROS can lead to the formation of sulphinic (-SOOH) and sulfonic acids (-SOOOH). Each step causing a reduction in the ability of the cell to reverse these modifications which leads to consistently reduced protein activity or ability to react to future changes in ROS concentrations (Chung et al., 2013). Interestingly, Sulfiredoxin has been demonstrated to be capable of reducing sulphinic acids on certain peroxiredoxins (Jeong et al., 2012). The inactivation of a protein by its substrate and subsequent re-activation would suggest that these proteins may play a signalling role in response to endogenous generation of H_2O_2 (Chung et al., 2013). Another intermediate from sulphenic acid is the reaction with RNS producing a sulphenylamide (-SN-). Both –SOH and –SN can react with glutathione (GSH) to produce reversibly modified glutathionylated thiols (-SSG) (Chung et al., 2013, Hazelton and Lang, 1980). Glutathionylated thiols can be reduced by another set of proteins called glutaredoxins using GSH and NADPH. S-Nitrosothiols (-SNO) are an intermediate of the reactions between glutathionylated thiols and Sulphydrated thiols. S-nitrosylation, is the covalent attachment of a nitric oxide group to the thiol side chain of cysteine and is an important mechanism for post-translational regulation of a large range of proteins. This also highlights

part of the ubiquitous influence of nitric oxide (NO) on cellular signal transduction providing a mechanism for redox-based physiological regulation. Sulphydrated thiols (-SSH) can occur via glutathionylation of S-Nitrosothiols or by Hydrogen sulphide (H_2S). Sulphydration of thiols is not well documented however it has been proposed that this can occur due to an increase in H_2S reflecting sarcoplasmic reticulum stress (Chung et al., 2013, Lo Conte and Carroll, 2013, Hess et al., 2005).

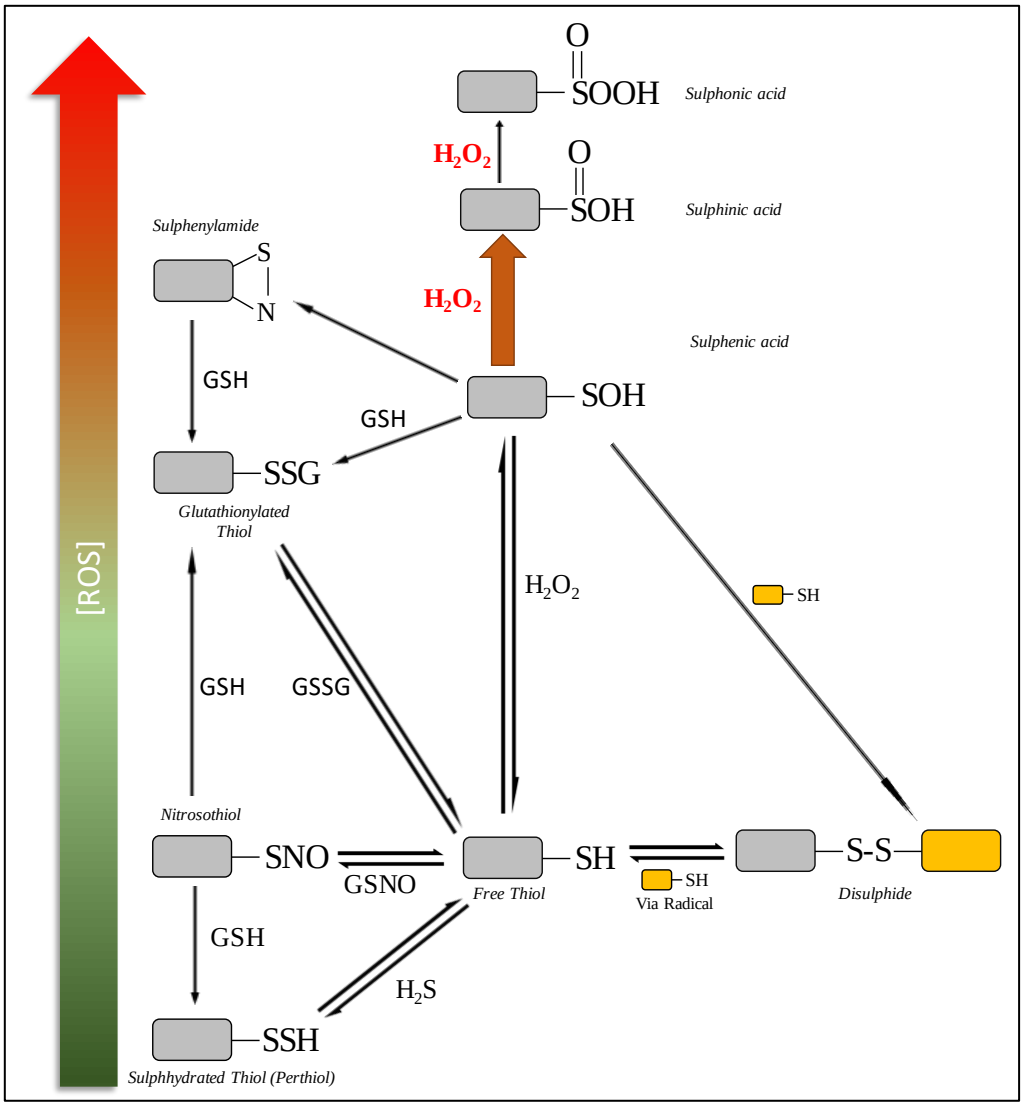

Figure 1.4.1 Cysteine modifications following an increase in the concentration of reactive oxygen species, specifically H_2O_2. The antioxidant glutathione (GSH) can reduce certain modifications and its reduced form (GSSG) can lead to reversible reactions producing free thiols. Nitrosylation produces Nitrosothiols (-SNO) which can be produced by S-Nitrosoglutathione (GSNO) involving the nitric oxide signalling pathways. The orange arrow indicates possible reversal of Peroxiredoxin-sulphinilation via Sulfiredoxin (adapted from (Chung et al., 2013)).

Redox signalling is a crucial mechanism that enables a cell to respond to changes in its oxidation state. A range of redox response systems have been identified such as those in the mitochondria, linking energy metabolism to changes in the cellular redox state, protein folding response involving heat-shock proteins such as HSP70 acting in combined roles as both redox sensors and protein chaperones (Collins et al., 2012, Vasilaki et al., 2006b). This thesis specifically considers skeletal muscle redox proteins, however similar mechanisms occur across a range of other biological systems. They enable a fast and efficient means of responding to changes in the cellular redox state. In skeletal muscle, a range of redox signalling mechanisms have been identified including the glutathione and thioredoxin systems, along with various antioxidant proteins such as peroxiredoxins and superoxide dismutases. The former can act both as a redox sensor and as an antioxidant protein. These systems enable the muscle to detect and respond to changes in the intracellular microenvironment. All systems rely on the previously described reduction-oxidation chemical mechanism and utilise cysteine amino acids thanks to their ability to form and break disulphide bonds (Forman et al., 2014). Furthermore, recent work has gone so far as to demonstrate the requirement of ROS in signalling for maintenance and repair of plasma membranes via the requirement of mitochondria (Horn et al., 2017).

Irrespective of the origin of the ROS, the mechanism relies on the reversible formation of disulphide bonds utilising the thiol group of a cysteine amino acid, enabling a response to changes in intracellular ROS concentrations.

A range of protein systems exist to finely react to and control intracellular ROS. Peroxiredoxins are antioxidant enzymes that reduce hydrogen peroxide to water in the presence of an electron donor. Six isoforms have been identified in mammals with Peroxiredoxin 3 and 5 occurring in the mitochondria and 1, 2, 4 and 6 being cytosolic (Sobotta et al., 2015). Their presence in all species indicates their importance for survival across a wide range of organisms

(Rhee et al., 2001). Peroxiredoxins 1-5 contain two redox cysteines which enables them to be reduced by Thioredoxin. Peroxiredoxin 6 contains one cysteine which can be reduced by glutathione with Glutathione *S*-Transferase π (Monteiro et al., 2007). Peroxiredoxin 4 is membrane-bound but appears to be secretory in nature as it contains an amino-tail group that may be subject to a post translational cleavage (Sasagawa et al., 2001, Rhee et al., 2001).

The Thioredoxin system contains the low molecular weight oxidoreductase enzyme Thioredoxin. It maintains substrates such as the peroxiredoxins in their active form. Thioredoxin relies on Thioredoxin Reductase (and NAD(P)H) to maintain it in a reduced, active form. Both proteins contain a selenocysteine at their active sites and occur in two forms: Thioredoxin 1/Thioredoxin Reductase 1 which are cytosolic and Thioredoxin2/Thioredoxin Reductase 2 which are mitochondrial. A third form of Thioredoxin Reductase has been identified in the testes called Thioredoxin glutathione reductase (TGR) and it is this third form that demonstrates the conjunction between Thioredoxin and Glutathione systems. Additionally, a secreted form of Thioredoxin is known although few details are known about its specific effects (Kalinina et al., 2008).

The glutathionylation system reacts to changes in hydrogen peroxide by oxidation of reduced glutathione (GSH) to its oxidised form (GSSG). These changes can lead to *S*-glutathionylation of other proteins as a post-translational modification, thus affecting their activities. This is another mechanism that links redox changes within the cell to protein modifications and enables a response to those changes (Munro and Treberg, 2017). Glutathione reduces the oxidised glutaredoxin proteins followed by reactivation of glutathione by glutathione reductase (Fernandes and Holmgren, 2004). Glutaredoxins are small redox sensitive proteins that contain a redox-active cysteine at their active sites (Holmgren, 1988). One paper has described glutaredoxin as a neuronal cell back-up to maintain Thioredoxin Reductase in a reduced state to maintain Thioredoxin functionality during times of high stress

(Branco et al., 2017). Glutathione peroxidases consist of eight currently known variants which convert Hydrogen peroxide to water in addition to reducing lipid hydroperoxides (Bhabak and Mugesh, 2010). These are also of importance for reducing oxidative stress within an organism.

Chronic exposure to high concentrations of ROS (as seen in figure 1.3.2.1) may lead to either the formation of disulphide bonds, or irreversible modifications of the redox cysteine residues in a range of redox sensitive proteins. This may negatively affect a protein's ability to react to changes in intracellular ROS due to conformational changes or steric hindrance of the enzyme's active site (Poole, 2015).

1.5 Skeletal Muscle Ageing

Skeletal muscle ageing is associated with a loss of muscle mass and force which is generally referred to as sarcopenia. By 70 years old, human muscle cross sectional area is reduced by 25-30% and strength by up to 40% and a similar reduction is observed in rodents (Jackson, 2013). As the current work was performed on mouse skeletal muscle, consideration was given to how they change with age. Mouse skeletal muscle ageing involves the loss of muscle mass and force and hence are an appropriate model for investigating the changes in different skeletal muscles with age. One example is the autophagy response which has been demonstrated to react to the metabolic adaptation to exercise. In aged models the autophagic response appears to be impaired (O'Leary et al., 2013, Ferraro et al., 2014).

Mouse quadriceps are fast glycolytic muscles responsible for swift responses to movement and sprinting in short bursts. As previously described, quadriceps energy metabolism predominantly utilises glycolysis to produce energy which can lead to a build-up of lactic acid due to an inability for the muscle to degrade it quickly enough. In comparison soleus muscles predominantly contain slow twitch fibres and use oxidative phosphorylation for the majority of their energy production. They are recruited for longer lasting muscle requirements such as maintaining posture and long-distance running. Studies of fast twitch

fibres has revealed they are more susceptible to age related loss than slow twitch fibres and fast twitch fibres appear to be more greatly affected by fibre type and size changes with age than their slow-twitch counterparts (Lexell, 1995). Oxidative phosphorylation appears to also change with age, with one study suggesting a decrease in mitochondrial ability to react to increased energy demand with age although this study examined liver samples from rats (Darnold et al., 1990).

While there are several theories of ageing there is no one alone wholly explains the cellular mechanisms that underlie it (Jang et al., 2009). One theory is the DNA damage theory of ageing which postulates that defects in DNA machinery or chromatin affect the genes required for normal cellular function. Therefore when transcribed in later life, having been accessed many times already, the errors in the gene code build to a point where the protein loses functionality, either partially or wholly (Lenart and Krejci, 2016). Of specific interest to this thesis is the free radical theory of ageing (Harman, 1956). This has been developed over more than 50 years of biochemical research and suggests that the cellular production of ROS leads to the partial or full destruction of various proteins (Harman, 1956). ROS were initially considered as only having a negative impact on cellular function but more recently they have been observed as necessary for normal cellular function. Indeed, some studies have also demonstrated that reducing ROS across the board may have a negative impact upon cellular signalling responses to changes in oxidation states (Schieber and Chandel, 2014, D'Autreaux and Toledano, 2007, Ray et al., 2012).

1.6 Thesis Aims and Hypothesis

The aim of the work reported in this thesis was to assess changes to two murine skeletal muscle types, differentiated by their primary energy production mechanism for contractions, via the use of global label free proteomics and differential labelling for redox proteomics. This will increase the understanding of how ageing affects two metabolically distinct murine

skeletal muscles at the proteomic scale and in relation to the redox state of individual cysteine residues. Thiol signalling was specifically investigated since it provided a rapid and reversible mechanism for intracellular redox concentrations to be controlled in a healthy cell and the mechanism by which this is controlled is thought to be susceptible to changes in the intracellular redox state.

The novelty of the work in this thesis is the proteomics analysis of how mouse skeletal muscle changes with age in relation to its redox proteome as this has not been previously performed. The study considered the quadriceps and soleus tissues from the mouse hind limbs due to their differences in physiological function and energy metabolism as described earlier.

LC-MS/MS or tandem mass spectrometry was the primary technique employed. Widely used and quantitative, it's ideal for studying complex samples such as tissues and characterising them. A two-pronged strategy used the relative quantitation of global label free proteomics data to determine large scale changes to the muscles along with differential labelling of specific cysteine residues which enabled the identification of changes to the redox state of individual proteins with age.

It was hypothesised that the two muscle types will age differently due to their different metabolic and functional backgrounds. This was because the quadriceps, as a fast twitch muscle using predominantly glycolysis for energy metabolism, uses a different set of proteins for structure and function compared to the slow twitch soleus that uses oxidative phosphorylation for its energy metabolism.

It was also hypothesised that differences in the changes to the redox state of each muscle type with age would be observed. It was thought this may be demonstrated by changes to quadriceps proteins involved in glycolysis (e.g. GAPDH) or soleus proteins involved in oxidative phosphorylation (e.g. ATP Synthase) which may decline in abundance with age.

CHAPTER 2

EXPERIMENTAL METHODS

2.1 Chemical Reagents

Unless otherwise stated, all reagents used were obtained from Sigma Chemical Company, Dorset, UK.

2.2 C57BL/6 Mice: Quadriceps and Soleus Muscles Dissection

C57BL/6 male mice were purchased from Charles River and housed in the Specific Pathogen-Free (SPF) facility at the University of Liverpool for a minimum of 2 weeks prior to use. All mice had free access to standard chow and water. Experiments were performed under U.K. Home Office guide lines in accordance with the U.K. Animals (Specific Procedures) Act 1986 and received ethical approval from the University of Liverpool Animal Welfare and Ethical Review Board. Sacrifice was by cervical dislocation. Only healthy, male mice were used to reduce variability and effects of hormones. Mice were selected at adult (12 months) and old (24 months) ages for mass spectrometry. Later, young (3 months old) mice became available and these tissues were used in western blotting and enzyme activity assays.

Quadriceps and soleus muscles were removed and one of each type was cut and mounted transversely on a cork block in OCT before being frozen prior to histological examination. A portion of each was prepared for redox proteomic analysis the muscles were placed in 25 mM *d*0-*N*-ethylmaleimide (NEM) and 25 mM Ammonium Bicarbonate (pH 8). Whilst the remaining muscle was used for western blotting and immediately frozen in liquid nitrogen prior to storage at -80°C.

2.3 Skeletal Muscle Homogenisation for Western Blotting

Homogenisation required the samples to be kept on ice throughout the process. Samples were moved to a 1.5 mL microcentrifuge tube containing ≤ 200 μL RIPA (Radioimmunoprecipitation Assay lysis buffer containing 50 mM Tris-HCl (pH=7.5), 1 mM EDTA, 150 mM NaCl, 0.1% w/v Sodium Deoxycholate and 1:1000 Protease Inhibitor Cocktail). The samples were initially minced with scissors followed by disruption with a

handheld homogeniser (Kontes Pellet Pestle Motor, Sigma Aldrich, Dorset) to further break down the muscle using three one-minute full-power bursts per sample. The samples were then centrifuged at 13,000 g for one minute at room temperature and the pellet formed was homogenised again (one one-minute burst per sample). A second centrifugation step at 12,000 g for 15 minutes at 4°C was then performed. The supernatant was decanted into a new 0.5 mL microcentrifuge tube and stored at -80°C for further use and the pellet was discarded.

2.4 Proteomics Sample Preparation and Analysis

2.4.1 Proteomics Sample Preparation: Muscle Homogenisation

The samples were removed from -80°C storage, defrosted on ice and briefly centrifuged at 5,000 *g* for three minutes at 4°C. Samples were minced with scissors then homogenised using a hand-held homogeniser (Kontes Pellet Pestle Motor) in a solution of ≤ 200 µL containing 20 µM Ammonium Bicarbonate and 25 µM *N*-ethylmaleimide (NEM) was used to block free thiols on proteins in the sample. A Bradford assay was performed to calculate initial protein concentrations (see 2.5.1, p.50). Desalting removed excess NEM using Zebra spin columns (Thermo Scientific, Hemel Hempstead, UK) and a second Bradford assay performed to recalculate protein concentrations and determine any protein loss during the desalting step.

2.4.2 Proteomics Sample Preparation: Differential Labelling

100 µg of desalted protein extract was added to 25 mM Ammonium Bicarbonate up to a volume of 160 µL followed by 10 µL RapiGest (Waters, Hertfordshire, UK) with a 1% (w/v) starting concentration and ~0.05% (w/v) final concentration. Samples were incubated at 80°C for 10 minutes followed by reduction with the addition of 10 µL TCEP (100 mM). Samples were incubated at 60°C for ten minutes then allowed to cool to room temperature and briefly centrifuged to collect liquid. Alkylation was performed by adding 10 µL of *d*5-NEM (200 mM). Samples were incubated in darkness at room temperature for 30 minutes. Following this quality control sample "A" was collected by sampling 10 µL into a new microcentrifuge tube. 10 µL

of a 200 μg/mL stock solution containing Trypsin and Ammonium Bicarbonate (in a 50:1 protein:trypsin ratio) was then added and samples were incubated at 37°C for twelve to sixteen hours. Quality control sample "B" (10 μL per sample) was collected following Trypsin digestion. Samples were briefly microcentrifuged to collect the digest and Trypsin was inactivated using Trifluoroacetic Acid (TFA) and incubated at 37°C for thirty to forty-five minutes. Samples were centrifuged at 13,000 *g* for fifteen minutes to remove any insoluble particles and the supernatant was carefully removed for immediate use in mass spectrometry. Quality control sample "C" was collected at this point (10 μL).

2.4.3 Tandem Mass Spectrometry and Label Free Relative Quantification

An Ultimate 3000 RSLC (fast liquid chromatography) Nano system (Thermo Scientific) was coupled to a Q-Exactive mass spectrometer (Thermo Scientific) to perform the data-dependent label free analysis.

5 μL (250 ng of protein) of sample was loaded onto a trapping column (Thermo Scientific, PepMap100, C18, 75 μm x 20 mm), using partial loop injection, for seven minutes at a flow rate of 4 μL /min with 0.1% (v/v) TFA. Resolution was performed on an analytical column (Easy Spray C18, 75 μm x 500 mm, 2 μm column) by preparing two solutions individually, prior to mixing in a specific ratio. An A gradient of 97% (containing 0.1% formic acid) and 3% B (99.9% Acetonitrile (CAN) and 0.1% Formic acid) to 60% A and 40% B over two hours at a flow rate of 300 nL/min. The program for data dependent acquisition consisted of a 70,000 resolution full scan for MS (Automated gain control (AGC) was set to 10^6 ions with a maximum fill time of 250 ms). The ten most abundant peaks were selected for MS/MS using a 17,000 resolution scan (AGC set to 5 x 10^4 ions with a maximum fill time of 250 ms) with an ion selection window of 3 *m/z* and a normalised collision energy of 30. A 30 s dynamic exclusion window was used to avoid repeat peptide selection in MS/MS. Detection of the peptides was performed by data dependent acquisition (DDA) which takes a select number of

peptide peaks from the initial scan according to a rule set and the corresponding ions were then verified against this initial set via tandem mass spectrometry (MS/MS).

Raw spectra were converted to Mascot Generated Files (.mgf) using the Proteome Discoverer software (Thermo Scientific). These .mgf files were then searched against the Uniprot mouse sequence database (database last updated on 12th May 2012; 16,376 sequences were identified for *Mus musculus*) via an in-house Mascot database server (Matrix Science, London, UK). The search parameters were: peptide mass tolerances, 10 ppm; fragment mass tolerance, 0.01 Da, 1+, 2+ and 3+ ions; missed cleavages, 1; instrument type, ESI-TRAP. Variable modifications were included as: *d*0-NEM, *d*5-NEM, mono-, di-, and tri-oxidation of cysteine residues and oxidation of methionine.

Label-free relative quantification software PEAKS 7 (Bioinformatics Solutions Inc., Waterloo, Canada) was used to analyse RAW data files against the same mouse protein database for identifications with Mascot (Zhang et al., 2012). Proteins were considered significantly changed between muscles in adult and old mice samples using the following criteria: -10 log P score of >20 (equivalent to a *p* value of 0.01), a fold change ≥ 1.5 and using a quality value of 0.8. Data normalisation was performed using the total ion current (McDonagh et al., 2014b).

PEAKS7 software includes a post-translational modification (PTM) algorithm applying the *de novo* sequencing module to search for a limited number of PTMs. All identified PTMs using this method adhere to the above search criteria and FDR validation.

2.4.4 Targeted Analysis of Differential Cysteine Labelling

Redox cysteines were detected as being simultaneously reduced and oxidised, giving rise to their cellular redox flexibility as they can adjust to changes in predominantly reduced or oxidised environments. In our experiment cysteine containing peptides that were labelled with both *d*5-NEM and *d*0-NEM were identified as redox cysteine residues, those that reacted with

only *d*0-NEM were reduced and those with only *d*5-NEM were reversibly oxidised. Redox cysteine peptides were identified by detecting identical amino acid sequences containing *d*0 and *d*5-NEM, confidence was determined by using a peptide score of >20.

Peptides detected from Proteome Discoverer analysis of RAW files were selected for targeted analysis using *m/z* data and retention with the open software Skyline (version 3.5) (MacLean et al., 2010). Targeted analysis applying *m/z*, retention times and fragmentation spectra for peptide selection allowed the calculation of the reduced/oxidised ratio (or *d*0/*d*5-NEM) of the individual cysteine residues using the individual parent ion intensities with Skyline. For redox peptides the individual reduced/oxidised ratio for each redox cysteine peptide was used to calculate an average ratio of specific cysteine oxidised/reduced peptides.

Filtration parameters for proteomics results of the label free comparison contained a false detection rate (FDR) of 1%, a mass error tolerance of 10.0 ppm and a retention time shift tolerance of 0.5 minutes.

2.4.5 Proteomic Data Analysis

Skyline (MacLean et al., 2010) was used to quantify redox peptides. The ratio of the peptide labelled with light/heavy NEM allowed the calculation of an estimated of redox state of individual cysteine residues. This was performed on adult and old muscle enabling a change in redox state of individual cysteine amino acids to be determined.

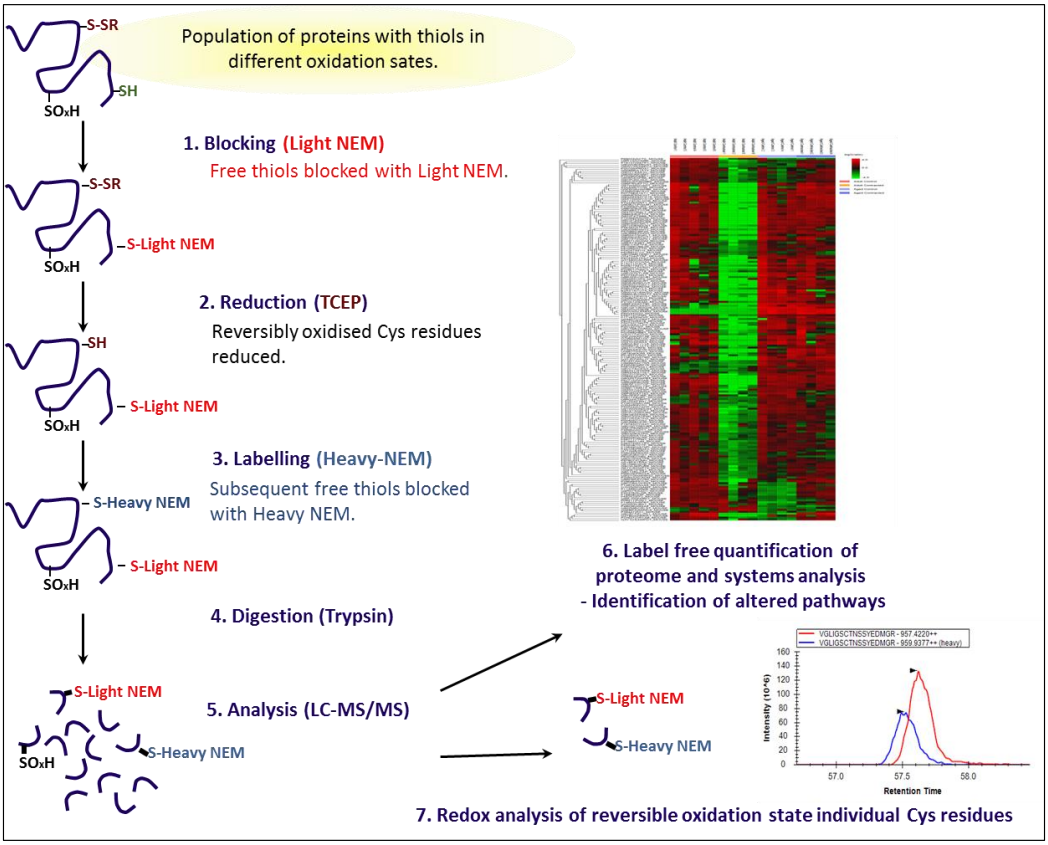

Figure 2.4.5.1 Schematic demonstrating differential labelling of proteins with light and heavy *N*-Ethylmaleimide. Following homogenisation, the protein free thiol groups are blocked with light NEM (*d*0-NEM). Excess NEM was removed and oxidised thiol groups are reduced in TCEP, the heavy isoform (*d*5-NEM) was then added to label the reversibly oxidised thiol groups within the protein and the excess removed. The labelled proteins are digested with Trypsin and injected into the HPLC column for mass spectrometry analysis. This approach enables a label free analysis of all detected peptides within the sample along with differentially labelled proteins which can indicate changes to their redox state. Peaks was used to analyse the label free data whilst Skyline was used for analysis of the differentially labelled peptides (reproduced with permission from B. McDonagh (McDonagh et al., 2014b)).

Figure 2.4.5.2 describes the layout of the Skyline desktop used for quantifying the redox state of specific cysteine residues. The left-hand panel contains the list of redox cysteine-containing peptides identified using Proteome Discoverer (v 1.4). The highlighted peptide then has its corresponding information displayed in the other three panels onscreen. The peptide information corresponds to a peptide library as identified by MS/MS fragmentation and corresponding to the mass of the peptide plus the *d*0-NEM (+125.14) or *d*5-NEM (+130.14).

The upper central pane contains the chromatogram for the selected peptide strand, the lower central panel contains the peptide retention times and the right-hand panel contains the peak area. It is this final panel that is used to determine the differences in oxidation state of the redox cysteine. The red line indicates the peak intensity for a peptide fragment detected with a redox cysteine labelled with *d*0-NEM (light isotope), and the blue is *d*5-NEM (heavy isotope) labelled redox cysteine. The samples are quadriceps and soleus muscles from five adult mice and six old mice.

The supplementary information at the end of this thesis contains label free protein details for the appropriate Venn diagrams and tables However the proteomics data was submitted to an online repository called DataCat at the University of Liverpool due to the size and formatting of the data. The online archive contains the following files in their original Excel (.xlsx) format. The files submitted are: S1 - Quadriceps All Detected Proteins; S2 – Quadriceps Significantly Changed Proteins; S3 – Adult Quadriceps Redox Proteins; S4 – Old Quadriceps Redox Proteins, S5 – Soleus All Detected Proteins; S6 – Soleus Significantly Changed Proteins; S7 – Soleus Adult Redox Proteins; S8 – Soleus Old Redox Proteins). They can be accessed at 10.17638/datacat.liverpool.ac.uk/437.

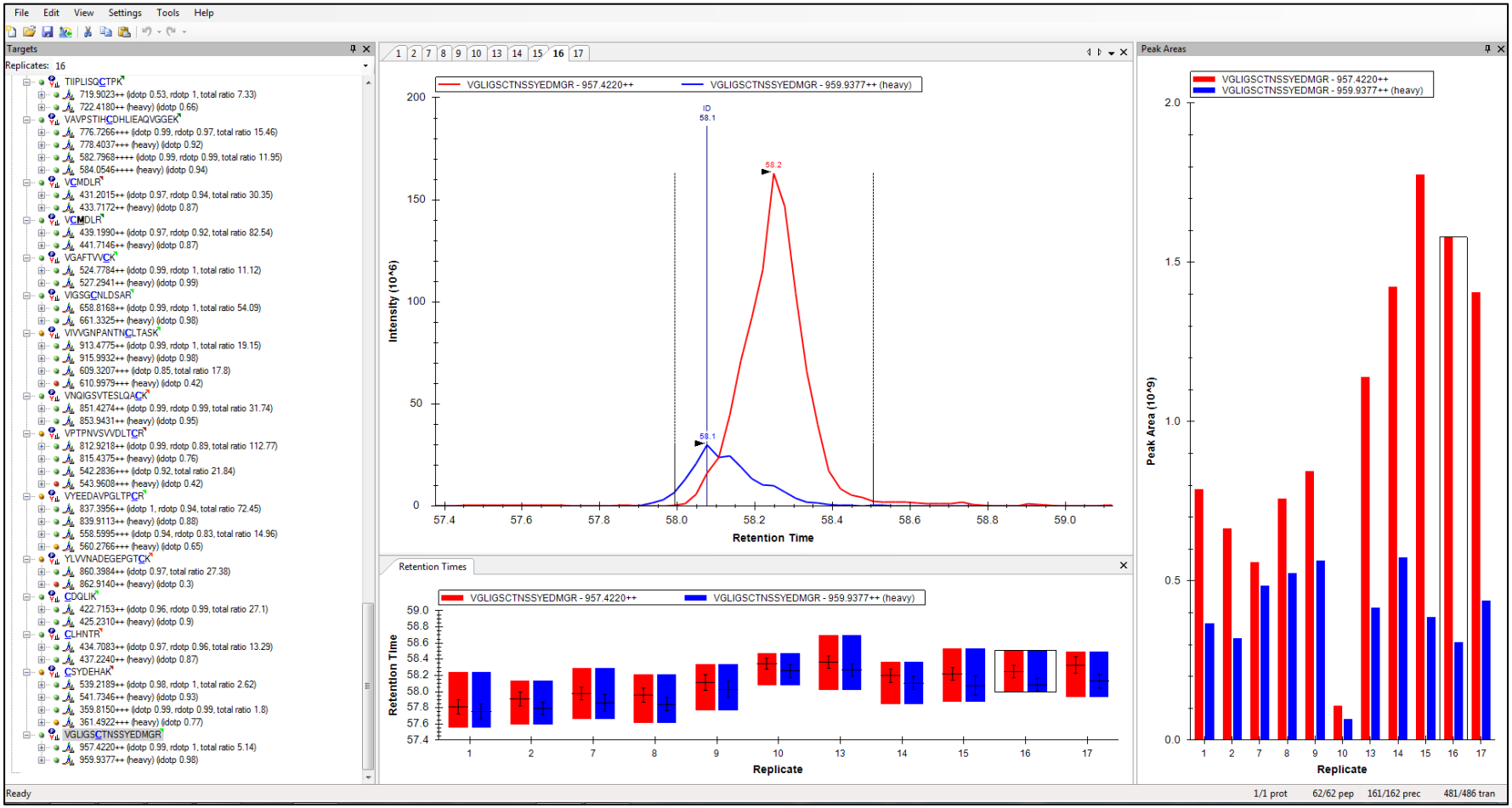

Figure 2.4.5.2 Skyline example desktop layout. Left-hand panel contains the redox peptide sequences, upper centre contains the chromatogram of the selected peptide and beneath it is the retention time for the samples containing this peptide. Right-hand panel contains the relative intensity (peak area) of the peptides as detected by the mass spectrometer and was used to determine redox ratio shifts for individual cysteine amino acids.

2.5 SDS-PAGE and Western Blotting

2.5.1 Determining Protein Concentration – Bradford Assay

A standard curve of known Bovine Serum Albumin (BSA) protein concentrations was prepared with a range of 0 to 10 µg/mL. Protein samples were removed from -80°C storage, defrosted on ice and briefly mixed using a pipette before diluting 1:1000 for quadriceps samples and 1:500 for soleus samples, in dH_2O. Quick Start Bradford Reagent (*BioRad*) was diluted 1:5. A Corning 96-well plate (Sigma Aldrich, Dorset, UK) was loaded with 100 µL of protein sample dilution and 100 µL of diluted Quick Start Bradford Reagent. The plate was analysed using a Spectrostar Nano (BMG-Labtech) spectrophotometer at 595 nm. The protein concentrations were determined using the standard curve. Confirmation of equal protein loading was initially performed via a Coomassie Blue stain for each sample at the beginning of the study. Subsequent equal loading checks were performed using the Ponceau S stain.

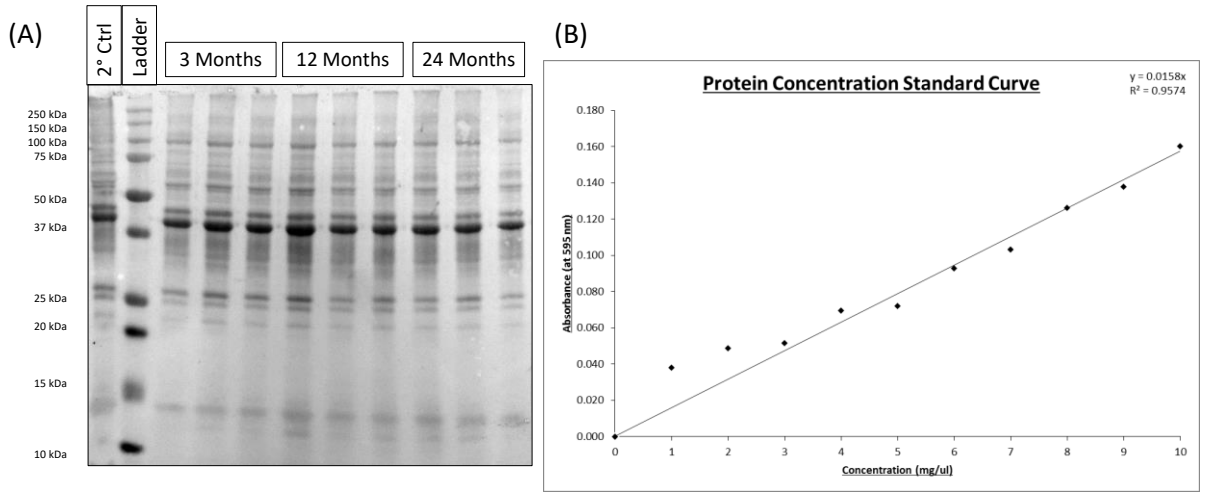

Figure 2.5.1 (A) Example Ponceau S stain showing the layout of a western blot of gels with a secondary antibody control sample (only used for the initial experiment with a new antibody). Dual Color marker was used to determine the relative molecular weights. Protein samples (25 µg) were loaded from left to right in ascending age. (B) An example standard curve produced with BSA for determining protein concentration following homogenisation.

2.5.2 Western Blotting

Protein concentrations were determined using a Bradford Assay (figure 2.5.1.1 (B)) and a specified amount of protein (in μg) was added to Laemmli buffer (Glycerol, Bromophenol Blue & 5% β-Mercaptoethanol). *N*-ethylmaleimide was added to inhibit oxidation of any remaining free thiols. Samples were denatured by heating to 95°C for 10 minutes then allowed to cool before loading 25 μg protein on 10% or 12% acrylamide resolving gels (comprising Acrylamide, Tris-HCl (pH 8.8), dH_2O, Ammonium Persulphate and TEMED (*N, N, N', N'*-Tetramethylethylenediamine). Separation of proteins based on molecular weight was performed at 120 V over two hours. Subsequently, the proteins were transferred to nitrocellulose membranes (unless otherwise stated) at 100 mA per gel over one hour. Ponceau S stain identified a successful transfer and even loading of the gel by highlighting the protein bands of similar size and location on the gel across all samples. Multiple band intensities per lane were used for image normalisation via total protein amount. Membranes were blocked using 3-5% non-fat dry milk (NFDM) dissolved in TBS-Tween20 (distilled H_2O, 20 mM Tris-HCl, 150 mM NaCl and 0.1% Tween 20, pH adjusted to 7.40) for one hour at room temperature, followed by washing three times for five minutes with TBS-T. A range of primary antibodies were used (Table 1) which were obtained from Abcam and Cell Signalling Technologies (diluted as required in either 3-5% NFDM or BSA). Primary antibodies were incubated with the membrane overnight at 4°C with constant agitation. Membranes were then washed with TBS-T three times for five minutes. Horseradish peroxidase-conjugated secondary antibodies (anti-mouse (7076 S, 1:3000) and anti-rabbit (7074 S, 1:3000) IgG (Cell Signalling Technologies, Hitchin, UK) and anti-goat IgG (A5420, 1:2000, Thermo Scientific, Loughborough, UK), were all diluted in TBS-T. Peroxidase activity was detected using the enhanced chemiluminescence (ECL) kit (Amersham International, Cardiff, UK) and band intensities were analysed on a BioRad ChemiDoc XRS+ (BioRad, US*)* using ImageLab (v5;

BioRad, US). Any potential cross reactivity of secondary antibodies was examined in initial blots by incubating protein samples with only the secondary antibody. Molecular weight was determined using Dual Color markers (BioRad, US).

In a handful of cases, it was necessary to re-probe a membrane due to the limited availability of soleus muscle tissue. In this case the membrane would first be washed three times with TBS-T at room temperature, followed by using a mild stripping buffer containing 15 g glycine, 1 g SDS and 10 mL Tween20 all in distilled H_2O and pH adjusted to 2.2. This was done with enough solution to cover the membrane and at room temperature whilst rocking for ten minutes. The solution was discarded, fresh buffer applied for another 10 minutes with rocking at room temperature. Finally, three washes with TBS-T were performed for five minutes each before checking the membrane with ECL to ensure sufficient removal of the antibodies. The membrane was washed again three times for five minutes each in TBS-T before adding the new primary antibody and following the protocol as previously detailed.

Normalisation of Data

Normalisation of the blots used the corresponding Ponceau S band intensities. Several bands per lane were measured in ImageLab (v5; BioRad, US) and the mean determined before dividing the band intensity by the corresponding Ponceau S value. This was performed for all western blot experiments.

Table 1 Western Blotting Primary Antibodies

Name	Abbreviation	Mw	Company	Product Code	LOT #	Dilution	Blocking Agent	Secondary Reqd.
AMP kinase alpha	AMPk	62 kDa	Cell Signalling Technology		#19	1:1000	3% BSA	Anti-Rabbit
p-AMPKinase-alpha	p-AMPKa	60 kDa	Cell Signalling Technology	2531 S	#13	1:1000	3% BSA	Anti-Rabbit
beta-Actin	b-Actin	42 kDa	Abcam	ab8224	GR180618-1	1:5000	3% Milk	Anti-Rabbit
Aconitase	Acon.	86 kDa	Abcam	ab129069	GR81376-7	1:5000	3% Milk	Anti-Rabbit
Carbonylation (Whole Blot)	Anti-DNP	Full Blot	Invitrogen	713500		1:1000	5% Milk	Anti-Rabbit
Catalase	Cat	60 kDa	Abcam	ab16731		1:2000	3% Milk	Anti-Rabbit
Copper-Zinc Super Oxide Dismutase	SOD1	16 kDa	Enzo	ADI-SOD-100	1051228	1:1000	3% Milk	Anti-Rabbit
DJ-1/PARK7	DJ-1/PARK7	20 kDa	Abcam	ab76241	YF021904	1:1000	3% Milk	Anti-Rabbit
DJ-1/PARK7 - SO3H	DJ-1/PARK7-SO3H	20 kDa	Abcam	ab169520	GR121877-7	1:1000	3% Milk	Anti-Rabbit
Glutathione-S-Transferase mu	GST-mu	26 kDa	Abcam	ab108524	YK080204PS	1:1000	3% Milk	Anti-Rabbit
Glucose regulated protein-78 (or Binding immunoglobulin protein)	Grp78	72 kDa	Enzo	ADI-SPA-826		1:1000	3% Milk	Anti-Goat
Glutathionylation (Whole Blot)	GSH	Full Blot	Virogen	101-A-100		1:3000	3% Milk	Anti-Mouse
Glyceraldehyde-3-Phosphate Dehydrogenase	GAPDH	36 kDa	Abcam	ab8245-100	GR663132	1:30000	3% Milk	Anti-Mouse
Glutaredoxin 1	Grxn1	12 kDa	Abcam	ab187507	GR198757-1	1:2500	3% BSA	Anti-Rabbit
Glutaredoxin 2	Grx2	18 kDa	Abcam	ab85267	GR26904-9	1:500	5% Milk	Anti-Rabbit
Glutathione Peroxidase 1	Gprx 1	22 kDa	Abcam	ab22604	GR172870-1	1:500	5% Milk	Anti-Rabbit
HSC70	HSC70	73 kDa	Stressgen Bioreagents		#04190606	1:4000	5% Milk	Anti-Rat
HSP70/HSP72 (Inducible form under RO stress)	HSP70	70 kDa	Enzo	ADI-SPA-810	#12071118	1:1000	3% Milk	Anti-Rabbit
Manganese Superoxide Dismutase	SOD2	25 kDa	Enzo	ADI-SOD-111		1:1000	3% Milk	Anti-Rabbit
Mitochondrial Brown Fat Uncoupling Protein 1	UCP1	32 kDa	Abcam	ab10983	GR169579-4	1:1000	5% Milk	Anti-Rabbit
Mitochondrial Uncoupling Protein 3	UCP3	36 kDa	Abcam	ab3477	GR150688-5	1:1000	3% BSA	Anti-Rabbit
Sulfiredoxin 1	Srxn1	14 kDa	Abcam	ab92298	GR40165-6	1:1000	3% Milk	Anti-Goat
Peroxiredoxin 1	Prdx1	22 kDa	Abcam	ab15571	GR49827-2	1:1000	3% Milk	Anti-Rabbit
Peroxiredoxin 2	Prdx2	27 kDa	Abcam	ab59539	GR106211-1	1:1000	3% Milk	Anti-Rabbit
Peroxiredoxin 3	Prdx3	27 kDa	Abcam	ab16751	GR40935-1	1:1000	3% Milk	Anti-Rabbit
Peroxiredoxin 4	Prdx4	29 kDa	Abcam	ab16943	GR140162-1	1:1000	3% Milk	Anti-Mouse
Peroxiredoxin 5	Prx5	22 kDa	Abcam	ab16944	GR64420-11	1:1000	3% Milk	Anti-Mouse or Anti Human
Peroxiredoxin 6	Prdx6	25 kDa	Abcam	ab133348	GR145006-1	1:1000	3% Milk	Anti-Rabbit
Peroxiredoxin-SO3	Prx-SO3	Full Blot	Abcam	ab16830		1:1000	3% Milk	Anti-Rabbit
Protein Disulphide Isomerase	PDI/P4HB	57 kDa	Abcam	ab137110	GR104170-8	1:1000	3% Milk	Anti-Rabbit
Sirtuin 1	Sirt1	80-110 kDa	Abcam	ab12193	GR79677-24	1:1000	5% Milk	Anti-Rabbit
Sulfiredoxin 1	Srxn1	14 kDa	Abcam	ab92298	GR40165-6	1:1000	3% Milk	Anti-Goat
Thioredoxin 1	Trx1	12 kDa	Abcam	ab86255	GR43357-5	1:1000	3% Milk	Anti-Rabbit
Thioredoxin 2	Trx2	26 kDa	Abcam	ab16857	GR53127-10	1:1000	3% Milk	Anti-Goat
Thioredoxin Reductase 1	TrxR1	55 kDa	Santa Cruz	sc20147; H-270	A1604	1:1000	3% Milk	Anti-Rabbit
Thioredoxin Reductase 1	TXNRD1	55 kDa	Abcam	ab16840	GR172892-1	1:2000	3% BSA	Anti-Rabbit
Thioredoxin Reductase 2	TXNRD2	55 kDa	Abcam	ab16841	GR779345	1:1000	3% Milk	Anti-Mouse
Thioredoxin Interacting Protein	TXNIP	45 kDa	Abcam	ab86993	GR132784-1	1:1000	3% Milk	Anti-Mouse

Table 1. List of all primary antibodies used throughout this study, with their accompanying details, including, where noted, their product codes/Lot#.

2.6 Analysis of Carbonylation

A denaturation solution (50 mM Tris-HCl (pH 7.50), 8M Urea, 2% (w/v) CHAPS (3-[(3-Cholamidopropyl) dimethylammonio]-1-propanesulfonate)) was prepared along with 4 μM DNPH ((2, 4-dinitrophenyl) hydrazine) solution (initially prepared as 40 μM DNPH in 100 μL TFA followed by a 1:10 dilution in dH_2O due to DNPH's poor solubility). 100 μg protein was denatured with 10 μL denaturation solution then 10 μL DNPH solution. Samples were briefly vortexed then incubated at room temperature (25°C) for fifteen minutes, agitated throughout. 2 M Tris neutralised the denaturants and a colour change from light to very dark orange was observed. Excess acetone was then added to precipitate the protein and incubation at -20°C for less than one hour (vortexing throughout). Samples were then pelleted at 12,000 *g* for five minutes at 4°C. Supernatant was removed and 50 μL dH_2O was added to remove salts along with another excess of acetone. Precipitation was repeated for >1 hour at -20°C, vortexing throughout and pelleting again at 12,000 *g* for five minutes at 4°C. The supernatant was removed, and the pellet allowed to air dry. The pellet was resuspended in denaturation solution and a Bradford Assay indicates the carbonylated protein concentration.

2.7 Analysis of Glutathionylation

The glutathionylation blot shows proteins conjugated to glutathione suggesting a change in overall cellular redox state. Samples were prepared under non-reducing conditions, containing no β-Mercaptoethanol. All other aspects of the blot were the same as performed for a standard western blot.

2.8 Enzyme Activity Assays

2.8.1 Aconitase Enzyme Activity

The enzyme activity of aconitase was determined by measuring the reaction of citrate to isocitrate. This is a coupled reaction requiring aconitase along with the conversion of NAD^+

to NADH and the outcome is measured using colorimetry. Throughout the experiment all samples and reagents were kept on ice.

A stock solution of 50 mM Tris-HCl was prepared and adjusted to pH 7.40. Two buffer solutions were prepared: 5 mM Tri-sodium citrate dehydrate and 0.6 mM Manganese (II) chloride tetrahydrate. Finally, the enzymatic reagents were prepared: 20 mM β-$NADP^+$ (Nicotinamide adenine dinucleotide phosphate) and two units of IDH (Isocitrate Dehydrogenase; 9.4 mg/mL equal to 9.4 units/mg). The reaction solution was then prepared by mixing the β-$NADP^+$, IDH, 50 μg protein and the buffer solution in a 50 μL reaction mixture for each well. Experiments used a Costar 3603 96-well glass bottomed plate (Sigma-Aldrich UK, Dorset) and measurements made on a Fluostar Optima (BMG Labtech, Germany) with emission at 340 nm and absorption at 440 nm with controls measured against blanks. Results are expressed as nmol/min/mg protein.

2.8.2 Thioredoxin and Thioredoxin Reductase Enzyme Activity Assays

Enzyme activity for Thioredoxin and Thioredoxin Reductase was determined using an end-point insulin-dependent reduction assay or Ellman assay. This utilises the reaction between thiols and TNB^- which produces a yellow colour that can be quantified by spectrometry. A buffer solution was prepared containing 84 mM HEPES (4-(2-hydroxyethyl)-1-piperazineethanesulfonic acid) at pH 7.60, 1.3 mM NADPH (reduced nicotinamide adenine dinucleotide phosphate), 12.5 mM EDTA (Ethylene diamine tetra-acetic acid) and 314 μM Insulin. An activating solution contained 1 M HEPES at pH 7.60 and 1mM DTNB (5,5'-dithiobis-(2-nitrobenzoic acid). Finally, a stopping solution was prepared containing 6 M Guanidine-HCl and 1 mM DTNB. A Costar 3603 96-well glass bottomed plate (Sigma-Aldrich UK, Dorset) was used and 50 μg protein was added to the buffer and activating solutions mixed in a well. Control wells contain buffer and activating reagents, no sample and have stopping solution added immediately. Following preparation of the plate, it was incubated at 37°C for

forty minutes after which an excess of stopping solution was added to all wells and the plate analysed at 412 nm on a Fluostar Optima (BMG Labtech, Germany). The resulting units were expressed as nano-moles per minute per milligram of protein (nmol/min/mg Protein) (Arner et al., 1999, Prigge et al., 2012).

2.9 Cell culture

2.9.1 Media Preparation

C2C12 standard growth and maintenance used Dulbecco's Modified Eagle's Medium High Glucose (DMEM; Sigma-Aldrich, Dorset, UK) containing 10% Foetal Bovine Serum (Gibco, Thermo-Fisher Scientific, Paisley, UK), 1% L-Glutamine (Lonza, Yorkshire, UK; 200mM) and 1% Penicillin-Streptomycin (5,000 units of penicillin and 5 mg/mL streptomycin).

Phosphate buffered saline (PBS; Sigma-Aldrich, Dorset, UK) contained 1% Penicillin-Streptomycin.

Differentiation of cells required DMEM with 2% horse serum (HS; Sigma-Aldrich, Dorset, UK), 1% L-Glutamine (200mM) and 1% Penicillin-Streptomycin.

Cell storage media contains 80% standard DMEM + 20% DMSO (Dimethyl sulfoxide; Sigma-Aldrich, Dorset, UK). As DMSO is toxic to the cells at room temperature, this time was minimised. All percentage values are final concentrations unless otherwise stated.

2.9.2 C2C12 Myoblast Culture, Differentiation and Storage

1-1.5 mL aliquots of C2C12 cells were stored in 2 mL cryovials in liquid nitrogen. Cells were thawed at 37°C for five minutes, resuspended in standard media and centrifuged at 1,000 rpm for ten minutes. The supernatant was discarded, and the pellet resuspended in 1 mL fresh

media. Cells were seeded in a T25 containing 4 mL standard DMEM and grown to 70% confluence. In all cases cells were checked daily to ensure normal and regular growth.

At 70% confluency cells were detached from the T25 surface using 1 mL Trypsin-EDTA solution (Sigma-Aldrich, Dorset, UK) and incubated at 37°C for 5 minutes followed by a brief but severe agitation to dislodge any remaining cells. Successful trypsinisation was confirmed by light microscopy. Trypsinised cells were suspended in standard media and pelleted at 1,000 *g* for ten minutes. The supernatant was discarded, and the pellet resuspended in 10 mL standard media. Cell numbers were determined using a Trypan Blue stain (Sigma-Aldrich, Dorset, UK) via haemocytometry. 10 µL of cells were mixed with 10 µL Trypan Blue and allowed to stand for five minutes. 2 x 10 µL of mixture was then loaded onto a haemocytometer on each grid. A glass cover slip was applied ensuring no bubbles were present in the cell counting regions. Cells were manually counted using a light microscope at 10X magnification.

For general cell maintenance after pellet resuspension C2C12s were diluted 1:10, seeded in a T75 and grown to 70% confluence over twenty-four hours. Incubator conditions were 37°C, 5% CO_2 and 21% O_2. Seeding of 6-well plates required 5.0-7.5x10^5 cells per well in standard media. 70% confluency was achieved in less than twenty-four hours. Differentiation of C2C12 myoblasts to myotubes was performed in their flask or plate. At approximately 80% confluency the standard growth media was removed and replaced with differentiation media. Storage of C2C12 cells required removal of DMEM and washing twice in 12 mL standard PBS. 2 mL Trypsin was added to each flask and incubated for approximately three minutes. Then 10 mL fresh standard DMEM was added to dilute the Trypsin and the cells moved to a falcon tube for centrifugation at 1000 rpm for five minutes. The old DMEM was removed and replaced with freezing media. 1-2 mL freezing media was added per 2.5 mL cryovials. The vials were labelled with cell type, name, date of freezing and the passage number

of the cells. Initially the vials were cooled for two to four hours at -80°C before being moved to a liquid nitrogen dewar for long term storage.

2.9.3 C2C12 Myotube Stretching

C2C12 cells were isolated and seeded at $7.5x10^5$ cells per well onto three BioFlex® Culture Plates coated with Collagen I. These plates had a flexible bottom membrane that allowed stretching of cell in a radial and circumferential manner. >90% confluency was achieved in twenty-four hours after which standard media was removed, the cells washed twice with PBS and differentiating media added. Cells were allowed to grow under differentiating conditions for two days before the differentiation media was renewed. Cells were not washed with PBS during differentiation stage. Following four days differentiation, the cells were stretched on the FlexCell® Loading Station™ attached to a PC with FlexCell's FX-4000 International v4.0 software for controlling experimental parameters.

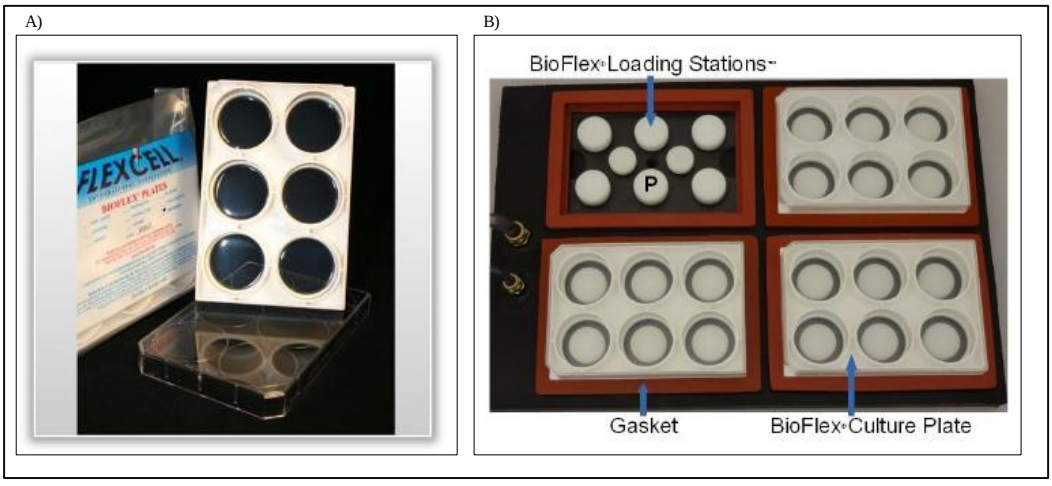

Figure 2.9.3.1 (A) FlexCell 6-well plates with stretchable bases. (B) The rubber gasket and loading station. P indicates one of the platforms for the well to sit on. The vacuum then pulls the edges of the well at intervals set in the software (see also figure 2.10.3.2). This was stationed in the incubator to maintain experiments at 37°C and 5%CO_2. Silicone gel was spread around the edge of the plates to ensure an air-tight seal with the gasket. The image was adapted from FlexCell™ marketing media.

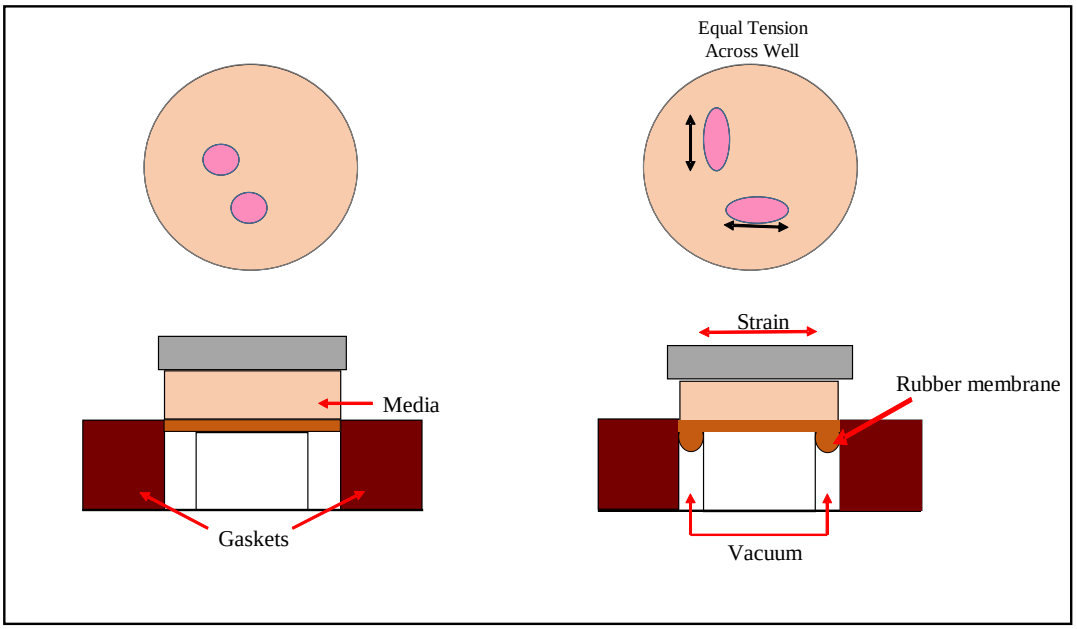

Figure 2.9.3.2 The left hand image is representative of normal set up under atmospheric conditions. The right hand image indicates how the vacuum pulls down on the edges of the elasticated well causing biaxial stretching of cells adhered to the membrane. The image is adapted from FlexCell™ marketing media.

The device applied radial and circumferential force to the membranes across three experiments. The membranes were subjected to 12% elongation (69.94 kPa pressure or 0.120 strain) at 1 Hz over a varying time course. A control plate was cultured with no force applied to the membranes. A second plate was stretched for fifteen minutes and a third plate was stretched for two hours to identify differences in cells following stimulation.

2.10 Analysis of Succinate Dehydrogenase in Histological Sections of Mouse Skeletal Muscle

All reagents were obtained from Sigma Aldrich, Dorset, UK unless otherwise stated.

The following solutions were prepared:

- 0.2 M Sodium phosphate monobasic
- 0.2 M Sodium phosphate dibasic

- 0.2 M Phosphate buffer, pH 7.6
- 0.2 M Sodium succinate solution
- NBT solution (0.1 g Nitrotetrazolium Blue in 50 mL dH_2O)
- Incubation medium contained 5 ml 0.2 M phosphate buffer, 5 ml sodium succinate solution, 5 ml NBT solution and 5 ml dH_2O.
- Physiological Saline contained 8.5 g NaCl in 1 L dH_2O.
- 50 mL of 10% Formalin-saline solution contained physiological saline and 40% formaldehyde
- 100 mL of 15% ethanol solution

Dissected quadriceps or soleus skeletal muscle from either adult or old mice was transversely orientated in OCT on cork following excision and snap-frozen in liquid nitrogen prior to storage. For histological analysis the samples were moved from -80°C storage to the Cryostat (Leica, Milton Keynes, UK) to acclimatise to -20°C. Cryo sections were cut at a thickness of 10 μm and stained for succinate dehydrogenase (SDH) activity. Individual Coplin jars containing each solution were prepared prior to the staining. First the slides were placed in incubation medium at 37°C for thirty minutes. Slides were rinsed in physiological saline then fixed in 10% formalin-saline solution for five minutes. Slides were rinsed in 15% ethanol solution for five5 minutes and finally aqueous mounting media was applied to the stained sample and a cover slip was applied. Slides were initially checked under a light microscope for sufficient staining or possible cryodamage. Analysis of the stain was performed on a Zeiss Axiovert 200M microscope connected to a PC running Windows XP and Axiovision 4.8.2 (SP3 08-2013). Images were taken using Axiocam ICc5 under bright field conditions at 10x/0.30 magnification for an exposure time of 2 ms giving a 2452 x 2056 pixel image with scale factors of x 0.55 μm/pixel, y 0.55 μm/pixel and z 1.00 pixel/pixel.

2.11 Software and Statistics

GOrilla

GOrilla highlighted protein interactions based on experimental evidence and highlights these linked processes, components or functions visually with flow diagrams. It also offers exporting of code into R for further adjustment of the visual output (Eden et al., 2009, Eden et al., 2007).

Motif-X

Motif-X showed overrepresented data patterns in protein sequences, also known as recurring short sequence elements, by searching a data set for a selected residue. Users can define the level of significance, the width or number of surrounding peptides, the occurrence (a minimum value for the number of times a sequence occurs) and the background data set (and foreground if so required) (Chou and Schwartz, 2011, Schwartz and Gygi, 2005). For our experiments, a cysteine was selected as the central amino acid and any conserved amino acids in surrounding sequences for each of the differentially labelled datasets reduced (*d*0-NEM), redox (*d*5-NEM + *d*0-NEM) and reversibly oxidised (*d*5-NEM) were identified. Search parameters were varied accordingly to identify, where possible, one conserved sequence. This enabled an alternative means of identification of potentially conserved amino acids and hence protein motifs within the reversibly labelled data sets.

PathVisio

PathVisio (v.3.2.3) is an open source software that was used to highlight proteins of particular pathways of interest using the global label free proteomics data (Kutmon et al., 2015, van Iersel et al., 2008). WikiPathways was used for the initial pathway layout before inserting the proteomics data on top to indicate up or down regulation of individual proteins (Kutmon et al., 2016, Kelder et al., 2012).

Perseus

Perseus software was used to identify statistical similarities based on a Pearson cluster of the accession numbers of proteins identified in the significantly changed global label free proteomics dataset (Tyanova et al., 2016).

Prism GraphPad

Prism's GraphPad (v6.0) software was used to produce the western blot and enzyme activity assays charts, displaying all individual data points. Statistical analysis of the normalised western blot data used GraphPad's internal analysis tool for analysis of age effect, ANOVA was performed with Tukey's post-hoc test. All significant differences relate to this analysis unless otherwise stated. Biological repeats were denoted by "N" and technical repeats by "n".

R Studio

R Studio (version 0.98.1102) was used to prepare the volcano plots of the label free proteomics data using the plot command within R Studio (RStudio Team (2015)). The volcano plot used input data from the global label free results for significantly changed proteins (those with a significance of -10logP (equivalent to $p = 0.01$) and a fold change of >1.5).

STRING

The STRING database (from here-on referred to simply as STRING) contains experimental evidence for protein-protein interactions based on both physical and functional associations. It enables pathway analysis of both the label free and differentially labelled proteomics data. These interactions can be defined with multiple coloured lines indicating the different forms of evidence or a single line whereby the thickness indicates the strength of that interaction. After input the data can be enriched for cellular components, functions or processes

highlighting specific aspects of changes between the muscle types and ages. Enrichment for KEGG pathway information highlights cell-wide information from molecular-level data. PFAM protein domains uses the protein family database and hidden Markov models (a statistical method for predicting future interactions based solely on current information) to identify evolutionarily related proteins. InterPro uses knowledge of current protein functions as applied to new protein sequences to identify domains and features that are currently uncharacterised. A combination of these enrichments then gives a clearer understanding of interactions within quadriceps for significantly changed proteins and those proteins detected in redox, reduced or reversibly oxidised conditions (Szklarczyk et al., 2015).

VennDIS

VennDIS (version 1.0.1) was used to prepare Venn diagrams for the visual comparison of detected protein numbers for age and muscle type comparison (Ignatchenko et al., 2015).

CHAPTER 3

STUDY OF THE QUADRICEPS MUSCLE

3.1 Introduction

Quadriceps skeletal muscles are located on the mouse hind limbs. The quadriceps contain four distinct muscles: the *rectus femoris*, *vastus lateralis*, *vastus intermedius* and the *vastus medialis*. The fibre type of quadriceps is a combination of fast twitch type IIa (glycolytic), type IIb (predominantly glycolytic) and type IIx (predominantly oxidative phosphorylation) fibres (Booth and Thomason, 1991). This combination of fibre type enables the rapid and explosive generation of force required for initial and short bursts of activity and as a consequence fatigue resistance is reduced (Khodabukus and Baar, 2015).

Contraction of skeletal muscle leads to an increase in the production of reactive oxygen species (ROS) by endogenous processes detailed in Chapter 1, p.30. A number of different ROS molecules are generated, ranging from the shorter-lived $^{\cdot}OH$ and $O_2^{\cdot-}$ species to the more sustained H_2O_2. Healthy skeletal muscle cells require these molecules to adapt to cellular fluctuations in ROS concentration, however high concentrations can lead to irreversible protein modifications. There are a number of mechanisms in place to control variations in these molecules. For instance, superoxide dismutases convert the superoxide radical to H_2O_2 whilst peroxiredoxins catalyse the conversion of H_2O_2 to H_2O. Of interest in this study are the intracellular ROS and the post translational modifications that are formed. Examples include sulphenic and sulphinic acids produced by increased H_2O_2 thereby affecting the activity of redox sensitive proteins and impacting some intracellular pathways causing an adaptive response of skeletal muscle to contractions. Healthy muscle can control these changes in ROS concentration and return proteins' functionality following exercise (Jackson, 2016b, McDonagh et al., 2014a, Jackson, 2009).

Several techniques have been used in this study to determine the changes in quadriceps muscles from ageing mice. One method used was succinate dehydrogenase (SDH) staining

which identified a decrease in mitochondrial complex III activity of the electron transport chain with age. This technique enabled visual identification of the changes in fibres between adult and old samples since the intensity of staining reflects the mitochondrial activity (Sher and Cardasis, 1976, Bloemberg and Quadrilatero, 2012). A two-pronged proteomics approach was performed to identify (i) global changes to the muscle protein content with age via label free relative quantification and (ii) changes to the redox proteome via differential labelling of cysteine amino acids with age. The abundance of specific proteins involved in redox signalling, metabolism and heat shock response proteins were also analysed via western blotting. The label free relative quantification together with western blot data complimented with enzyme activity assays elucidated changes in specific pathways. This is important as the overall protein abundance of individual proteins may not change with age, but reversible redox modification of regulatory cysteine residues can affect protein enzymatic activity, therefore where possible the label free proteomic data, redox analysis of individual cysteine residues of the protein together with analysis of activity allow for a broad understanding of the effects of age on selected proteins.

Pathway analysis of reduction and oxidation within the cell utilised GOrilla gene ontology to identify statistically significant pathways identified as altered with age via the label free proteomics data. STRING database analysis for protein-protein interaction also added to the evidence of various changes observed in mouse quadriceps with age. This combination of approaches enables a global analysis of mouse quadriceps ageing ranging from physiological analysis of the muscles through to the molecular changes observed for specific redox cysteines giving a thorough understanding of how they are affected by age.

3.2 Aims & Hypothesis

The aim of the work in this chapter was to identify age-related changes in the quadriceps using mass spectrometry for proteomic analysis of changes to intracellular proteins and their redox states. It was hypothesised that changes to the redox state of key intracellular proteins would occur with age.

3.3 RESULTS

3.3.1 Muscle Weights

Quadriceps were dissected from male C57BL/6 mice at 3 months (young), 12 months (adult) and 24 months (old) of age. Figure 3.3.1.1A indicates the whole mouse body weight and shows that one mouse at 24 months was significantly lighter than the others. This outlier was omitted from future analyses as western blotting only used three biological samples at 24 months of age while the mass spectrometry analyses shows six 12 months old and five 24 months old mice were used. The overall body weight of the mice increased from 3 to 12 months, as seen in figure 3.4.1.1A after which the body mass plateaued. Sarcopenia is the loss of muscle mass with age and the data in figure 3.3.1.1B demonstrates that between 12 and 24 months, mouse quadriceps mass decreased in agreement with previous studies (Romanick et al., 2013, Schiaffino et al., 2013).

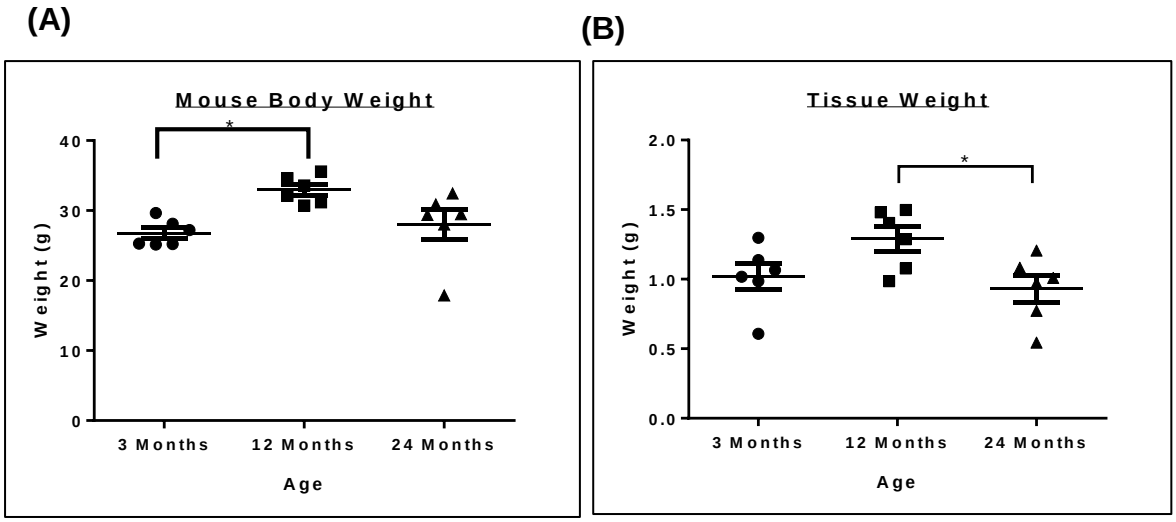

Figure 3.3.1.1 (A) Whole body weights of mice. (B) Quadriceps muscle weight. N=6 biological replicates were obtained for analysis. Significance p <0.05, *.

3.3.2 Succinate Dehydrogenase Activity of the Quadriceps Muscle

Succinate dehydrogenase (SDH) staining identified the oxidative capacity of cells by indicating the extent to which oxidation of NADH occurred via labelling with nitro-blue tetrazolium (NBT). Highly oxidised fibres stained a darker blue showing increased oxidative capacity (figure 3.3.2.1A and B). These images were not quantified and are presented to highlight the differences with age between fibres from adult and old mice prior to the detailed proteomic and biochemical analysis.

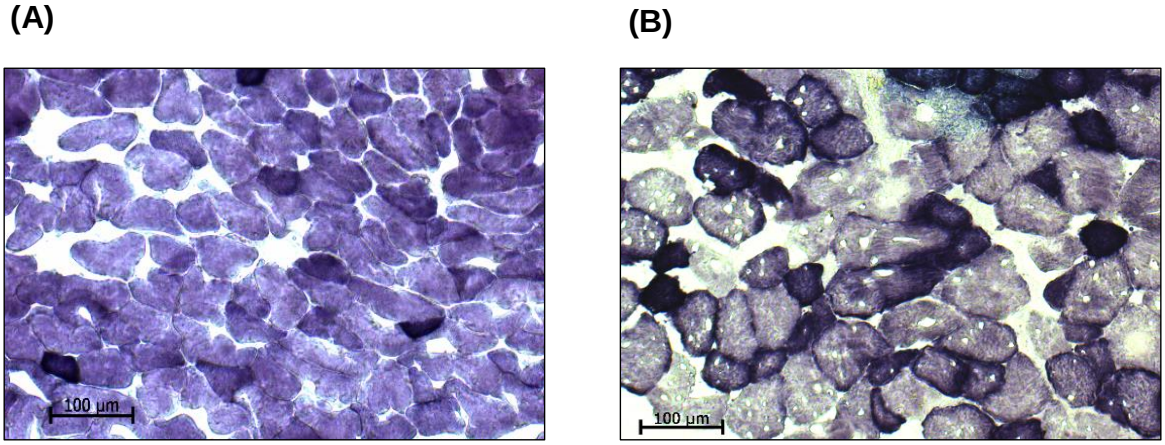

Figure 3.3.2.1 (A) SDH stain of quadriceps muscle from adult mice and (B) old mice showing a decrease in oxidative capacity of quadriceps fibres with age.

SDH staining suggested a decrease in oxidative capacity of the quadriceps fibre with age where figure 3.3.2.1A had a more intense blue stain identifying higher levels of oxidative fibres compared with figure 3.3.2.1B which has a less intense blue staining. The small white dots within cells of figure 3.3.2.1B are artefacts of the cryopreservation process and may affect apparent size by the formation of ice crystals within the cells.

3.3.3 Global Label Free Proteomics Data Analysis

A total of 640 proteins were detected via the label free method in mouse quadriceps (combining both adult and old samples) and of these 67 proteins were significantly changed with age from adult to old. The proteomics data were obtained from n=6 adult and n=5 old quadriceps muscle samples. The data is archived online as: S1 - Quadriceps All Detected Proteins; S2 – Quadriceps Significantly Changed Proteins at: 10.17638/datacat.liverpool.ac.uk/437.

A multicomponent analysis (MCA) acted as a quality control measure of the proteomics data. It indicates the extent of variance between samples and compared each adult sample with each old sample. Performed on the adult and old quadriceps samples, figure 3.3.3.1 highlights positive correlations within each age group. The blue values at the top of each box represent the R^2 value, indicating the statistical measure of fit for the regression line of the data. A higher value indicates a tighter fit to this line. The results in figure 3.3.3.1 showed high similarity within the adult and old mouse muscle sample data sets respectively and a high level of variance when comparing the data sets to each other.

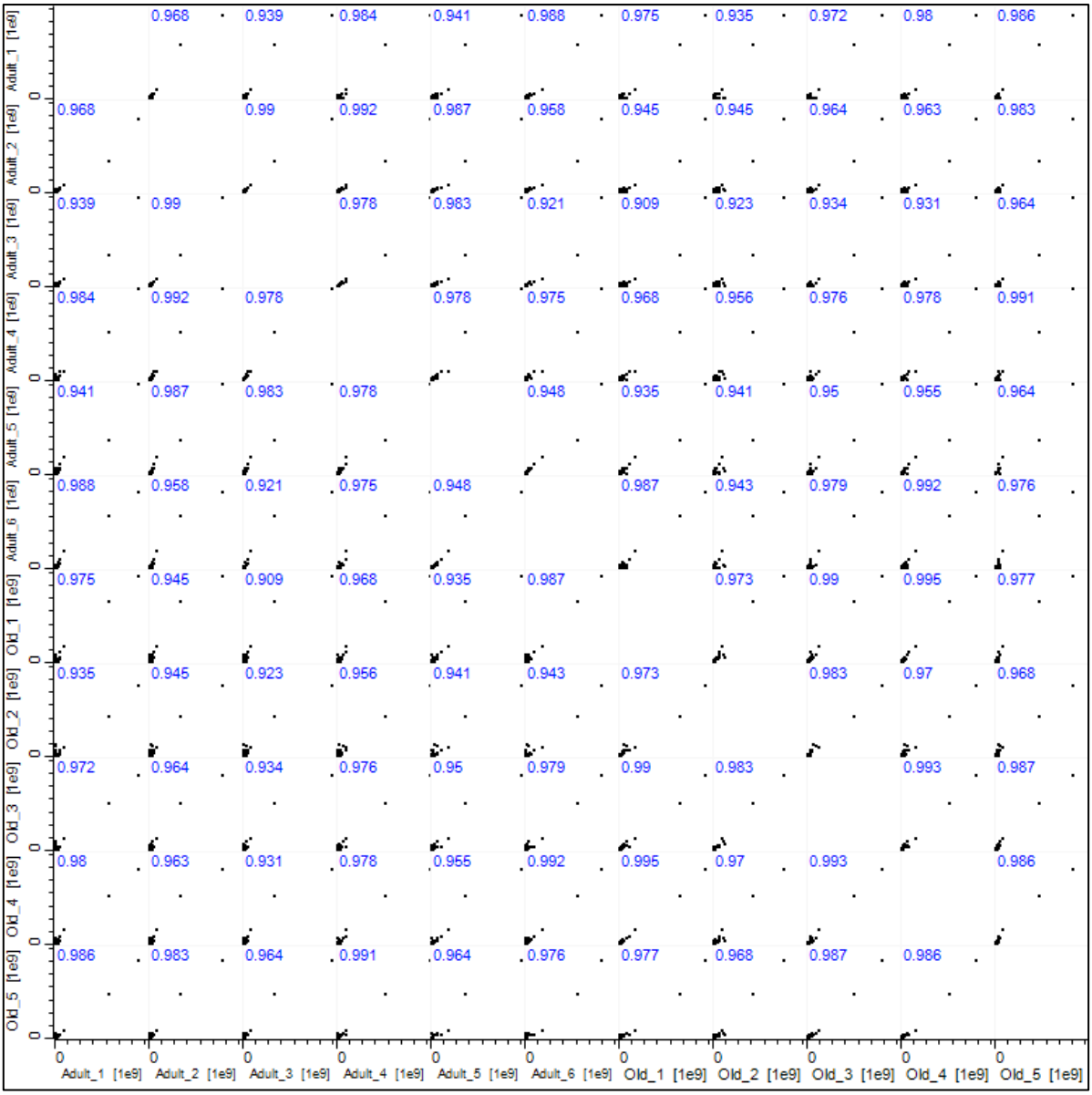

Figure 3.3.3.1 Multi-component analysis of proteins detected across all samples. Values in blue represent R^2 value for that data set.

Label free proteomics analysis utilised PEAKS7 to identify the proteins in the samples and perform label free relative quantification. For label free relative quantification, proteins were considered as significantly changed when they had a –10 log P of >20 (equivalent to *p* value of 0.01), fold change of >1.5 between adult and old and a quality value of 0.8, these parameters ensured a good minimum standard of confidence in the comparison of protein abundance (Ting et al., 2009, Oberg and Mahoney, 2012). The heat map in figure 3.3.3.2 shows

significantly changed proteins identified in quadriceps from adult and old mice. The datasets are included in an online data storage facility provided by Datacat a University of Liverpool data repository for research data. Excel files containing the combined label free and the differentially labelled proteomics data for the redox proteins as per the output from Proteome Discoverer are stored at 10.17638/datacat.liverpool.ac.uk/437.

Significant differences were observed between muscle from adult and old mice for a number of proteins. For example, significant increases with age were seen for cytoskeletal proteins such as troponins, tropomyosin and actin. Significant decreases were seen in the protein folding response and energy metabolism proteins such as HSP70 and phosphoglycerate mutase. Figure 3.3.3.3 indicates the $\log_2$ fold change as normalised against the total ion current for each run of proteins in adult and old samples.

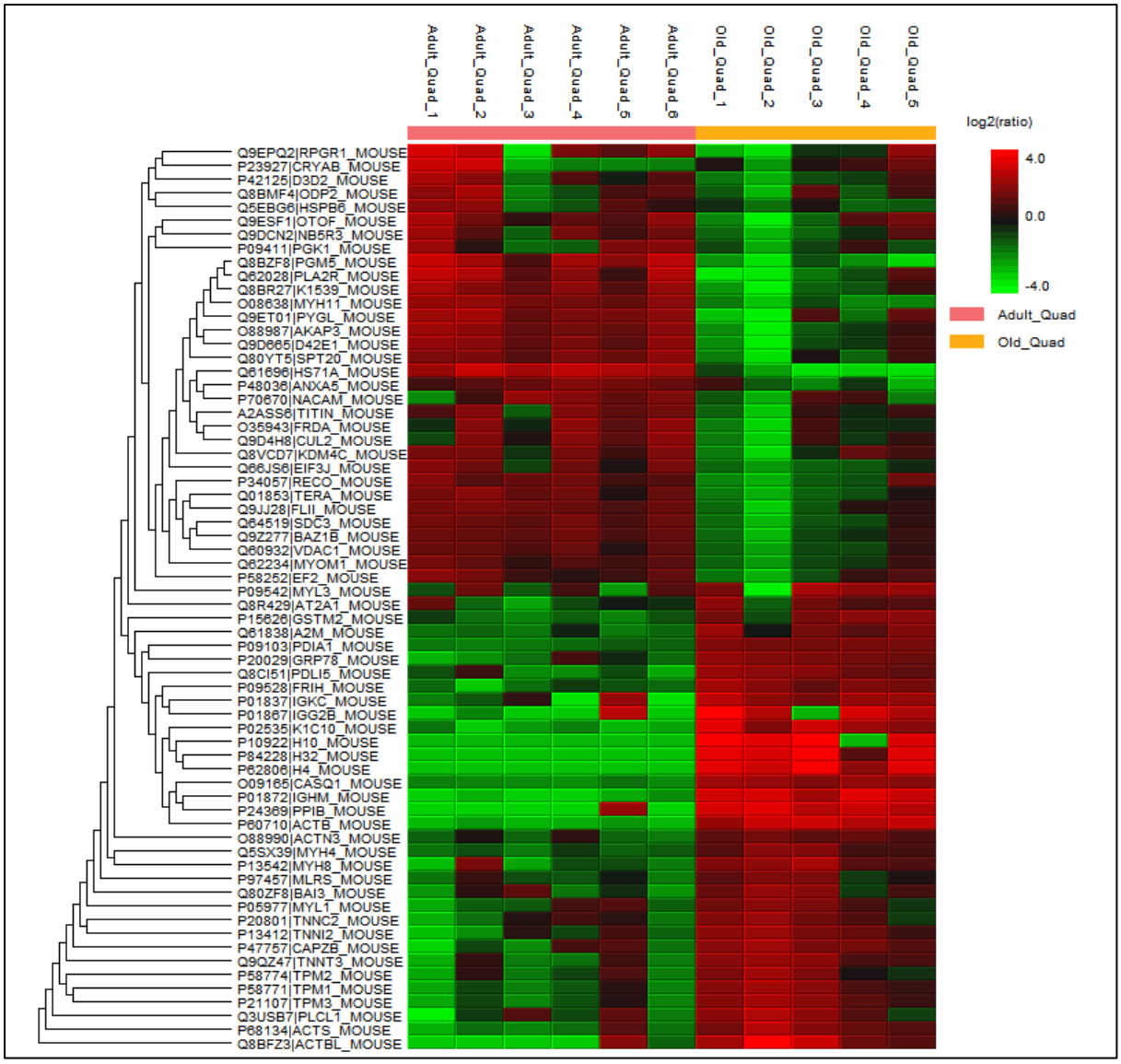

Figure 3.3.3.2 Heat map of the $\log_2$ ratio fold change of significantly changed quadriceps muscle proteins comparing adult (n=6) and old (n=5) mice. Red indicates an increase and green a decrease in fold change. Label free significance was determined using a minimum fold change of ≥ 1.5, a peptide quality of 0.8 and a significance $p < 0.01$.

A volcano plot was produced using the basic R Studio (version 0.98.1102) application and shows significantly changed proteins from a dataset of combined adult and old results. Figure 3.3.3.3 shows all significantly changed proteins identified in the label free proteomics assessment of the quadriceps samples. Those highlighted in red are significantly up-regulated and green shows those significantly down-regulated proteins (where a minimum fold change of ≥ 1.5, a peptide quality of 0.8 and a significance $p < 0.01$).

Significantly up-regulated proteins in quadriceps include the cytoskeletal proteins Tropomyosin 1 (TPM1), Troponin T (TNNT3), Myosin Light Chain 3 (MYL3) in addition to those involved in protein folding such as Grp78 (HSPA5) and Protein Disulphide Isomerase A3 (PDIA3). Significantly down-regulated proteins included the chaperone proteins HSP70 (HS71A) and HSPB6, both of which are involved in the heat-shock response. Nascent polypeptide-associated protein complex subunit α muscle specific form (NACAM) was also identified as down regulated with age in the quadriceps. This is involved in thick and thin myofibril assembly.

Volcano Plot of Quadriceps Proteins Significantly Changed with Age

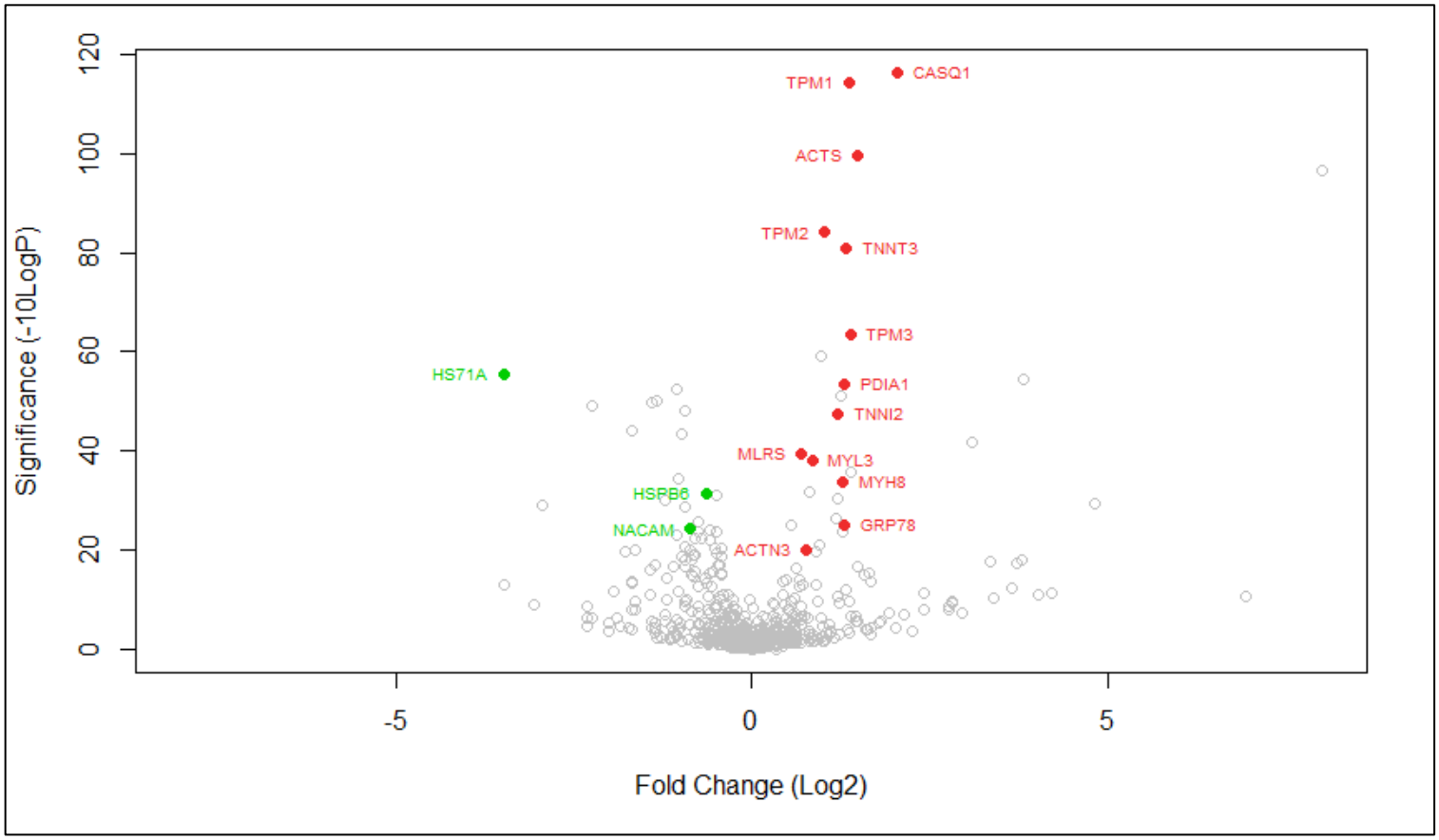

Figure 3.3.3.3 Volcano plot showing structural proteins identified from analysis of global label free proteomics data of all detected proteins in quadriceps (adult and old mice combined). Significantly up-regulated proteins highlighted are Calsequestrin1 (CASQ1), Tropomyosin α-1 chain (TPM1), Actin α skeletal muscle (ACTS), Tropomyosin β chain (TPM2), Troponin T fast skeletal muscle (TNNT3), Troponin α-3 chain (TPM3), Protein disulphide isomerase (PDIA1), Troponin-I fast skeletal muscle (TNNI2), Myosin regulatory light chain 2 skeletal muscle isoform (MLRS), Myosin light chain 3 (MYL3), Myosin heavy chain 8 (MYH8), Grp78 (GRP78) and A actin 3 (ACTN3). Significantly down-regulated proteins highlighted are HSP70 1A (HS71A), HSP β-6 (HSPB6) and Nascent polypeptide-associated protein complex subunit α muscle specific form (NACAM). Green indicates significantly decreased proteins and red indicates significantly increased proteins. Significance is defined as having –10 log P of >20 (equivalent to *p* value of 0.01), a >1.5 fold change.

3.3.4 Western Blotting and Enzyme Activity Assays

Western blots and enzyme activity assays were performed as described in Methods (2.5, p.53 and 2.8, p.56 respectively). The western blot primary and secondary antibodies used are presented on p.62-63. Where global label free proteomics data are included, significance values were defined as > 1.5 fold change, a significance score of -10 log P, > 20 (equivalent to $p < 0.01$) and a peptide quality of 0.8. In this section, mouse muscle ages are referred to as 3, 12 or 24 months for clarity.

Thioredoxin 1 (TRX1) was selected for western blot analysis due to its role in intracellular control of ROS (Dimauro et al., 2012, Munro and Treberg, 2017). It is a 12 kDa cytosolic antioxidant enzyme that performs the crucial task of reducing cytosolic Peroxiredoxins (PRDX1, PRDX2, & PRDX4). Oxidised TRX1 is inactive and requires Thioredoxin Reductase 1 (TRXR1) to reduce it back to its active form. In figure 3.3.4.1 no significant change was observed in protein abundance for TRX1 which agreed with the global label free proteomics data. TRXR1 also demonstrated no significant change in protein abundance between 12 and 24 months as shown in figure 3.3.4.2. Enzyme activities for both Thioredoxin and Thioredoxin Reductase showed no change with age.

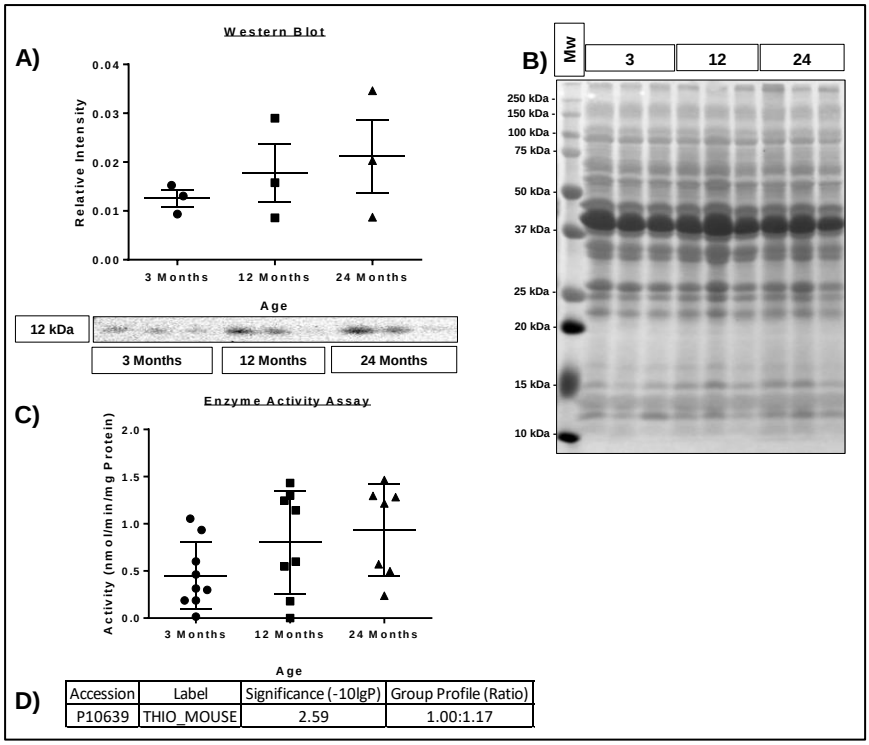

Figure 3.3.4.1 (A) Densiometric measurement for immunodetection by western blotting of Thioredoxin 1 (TRX1) in mouse quadriceps muscle. (B) Enzyme activity assay performed for Thioredoxin (non-specific, detecting both TRX1 and TRX2. (C) The Ponceau S stain used for normalisation of (A). (D) Label free proteomics result for Thioredoxin. N=3 biological replicates. Short bars indicate upper and lower interquartile range while the middle represents the median value following statistical analysis using ANOVA with Tukey's post-hoc test.

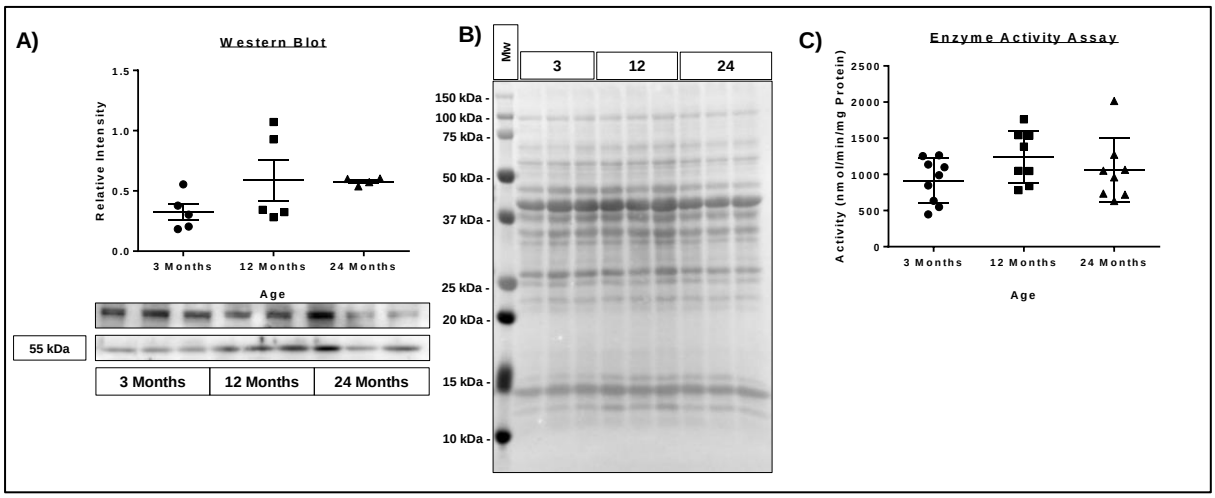

Figure 3.3.4.2 (A) Densiometric measurement for immunodetection by western blotting of Thioredoxin reductase (TRXR1) from 3, 12 and 24 month samples of quadriceps muscle. (B) The Ponceau S stain used for normalisation of (A). (C) Enzyme activity assay performed for Thioredoxin Reductase (non-specific, detecting both TRXR1 and TRXR2). Thioredoxin. N=3 biological replicates. Short bars indicate upper and lower interquartile range while the middle represents the median value following statistical analysis using ANOVA with Tukey's post-hoc test.

Thioredoxin 2 (TRX2) is a 26 kDa redox enzyme located in the mitochondria that has the same biochemical function as TRX1 and, along with Thioredoxin Reductase 2 (the mitochondrial equivalent of TRXR1) returns PRDX3 and PRDX5 back to activity. No significant change in protein abundance of either TRX2 or TRXR2 were observed with age and TRX2 was not detected in the global label free proteomics data.

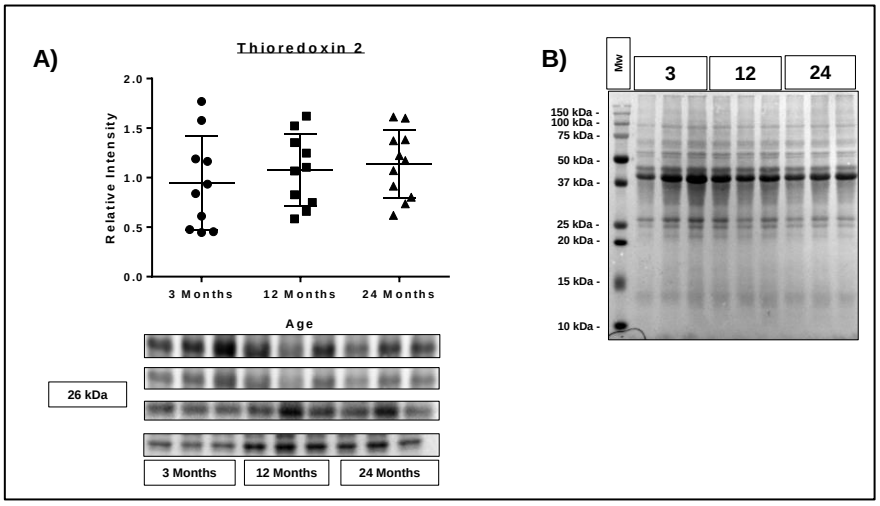

Figure 3.3.4.3 (A) Densiometric measurement for immunodetection by western blotting of TRX2. (B) Ponceau S stain used for normalisation of band intensities of (A). N=3 biological replicates. Short bars indicate upper and lower interquartile range while the middle represents the median value following statistical analysis using ANOVA with Tukey's post-hoc test.

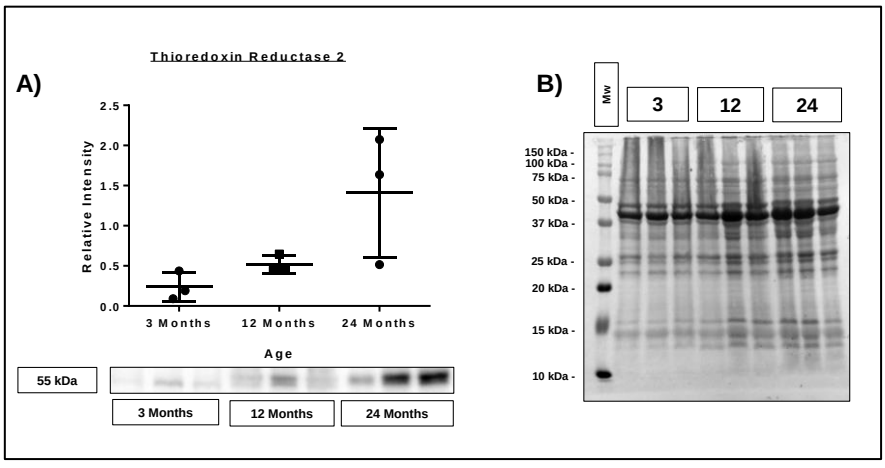

Figure 3.3.4.4 (A) Densiometric measurement for immunodetection by western blotting of Thioredoxin Reductase 2 (TRXR2). (B) Ponceau S stain used for normalisation of (A). N=3 biological replicates. Short bars indicate upper and lower interquartile range while the middle represents the median value following statistical analysis using ANOVA with Tukey's post-hoc test.

Thioredoxin interacting protein (TXNIP) may limit the availability of Thioredoxin in the cytosol, affecting the rate of turn-over of redox controlling proteins such as the Peroxiredoxins (Jeon et al., 2005). The data showed no significant change and was not detected in the total label free proteomic data set.

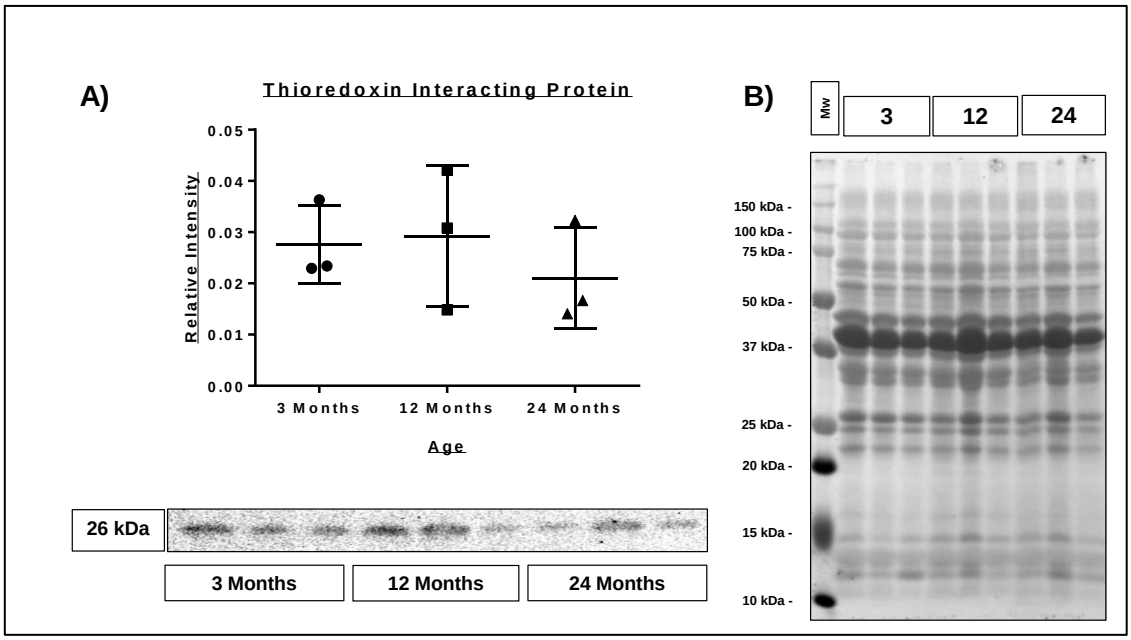

Figure 3.3.4.5 (A) Densiometric measurement for immunodetection by western blotting of Thioredoxin Interacting Protein (TXNIP). (B) Ponceau S stain used for normalisation of (A). N=3 biological replicates. Short bars indicate upper and lower interquartile range while the middle represents the median value following statistical analysis using ANOVA with Tukey's post-hoc test.

Peroxiredoxins (1-6) directly regulate intracellular ROS concentrations coupled with Thioredoxin 1 and 2. Thioredoxin 1 and 2. They catalyse the reduction of H_2O_2 to H_2O which causes the formation of a disulphide bond between the peroxidatic cysteine and resolving cysteine residues of the active site that can be reversed by Thioredoxin 1 or 2 depending on whether it is located in the cytosol or mitochondria respectively. Western blot data identified significant increases in protein abundance for mitochondrial PRDX3 (3 and 12 to 24 months, both $p < 0.01$) and PRDX5 (3 to 24 months, $p < 0.05$) with age. PRDX1, 2, 4 and 6 (all cytosolic) did not change in protein abundance with age. Relative quantification via global label free

proteomics (figure 3.3.4.6G) identified no significant changes to any of the peroxiredoxins with age.

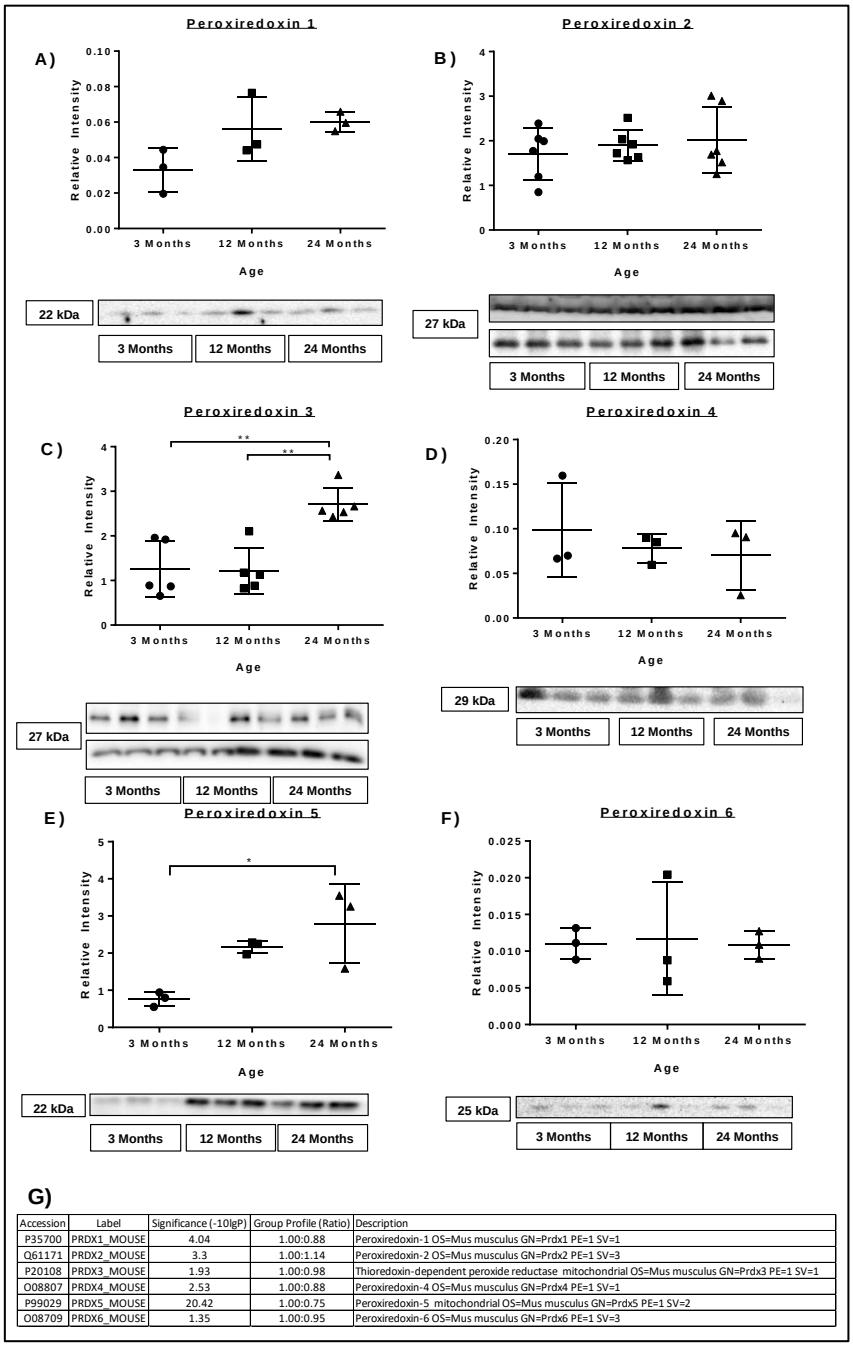

G)

Accession	Label	Significance (-10lgP)	Group Profile (Ratio)	Description
P35700	PRDX1_MOUSE	4.04	1.00:0.88	Peroxiredoxin-1 OS=Mus musculus GN=Prdx1 PE=1 SV=1
Q61171	PRDX2_MOUSE	3.3	1.00:1.14	Peroxiredoxin-2 OS=Mus musculus GN=Prdx2 PE=1 SV=3
P20108	PRDX3_MOUSE	1.93	1.00:0.98	Thioredoxin-dependent peroxide reductase mitochondrial OS=Mus musculus GN=Prdx3 PE=1 SV=1
O08807	PRDX4_MOUSE	2.53	1.00:0.88	Peroxiredoxin-4 OS=Mus musculus GN=Prdx4 PE=1 SV=1
P99029	PRDX5_MOUSE	20.42	1.00:0.75	Peroxiredoxin-5 mitochondrial OS=Mus musculus GN=Prdx5 PE=1 SV=2
O08709	PRDX6_MOUSE	1.35	1.00:0.95	Peroxiredoxin-6 OS=Mus musculus GN=Prdx6 PE=1 SV=3

Figure 3.3.4.6 Densiometric measurement for immunodetection by western blotting of Peroxiredoxins 1-6. (A) PRDX1, (B) PRDX2, (C) PRDX3 (**, $p < 0.01$), (D) PRDX4, (E) PRDX5 (*, $p < 0.05$), (F) PRDX6. (G) Label free proteomics data for PRDX1-6 between 12 months and 24 months. N=3 biological replicates. Short bars indicate upper and lower interquartile range while the middle represents the median value following statistical analysis using ANOVA with Tukey's post-hoc test.

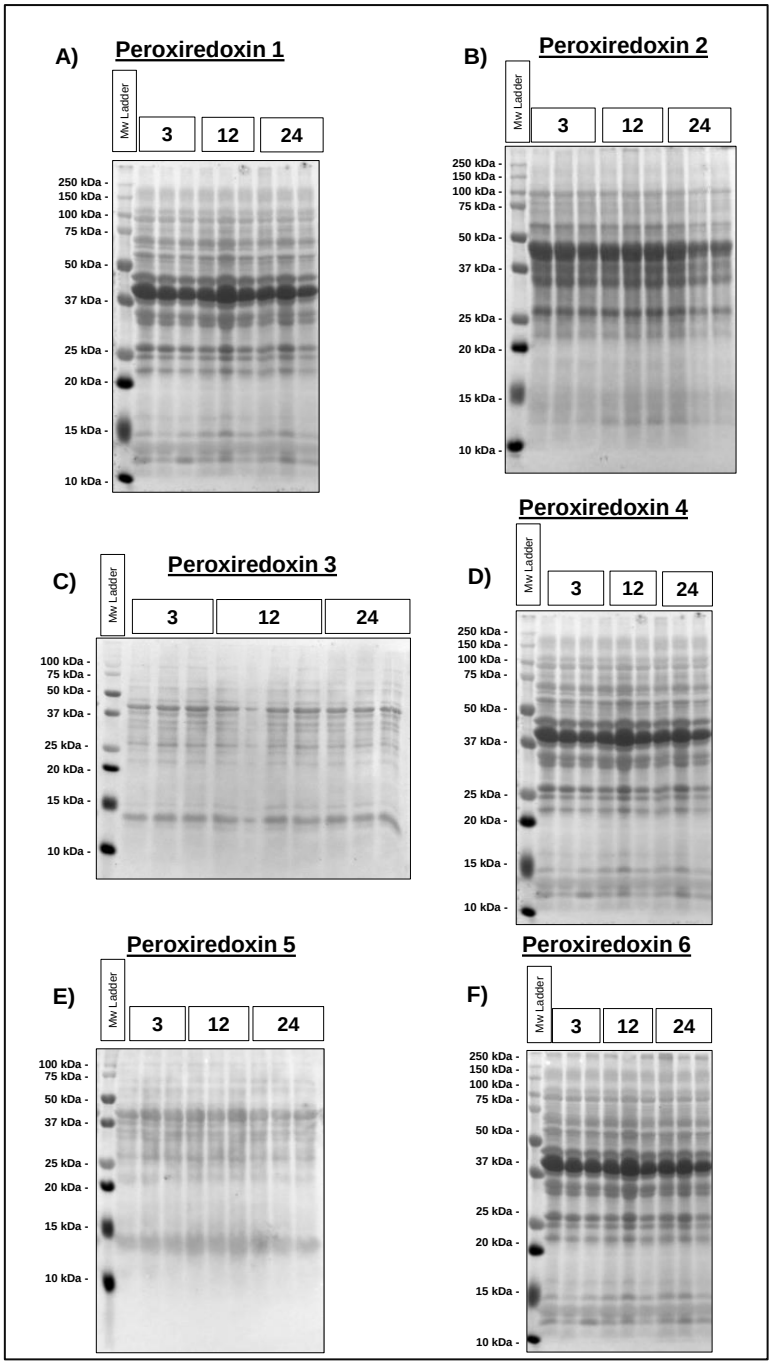

Figure 3.3.4.7 Ponceau S images used for normalisation of the corresponding blots in figure 3.3.4.6.

In addition to the individual peroxiredoxin blots and label free analysis, sulphonylated Peroxiredoxins 1-4 (Prdx-SO_3H) were analysed via western blot to identify long term effects of sustained ROS on peroxiredoxins. Figure 1.4.1 (p.36) describes the various post translational modifications resulting from changing and sustained intracellular ROS concentrations. The

results in figure 3.3.4.8 (A) showed a significant increase in the abundance of sulphonylated proteins with age (3 to 24 months ** $p < 0.01$ and 12 to 24 months *** $p < 0.001$).

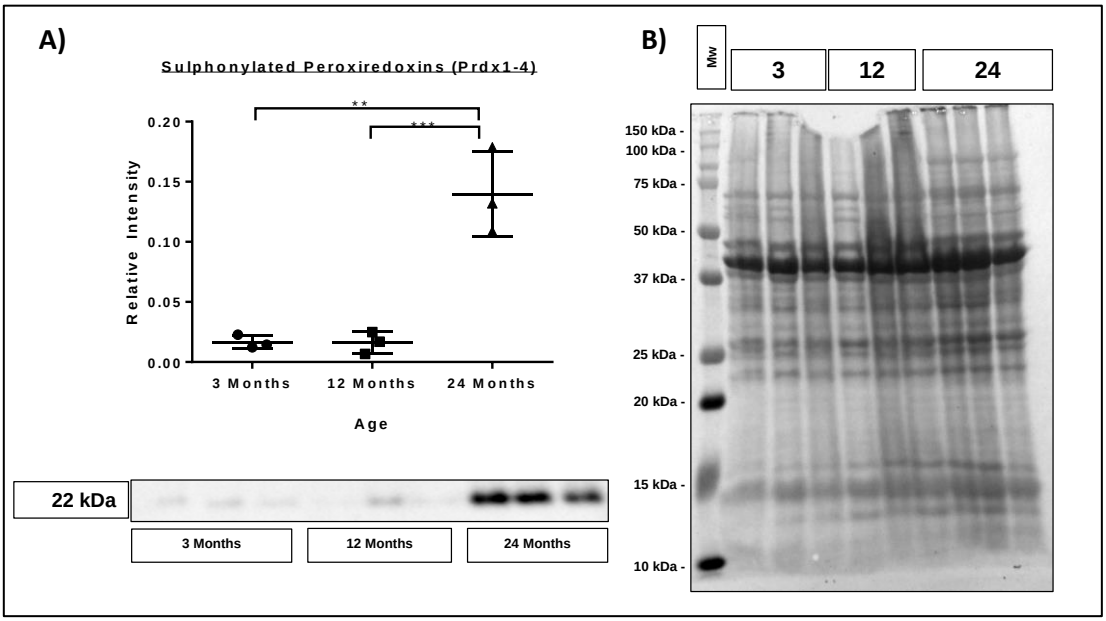

Figure 3.3.4.8 (A) Densiometric measurement for immunodetection by western blotting of sulphonylated peroxiredoxins (Prdx-SO_3H). ** $p < 0.01$, *** $p < 0.001$. (B) Ponceau S stain used for normalisation of (A). N=3 biological replicates. Short bars indicate upper and lower interquartile range while the middle represents the median value following statistical analysis using ANOVA with Tukey's post-hoc test.

Cu-Zn Superoxide dismutase (SOD1, cytosolic) and Mn Superoxide dismutase (SOD2, mitochondrial) were analysed via western blot to identify changes to these enzymes that are directly involved in the attenuation of superoxide free radicals. The results shown in figure 3.3.4.9A identified a significant increase in protein abundance from 3 to 12 months in SOD1, although there was no significant change in SOD2 (figure 3.3.4.9C) protein abundance and the label free proteomics data identified no change with age.

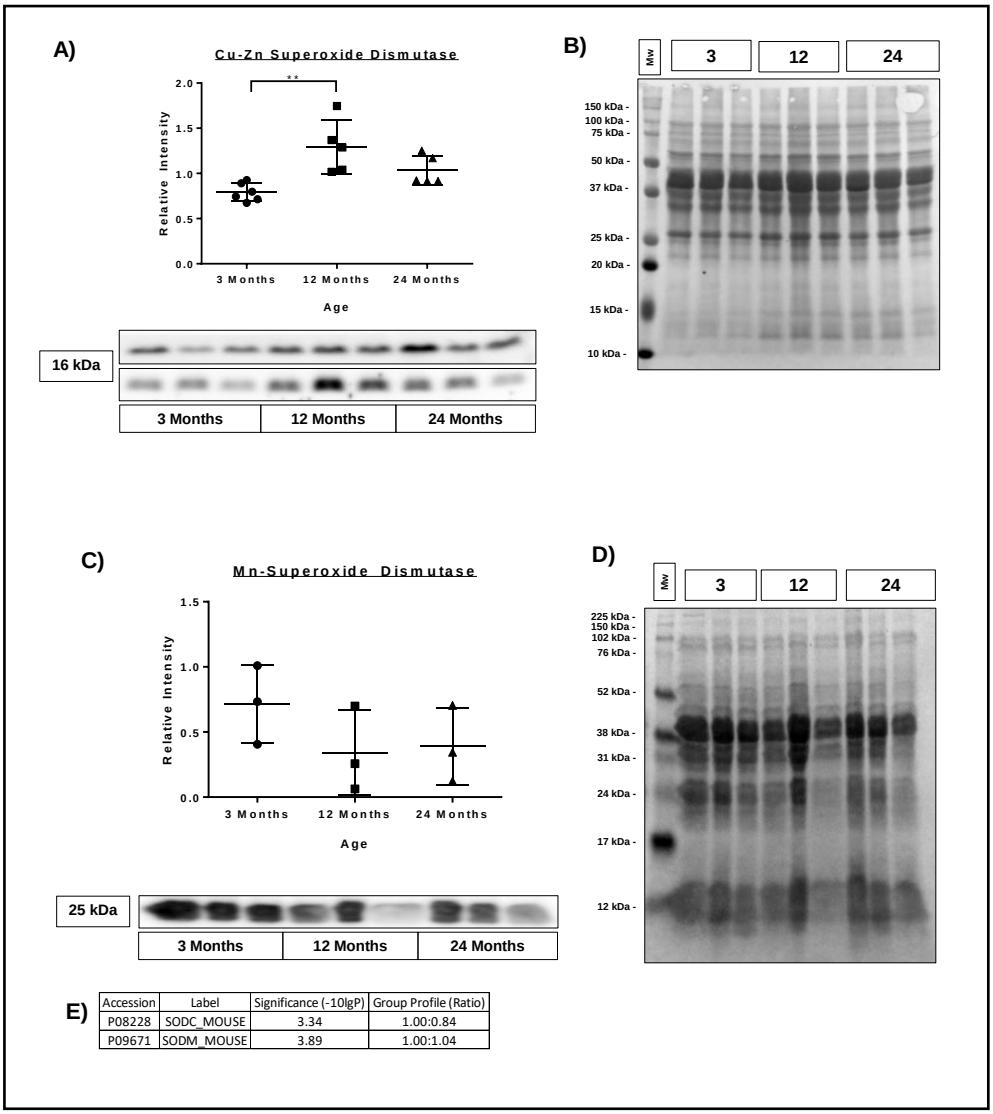

Figure 3.3.4.9 (A) Densiometric measurement for immunodetection by western blotting of Cu-Zn Superoxide Dismutase (SOD1). ** $p < 0.01$. (B) Ponceau S stain used for normalisation of (A). (C) Mn-Superoxide Dismutase (SOD2). (D) Ponceau S stain used for normalisation of (A). N=3 biological replicates. Short bars indicate upper and lower interquartile range while the middle represents the median value following statistical analysis using ANOVA with Tukey's post-hoc test.

Glutathione peroxidase 1 (GPX1) is one of several isoforms of glutathione peroxidase and catalyses the conversion of H_2O_2 to H_2O. Western blot analysis (figure 3.3.4.10A) identified no significant change in protein abundance with age. This protein was not detected in the label free proteomics analysis.

Glutaredoxin 2 (GRX2) is a mitochondrial based protein that contains an Fe-S (iron-sulphur) cluster. Western blot data shown in figure 3.3.4.11A showed a significant increase in protein abundance with age (p <0.05) from 12 to 24 months but this was not detected in the label free proteomics data.

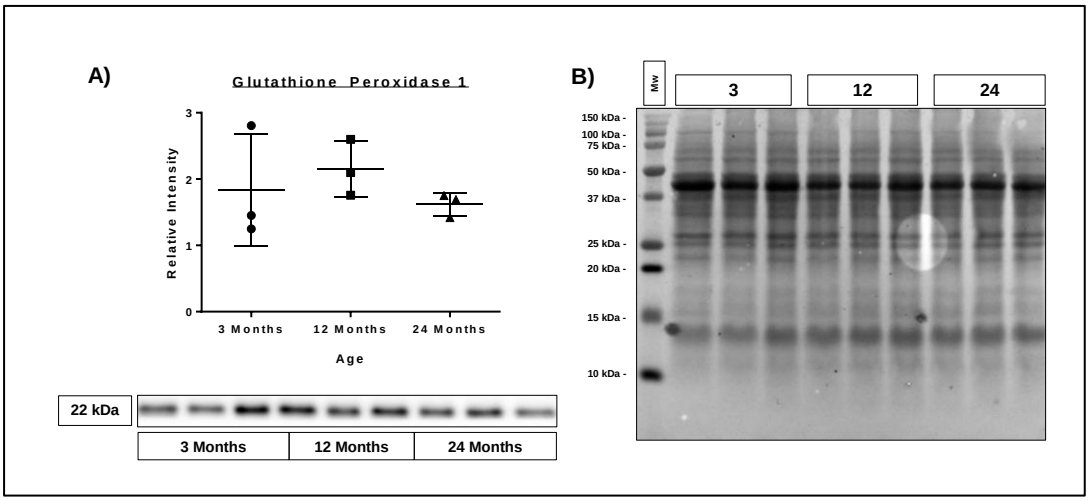

Figure 3.3.4.10 (A) Glutathione Peroxidase 1 (Gpx1). (B) Ponceau S stain used for normalisation of (A). N=3 biological replicates. Short bars indicate upper and lower interquartile range while the middle represents the median value following statistical analysis using ANOVA with Tukey's post-hoc test.

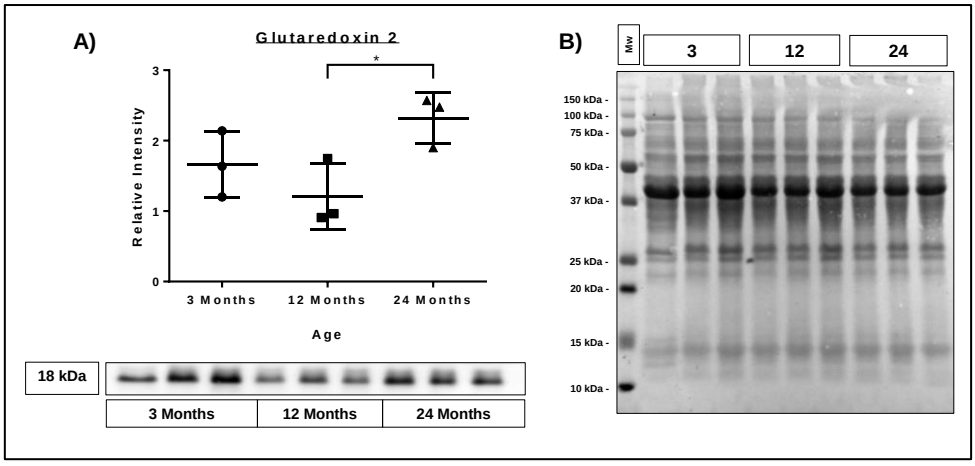

Figure 3.3.4.11 Glutaredoxin 2 (Grx2). (A) Densiometric measurement for immunodetection by western blotting, * p <0.05. (B) Ponceau S stain used for normalisation of (A). N=3 biological replicates. Short bars indicate upper and lower interquartile range while the middle represents the median value following statistical analysis using ANOVA with Tukey's post-hoc test.

Sulfiredoxin 1 (SRXN1) is involved in maintaining peroxiredoxin activity by reducing thiol groups. Western blotting data in figure 3.3.4.12A demonstrated no change in protein abundance with age and it was not detected in the label free proteomic analysis.

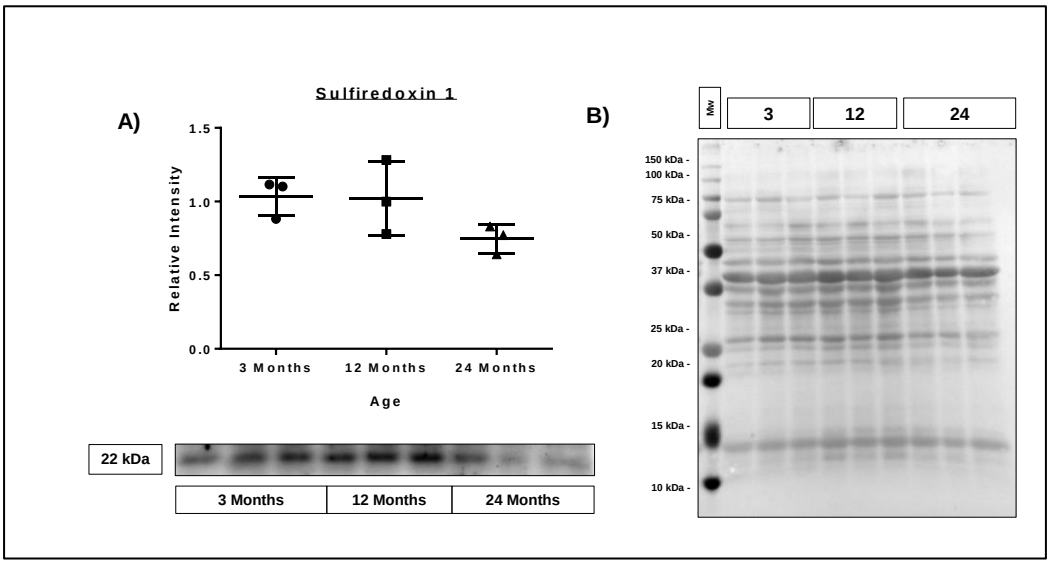

Figure 3.3.4.12 Sulfiredoxin 1 (Srxn1). (A) Densiometric measurement for immunodetection by western blotting. (B) Ponceau S stain used for normalisation of (A). N=3 biological replicates. Short bars indicate upper and lower interquartile range while the middle represents the median value following statistical analysis using ANOVA with Tukey's post-hoc test.

The heat shock and protein folding response are alternative indicators of both short-term and sustained cellular stress. In figure 3.3.4.13A, the constitutively expressed HSC70 showed a significant decrease (p <0.05) in protein abundance from 12 to 24 months in quadriceps muscle. Figure 3.3.4.13B shows the inducible form, HSP70, which did not significantly change with age. However relative quantification of these proteins in the label free proteomics data highlighted a significant decrease in the inducible HSP70 with age and no significant change to HSC70. Note that a 15% resolving gel was used for the HSC70 blot alone.

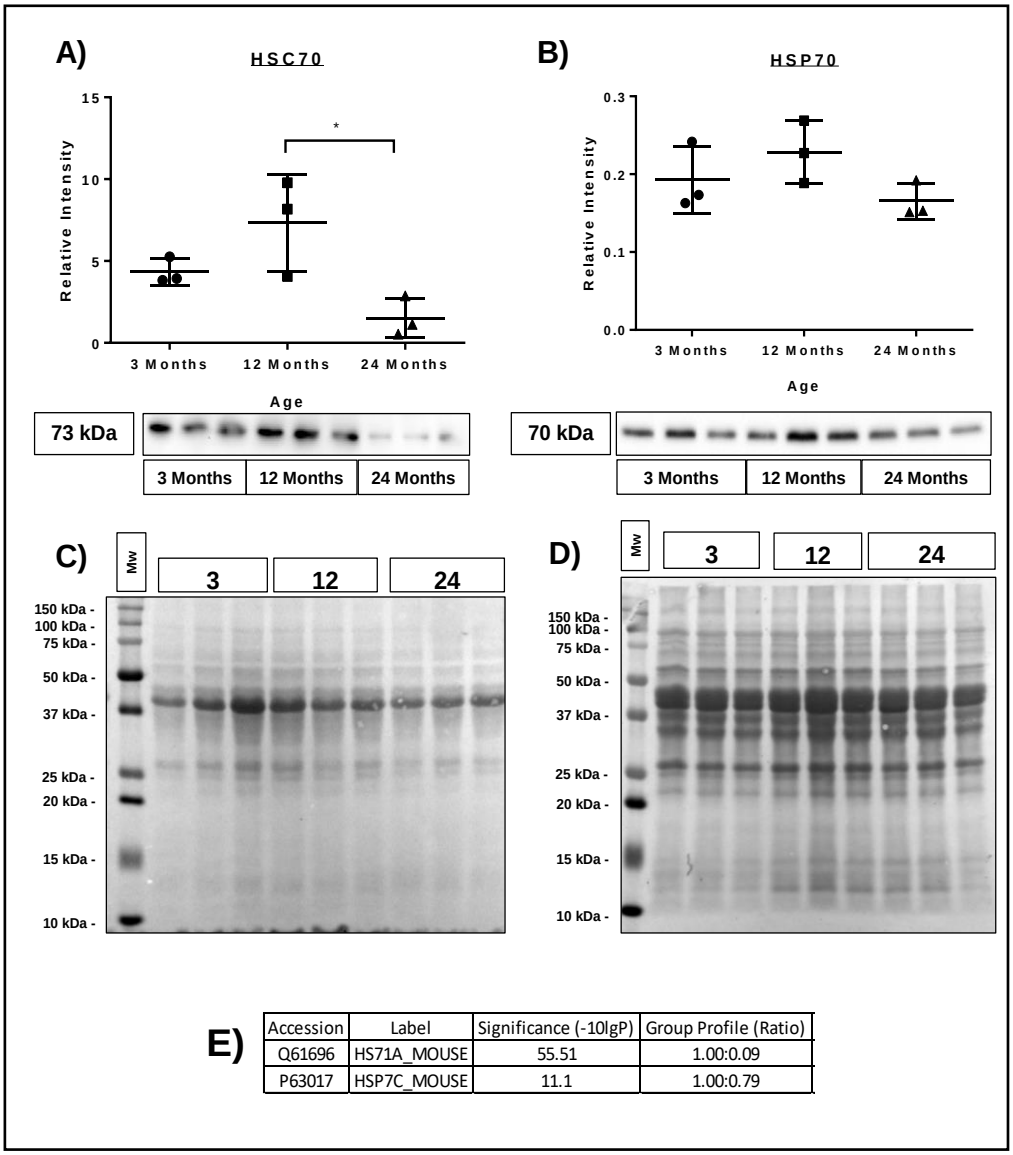

E)

Accession	Label	Significance (-10lgP)	Group Profile (Ratio)
Q61696	HS71A_MOUSE	55.51	1.00:0.09
P63017	HSP7C_MOUSE	11.1	1.00:0.79

Figure 3.3.4.13 Densiometric measurement for immunodetection by western blotting of (A) Constitutively expressed HSC70, * p <0.05. (B) Inducible variant HSP70. (C) Ponceau S stain used for normalisation of (A). (D) Ponceau S stain used for normalisation of (B). (E) Global label free proteomics data for HSP70 (HS71A) and HSC70 (HS70C). (A) Used a 15% resolving gel. N=3 biological replicates. Short bars indicate upper and lower interquartile range while the middle represents the median value following statistical analysis using ANOVA with Tukey's post-hoc test.

Protein disulphide isomerase analyses are shown in figure 3.3.4.14. The western blot identified a significant increase in Protein disulphide isomerase (P4HB) abundance from both 3 to 24 months (*** p <0.001) and 12 to 24 months (* p <0.05). This result was reflected in the label free global proteomics result where a significant increase with age was also observed.

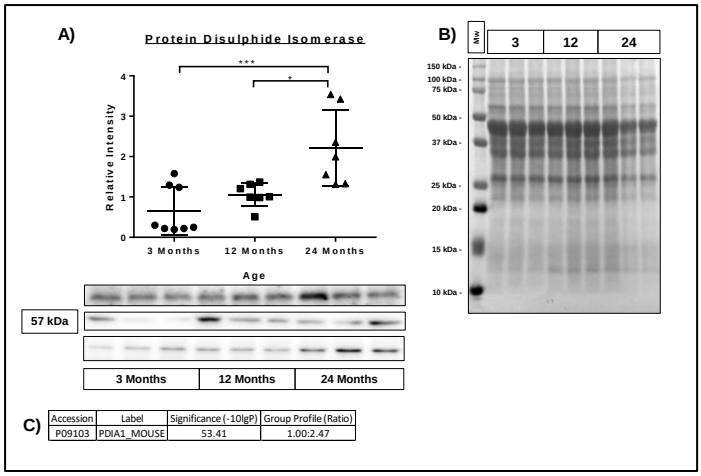

Figure 3.3.4.14 (A) Protein Disulphide Isomerase (PDI), * p <0.05, *** p <0.001 (B) Ponceau S stain used for normalisation of (A). (C) Label free data for PDI/P4HB. N=3 biological replicates. Short bars indicate upper and lower interquartile range while the middle represents the median value following statistical analysis using ANOVA with Tukey's post-hoc test.

Glutathione S-transferase μ (GST-μ) is a protein involved in conjugation of reduced glutathione for detoxification within the cell. In figure 3.3.4.15A data on protein abundance showed no change with age, however the global label free proteomics result showed a significant increase in protein abundance with age.

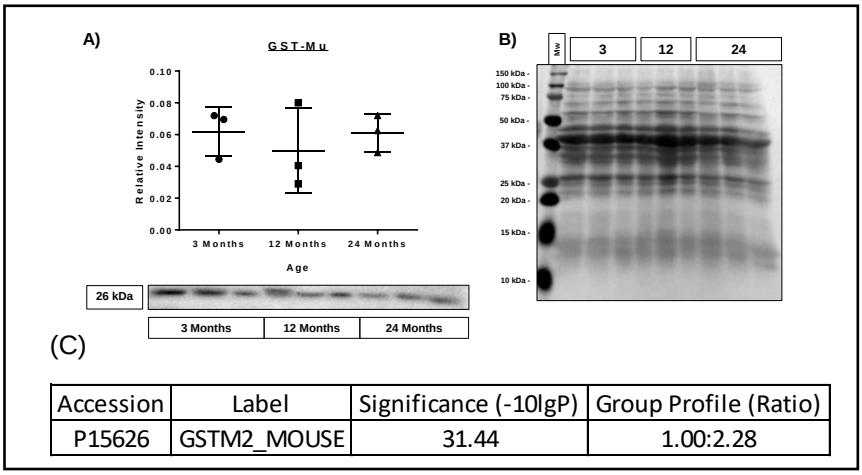

Figure 3.3.4.15 (A) Glutathione S-Transferase μ (GST- μ). (B) Ponceau S stain used for normalisation of (A). (C) Global label free proteomics result for GST-μ 2 isoform. N=3 biological replicates. Short bars indicate upper and lower interquartile range while the middle represents the median value following statistical analysis using ANOVA with Tukey's post-hoc test.

PARK7 is a protein with a multitude of functions including as a redox sensor in addition to its protein chaperone duties, western blot data in figure 3.3.4.16A showed significant increases (*, p <0.05) in protein abundance between both 3 and 12 to 24 months of age, however this was not reflected in the global label free data (Jin et al., 2016, Yu et al., 2014, Wang et al., 2016).

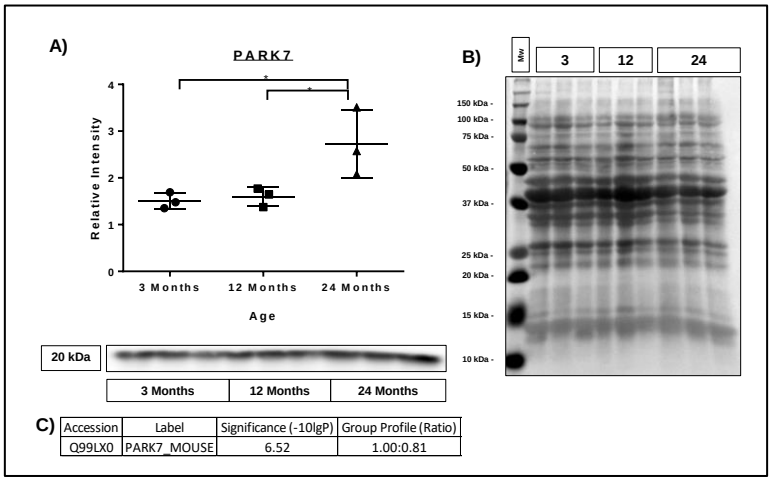

Figure 3.3.4.16 (A) Densiometric measurement for immunodetection by western blotting of PARK7 in mouse quadriceps. * p <0.05. (B) Ponceau S stain used for normalisation of (A). (C) Label free analysis of PARK7 indicating no significant change with age. N=3 biological replicates. Short bars indicate upper and lower interquartile range while the middle represents the median value following statistical analysis using ANOVA with Tukey's post-hoc test.

The sulphonylated form of PARK7 (PARK7-SO_3H) is thought to reflect the effects of sustained intracellular ROS upon proteins involved in chaperone and folding mechanisms. Figure 3.3.4.17A shows a substantial increase in protein abundance with age for PARK7-SO_3H. No protein was detected at 3 or 12 months, however clear bands were seen at 24 months. This significant increase (* p <0.05) in the modified form of PARK7 suggests that as a chaperone it is highly likely to be affected by sustained increased concentrations of ROS.

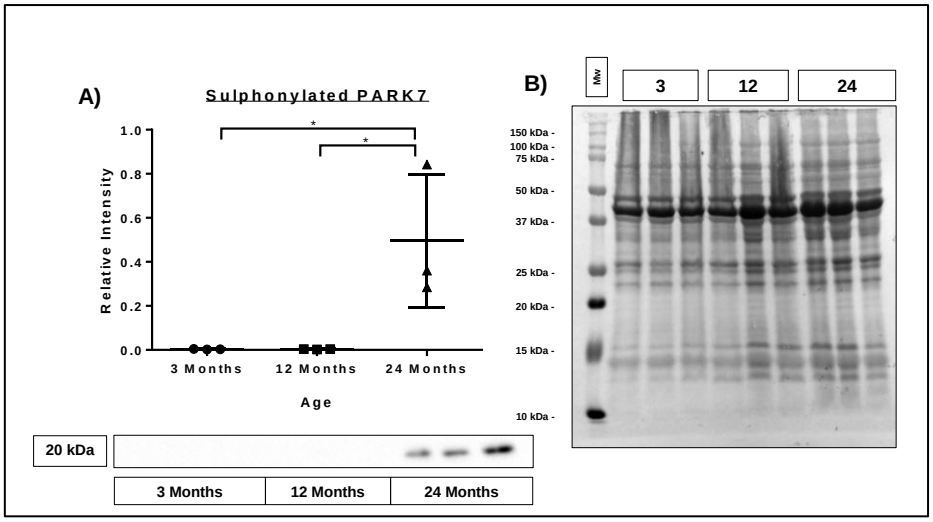

Figure 3.3.4.17 Sulphonylated PARK7 (PARK7-SO_3H) reflects the response to sustained reactive oxygen species over time leading to increasing modifications of the protein with sulfonyl groups. (A) Densiometric measurement for immunodetection by western blotting of PARK7-SO_3H. *, $p < 0.05$. (B) Ponceau S stain used for normalisation of (A). N=3 biological replicates. Short bars indicate upper and lower interquartile range while the middle represents the median value following statistical analysis using ANOVA with Tukey's post-hoc test.

Cellular energy metabolism changes with age were considered by assessing Aconitase, AMPK, its active form p-AMPK and GAPDH.

Aconitase demonstrated no change in protein abundance with age as shown in figure 3.3.4.18A with no change seen for enzymic activity. These results combined with the global label free proteomics data all indicate no change to Aconitase with age.

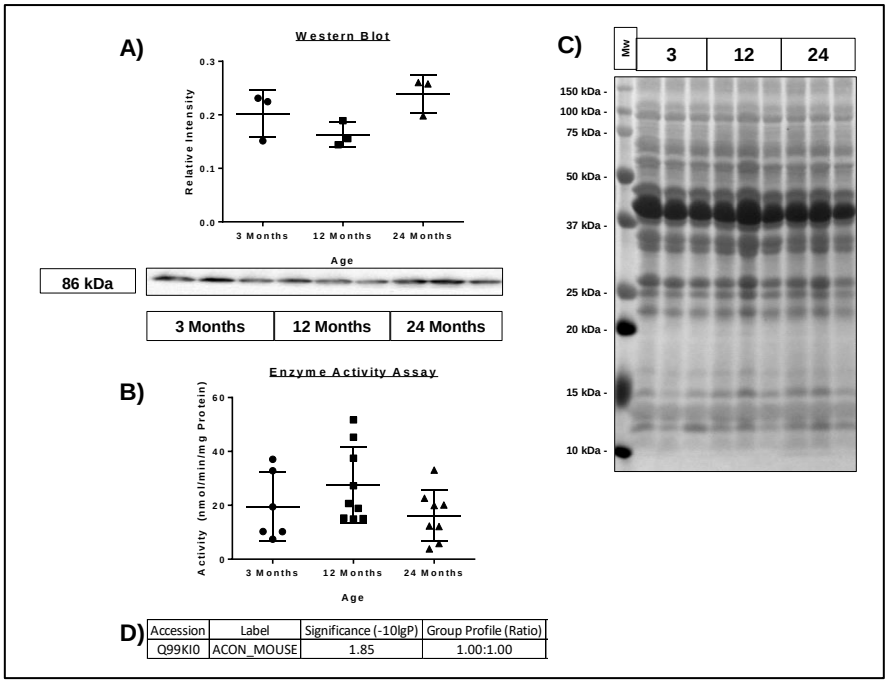

Figure 3.3.4.18 (A) Densiometric measurement for immunodetection by western blotting of Aconitase in mouse quadriceps muscle. (B) Enzyme activity assay of Aconitase. (C) Ponceau S stain used for normalisation of (A). (D) Global label free proteomics data. N=3 biological replicates. Short bars indicate upper and lower interquartile range while the middle represents the median value following statistical analysis using ANOVA with Tukey's post-hoc test.

AMP-kinase and p-AMP kinase (PRKAA1) are shown in figure 3.3.4.19A and 3.3.4.19D respectively. They both indicate no change in protein abundance which was supported by the global label free proteomics data for the two subunits of AMPK (PRKAR1A and PRKAR2A) both of which showed no significant change with age.

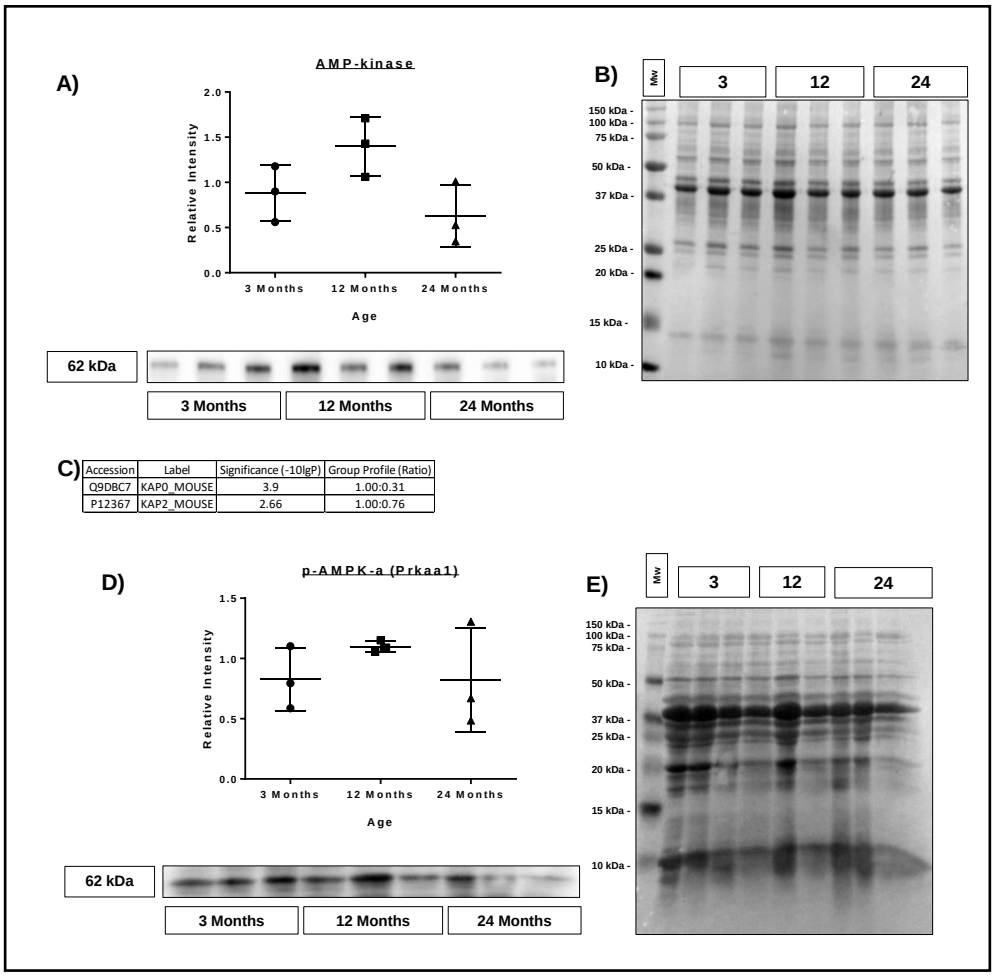

Figure 3.3.4.19 (A) Densiometric measurement for immunodetection by western blotting of AMPK. (B) Ponceau S stain used for normalisation of (A). (C) Label free data indicating no significant change with age. (D) Densiometric measurement for immunodetection by western blotting of Phosphorylated AMPK subunit (Prkaa1). (E) Ponceau S stain used for normalisation of (D). N=3 biological replicates. Short bars indicate upper and lower interquartile range while the middle represents the median value following statistical analysis using ANOVA with Tukey's post-hoc test.

Glyceraldehyde 3-phosphate dehydrogenase (GAPDH) is another crucial energy metabolism enzyme involved in glycolysis which is the predominant energy generating pathway in the quadriceps as previously described. Western blot results in figure 3.3.4.20A indicate a significant decrease in protein abundance with age from 3 to 24 months and 12 to 24 months of age. The global label free proteomics data did not reflect this, indicating no significant change with age.

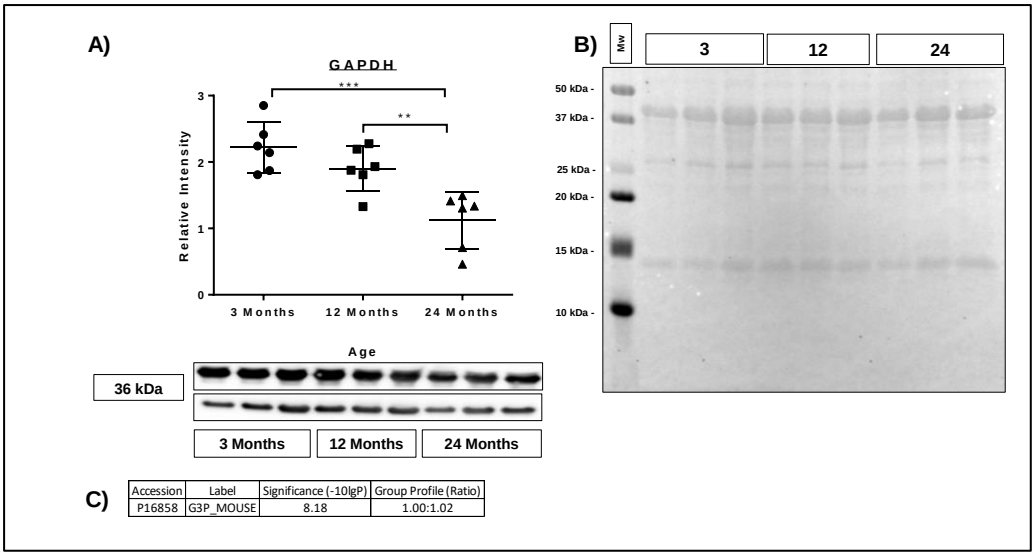

Figure 3.3.4.20 (A) Densiometric measurement for immunodetection by western blotting of Glyceraldehyde Phosphate Dehydrogenase (GAPDH). ** $p < 0.01$, *** $p < 0.001$. (B) Ponceau S stain used for normalisation of (A). (C) Label free proteomics data indicating no significant change with age. N=3 biological replicates. Short bars indicate upper and lower interquartile range while the middle represents the median value following statistical analysis using ANOVA with Tukey's post-hoc test.

P70-S6 Kinase was examined due to potential changes in the intracellular redox state affecting the mTOR (mammalian Target Of Rapamycin) signalling pathway as this pathway is crucial to adult skeletal muscle development (Marabita et al., 2016, Zhang et al., 2016a). The western blot data in figure 3.3.4.21A showed no significant change in protein abundance with age and the protein was not detected in the global label free data.

Sirtuin 1 (SIRT1) deacetylates proteins involved in cellular regulation. Therefore, it was considered whether this may be affected with age potentially impacting some cellular regulators downstream. The western blot result shown in figure 3.3.4.22A showed no significant change in protein abundance with age.

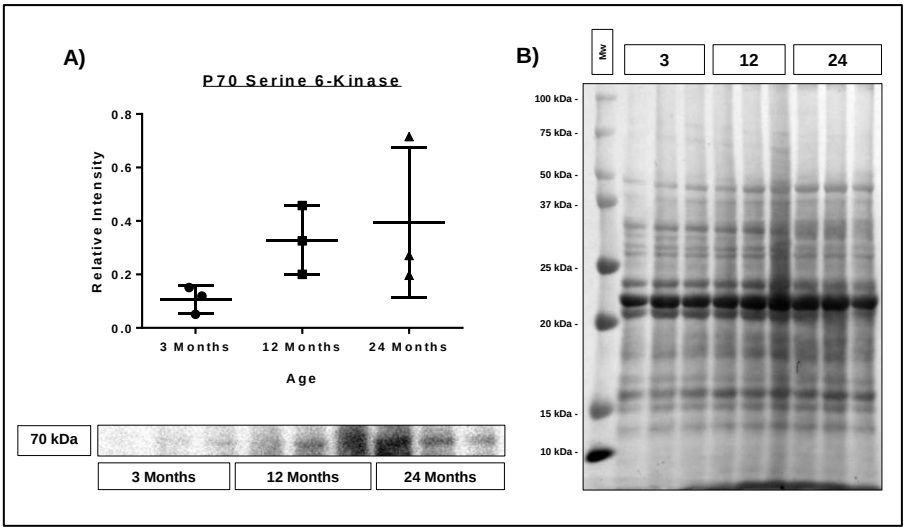

Figure 3.3.4.21 P70 S-6 Kinase (P70S6K). (A) Densiometric measurement for immunodetection by western blotting of P70S6K in mouse quadriceps muscle. (B) Ponceau S stain used for normalisation of (A). N=3 biological replicates. Short bars indicate upper and lower interquartile range while the middle represents the median value following statistical analysis using ANOVA with Tukey's post-hoc test.

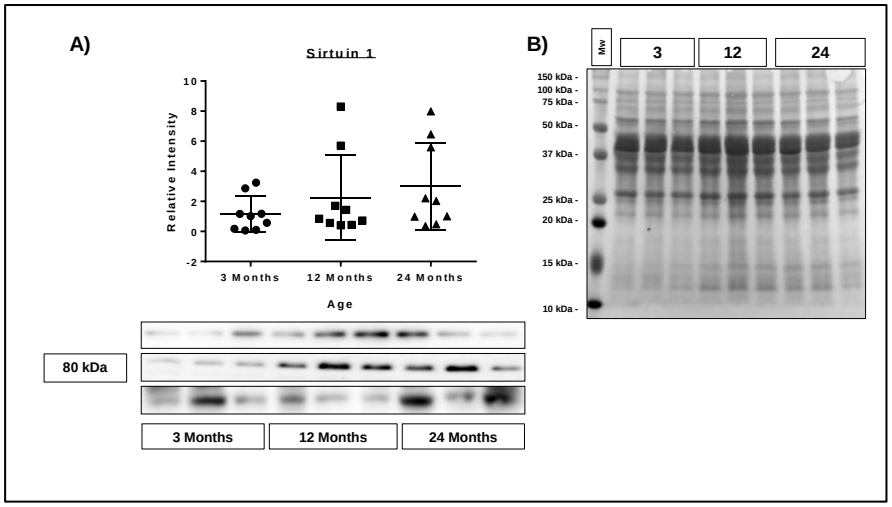

Figure 3.3.4.22 Sirtuin 1 (SIRT1). (A) Densiometric measurement for immunodetection by western blotting of Sirt1 in mouse quadriceps muscle. (B) Ponceau S stain used for normalisation of (A). N=3 biological replicates. Short bars indicate upper and lower interquartile range while the middle represents the median value following statistical analysis using ANOVA with Tukey's post-hoc test.

Carbonylation blots identify proteins modified with a carbonyl group (C=O) and is one of several indicators of sustained ROS within the cell that affects proteins over the long-term.

There was a significant decrease in carbonylated proteins with age in mouse quadriceps (figure 3.3.4.23A) when measuring the most abundant band at 37 kDa.

An alternative measure of oxidised protein is glutathionylation where cysteine residues are modified with the addition of a glutathione molecule. The process is redox dependent and thought to play a role in cellular signalling. The result of the glutathionylation blot shown in figure 3.3.4.24A indicates an increase in Glutathionylation of quadriceps proteins from 3 to 12 and 3 to 24 months.

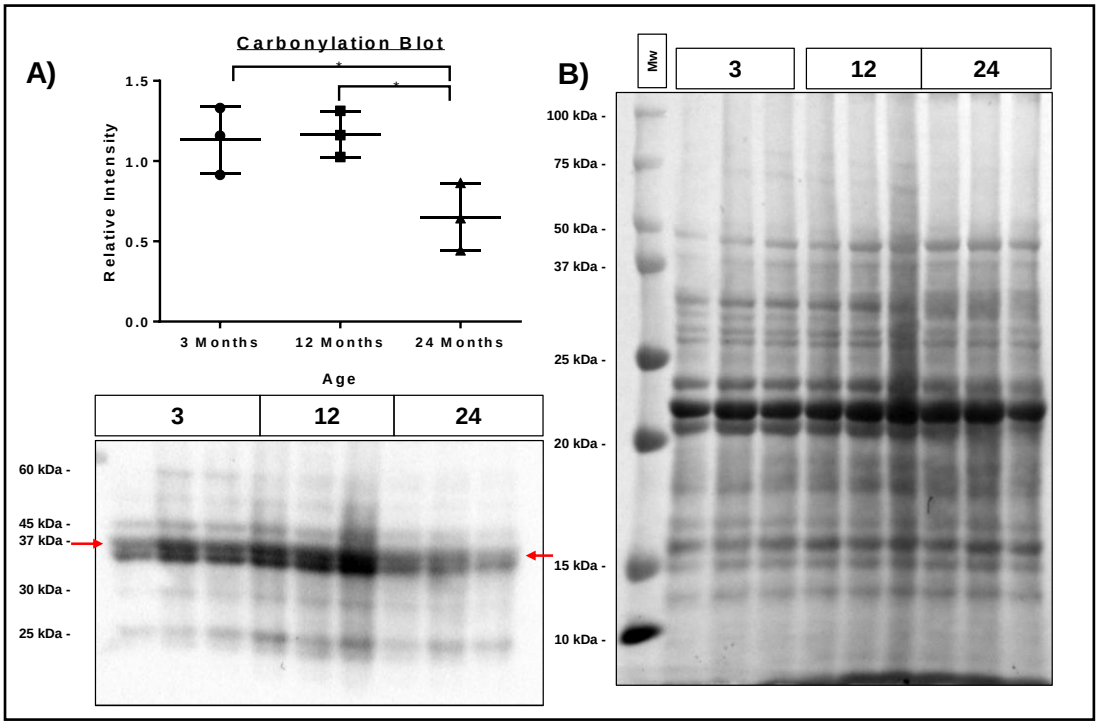

Figure 3.3.4.23 Carbonyl blot reflecting sustained intracellular ROS. (A) Densiometric measurement for immunodetection by western blotting of carbonylated proteins. The bands of interest are highlighted by the red arrows. * $p < 0.05$. (B) Ponceau S stain used for normalisation of (A). N=3 biological replicates. Short bars indicate upper and lower interquartile range while the middle represents the median value following statistical analysis using ANOVA with Tukey's post-hoc test.

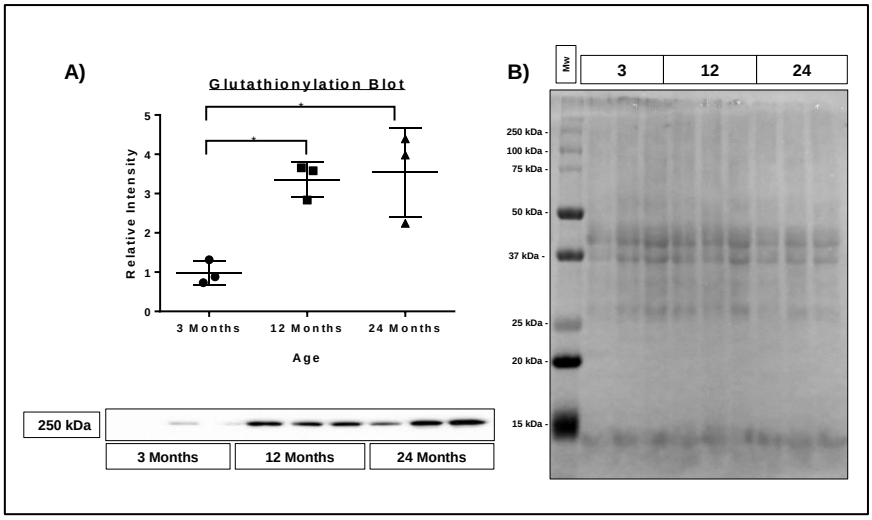

Figure 3.3.4.24 Glutathionylation blot. (A) Densiometric measurement for immunodetection by western blotting protein glutathionylation in mouse quadriceps. * $p < 0.05$. (B) Ponceau S stain used for normalisation of (A). N=3 biological replicates. Short bars indicate upper and lower interquartile range while the middle represents the median value following statistical analysis using ANOVA with Tukey's post-hoc test.

3.3.5 GOrilla Pathway Analysis

Use of GOrilla enabled a gene ontological (GO) pathway analysis of the quadriceps muscle label free proteomics data. This shows protein pathway associations and covers three aspects: biological processes, cellular components and molecular function. Significance was determined within the GOrilla software and the colour of the text box showed the associated *p* value described in figure.

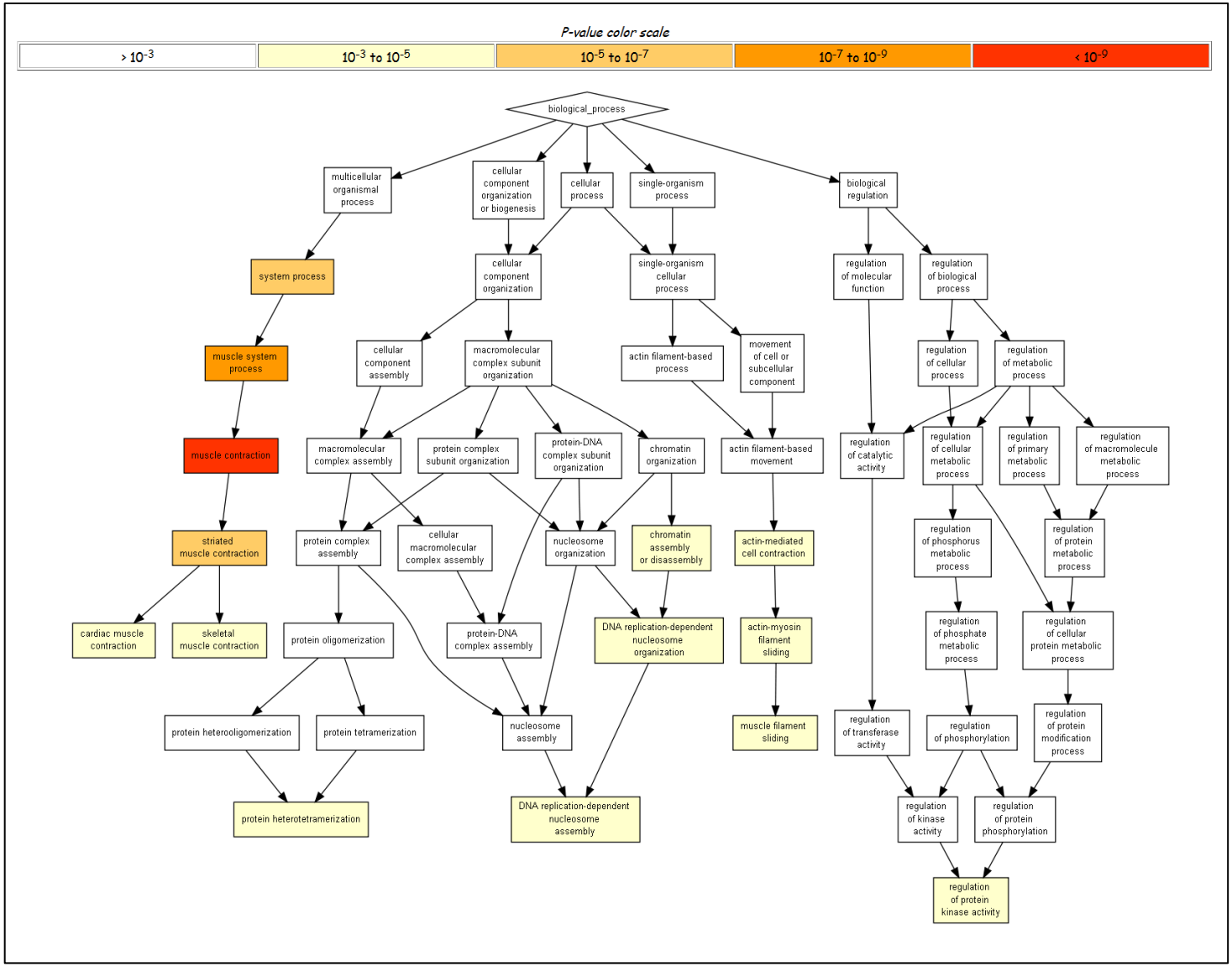

Figure 3.3.5.1 GOrilla biological process analysis of all detected proteins from the global label free analysis of quadriceps muscle. Statistically significant change in identified gene ontology relating to muscle contraction were identified ($p \leq 1 \times 10^{-9}$) with a number of other processes also shown to be significantly changed ($p \geq 1 \times 10^{-3} \leq 1 \times 10^{-5}$) which were predominantly contractile proteins.

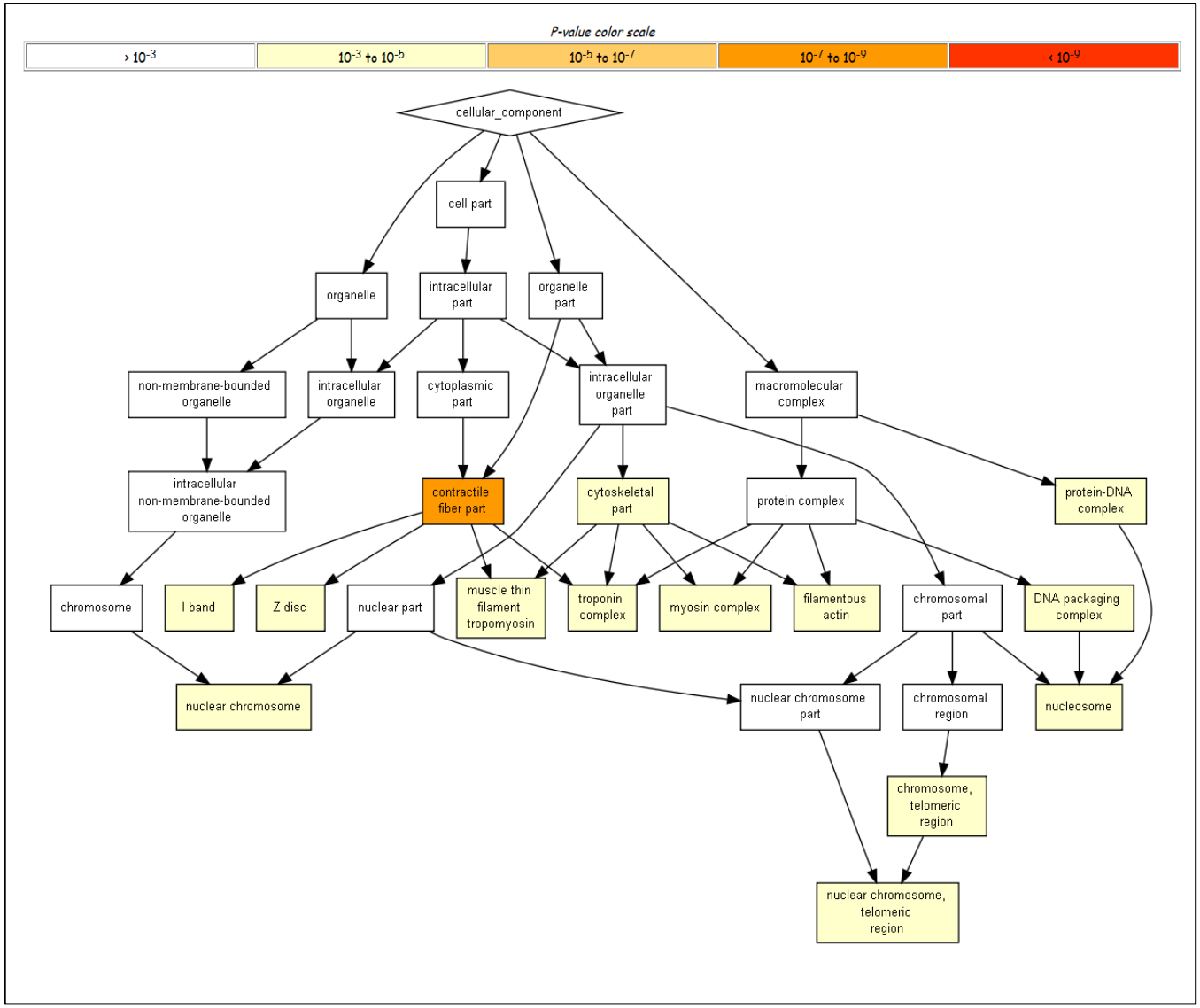

Figure 3.3.5.2 GOrilla analysis of the cellular components from all detected proteins from the global label free analysis of quadriceps muscle. Several cellular components were identified from the label free proteomics data such as 'contractile fibre part' (significantly changed, $p \geq 1 \times 10^{-7} \leq 1 \times 10^{-9}$), 'I band', 'Z disc', 'troponin complex', 'myosin complex' and 'protein-DNA complexes' all with a significance of $p \geq 1 \times 10^{-3} \leq 1 \times 10^{-5}$.

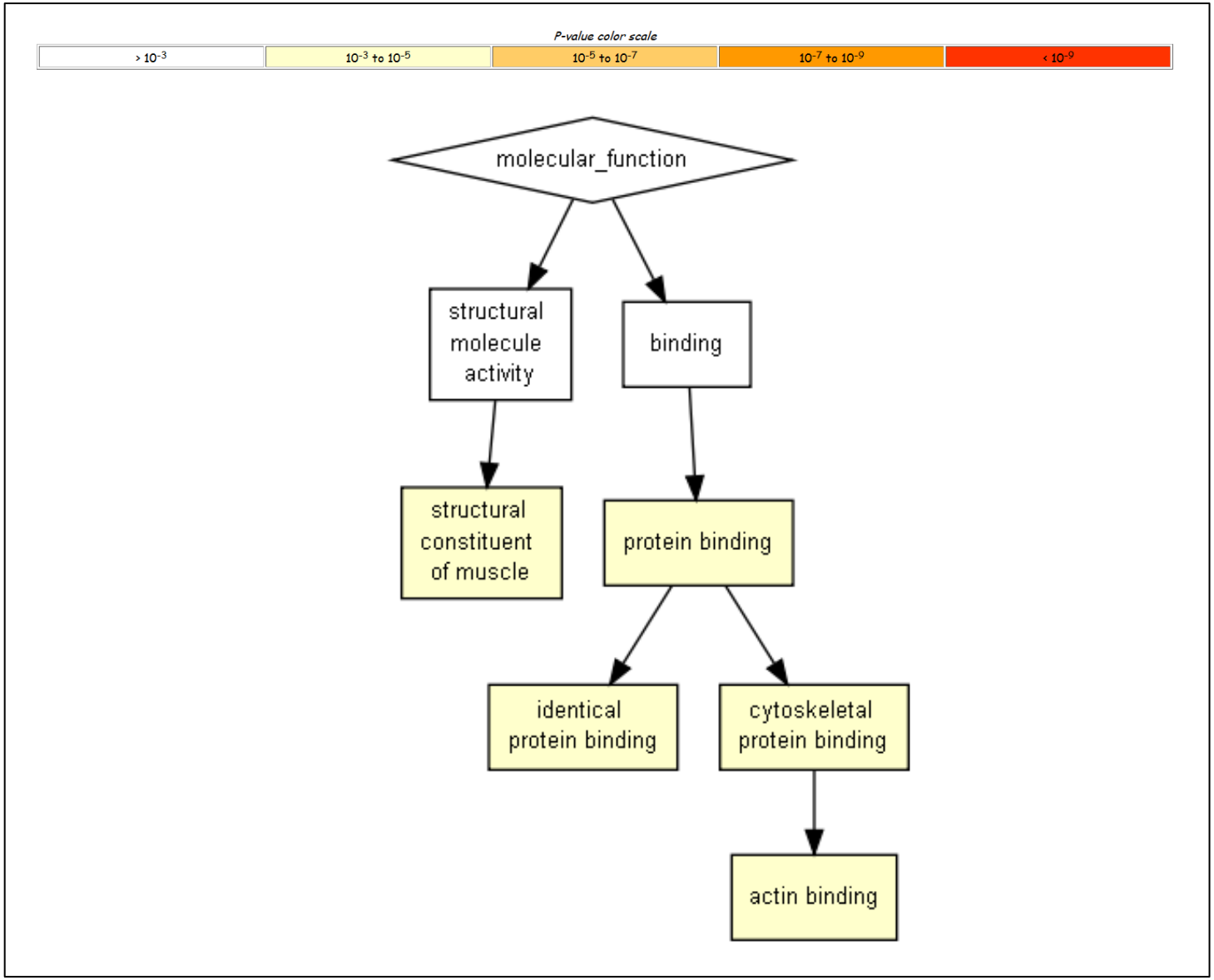

Figure 3.3.5.3 GOrilla analysis of molecular function from the global label free proteomics data from mouse quadriceps muscle. This identified two pathways: one highlighting 'structural constituent of muscle' and the other 'protein binding', both with a significance of $p \geq 1 \times 10^{-3} \leq 1 \times 10^{-5}$.

GOrilla analysis of quadriceps muscle highlighted significant GO enrichment in biological processes (figure 3.3.5.1) for muscle contraction, chromatin assembly, actin mediated cell contraction and regulation of protein kinase activity for quadriceps muscle. Analysis of cellular components in figure 3.3.5.2 identified contractile fibre parts, the I band, Z disc, troponin complex, myosin complex and protein-DNA complexes. Analysis of molecular function in figure 3.3.5.3 identified significant GO enrichment for structural constituents of muscle and the other 'protein binding. Together this information highlights that the predominant quadriceps proteins detected using the global label free proteomics data were associated with the cytoskeleton.

3.3.6 STRING Analysis of Significantly Changed Quadriceps Proteins

STRING analysis identified protein-protein interactions within the label free global proteomics data set. The reference to gene ontologies enables classification of groups of proteins detected to identify changes to protein-protein interactions within a group. Consideration is given to both protein-protein interactions as well as groups of proteins that perform a similar function. The analysis was performed on the quadriceps proteomics data for those proteins that showed significant changes between adult and old mice. Figures show the full, unenriched image to highlight all proteins used in the analysis and the enrichment for a specific trait e.g. cytoskeletal protein binding.

STRING analysis shown in figure 3.3.6.1 examined proteins detected in the quadriceps that were significantly up regulated in muscle from old compared with adult mice to determine any protein interactions within that data set. Figure 3.3.6.1A indicates the overall proteomics data examined in STRING prior to enrichment demonstrated in figure 3.3.6.1B. The overall analysis highlighted interactions between F-actin capping protein subunit β (CAPZB) and cytoplasmic actin (ACTB) on the left of the image and between Tropomyosin α-1 (TPM1),

Troponin T fast skeletal muscle (TNNT3), Troponin fast skeletal muscle (TNNI2) and Myosin light chain 3 (MYL3) on the right. Figure 3.3.6.1C Indicates the GO pathway ID for the analysis, the description of the pathway, the number of proteins used in this analysis and the false discovery rate (FDR). Figure 3.3.6.1D Is the global label free proteomics data for the significantly increased proteins shown in figures 3.3.6.1A and 3.3.6.1B.

A)

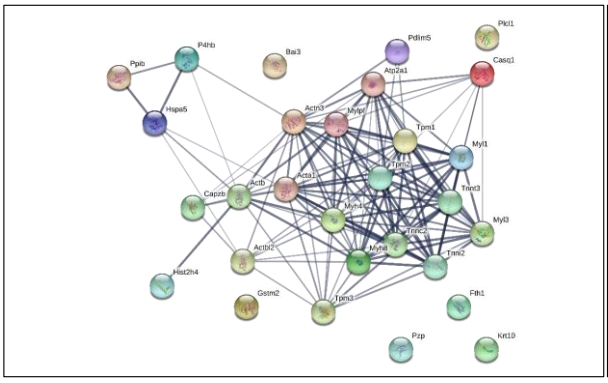

B)

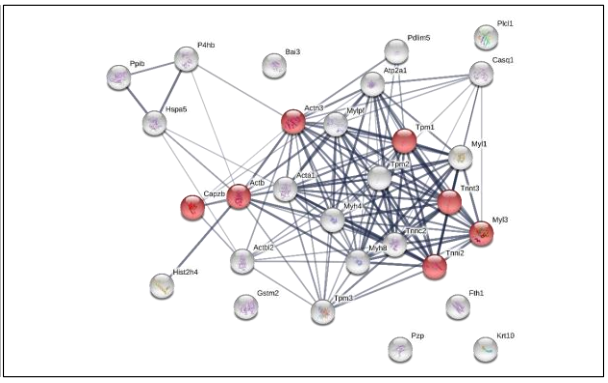

C)

#pathway ID	pathway description	observed gene count	false discovery rate
GO.0008092	cytoskeletal protein binding	7	0.0054

D)

Accession	Significance (-10lgP)	Group Profile (Ratio)	Description
P58771	115.68	1.00:2.60	Tropomyosin alpha-1 chain OS=Mus musculus GN=Tpm1 PE=1 SV=1
P47757	28.59	1.00:2.43	F-actin-capping protein subunit beta OS=Mus musculus GN=Capzb PE=1 SV=3
P60710	22.54	1.00:13.12	Actin cytoplasmic 1 OS=Mus musculus GN=Actb PE=1 SV=1
O88990	22.46	1.00:1.71	Alpha-actinin-3 OS=Mus musculus GN=Actn3 PE=2 SV=1
Q9QZ47	86.85	1.00:2.52	Troponin T fast skeletal muscle OS=Mus musculus GN=Tnnt3 PE=1 SV=3
P09542	44.1	1.00:1.80	Myosin light chain 3 OS=Mus musculus GN=Myl3 PE=1 SV=4
P13412	52.67	1.00:2.32	Troponin I fast skeletal muscle OS=Mus musculus GN=Tnni2 PE=1 SV=2

Figure 3.3.6.1 STRING analysis of protein interactions in quadriceps for proteins that were significantly up regulated between adult and old mice using the global label free proteomics data. (A) The overall, unenriched protein dataset for significantly up regulated quadriceps proteins. (B) The data set for enriched cytoskeletal protein binding in which several interactions were identified. (C) Table containing STRING pathway analysis information. (D) Global label free protein data for the significantly changed proteins in (A) and (B).

Figure 3.3.6.2 shows proteins that were significantly down regulated between quadriceps from adult and old mice. This figure shows the entire protein set submitted to STRING analysis prior to enrichment and following enrichment for myofibrils. This

enrichment only highlighted an interaction between Myomesin-1 (MYOM1) and myosin-11 (MYH-11) proteins. Both are involved in muscle contraction and Myomesin may link the intermediate filament of the cytoskeleton to the M disk (Gonzalez-Morales et al., 2017).

A)

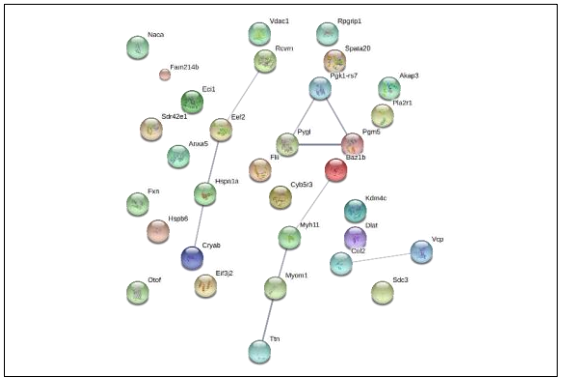

B)

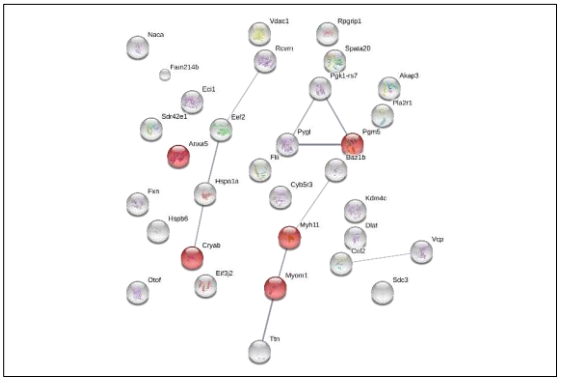

C)

#pathway ID	pathway description	observed gene count	false discovery rate
GO.0030016	myofibril	5	0.00289

D)

Accession	Significance (-10lgP)	Group Profile (Ratio)	Description
P23927	21.96	1.00:0.47	Alpha-crystallin B chain OS=Mus musculus GN=Cryab PE=1 SV=2
P48036	21.96	1.00:0.52	Annexin A5 OS=Mus musculus GN=Anxa5 PE=1 SV=1
Q62234	29.22	1.00:0.67	Myomesin-1 OS=Mus musculus GN=Myom1 PE=1 SV=2
O08638	23.37	1.00:0.29	Myosin-11 OS=Mus musculus GN=Myh11 PE=1 SV=1
Q8BZF8	32.93	1.00:0.13	Phosphoglucomutase-like protein 5 OS=Mus musculus GN=Pgm5 PE=1 SV=2

Figure 3.3.6.2 STRING analysis of protein-proteins interactions for significantly down regulated proteins. (A) Demonstrates the entire dataset. (B) Following enrichment for myofibrillar proteins, 5 proteins were identified. (C) STRING pathway information. (D) Global label free proteomics data for proteins enriched in (A).

3.3.7 Redox Changes in Mouse Quadriceps with Age

Differentially labelled proteins were analysed from the samples from adult and old mice. The total number of redox-cysteine containing proteins detected were 179 in adult and 166 in old mice. The difference in protein numbers between adult and old reflects a number of different proteins detected in each tissue set, rather than several proteins detected in one and not the other.

Differential labelling of cysteine residues followed by mass spectrometry analysis was used to determine changes to the redox state of individual cysteine containing peptides. They are of interest because under normal conditions their flexible oxidation states enable a swift response to changes in intracellular ROS. Our hypothesis was that they will change with age.

Figure 3.3.7.1 shows a reduction in the total number of redox proteins with an increase in the number of reduced proteins, with age. This change to intracellular redox flexibility with age may be related to exposure to sustained intracellular ROS which will be assessed in the next section looking at specific proteins and changes to their redox state with age. The online DataCat archive for the adult and old quadriceps redox protein lists S3 – Adult Quadriceps Redox Proteins; S4 – Old Quadriceps Redox Proteins are accessible at 10.17638/datacat.liverpool.ac.uk/437.

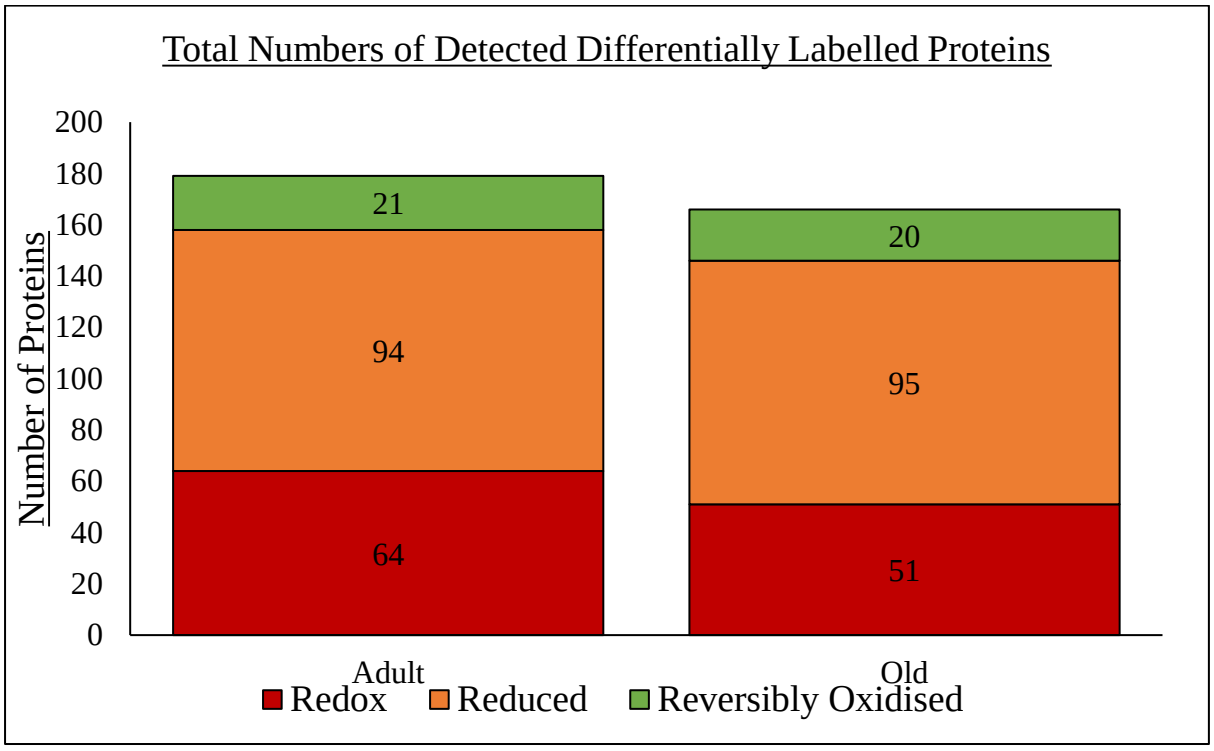

Figure 3.3.7.1 Numbers of proteins containing redox, reduced and reversibly oxidised cysteine-containing peptides from quadriceps muscle in adult and old mice.

Table 2 shows the combined data for redox proteins and includes protein accession number and name of the identified protein in the label free data along with the abundance change in label free data with age, the significance of that change (-10 log P), the redox peptide identified, the specific redox cysteine being analysed and the adult and old reduced:oxidised ratio change with age.

Table 2. Redox Cysteines in Quadriceps Muscle

Accession	Protein	Adult:Old	Significance (-10logP)	Peptide	Cysteine	Adult Red/Ox	Old Red/Ox
P62259	14-3-3 Protein Epsilon (Ywhae)	1.00:1.16	6.06	LICCDILDVLDK	97/98*	7.69	22.47
P61982	14-3-3 Protein Gamma (Ywhag)	1.00:1.04	6.62	NCSETQYESK	112	14.21	36.02
Q60597	2-Oxoglutarate Dehydrogenase (Mitochondrial) (Ogdh)	1.00:1.12	2.15	DVVVDLVCYR	507	0.53	0.71
P47857	6-Phosphofructokinase (Muscle Type)(Pkfm)	1.00:0.70	8.36	GITNLCVIGGDGSLTGADTFR	114	5.63	9.68
				LPLMECVQVTK	351	8.65	15.08
				CNENYTTDFIFNLYSEEGK	631	5.22	21.04
				IFANTPDSGCVLGMR	709	3.37	14.03
Q99KI0	Aconitate Hydratase (Mitochondrial) (Aco2)	1.00:1.00	1.85	VAVPSTIHCDHLIEAQVGGEK	126	61.41	26.17
				VGLIGSCTNSSYEDMGR	385	0.66	1.12
				DVGGIVLANACGPCIGQWDR	448/451*	0.13	0.33
				CTTDHISAAGPWLK	592	19.33	22.92
P07724	Serum Albumin (Alb)	1.00:1.25	9.00	CSYDEHAK	58	2.95	2.78
O88990	**Alpha-Actinin-3 (Actn3)**	**1.00:1.71**	**20.02**	LCYVALDFENEMATAASSSSLEK	218	4.65	6.16
				CDIDIR	286	4.36	6.32
P05201	Aspartate Aminotransferase (Cytoplasmic) (Got1)	1.00:1.10	4.28	INMCGLTTK	391	3.54	7.45
P05202	Aspartate Aminotransferase (Mitochondrial) (Got2)	1.00:1.13	4.92	EYLPIGGLAEFCK	106	5.36	10.69
				TCGFDFSGALEDISK	187	4.31	3.99
				VGAFTVVCK	295	0.16	0.06
Q9DCX2	ATP Synthase Subunit D Mitochondrial (Fragment) (Atp5h)	1.00:1.27	8.20	SCAEFVSGSQLR	101	51.73	37.60
P45591	Cofilin-2 (Cfl2)	1.00:1.07	5.60	LLPLNDCR	80	1.90	13.71
P07310	Creatine Kinase M-type (Ckm)	1.00:1.14	3.01	GYTLPPHCSR	146	6.40	18.06
				FCVGLQK	254	11.50	28.41
Q6P8J7	Creatine Kinase S-Type (Mitochondrial) (Ckmt2)	1.00:0.95	5.14	SEVELVQIVIDGVNYLVDCEK	397	3.60	7.42
Q9CZ13	Cytochrome b-c1 Complex Subunit 1 (Mitochondrial) (Uqcrc1)	1.00:0.92	9.70	LCTSATESEVTR	380	1.96	1.60
Q9DB77	Cytochrome b-c1 complex subunit 2 (Mitochondrial) (Uqcrc2)	1.00:1.09	6.20	NALANPLYCPDYR	192	0.02	0.02
O08749	Dihydrolipoyl Dehydrogenase (Mitochondrial) (Dld)	1.00:1.99	8.53	NETLGGTCLNVGCIPSK	80/85*	71.21	307.42
Q99LC5	Electron Transfer Flavoprotein Subunit Alpha (Mitochondrial) (Etfa)	1.00:0.85	12.77	LGGEVSCLVAGTK	53	15.40	5.53
P58252	**Elongation Factor 2 (Eef2)**	**1.00:0.59**	**25.73**	EGALCEENMR	693	14.47	17.27
				ETVSEESNVLCLSK	591	2.86	6.59
P17182	Alpha-Enolase (Enoa)	1.00:1.32	1.46	TGAPCR	331	4.18	8.93
				FGANAILGVSLAVCK	119	2.14	8.36
P21550	Beta-Enolase (Enob)	1.00:0.89	8.60	SGETEDTFIADLVVGLCTGQIK	321	3.60	6.42
P05064	Fructose Bisphosphate Aldolase A	1.00:1.04	3.97	YASICQQNGIVPIVEPEILPDGDHDLK	178	0.53	2.08
				CQYVTEK	202	2.50	6.56
				ALANSLACQGK	339	5.77	11.37
P06745	Glucose 6-Phosphate Isomerase (Gm1840)	1.00:1.25	6.57	MIPCDFLIPVQTQHPIR	321	0.48	2.89
P16858	Glyceraldehyde-3-Phosphate Dehydrogenase (Gapdh)	1.00:1.02	8.18	IVSNASCTTNCLAPLAK	150/154*	127.86	554.21
				VPTPNVSVVDLTCR	245	17.90	26.74
Q9WUB3	Glycogen Phosphorylase (Muscle Form) (Pygm)	1.00:0.98	10.01	ICGGWQMEEADDWLR	172	6.47	10.09
				TCAYTNHTVLPEALER	373	4.81	10.53
				WLVLCNPGLAEVIAER	496	14.05	18.31
				QLLNCLHIITLYNR	581	30.97	12.73
P63017	Heat Shock Cognate 71 kDa Protein (Hspa8)	1.00:0.79	11.10	VCNPIITK	584	10.88	8.79

P02089	Hemoglobin Subunit Beta-2 (Hbb-b2)	1.00:1.54	5.99	GTFASLSELHCDK	94	100.34	91.44
P06151	**L-Lactate Dehydrogenase A Chain (Ldha)**	**1.00:0.71**	**23.73**	DYCVTANSK	84	13.62	20.01
				VIGSGCNLDSAR	163	1.33	4.29
P14152	Malate Dehydrogenase (Cytoplasmic) (Mdh1)	1.00:1.06	6.17	ENFSCLTR	154	0.94	6.36
				VIVVGNPANTNCLTASK	137	15.57	35.51
P08249	Malate Dehydrogenase (Mitochondrial) (Mdh2)	1.00:0.76	10.78	GCDVVVIPAGVPR	93	0.69	2.52
				TIIPLISQCTPK	212	22.06	82.92
				EGVVECSFVQSK	275	2.44	9.84
				ETECTYFSTPLLLGK	285	4.35	9.62
Q5XKE0	Myosin-Binding Protein C Fast-Type (Mybpc2)	1.00:0.81	12.24	IFSENICGLSDSPGVSK	1007	48.64	77.79
P97457	**Myosin Regulatory Light Chain 2 Skeletal Muscle Isoform (Mylpf)**	**1.00:1.63**	**39.47**	QFLEELLTTQCDR	128	16.04	22.38
				NICYVITHGDAK	157	7.32	13.91
P15532	Nucleoside Diphosphate Kinase A (Nme1)	1.00:0.59	12.77	GDFCIQVGR	109	14.89	14.54
P17742	Peptidyl Prolyl Cis-Trans Isomerase (PpiA)	1.00:0.90	2.84	IIPGFMCQGGDFTR	62	2.52	5.76
P09411	**Phosphoglycerate Kinase 1 (Pgk1)**	**1.00:0.59**	**23.68**	GCITIIGGGDTATCCAK	367/79/80*	47.50	95.40
Q9D0F9	Phosphoglucomutase-1 (Pgm1)	1.00:0.75	14.98	TIEEYAICPDLK	160	15.52	16.76
				LSLCGEESFGTGSDHIR	374	3.25	8.42
Q99LX0	Protein DJ-1 (Park7)	1.00:0.81	6.52	DPVQCSR	46	8.50	17.53
Q9QYG0	Protein NDRG2 (Ndrg2)	1.00:0.83	9.86	CPVMLVVGDQAPHEDAVVECNSK	255/274*	14.57	32.14
Q9D051	Pyruvate Dehydrogenase E1 Component Subunit Beta (Mitochondrial) (Pdhb)	1.00:0.82	6.78	EGIECEVINLR	263	6.80	9.97
P52480	Pyruvate Kinase Isozymes M1/M2 (Pkm2)	1.00:0.98	3.86	NTGIICTIGPASR	49	12.06	17.11
				CDENILWLDYK	152	5.75	8.62
				GIFPVLCK	474	23.16	29.64
P17751	Triosephosphate Isomerase (Tpi1)	1.00:0.84	8.68	IAVAAQNCYK	117	0.63	2.40
				VSHALAEGLGVIACIGEK	177	9.15	11.75
				IIYGGSVTGATCK	268	7.29	13.17
P58771	**Tropomyosin Alpha-1 Chain (Tpm1)**	**1.00:2.60**	**115.68**	CAELEEELK	154	5.65	9.46
P58774	**Tropomyosin Beta Chain (Tpm2)**	**1.00:2.04**	**84.11**	CGDLEEELK	154	6.34	7.89
P13412	**Troponin-1 Fast Skeletal Muscle (Tnni2)**	**1.00:2.32**	**52.67**	VCMDLR	134	6.79	10.27

Table 2. Redox-cysteine containing proteins detected via differential labelling. Significantly changed proteins are highlighted in **bold** and tryptic peptides are denoted with an asterisk (*).

Figure 3.3.7.1 shows the whole dataset of redox proteins listed in Table 2 that were identified via differential labelling of quadriceps muscle from adult and old mice. Specific cysteine residues highlighted in the figure show marked increased in reduced state for Cofilin 2 (Cys80, increased by 7.21 fold), Glucose 6-phosphate isomerase (Cys404, increased by 6.06 fold) and Malate dehydrogenase (Cys154, increased by 6.8 fold). Conversely, Aconitase (Cys126, decreased by 0.42 fold), mitochondrial Aspartate aminotransferase (Cys295, decreased by 0.38) and Glycogen phosphorylase (Cys581, decreased by 0.41).

Redox Cysteines in Adult and Old Mouse Quadriceps Muscle

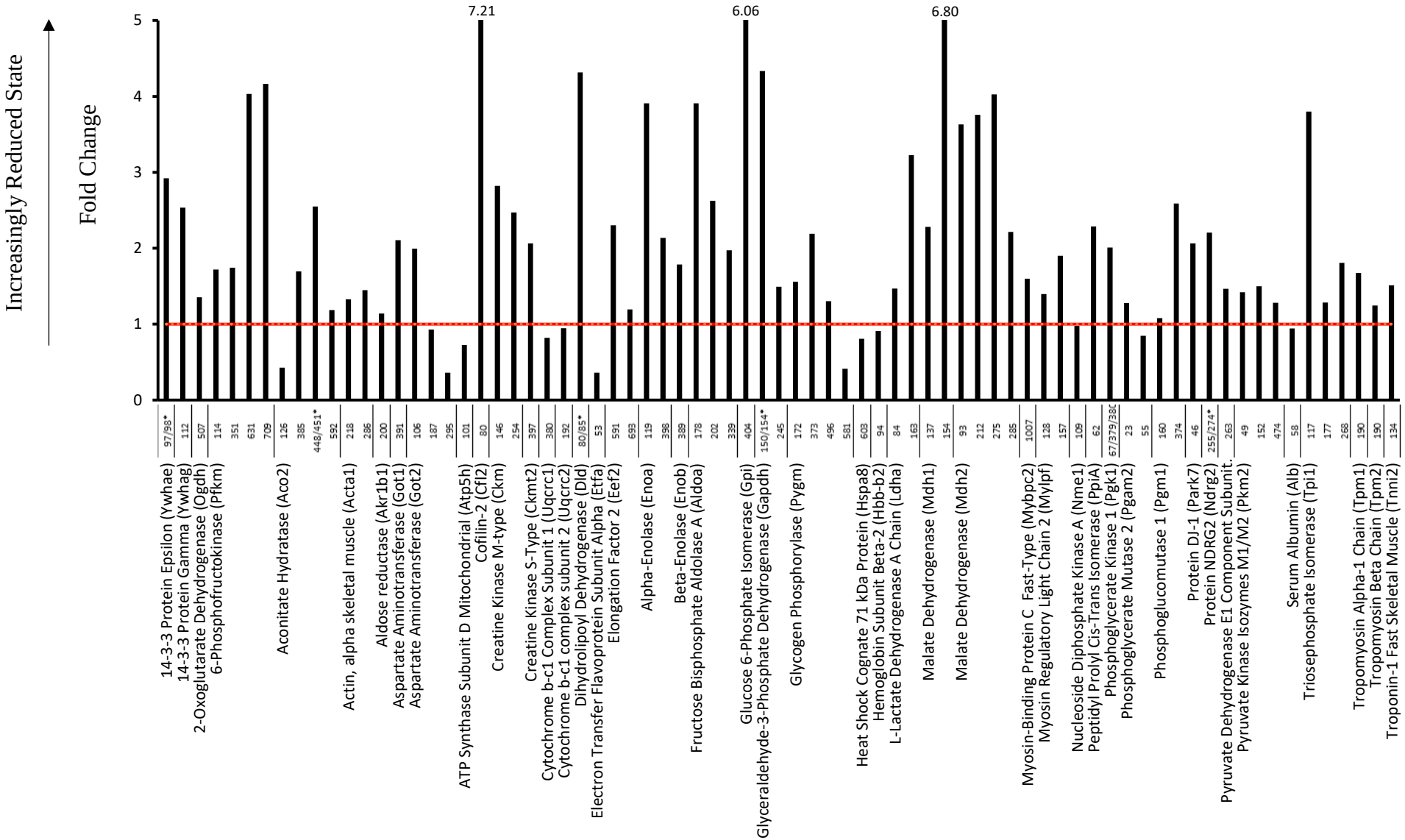

Figure 3.3.7.2 All detected redox labelled cysteine proteins demonstrating changes to the reduced:reversibly oxidised ratios with age in quadriceps. Values > 1.0 are reduced, values < 1.0 are reversibly oxidised. Higher values indicate an increased reduced state. Data are derived from table 2.

3.3.8 Comparison of Differentially Labelled Proteins

Venn diagrams were produced using VennDIS (version 1.0.1) software to compare redox, reduced and reversibly oxidised proteins to identify those that were conserved or changed with age.

Figure 3.3.8.1 compares the redox, reduced and reversibly oxidised through differential labelling of cysteine in adult and old quadriceps muscles. This highlighted 133 proteins that were present in both adult and old quadriceps muscles, 44 proteins only in adult and 33 only in old. In the adult dataset, proteins detected included the energy metabolism proteins ATP Synthase polypeptides and subunits (ATP1A2, ATP5C1 and ATP5F1 respectively), redox proteins Glutathione peroxidase (Gpx4) and Thioredoxin (Txn1) and the Heat shock proteins (HSPA1A and HSPB6). The 133 proteins identified in both adult and old muscle for all forms of differentially labelled proteins highlighted a range of different types covering energy metabolism (NADH dehydrogenases 1 α sub-complexes and ATP Synthase subunits), cytoskeleton (Tropomyosin 1 α and Tropomyosin 4, Troponin 1 and C2, various Myosins, Myomesins etc.) and redox control (e.g. Peroxiredoxins 1, 3 and 5). The proteins found only in old were fewer but of note were Glutathione S-Transferase π 1 and Peroxiredoxin 6 (see the supplementary information "Table 3.3.8.1 A/B/C" (p.262-264) for the lists of individual proteins in each section of the Venn diagram).

Further to this initial information, the lists of differentially labelled proteins were later separated to determine any age or effects to redox proteins in quadriceps muscle.

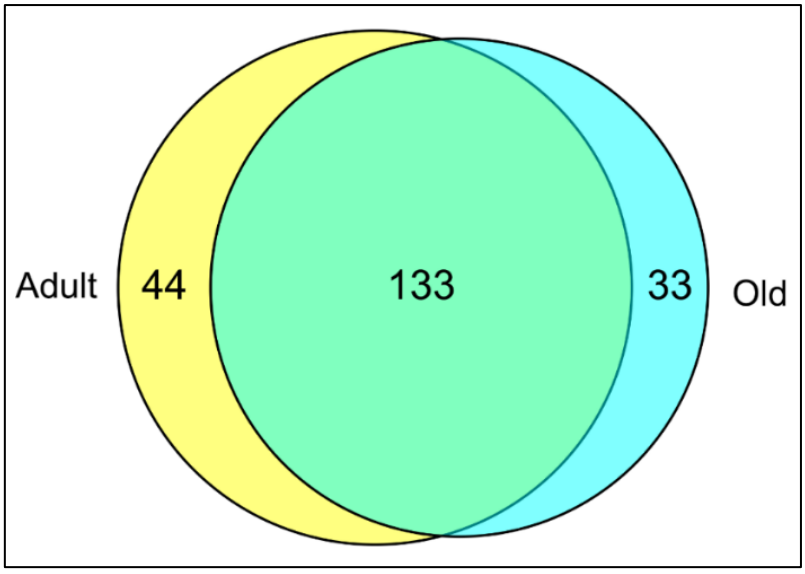

Figure 3.3.8.1 Venn diagram comparing redox, reduced and reversibly oxidised protein numbers in quadriceps muscle from adult and old mice. See also the supplementary information table 3.3.8.1 A/B/C on p.262-264 for the lists of proteins in individual segments.

Figure 3.3.8.2 highlights the redox proteins (labelled with both *d*0-NEM and *d*5-NEM) identified from quadriceps muscle in adult and old mice. This highlighted 21 redox proteins solely in the adult, 8 in the old and 43 in both adult and old quadriceps muscle. In tissue from adult mice, the redox control chaperone protein PARK7 was observed along with the Myosin binding protein C (MBPC2) and the glycolytic enzyme Phosphoglycerate kinase 1-related sequence (PGK-RS7) and the folding protein Peptidylprolyl isomerase A (PPIA). In tissue from both adult and old mice several energy metabolism enzymes such as Enolase 1 and 3 (ENO1 and ENO3), Creatine kinase (both muscle (CKM) and mitochondrial (CKMT2) forms) and the redox control protein Superoxide dismutase 1 (SOD1) were present. The dataset from old mice only highlighted 8 proteins, mostly involved in energy metabolism and one Myosin heavy polypeptide 2 (MYH2) (see the supplementary information "Table 3.3.8.2 A/B/C" (p.265-266) for the lists of proteins included in this Venn diagram).

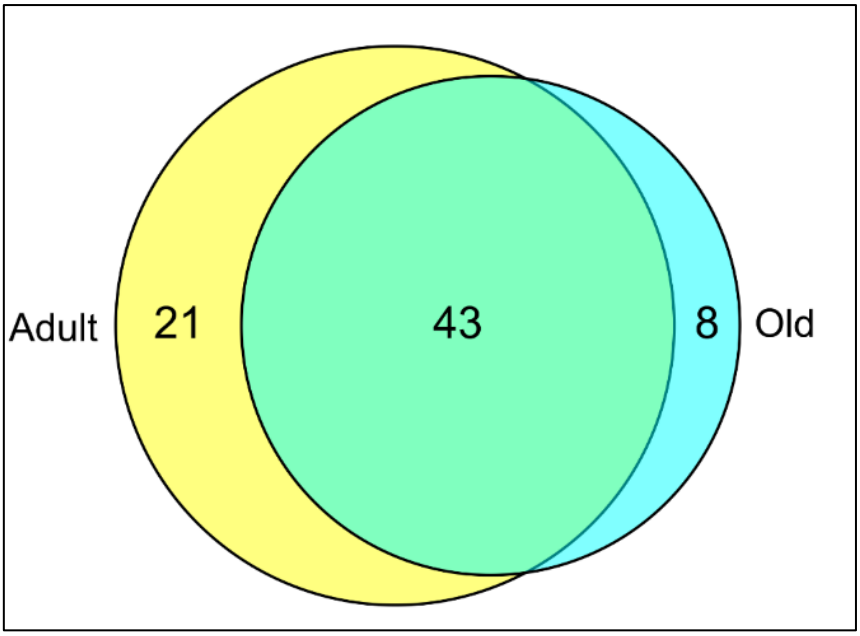

Figure 3.3.8.2 Venn diagram of redox proteins detected in mouse quadriceps. See also the supplementary information table 3.3.8.2 A/B/C on p.265-266 for diagram segment protein lists of individual segments.

Figure 3.3.8.3 compared reduced proteins found in the adult, old and both datasets. The 37 proteins only found in muscle from adult mice included the Heat shock protein Hspb6, the redox protein Thioredoxin 1 (TXN1) and Glutathione peroxidase (GPX4) along with a range of energy metabolism proteins such as ATP synthases (ATP1A2, ATP5C1, ATP5F1), Isocitrate dehydrogenase 3 (IDH3) and Protein kinases (PRKAR2A and PRKAB2). Of the 43 proteins found in both datasets, Glutathione S-transferase μ-1, 2 and 5 (GSTM1, GSTM2 and GSTM5), cytoskeletal proteins Myosin 1 (MYL1) and Myosin 3 (MYL3) and redox proteins Peroxiredoxin 1, 3 and 5 (PRDX1, PRDX3 and PRDX5). In the proteins found in muscle from old mice a number were involved in energy metabolism such as Citrate synthase (CS), ATP Synthase (ATP5H) and Fructose bisphosphatase 2 (FBP2) were found in addition to the chaperone and redox sensor PARK7 (see the supplementary information "Table 3.3.8.3 A/B/C" (p.267-269) for the lists of proteins included in this Venn diagram).

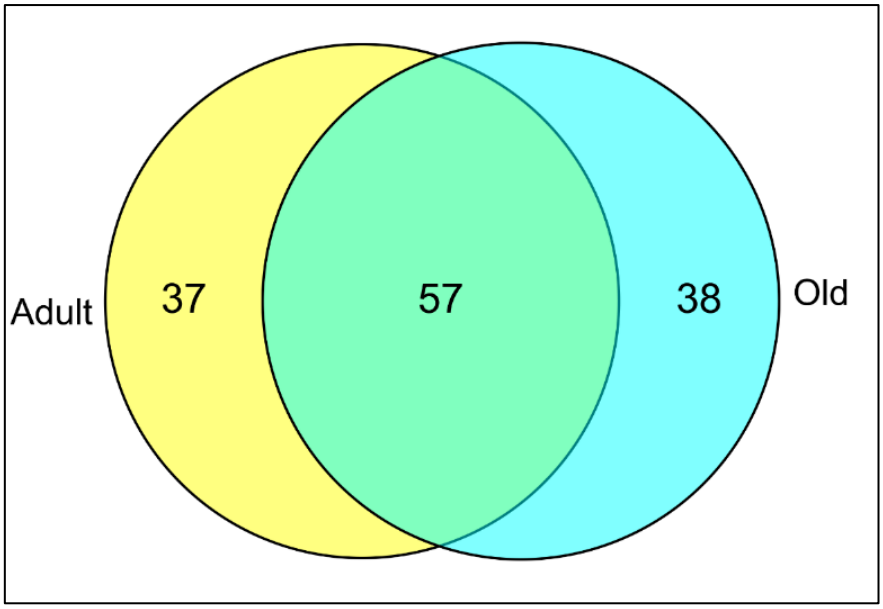

Figure 3.3.8.3 Venn diagram of reduced proteins detected in mouse quadriceps. See also the supplementary information table 3.3.8.3 A/B/C on p.267-269 for protein lists of individual segments.

Figure 3.3.10.4 shows reversibly oxidised proteins found in muscle from adult, old and both ages of mice. Few proteins of note were observed in each of the datasets. Example proteins found in the adult included the Heat shock protein Hspa1a and the energy metabolism protein Cytochrome c oxidase (COX5B). In the protein datasets from both adult and old mice, the energy protein NADH dehydrogenase (NDUFB7) and the endoplasmic reticulum folding control protein Calreticulin (CALR) were observed. In the proteins found in old mice, Peroxiredoxin 6 (PRDX6) and two immunoglobulins (Ig κ chain V-V regions and Ig heavy chain V region and lysosome degradation proteins Cathepsin B and D (CTSB and CTSD) were observed (see supplementary information "Table 3.3.8.4 A/B/C" (p.270) for the lists of proteins included in this Venn diagram).

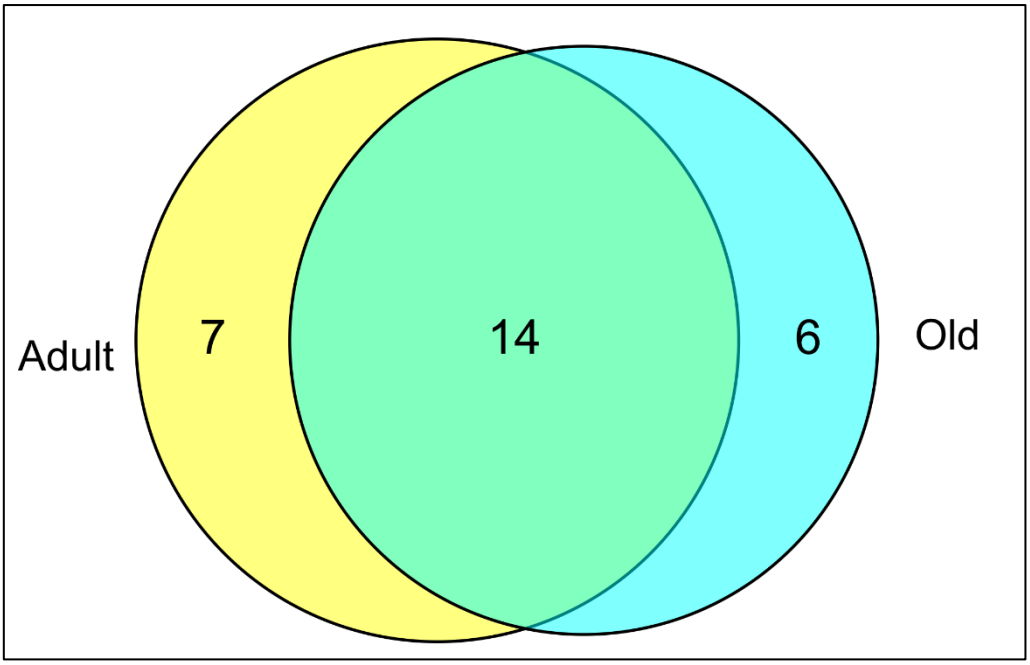

Figure 3.3.8.4 Venn diagram of reversibly oxidised proteins in mouse quadriceps. See also the supplementary information table 3.3.8.4 A/B/C on p.270 for the protein lists of individual segments.

The VennDIS highlighted the variety of proteins from muscle in adult, old and both ages of mice. Interestingly fewer cytoskeletal proteins were observed in the differential labelling data when compared with the global label free proteomics results. These data were used for the subsequent STRING pathway analysis of the individual label datasets in the following section 3.3.9.

3.3.9 STRING Analysis of Differentially Labelled Proteins

STRING (Search Tool for the Retrieval of Interacting Genes/Proteins) analysis was performed on the differentially labelled proteins, described previously for quadriceps muscle from adult and old mice. The STRING database enables identification of protein-protein interactions based on experimental evidence. The thickness of the lines joining two proteins

indicates the strength of the experimental evidence for the interaction. STRING requires a minimum number of proteins available to be input to enable statistically accurate results to be determined. Due to the limited number of proteins identified for reversibly oxidised proteins from adult, redox proteins from old and the reversibly oxidised proteins from old mice, their interactions were unable to be computed using STRING.

To perform the analysis accession numbers of proteins highlighted in the Venn diagrams of section 3.3.8 and identified as redox-flexible cysteine containing proteins that may have changed with age (see Table 2, p.105-106), were inserted into STRING to determine redox protein specific interactions.

Figure 3.3.9.1 shows interactions of the reduced proteins and highlights oxidative phosphorylation in quadriceps from adult mice. In (A) this highlights two ATP Synthase subunits (ATP5G1 and ATP5C1), the mitochondrial Acyl carrier protein (NDUFAB1) and NADH dehydrogenase 1 α sub-complex subunit 5 (NDUFA5). The GO pathway information and descriptions are shown in (B) along with three identified genes from within the pathway. (C) Shows the global label free proteomics results for the proteins highlighted in (A). This result showed interactions between reduced ATP synthase and NADH dehydrogenase protein subunits in adult quadriceps.

(A)

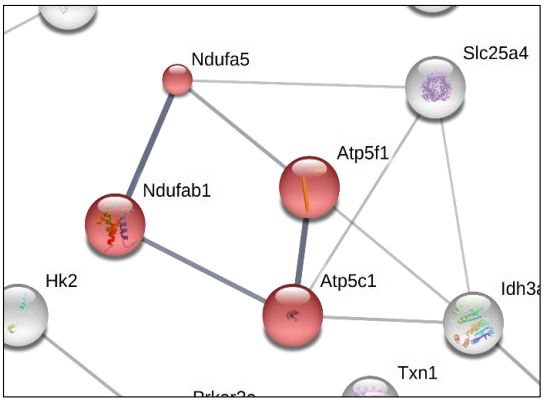

(B)

#pathway ID	pathway description	observed gene count	false discovery rate
190	Oxidative phosphorylation	3	0.025

(C)

Accession	Label	Significance (-10lgP)	Group Profile (Ratio)	Description
Q9CPP6	NDUA5_MOUSE	1.92	1.00:0.62	NADH dehydrogenase [ubiquinone] 1 alpha subcomplex subunit 5 OS=Mus musculus GN=Ndufa5 PE=1 SV=3
Q9CQQ7	AT5F1_MOUSE	1.14	1.00:1.05	ATP synthase subunit b mitochondrial OS=Mus musculus GN=Atp5f1 PE=1 SV=1
Q91VR2	ATPG_MOUSE	10.69	1.00:0.65	ATP synthase subunit gamma mitochondrial OS=Mus musculus GN=Atp5c1 PE=1 SV=1
Q9CR21	ACPM_MOUSE	0.68	1.00:1.36	Acyl carrier protein mitochondrial OS=Mus musculus GN=Ndufab1 PE=1 SV=1

Figure 3.3.9.1 STRING analysis of reduced protein interactions in mouse quadriceps muscle from adult mice. (A) Protein interactions highlighted following STRING enrichment for oxidative phosphorylation. (B) Pathway information, description gene count and false discovery rate. 3 genes are highlighted due to Ndufa5 being a sub-complex subunit. (C) Global label free proteomics results for proteins in (A).

Figure 3.3.9.2 shows redox protein interactions in muscle from adult and old mice. The proteins were enriched for glycolysis/gluconeogenesis and highlighted interactions between a number of energy metabolism proteins: Triosephosphate isomerase 1 (TPI1), 6-Phosphofructokinase muscle-type (PFKM), α-Enolase (ENO1), β-Enolase (ENO3), Phosphoglycerate mutase 2 (PGAM2), Pyruvate kinase isozymes M1/M2 (PKM) and Fructose bisphosphate aldolase A (ALDOA). This result indicates the sensitivity of certain proteins involved in glycolysis to changes in the intracellular redox environment.

(A)

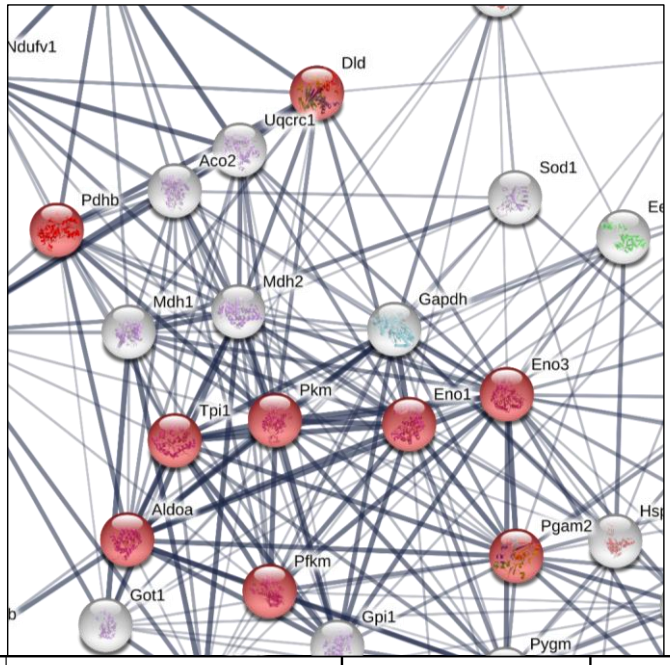

(B)

#pathway ID	pathway description	observed gene count	false discovery rate
10	Glycolysis / Gluconeogenesis	9	1.10E-13

(C)

Accession	Label	Significance (-10lgP)	Group Profile (Ratio)	Description
O08749	DLDH_MOUSE	4.49	1.00:1.99	Dihydrolipoyl dehydrogenase mitochondrial OS=Mus musculus GN=Dld PE=1 SV=2
Q9D051	ODPB_MOUSE	6.78	1.00:0.82	Pyruvate dehydrogenase E1 component subunit beta mitochondrial OS=Mus musculus GN=Pdhb PE=1 SV=1
P17751	TPIS_MOUSE	8.68	1.00:0.84	Triosephosphate isomerase OS=Mus musculus GN=Tpi1 PE=1 SV=3
P52480	KPYM_MOUSE	3.86	1.00:0.98	Pyruvate kinase isozymes M1/M2 OS=Mus musculus GN=Pkm2 PE=1 SV=4
P17182	ENOA_MOUSE	1.46	1.00:1.32	Alpha-enolase OS=Mus musculus GN=Eno1 PE=1 SV=3
P21550	ENOB_MOUSE	5.88	1.00:0.89	Beta-enolase OS=Mus musculus GN=Eno3 PE=1 SV=3
P05064	ALDOA_MOUSE	2.12	1.00:1.04	Fructose-bisphosphate aldolase A OS=Mus musculus GN=Aldoa PE=1 SV=2
P47857	K6PF_MOUSE	8.36	1.00:0.70	6-phosphofructokinase muscle type OS=Mus musculus GN=Pfkm PE=1 SV=3
O70250	PGAM2_MOUSE	30.92	1.00:0.71	Phosphoglycerate mutase 2 OS=Mus musculus GN=Pgam2 PE=1 SV=3

Figure 3.3.9.2 STRING analysis of redox proteins from mouse quadriceps muscle in adult and old mice. (A) Protein interactions following enrichment for glycolysis/gluconeogenesis. (B) Pathway information, description and false discovery rate for the enrichment performed for (A). (C) Global label free proteomics data for proteins highlighted in (A).

Figure 3.3.9.3 presents reduced proteins of adult and old mice and used STRING to enrich for protein interactions of both oxidoreductase activity and oxidative phosphorylation. The interactions show proteins involved in oxidoreductase activity and highlighted three main groups of proteins. Reading from left to right, the first group consisted of three proteins interacting strongly based on various forms of experimental and computational evidence: Trifunctional enzyme subunit α (HADHA), short chain acyl-co-A dehydrogenase (ACADS; mitochondrial), very long chain specific acyl co-A dehydrogenase (ACADYL; mitochondrial)

and Aldehyde dehydrogenase (ALDH; mitochondrial). A central group of five proteins included three Succinate dehydrogenases (SDHA, SDHB and SDHC), Isocitrate dehydrogenase subunit γ (IDH3G; mitochondrial) and Pyruvate dehydrogenase E1 (PDHA1). Finally, the third group of four proteins on the right included three peroxiredoxins (PRDX1, PRDX3 and PRDX5) and Protein disulphide isomerase (P4HB). These interactions highlight the range of energy metabolism proteins involved in oxidoreductase activity and a number of antioxidant proteins. Combined with the global proteomics information. Furthermore, as these proteins were all reduced in samples from adult and old mice, suggesting a marked impact on energy metabolism in terms of redox biochemistry as the quadriceps age.

Figure 3.3.9.3B shows the reduced proteins from adult and old mice following enrichment for oxidative phosphorylation. This identified links between succinate dehydrogenase (SDHA, SDHB and SDHC) and ATP synthase subunits (ATP5A1) and then via the NADH dehydrogenase subunit (NDUFA10) to NADH ubiquinone oxidoreductase (MTND3). From these data, the STRING results demonstrate redox changes to energy metabolism proteins with age.

(A)

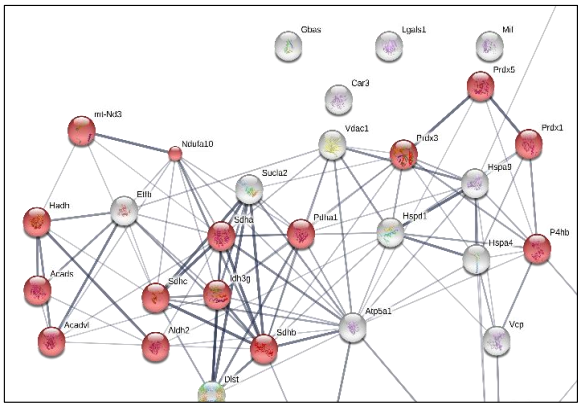

(B)

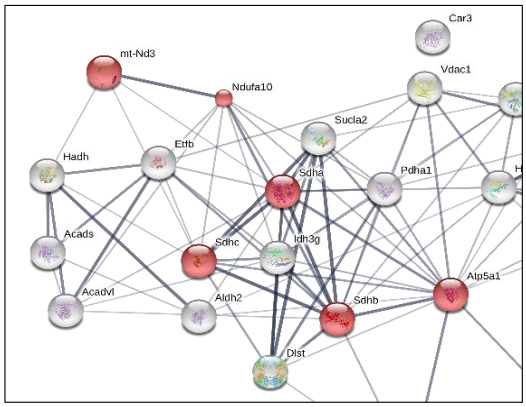

(C)

#pathway ID	pathway description	observed gene count	false discovery rate
GO.0016491	oxidoreductase activity	15	1.04E-07
190	Oxidative phosphorylation	6	4.41E-05

(D)

Accession	Significance (-10lgP)	Group Profile (Ratio)	Description
P47738	3.95	1.00:1.09	Aldehyde dehydrogenase mitochondrial OS=Mus musculus GN=Aldh2 PE=1 SV=1
P70404	1.16	1.00:0.77	Isocitrate dehydrogenase [NAD] subunit gamma mitochondrial OS=Mus musculus GN=Idh3g PE=1 SV=1
Q99LC3	1.42	1.00:0.71	NADH dehydrogenase [ubiquinone] 1 alpha subcomplex subunit 10 mitochondrial OS=Mus musculus GN=Ndufa10 PE=1 SV=1
P03899	0.42	1.00:1.12	NADH-ubiquinone oxidoreductase chain 3 OS=Mus musculus GN=Mtnd3 PE=3 SV=3
P35700	4.04	1.00:0.88	Peroxiredoxin-1 OS=Mus musculus GN=Prdx1 PE=1 SV=1
P99029	20.42	1.00:0.75	Peroxiredoxin-5 mitochondrial OS=Mus musculus GN=Prdx5 PE=1 SV=2
P09103	53.41	1.00:2.47	Protein disulfide-isomerase OS=Mus musculus GN=P4hb PE=1 SV=1
P35486	19.44	1.00:0.71	Pyruvate dehydrogenase E1 component subunit alpha somatic form mitochondrial OS=Mus musculus GN=Pdha1 PE=1 SV=1
Q07417	4.45	1.00:1.35	Short-chain specific acyl-CoA dehydrogenase mitochondrial OS=Mus musculus GN=Acads PE=2 SV=1
Q8K2B3	0.97	1.00:1.03	Succinate dehydrogenase [ubiquinone] flavoprotein subunit mitochondrial OS=Mus musculus GN=Sdha PE=1 SV=1
Q9CQA3	3.5	1.00:0.78	Succinate dehydrogenase [ubiquinone] iron-sulfur subunit mitochondrial OS=Mus musculus GN=Sdhb PE=1 SV=1
Q9CZB0	1.05	1.00:0.65	Succinate dehydrogenase cytochrome b560 subunit mitochondrial OS=Mus musculus GN=Sdhc PE=2 SV=1
P20108	1.93	1.00:0.98	Thioredoxin-dependent peroxide reductase mitochondrial OS=Mus musculus GN=Prdx3 PE=1 SV=1
Q8BMS1	3.9	1.00:1.44	Trifunctional enzyme subunit alpha mitochondrial OS=Mus musculus GN=Hadha PE=1 SV=1
P50544	1.47	1.00:1.13	Very long-chain specific acyl-CoA dehydrogenase mitochondrial OS=Mus musculus GN=Acadvl PE=1 SV=3

(E)

Accession	Significance (-10lgP)	Group Profile (Ratio)	Description
Q03265	6.54	1.00:0.85	ATP synthase subunit alpha mitochondrial OS=Mus musculus GN=Atp5a1 PE=1 SV=1
Q99LC3	1.42	1.00:0.71	NADH dehydrogenase [ubiquinone] 1 alpha subcomplex subunit 10 mitochondrial OS=Mus musculus GN=Ndufa10 PE=1 SV=1
P03899	0.42	1.00:1.12	NADH-ubiquinone oxidoreductase chain 3 OS=Mus musculus GN=Mtnd3 PE=3 SV=3
Q8K2B3	0.97	1.00:1.03	Succinate dehydrogenase [ubiquinone] flavoprotein subunit mitochondrial OS=Mus musculus GN=Sdha PE=1 SV=1
Q9CQA3	3.5	1.00:0.78	Succinate dehydrogenase [ubiquinone] iron-sulfur subunit mitochondrial OS=Mus musculus GN=Sdhb PE=1 SV=1
Q9CZB0	1.05	1.00:0.65	Succinate dehydrogenase cytochrome b560 subunit mitochondrial OS=Mus musculus GN=Sdhc PE=2 SV=1

Figure 3.3.9.3 STRING analysis of interactions of reduced proteins in quadriceps muscle of adult and old mice. (A) Enrichment of proteins for oxidoreductase activity. (B) Enrichment of proteins for oxidative phosphorylation. (C) STRING pathway information. (D) Global label free data for proteins in (A). (E) Global label free data for proteins in (B).

Figure 3.3.9.4 shows STRING analysis of reversibly oxidised proteins from quadriceps muscle from adult and old mice. Figure 3.3.9.4A shows protein interactions between Cytochrome c oxidase (COX6B1), NADH dehydrogenase (NDUFB7) and Cytochrome b-c1 complex (UQCRH). Figure 3.3.9.4B shows the STRING pathway information and figure 3.3.9.4C shows the global proteomics data for the enriched proteins in figure 3.3.9.4A. As the

proteins were reversibly oxidised, this showed that disulphide bridges could have been formed within these proteins in quadriceps muscle from adult and old mice. The interactions identified via STRING demonstrated that only a handful of proteins involved in energy metabolism were observed with this modification.

(A)

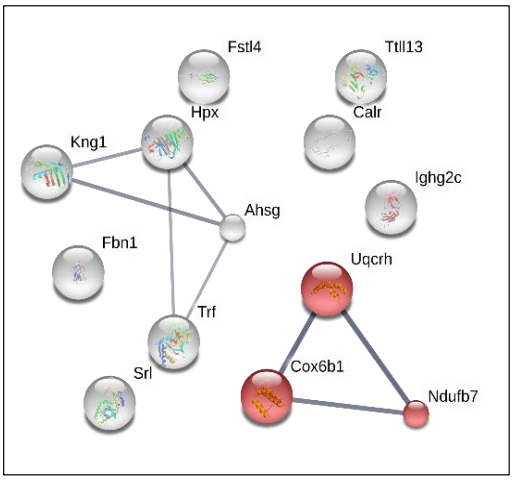

(B)

#pathway ID	pathway description	observed gene count	false discovery rate
190	Oxidative phosphorylation	3	0.00694

(C)

Accession	Label	Significance (-10lgP)	Group Profile (Ratio)	Description
P56391	CX6B1_MOUSE	0.86	1.00:1.07	Cytochrome c oxidase subunit 6B1 OS=Mus musculus GN=Cox6b1 PE=1 SV=2
Q9CR61	NDUB7_MOUSE	1.85	1.00:1.31	NADH dehydrogenase [ubiquinone] 1 beta subcomplex subunit 7 OS=Mus musculus GN=Ndufb7 PE=1 SV=3
P99028	QCR6_MOUSE	2.6	1.00:1.25	Cytochrome b-c1 complex subunit 6 mitochondrial OS=Mus musculus GN=Uqcrh PE=1 SV=2

Figure 3.3.9.4 STRING of reversibly oxidised protein interactions for proteins identified in both quadriceps muscle from adult and old mice. (A) Protein interactions following enrichment for oxidative phosphorylation. (B) STRING pathway information. (C) Global label free proteomics data for proteins in (A).

3.3.10 Motif-X Analysis of the Cysteine Microenvironment

Motif-X enabled the identification of a recurring short sequence element or motif surrounding a selected central amino acid. Parameters can be set for the foreground and background search data sets as well as significance, frequency of occurrence and the width of the amino acid string. Analysis of data for redox, reduced and reversibly oxidised proteins from the adult mouse revealed a motif containing a central cysteine, surrounded by seven peptides.

This analysis helped in determining whether the surrounding microenvironment of redox, reduced or reversibly oxidised cysteines would encourage oxidation.

Figure 3.3.10A shows a conserved threonine amino acid was identified in redox peptides from adult muscle. It contains an aliphatic hydroxyl group making the molecule hydrophilic along with a chiral centre. The amino acid is uncharged but polar meaning that while it has no overall charge, specific groups are particularly electronegative giving a tendency to hold electrons slight closer and thereby giving a slight (δ) charge. Only one isomer of threonine is present in proteins (Berg et al., 2002).

Glycine is the simplest amino acid and in figure 3.3.10B it was detected as conserved in reduced peptides from quadriceps muscle of adult mice. Like isoleucine below, it is a hydrophobic molecule and its small size enables the formation of particularly compact structures when in water (Berg et al., 2002).

Aspartate, the deprotonated form of aspartic acid, was identified in reversibly oxidised peptides in quadriceps of adult mice (figure 3.3.10C). It contains a carboxylate side chain and in certain instances can accept a proton making it functionally important (Berg et al., 2002).

Figure 3.3.10D identified an Isoleucine as a conserved amino acid sequence at +4 from the central cysteine. Isoleucine contains one less hydrogen atom than leucine giving it a chiral centre. The aliphatic side gives the molecule hydrophobic properties enabling stabilisation in water (Berg et al., 2002).

Glutamate (the deprotonated form of glutamic acid, giving an overall negative charge to the molecule) was detected as a conserved amino acid in reduced peptides of old mice (figure 3.3.10E). Similar in structure to aspartate, it also contains an acidic side chain (Berg et al., 2002).

Reversibly oxidised peptides in muscle from old mice (figure 3.3.10F) appeared to also have a conserved glutamate amino acid at -5 from the central cysteine. As previously described glutamate contains an acidic side chain and is negatively charged (Berg et al., 2002).

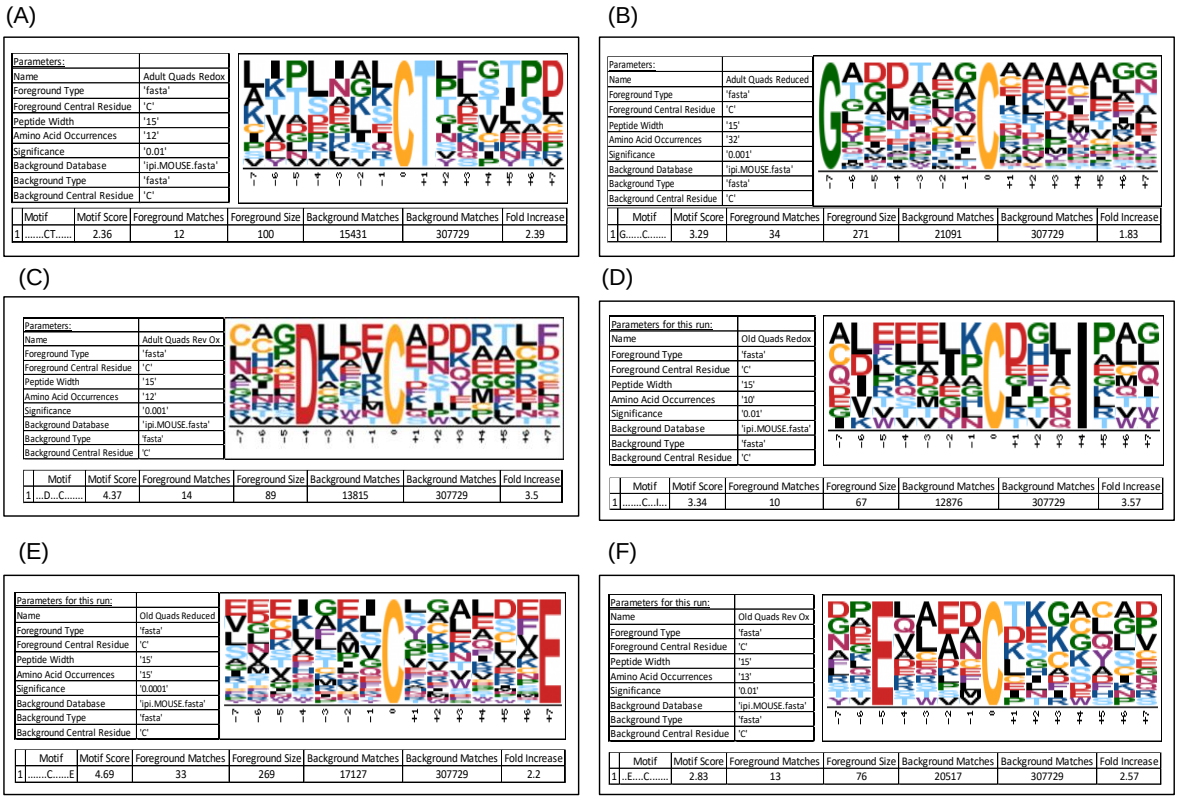

Figure 3.3.10. Motif-X analysis of redox cysteine-containing proteins. (A) Redox peptides from adult mouse quadriceps muscle and identifying a conserved threonine residue at +1, next to the central cysteine. (B) Reduced peptides from quadriceps muscle of adult mice and identifying a conserved glycine -7 away from the central cysteine. (C) Reversibly oxidised peptides from quadriceps from adult mice identifying a conserved aspartic acid -4 away from the central cysteine. (D) Redox peptides from quadriceps muscle of old mice and identifying isoleucine as a conserved residue +4 from the central cysteine. (E) Reduced peptides in quadriceps muscle from old mice and identifying Glutamic acid +7 from the central cysteine. (F) Reversibly oxidised peptides in quadriceps muscle of old mice and identifying glutamic acid -5 from the central cysteine.

The changes identified in quadriceps muscle using Motif-X analysis to highlight amino acid modifications may help in understanding changes to protein conformations via

changes to the microenvironment of specific amino acids. A future step would be to combine this information with structural biology data to characterise these changes.

3.4 Discussion

In a healthy adult the quadriceps muscle is responsible for the fast and explosive action of a sprint start. With age, a loss of muscle mass and strength is referred to as sarcopenia (Deepa et al., 2017, Sakellariou et al., 2016). In quadriceps, several proteins were observed to change in activity and redox state between adult and old mice. I hypothesised that a change in the redox state of intracellular proteins would occur with age (section 3.2, p.67) and the results generally supported this hypothesis, demonstrating that predominantly cytoskeletal proteins were detected as being down regulated with age in the label free data. Differential labelling identified changes to specific redox control proteins too, perhaps affecting protein function in relation to both redox intracellular sensitivity and redox control.

In figure 3.3.3.3 the volcano plot highlighted some cytoskeletal proteins such as the Tropomyosin 1, 2 and 3 (TPM1, TPM2, TPM3), Troponins (TNNT3, TNNI2), Myosin light chain 3 (MYL3), Myosin heavy chain 8 (MYH8), A-actin 3 (ACTN3) and Myosin regulatory light chain (MLRS). In addition, the ER stress proteins Grp78 and Protein disulphide isomerase (PDIA or P4HB) were significantly up regulated with age in mouse quadriceps. Tropomyosin has over 40 isoforms and is a key component of the actin cytoskeleton (Kee et al., 2004), therefore an increase in protein abundance with age within the quadriceps may suggest an increase in muscle physiological stiffness thereby reducing physical flexibility as observed previously in humans (Palmer and Thompson, 2016). This, in addition to work by Lexell & Brooks then demonstrated muscle fibre atrophy with age (Lexell et al., 1988, Brooks and Faulkner, 1988, Lexell et al., 1986, Lexell et al., 1984). Conversely, significantly down regulated proteins included Heat shock protein 70kDa (HSP70), Heat-shock protein β-6

(HSPB6) and Nascent polypeptide-associated complex subunit α (NACAM). HSP70 is a crucial for protein folding and involved in the heat shock response (the rest of the associated data will be discussed later in this chapter, see p.126). HSPB6 is also involved in protein folding control and chaperoning and was reduced in quadriceps muscle for old mice. Finally, NACAM is a transcription factor involved in regulation of thick and thin filaments during muscle growth and regeneration (Yotov and St-Arnaud, 1996, Park et al., 2010). The significant reduction in abundance found in quadriceps from old mice may suggest a partial reduction in skeletal muscle regeneration capabilities although why this occurs, in addition to the reduction in HSP70 and HSPB6 is unclear. These results support the concept of age-related physiological decline in skeletal muscle flexibility to respond to changes in the intracellular redox balance (Brook et al., 2016).

Mouse body weights and quadriceps muscle weights were measured to identify any general physiological differences between individual mice and between individual quadriceps muscles. Figure 3.3.1.1A showed a significant increase in body weight from 3 to 12 months which was expected due to growth. A single outlier with lower weight than the rest of the mice was identified. The quadriceps showed a significant decrease in weight with age. Both the whole body and quadriceps tissue-specific data agreed with another study that identified significant increases in mouse body weight between 3 and 12 months of age and a decrease in "hind limb muscle mass" between 18 and 24 months of age (Hamrick et al., 2006).

Redox Ageing

Redox control proteins such as Peroxiredoxin 3 and 5 (mitochondrial based) demonstrated an increase in abundance (via western blotting) with age. The sulphonylated versions of Peroxiredoxins 1-4 also showed an increase in ROS with age to levels that cause sustained changes to free thiol groups. Interestingly protein carbonylation, another indicator or

sustained ROS showed a decrease with age in mouse quadriceps muscle while the protein chaperone PARK7 increased in abundance with age along with the sulphonylated form. Briefly, these results indicate some of the changes observed in ageing mouse quadriceps muscle and generally support an increase in oxidation with age in quadriceps muscle. The results are considered in greater detail below.

Changes to numbers of redox proteins were represented in figure 3.3.7.1 and highlight a decrease in redox proteins. These are of particular interest as they allow for reduction and oxidation of specific cysteine residues which enables the cell to react to changes in ROS concentration. An increase in the number of reduced proteins was also observed and this indicates a potential loss of protein function with age in the quadriceps. Redox proteins are defined in this regard as those involved in the intracellular control of redox reactions and maintenance of a balanced redox state. Table 2 listed the redox proteins detected via differential labelling in mouse quadriceps and figure 3.3.7.2 highlighted these changes as fold change. This indicated significant increases in the reduced state to the actin-controller and translocation protein Cofilin-2 (CFL2) at Cys80 by 7.21 fold. The glycolysis and pentose phosphate pathway protein Glucose-6-phosphate isomerase (GPI) at Cys404 by 6.06 fold and the cytoplasmic Malate dehydrogenase-1 (MDH1) at Cys154 by 6.8 fold (Gillett et al., 1996, Berg et al., 2002). This may suggest a significant change to the microenvironment, however this did not appear to be translated into changes in protein abundance as none of those mentioned significantly changed. Interestingly, Glucose-6-phosphate changed its redox state entirely from being reversibly oxidised in adult mouse quadriceps to becoming reduced in old mouse quadriceps. Conversely, the metabolism protein Aconitase (ACO2) at Cys126 reducing by 0.42 fold, the amino acid metabolism protein Aspartate aminotransferase (GOT2) at Cys295 by 0.38 fold and the glyconeogenesis protein Glycogen phosphorylase (PYGM) at Cys581 by 0.41 fold. All

appeared to reduce in the redox state, becoming reversibly oxidised in the old mouse quadriceps.

In addition to the differential labelling of redox proteins in skeletal muscle, western blotting was performed on a number of proteins of interest in addition to the mass spectrometry analysis. The first of those proteins examined was Thioredoxin 1, a cytosolic enzyme containing a disulphide bridge at its active site which enables redox signalling and the maintenance of normally functioning peroxiredoxins (Dimauro et al., 2012). It is among several redox proteins constitutively expressed by skeletal muscle and was assessed to begin with due to the integral part of the thioredoxin system in maintaining the functionality of other redox control proteins and therefore the regulation of intracellular ROS concentration (Manabe et al., 2014, Dimauro et al., 2012). No significant change was observed for Thioredoxin 1 or 2 or Thioredoxin reductase 1 or 2 suggesting the thioredoxin system for redox sensing and control of both cytosolic and mitochondrial proteins was not affected with age. This was a surprising result and contradicts previous data from C2C12 myoblasts and myotubes that showed changes to the Thioredoxin system do occur (Dimauro et al., 2012).

Thioredoxin interacting protein (TXNIP) negatively regulates the function and expression of Thioredoxin and has been demonstrated to reduce insulin sensitivity in skeletal muscle following overexpression (Alhawiti et al., 2017). Figure 3.3.4.5A showed a significant increase in protein abundance with age from 3 to 12 months and 3 to 24 months of age (both $p < 0.05$). This was a surprising result given the Thioredoxin system proteins did not change in abundance or activity and suggests regulation at a number of different levels.

Peroxiredoxins 1-6 were assessed to determine which of these crucial antioxidant proteins are affected by ageing via changes to their protein abundance. Western blots in figure 3.3.4.6A-F (p.83) showed significant increases in abundance for Peroxiredoxin 3 (3.3.4.6C

from 3 to 12 months, p <0.01 and 3 to 24 months p <0.01) and Peroxiredoxin 5 (3.3.4.6E from 3 to 24 months, p <0.05). Both Peroxiredoxins are located in the mitochondria suggesting that ageing in mouse quadriceps affects the organelle more than the general cytosolic systems. None of the Peroxiredoxins demonstrated significant changes to abundance in the global proteomics data.

A sustained increase in ROS may affect Peroxiredoxins via oxidation of their thiol groups. As described in figure 1.4.1 (p.35), a sustained increase in ROS leads to increasing degrees of oxidation of thiol groups starting with sulphenylation (-SOH), then sulphinylation ($-SO_2H$) and finally sulphonylation ($-SO_3H$). These modifications inhibit protein activity by increasingly irreversible modifications and therefore any increase detected by this blot for $–SO_3H$ would significantly impact protein function. A previous study has highlighted that the addition of the $–SO_3H$ leads to negative effects impacting health (Pan and Carroll, 2014). One study demonstrated a circadian rhythm for PRDX2 hyperoxidation, oscillating over a 24-hour period. The study noted this oscillation was not observed for PRDX6 or GAPDH, however this suggests that certain redox proteins can function cyclically. This hyperoxidation leads to the degradation of PRDX2 and eventually its decline in abundance from the cell surface. One aspect of future work would be to assess circadian changes to redox protein in skeletal muscle to determine if PRDX2 or others follow a similar oscillation (Cho et al., 2014).

Figure 3.3.4.8A showed a significant increase in sulphonylated peroxiredoxins (1-4) protein abundance from 3 to 24 months of age (p <0.01) and 12 to 24 months of age (p <0.001) compared with almost none detected in quadriceps muscle samples from young and adult mice. The antibody detects Peroxiredoxins 1-4 and although individual Peroxiredoxins could not be distinguished, it represents modifications to both the cytosolic and mitochondrial antioxidant proteins with age.

Following from the Peroxiredoxin redox sensor and controllers, Cu-Zn Superoxide Dismutase (SOD1) and Mn-Superoxide Dismutase (SOD2) were examined as they are key antioxidant proteins located in the cytosol and mitochondria respectively. Figure 3.3.4.9A showed a significant increase in SOD1 from 3 to 12 months in protein abundance (p <0.01), however no change was observed for SOD2 indicating ageing may impact ROS control predominantly in the cytosol rather than the mitochondria for mouse quadriceps muscle (Powers and Jackson, 2008, Powers et al., 2011).

To better understand the longer-term effects of reactive oxygen species, protein Carbonylation and Glutathionylation western blots were examined. Figure 3.3.4.23A showed a significant decrease in protein carbonylation with age. The result showed significant decreases for proteins from both 3 to 12 months and 3 to 24 months (both p <0.05). This is highly surprising as one would expect an increase in carbonylated proteins with age as an indicator of sustained concentrations of ROS due to the variations previously seen in redox control proteins. These results contrast with other work that has identified increases in the carbonylation of proteins with age (Rabek et al., 2003, Tohma et al., 2014). The Glutathionylation blot in figure 3.3.4.24A showed a significant increase in glutathionylated proteins with age (p <0.05 for both 3 to 12 months and 3 to 24 months of age). Glutathionylation has been described as a reversible form of protein modification following sustained exposure to ROS (Fratelli et al., 2002, Brigelius et al., 1983).

The observations for age related changes to carbonylated and S-glutathionylated proteins in mouse quadriceps are supported by two other studies which demonstrate glutathione pools and carbonylation work in opposite directions where an increase in carbonylated proteins results from a decrease in available glutathione. One caveat regarding these published studies is that they were performed in neuronal tissues, whereas our data showed similar changes occur in ageing mouse quadriceps (Bizzozero et al., 2006, Dasgupta et al., 2012).

In summary the results of the redox proteins indicate a varied number of changes in the different redox systems considered. Notwithstanding the differences sometimes observed between western blot and proteomics data (to be discussed in detail later in Chapter 7, p.221), these results demonstrate that the impact of ageing is complex in relation to the redox proteome since both cytosolic and mitochondrial proteins are affected and some redox control systems examined are not affected by ageing.

Protein Folding Response

Protein folding is crucial to the production of fully functioning proteins. Both the constitutively expressed HSC70 (HSPA1, figure 3.3.4.13A) and the inducible HSP70 (HSPA8, figure 3.3.4.13B) heat shock proteins were looked at. Western blot data showed a significant decrease (p <0.05) in the constitutive variant from 12 to 24 months of age but not for the inducible form. Interestingly the proteomics results were the opposite of that observed with western blotting. Whilst experimental limitations are discussed in detail later (see Chapter 7, p.221), the proteomics result may be considered a more robust due to the stringent requirement of at least three peptide fragments required for a confirmed detection and measurement. In addition to changes in protein abundance, the redox state for HSC70 was tested via differential labelling. Cys584 showed a decrease in the redox ratio (adult reduced: oxidised versus old reduced: oxidised) with age from 10.9 to 8.7 reflecting the susceptibility of this particular cysteine to changes in the redox environment over time, however this specific cysteine does not appear to be crucial to enzyme function (UniProt, 2017d). Overall these results indicate an ongoing requirement for the inducible form of HSP70, and a reduced requirement for the constitutively expressed variant as mouse quadriceps age. These results support a number of other studies in relation to increased inflammation in skeletal muscle ageing (Ferrucci et al., 2002, Hiona and Leeuwenburgh, 2008, Vabulas et al., 2002). HSP70 was identified as a cytokine in 2000 and the increase in abundance observed here, with a the reduction in HSC70,

suggests an attempted intracellular response to changing redox environment, perhaps as showed by the slight change observed for Cys584 of HSC70 and the work of others identifying an increase in misfolded proteins occurring with age and age-related illnesses (Selkoe, 2004, Basaiawmoit and Rattan, 2010, Asea et al., 2000). Additionally overexpression of HSP70 has been demonstrated to attenuate the age-related reduction in muscle function (McArdle et al., 2004a).

A key redox sensor protein involved in the folding response is PARK7. There have been a range of functions described for this protein including a requirement for autophagy in mitochondria (Krebiehl et al., 2010), stability of the antioxidant transcription regulator NRF2, a peroxiredoxin-like function, skeletal muscle calcium homeostasis and effects on myotube size and expression where an increase in PARK7 was demonstrated to cause hypertrophy in mouse skeletal muscles (Clements et al., 2006, Andres-Mateos et al., 2007, Shtifman et al., 2011, Yu et al., 2014). The western blot data in figure 3.3.5.17A showed a significant increase (both $p < 0.05$) in protein abundance with age from both 3 to 24 and 12 to 24 months, but relative quantification via global label free proteomics did not indicate a significant change in abundance with age from 12 to 24 months. Furthermore the redox Cys46 of PARK7 was shown to be susceptible to oxidation as identified via an increase in the reversibly oxidised form suggesting a decrease in redox flexibility via the formation of disulphide bonds (Ito et al., 2006). Relative quantification to determine any change to the redox state of PARK7 Cys46 showed an increase in reduced state from 8.5 to 17.5. Interestingly, this cysteine has been suggested to undergo conversion to alanine in the presence of hydrogen peroxide which may impact enzyme performance (Andres-Mateos et al., 2007). Furthermore, the same conversion in humans has been implicated in reduced protein stability (Canet-Aviles et al., 2004). The results in figure 3.3.3.17 showing an increase in PARK7 protein abundance, combined with the increase in the reduced in redox state of Cys46, may reflect increased oxidative stress with

age. Additionally, the redox results for Cys46 also reflect inactivation of PARK7 in the old mouse quadriceps (Richarme et al., 2015). To consider this in greater detail a western blot of the sulphonylated form of PARK7, PARK7-SO_3H was examined and figure 3.3.5.18A shows a significant increase (p <0.05) in protein abundance with age. The formation of PARK7-SO_3H occurs on Cys106 and is due to the ease with which this relatively unstable PARK7-SO_2H undergoes further oxidation (Wilson, 2011), although this particular cysteine was not observed in our differential labelling data. Considering the combined results of PARK7 and PARK7-SO_3H, these suggest an intracellular attempt to control increased reactive oxygen species that are known to occur in mouse skeletal muscle with age (McArdle et al., 2001).

Protein disulphide isomerase (PDI, PDIA or P4HB) is required in the formation and breakage of nascent disulphide bonds. However, this dynamic protein has a range of other functions described in human studies, such as a chaperone function at high concentrations, an aggregation facilitator at low concentrations and a reductase function when localised to the cell exterior (Lumb and Bulleid, 2002, Bi et al., 2011). The western blot shown in figure 3.3.5.14A demonstrates a significant increase for both 3 to 24 months (p <0.001) and 12 to 24 months (p <0.05) of age. Global label free proteomics correlated with this result indicating a significant increase in abundance with age between adult and 24 months of age.

In summary, protein chaperones perform a vital task in maintaining intracellular functions by ensuring misfolded proteins are broken down. They are correctly folded with complete proteins being successfully translocated. The results indicate that a number of those involved in protein folding were significantly increased in abundance with age in the mouse quadriceps. This suggests an increased demand for protein folding control with age also supports previous results considering redox control proteins, where those systems were sporadically affected by changes observed for some, but not all proteins. Overall this suggests an attempt to control the effects of increased intracellular ROS by skeletal muscle is only

partially successful for the redox systems and therefore an increase in certain protein chaperone abundance is required to mitigate this.

Energy Metabolism and Ageing

Mitochondrial activity in the quadriceps was assessed through age-related changes in succinate dehydrogenase (SDH) staining, as shown in figure 3.3.2.1A for adult and old (figure 3.3.2.1B) tissue. The SDH staining method causes the precipitation of nitro-blue tetrazolium (NBT) which relates to SDH activity indicating changes to Complex II of the electron transport chain with age (Trifunovic et al., 2004). The results in figure 3.4.2.1 highlight a reduction in oxidative capacity from adult to old as demonstrated by a decrease in the intensity of from 3.4.2.1A to 3.4.2.1B. In addition to this a number of human studies have identified a decrease in fibre number and size with age in quadriceps muscle (Frontera et al., 2000, Kent-Braun et al., 2000), although Sheard and Anderson report more varied fibre type changes with age (Sheard and Anderson, 2012).

Aconitase (mitochondrial form) is a redox sensitive enzyme crucial to the tricarboxylic acid cycle as it is involved in the isomerisation of Citrate to Isocitrate via *cis*-Aconitase. It contains an Iron-Sulphur cluster at its active site that is readily oxidised thus impacting its redox performance (Larsen et al., 2016). Figure 3.3.5.18 shows no significant change in Aconitase abundance with age (supported by the proteomics result) and no significant change in enzyme activity. Redox analysis of Aconitase showed that Cys126 decreased its reduced state from 61.4 to 26.2. Cys385 changed from a reversibly oxidised form in quadriceps from adult mice to a reduced form in quadriceps from old mice, moving from 0.7 to 0.1. Given its crucial role, this modification may hinder the enzyme's ability to correctly function. Cys448/451 was found to become slightly more reversibly oxidised with age, changing from 0.1 to 0.3 and Cys592 to become more reduced with age changing from 19.3 to 22.9. Cys385

and Cys448/451 are involved in the Iron-Sulphur active site complex, Cys126 and Cys592 are located near the catalytic binding site. It has been widely reported that because of their positioning, the four active site cysteines are susceptible to modification by ROS and this makes Aconitase vulnerable to increased ROS within the cell. Furthermore, the location of Cys126 and Cys592 means that any effect upon these cysteines will affect protein function (Talib and Davies, 2016, Han et al., 2005, Kennedy et al., 1988). While other studies have identified changes to Aconitase abundance in different organs such as mouse kidneys (Yarian et al., 2006) and mouse heart mitochondria (Yarian et al., 2005), the current results support other data from skeletal muscle which demonstrated no significant change in Aconitase : Citrate synthase ratio with age (Lyons et al., 2006).

Glyceraldehyde 3-Phosphate dehydrogenase (GAPDH) is involved in glycolysis and has often been used as a housekeeping gene due to its ubiquity. Western blot data (figure 3.3.5.20) identified a significant decrease in protein abundance from 3 to 24 months ($p < 0.001$) and adult to 24 months of age ($p < 0.01$). However, the proteomics data showed no significant change to GAPDH protein abundance with age. Despite the discrepancy, it has been identified elsewhere that GAPDH changes with age. This questions its reliability as a housekeeping protein for western blotting, at least for quadriceps muscle in mice (Vigelso et al., 2015). In addition to protein abundance the redox state in adult and old were measured via differentia labelling. This highlighted GAPDH Cys150 was increased in redox state from 127 to 554 and Cys245 increased from 17 to 26. As Cys150 is located at the enzyme active site, the result suggest a direct impact of the increased reduced state on GAPDH's activity in old mouse quadriceps (Kornberg et al., 2010).

Differential labelling highlighted changes to two other energy metabolism proteins in mouse quadriceps. Phosphoglycerate kinase (PGK1) in which Cys379 remained reduced but increased from 47.5 to 95.4. This specific cysteine is located near to a nucleotide binding site

and a hinge region, thus changes to the redox state of Cys379 may affect protein conformation (Lay et al., 2002). ATP Synthase subunit D (ATP5H) was identified as redox sensitive for Cys101 and although remaining in reduced form in both adult and aged samples, the reduced state decreased from 51.7 to 37.6.

In summary, although a number of changes were observed in energy metabolism proteins in mouse quadriceps, only the changes to GAPDH appeared to have a sufficient impact on enzyme function, reducing it with age.

Label Free Analysis with GOrilla and STRING

GOrilla pathway analysis enabled a gene ontology assessment using the label free proteomics data and STRING helped to identify protein-protein interactions but also included information regarding gene ontology to better categorise functional groups of proteins. Combined, these results build on the global label free data heat map (figure 3.3.3.2) and volcano plot (figure 3.3.3.3) by highlighting the quadriceps proteomics data containing key proteins involved in the cytoskeleton and contractile activity. This is an important finding as it indicates which types of proteins are predominantly susceptible to ageing in the mouse quadriceps.

Differentially Labelled Protein Datasets Comparison using VennDIS Followed by STRING Analysis of this Data

Initially the data was prepared via VennDIS to isolate just redox proteins in muscle from adult, old or both ages of mice. This was repeated for reduced and reversibly oxidised proteins. In summary, the VennDIS analysis of differentially labelled proteins helped to identify some changes to proteins of interest. In the redox and reduced proteins many energy metabolism proteins were observed in adult but not old mice indicating a change in energy

metabolism. This initial insight was then taken a stage further to attempt to identify any protein interactions via the use of STRING.

Pathway analysis took the differentially labelled proteins and used VennDIS to initially examine data from muscles of adult and old mice (section 3.3.9), and subsequently into redox, reduced and reversibly oxidised proteins. Reduced proteins in muscle of adult mice were enriched for oxidative phosphorylation in figure 3.3.9.1. This highlighted three interactions between two ATP synthase subunits, an NADH dehydrogenase subunit and an acyl carrier protein.

The data in figure 3.3.9.2 looked at redox proteins from adult and old mice enriched for glycolysis/gluconeogenesis. This highlighted several metabolomics proteins that had undergone redox labelling. Of those Pyruvate dehydrogenase is a key metabolome protein which links the tricarboxylic cycle to the glycolytic pathway (Seifert et al., 2007). Reduced proteins from adult and old mice enriched for both oxidoreductase figure 3.3.9.2A and oxidative phosphorylation (figure 3.3.9.2B). In both figures metabolic proteins were identified. In 3.3.9.2A Peroxiredoxin 1 and 5 suggested a maintained requirement for mitochondrial and some cytoplasmic control of ROS (specifically H_2O_2), along with Protein disulphide isomerase and a number of metabolic proteins. Enrichment was also performed for oxidative phosphorylation and highlighted succinate dehydrogenase and ATP synthase amongst other proteins highlighting alternative metabolic pathways.

Figure 3.3.9.4 shows reversibly oxidised proteins from adult and old mice enriched for oxidative phosphorylation. Reversibly oxidised data was enriched for oxidative phosphorylation and identified two cytochrome b-c1 complex proteins and NADH dehydrogenase both of which are involved in the mitochondrial respiratory chain. Reversibly oxidised proteins suggest disulphide bridge formation prior to detection.

The cytochrome b-c1 complex is involved in the mitochondrial respiratory chain and changes have been implicated due to increases in ROS with age (Crofts, 2004, Boffoli et al., 1996). Furthermore, the redox cysteine data for subunits 1 and 2 of cytochrome b-c1 complex became more reversibly oxidised with age. This was seen in the reversibly oxidised data for old mice and may suggest irreversible modifications of the protein with age in quadriceps. Another energy metabolism protein, NADH dehydrogenase, is a known producer of ROS in mitochondria (Marchi et al., 2012) and was observed in the reversibly oxidised list. Interestingly, one study identified a mutation to NADH dehydrogenase which imparted longevity on fibroblasts (Schauer et al., 2015). Reversibly oxidised protein from adult and old mice had no STRING datasets due to limited numbers of identified proteins within these categories therefore no statistically significant interactions could be inferred by the software.

Overall, the STRING protein-protein interactions analysis of the redox cysteine data has highlighted a range of protein interactions that support other data regarding the predominant changes in quadriceps with age affecting cytoskeletal proteins.

Motif-X Analysis of Redox Data

Motif-X analysed conserved amino acids in redox, reduced and reversibly oxidised peptides lists for adult and old mice with all parameters including a significance of $p \leq 0.01$. Figure 3.3.10A (redox peptides from adult mice) highlighted a conserved threonine at +1 from a central cysteine residue in adult quadriceps muscle. Figure 3.3.10D (quadriceps from old mice) highlighted a conserved isoleucine at +4 from the central cysteine. These two results highlight the likelihood of changes to the amino acid sequence and in addition to previous data demonstrating the effect of a change in redox state. Furthermore, both serve to highlight the variety of changes that a protein can undergo with age and lead the way to investigating how this impacts protein function as a possibility for future studies.

3.5 Conclusions

In conclusion this work has successfully identified changes to redox-sensitive and cytoskeletal proteins that occur in the quadriceps with increasing age. The results indicate that the predominant change with age affects cytoskeletal and contractile proteins. Other changes seen included redox sensitive proteins such as PARK7 and its sulphonylated form. This and the differential labelling data together indicate an increase in the reduced state of a range of proteins. It is thought this may impart an increased 'redox stiffness' as the proteins are less able to react to redox changes. The physiological outcome may be the observed increase in 'stiffening' of skeletal muscle, caused by this increase in abundance of cytoskeletal proteins.

CHAPTER 4

STUDY OF THE SOLEUS MUSCLE

4.1 Introduction

The soleus muscle is predominantly made up of slow twitch fibres and is located under the quadriceps on the lower mouse hind limbs (Wang and Kernell, 2001, Kammoun et al., 2014). This muscle was selected for study due to its primary use of oxidative phosphorylation for energy generation and to investigate if ageing affects this muscle in a similar way to the quadriceps. Energy metabolism for soleus muscle is predominantly via oxidative phosphorylation, an aerobic mechanism that occurs in the inner mitochondrial membrane and produces Adenosine Triphosphate (ATP) following the degradation of succinate produced via the tricarboxylic acid cycle (TCA). This takes longer to act and therefore soleus muscle fibres are utilised in endurance actions (Leijendekker and Elzinga, 1990). The techniques performed in this chapter and details regarding proteins of interest have been discussed previously in the overall Introduction of chapter one and the introduction to the Quadriceps muscle results (chapter 3).

4.2 Aims and Hypothesis

The aim of this study was to identify age-related changes to the soleus via the use of mass spectrometry for proteomics analysis of intracellular proteins and their redox states.

It was hypothesised that the redox state of intracellular soleus proteins would change with age.

4.3 RESULTS

4.3.1 Muscle Weights

Soleus muscles were dissected from male C57BL/6 mice at 3, 12 and 24 months of age and the weights of both the mice and the individual soleus muscles were recorded. Body weights (figure 3.4.1.1A) demonstrated a significant increase from 3 to 12 months. Figure 4.4.1.1, below, shows no significant change occurred in soleus muscle weight with age.

Figure 4.3.1.1 Soleus muscle weights. N=6 biological replicates for each age.

4.3.2 Succinate Dehydrogenase Staining of Soleus Muscle

Succinate dehydrogenase (SDH) staining showed the overall oxidative capacity mouse skeletal muscle cells. The data in figure 4.3.2.1 highlights differences in the soleus muscles between adult (4.3.2.1A) and old (4.3.2.1B). Visual analysis of the images shows a reduction in the cellular oxidative capacity with age by the reduction in intensity of the blue/purple dye. As per the previous chapter, these images were not quantified and are presented to highlight the differences with age between fibres from adult and old mice prior to the detailed proteomic and biochemical analysis that follows.

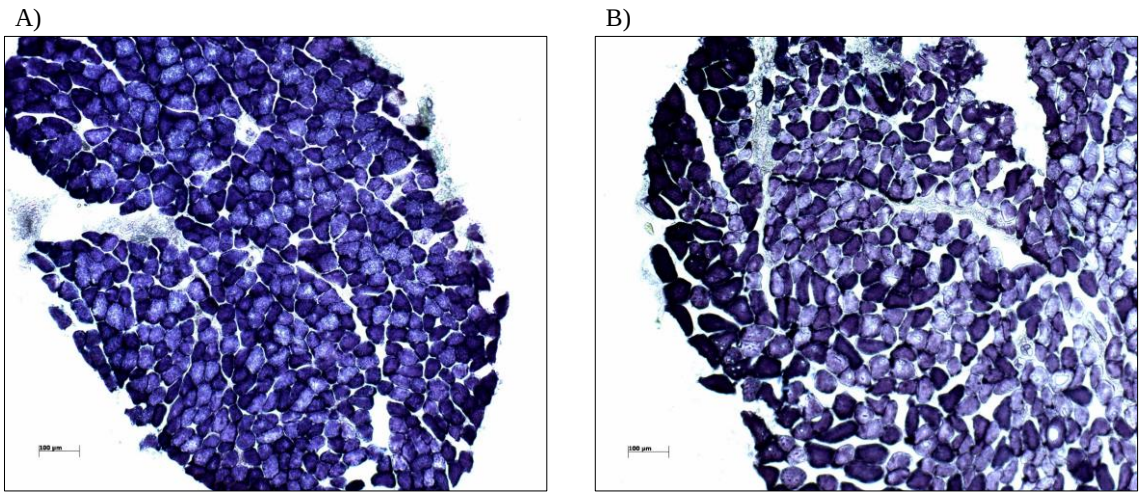

Figure 4.3.2.1 (A) Adult soleus muscle stained for succinate dehydrogenase and (B) old soleus muscle.

4.3.3 Global Label Free Proteomics Data Analysis

For proteomic assessment, PEAKS7 was used to identify detected proteins in the samples and perform label free relative quantification. For label free relative quantification, proteins were deemed significantly changed when they had a –10 log P of >20 (equivalent to *p* value of 0.01), a fold change of >1.5 and a quality value of 0.8. These parameters ensured a good minimum standard of confidence in the comparison of protein abundance. The heat map in figure 4.3.3.1 shows the significantly changed proteins identified in soleus muscle from adult and old mice. Red signifies an up regulation and green a down regulation of the protein via the $\log_2$ ratio. The label free proteomics data can be accessed online as S5 – Soleus All Detected Proteins; S6 – Soleus Significantly Changed Proteins at 10.17638/datacat.liverpool.ac.uk/437.

A multicomponent analysis (MCA) of the global label free proteomics data highlighted correlations within each data set and between the adult and old data. The blue value at the top of each box is the R^2 value, indicating the statistical measure of the data to the fitted regression

line. A high value indicates a tight fit to the regression line. A number of data points appear to be more widely spread suggesting increased variation amongst proteins in the soleus samples.

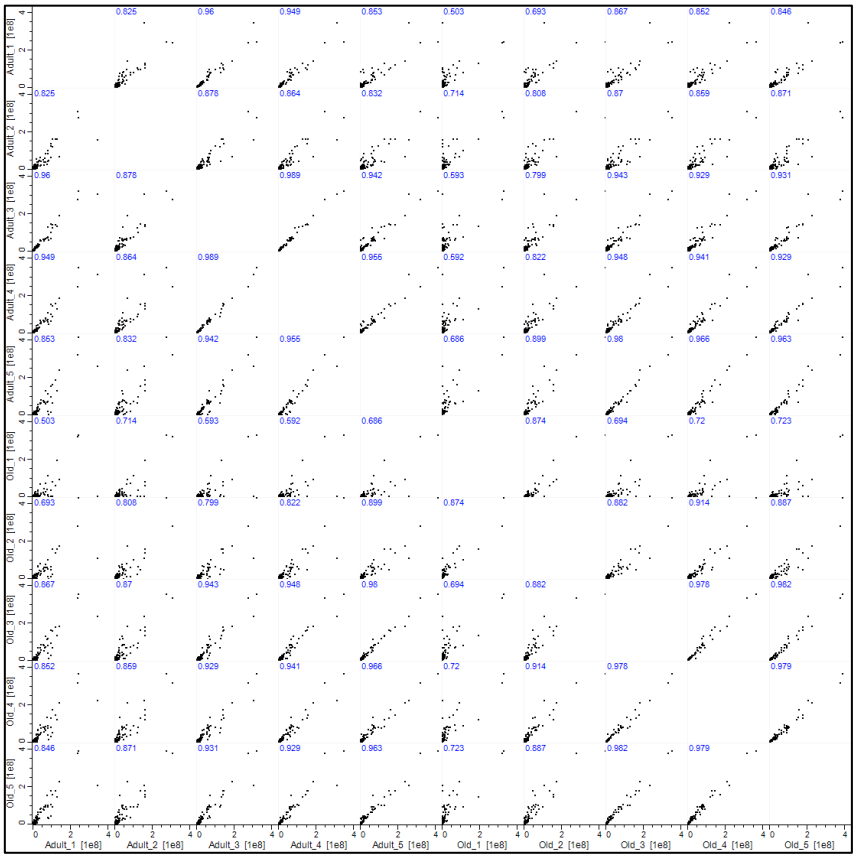

Figure 4.3.3.1 Multicomponent analysis of detected soleus proteins when compared across different samples to identify variation between samples.

The heat map in figure 4.3.3.2 illustrates differential expression of a number of proteins including many involved in the energy metabolism pathways such as the cytosolic proteins cAMP dependent protein kinase (KAP2), Glycogen phosphorylase (PYGM) and Glyceraldehyde 3-Phosphate dehydrogenase (G3P) all of which were significantly decreased with age. Conversely, Heat shock protein β-3 (HSPB3) occurs in the cytoplasm (and nucleus) and was significantly increased with age. Mitochondrial proteins detected include Isocitrate dehydrogenase (IDH3A), 2-oxoglutarate dehydrogenase (ODO1), Pyruvate dehydrogenase

(ODPB) and Cytochrome c oxidase (COX7C) all of which are significantly decreased with age and mitochondrial Aconitate hydratase (ACON) was significantly increased with age.

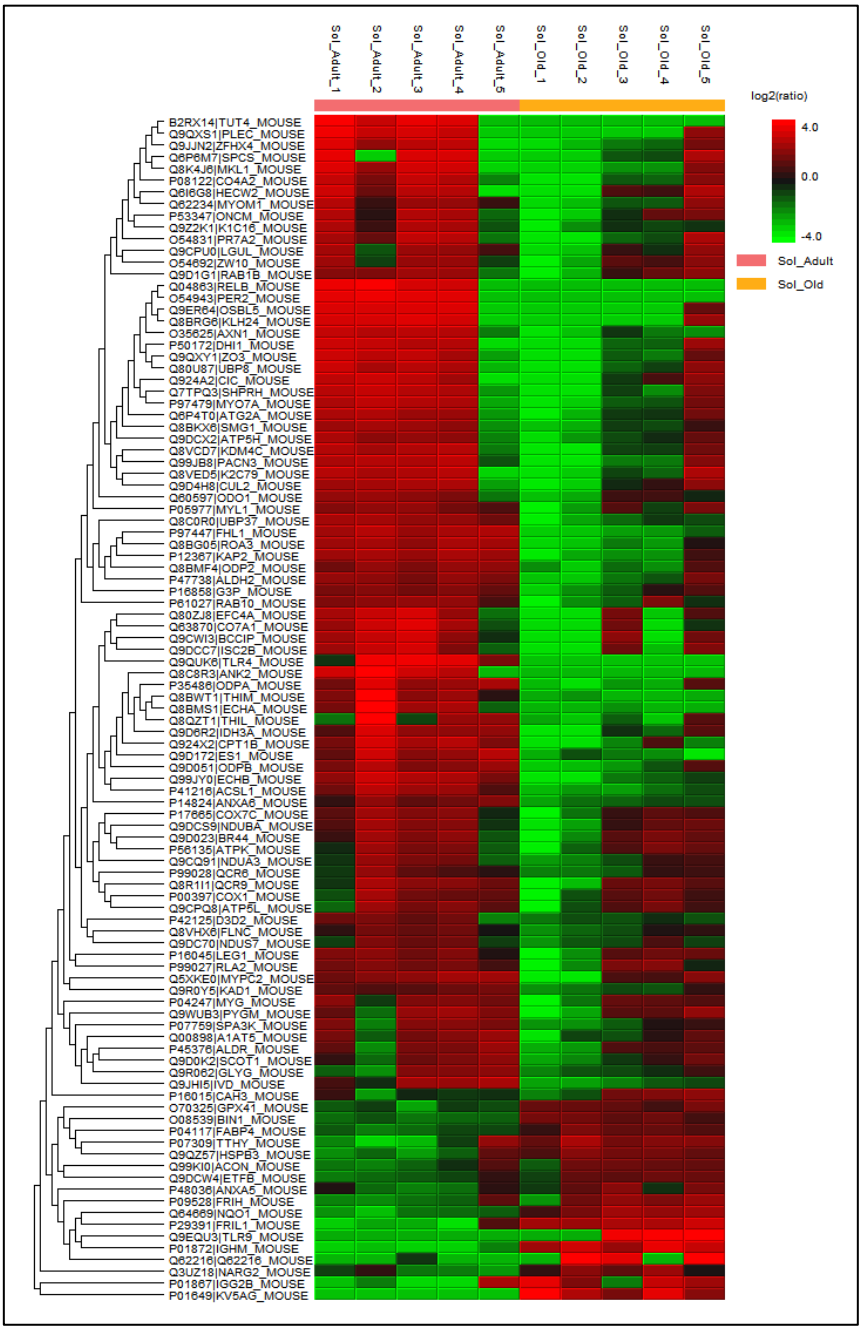

Figure 4.3.3.2 Heat map of the $\log_2$ ratio fold change of significantly changed soleus muscle proteins comparing muscle of adult (n=5) and old (n=5) mice. Clear differences in up and down regulation of detected proteins are identified. Red indicates an increase and green a decrease in fold change. Label free significance was determined using a peptide quality of 0.8, a significance score of –10 log P of >20 (equivalent to *p* value of < 0.01) and a fold change of >1.5.

A volcano plot was used to highlight a number of significantly changed metabolic proteins from the global label free proteomics data by comparing significance -10 log P significance with log_2 fold change (figure 4.3.3.3). Proteins significantly down-regulated according to the label free proteomics data were highlighted and included a large number of energy metabolism proteins such as cAMP-dependent protein kinase type II-α regulatory subunit (KAP2/PRKAR2A), trifunctional enzyme subunit β (ECHB/HADHB, mitochondrial), glyceraldehyde-3-phosphate dehydrogenase (G3P/GAPDH), pyruvate dehydrogenase E1 component subunit α (ODPA/PDHA1, mitochondrial), dihydrolipoyllysine-residue acetyltransferase component of pyruvate dehydrogenase complex (ODP2/DLAT, mitochondrial), 2-oxoglutarate dehydrogenase (ODO1/OGDH, mitochondrial), pyruvate dehydrogenase E1 component subunit β (ODPB/PDHB, mitochondrial), ATP synthase subunit d (ATP5H, mitochondrial), cytochrome c oxidase subunit 7C (COX7C, mitochondrial), Aldehyde dehydrogenase (ALDH2, mitochondrial), 3-ketoacyl-CoA thiolase (THIM/ACAA2, mitochondrial), acetyl-CoA acetyltransferase (THIL/ACAT1, mitochondrial), cytochrome b-c1 complex subunit 6 (QCR6/UQCRFS1, mitochondrial), cytochrome b-c1 complex subunit 9 (QCR9/UQCR10), NADH dehydrogenase 1 β subcomplex subunit 10 (NDUBA/NDUFB10), ATP synthase subunit g (ATP5L, mitochondrial). Another protein, the four and a half LIM domains protein 1 (FHL1) has been implicated in maintaining striated muscle function by aiding development or hypertrophy (Chu et al., 2000). Galectin-1 (LEG1/LGALS1) is involved in apoptosis, proliferation and differentiation, possibly enabling the physiological adaptation of skeletal muscle (Kami and Senba, 2005). The glycolytic and muscle contraction protein phosphoglycerate mutase 2 (PGAM2), prostaglandin G/H synthase 1 (COX1/PTGS1) involved in a range of functions and the phosphate transporter phosphate carrier protein (MPCP SLC25A3, mitochondrial). The significantly up-regulated proteins were highlighted in red and included Ig μ chain C region (IGHM), the key energy metabolism proteins aconitate hydratase

(ACON/ACO2, mitochondrial), ATP synthase subunit α (ATPA/ATP5A1, mitochondrial), electron transfer flavoprotein subunit β (ETFB), fructose-bisphosphate aldolase A (ALDOA). The lipid peroxidation protection protein phospholipid hydroperoxide glutathione peroxidase (GPX41/GPX4, mitochondrial) and the Calcium binding and storage protein calsequestrin-1 (CASQ1). Significance is defined as -10 log P (equivalent to p <0.01), a fold change >1.5 and a peptide quality of 0.8. Together these results indicate a general down regulation of energy metabolism proteins in the soleus muscle as it ages in mice.

Proteins Significantly Changed in Abundance for Soleus Muscle

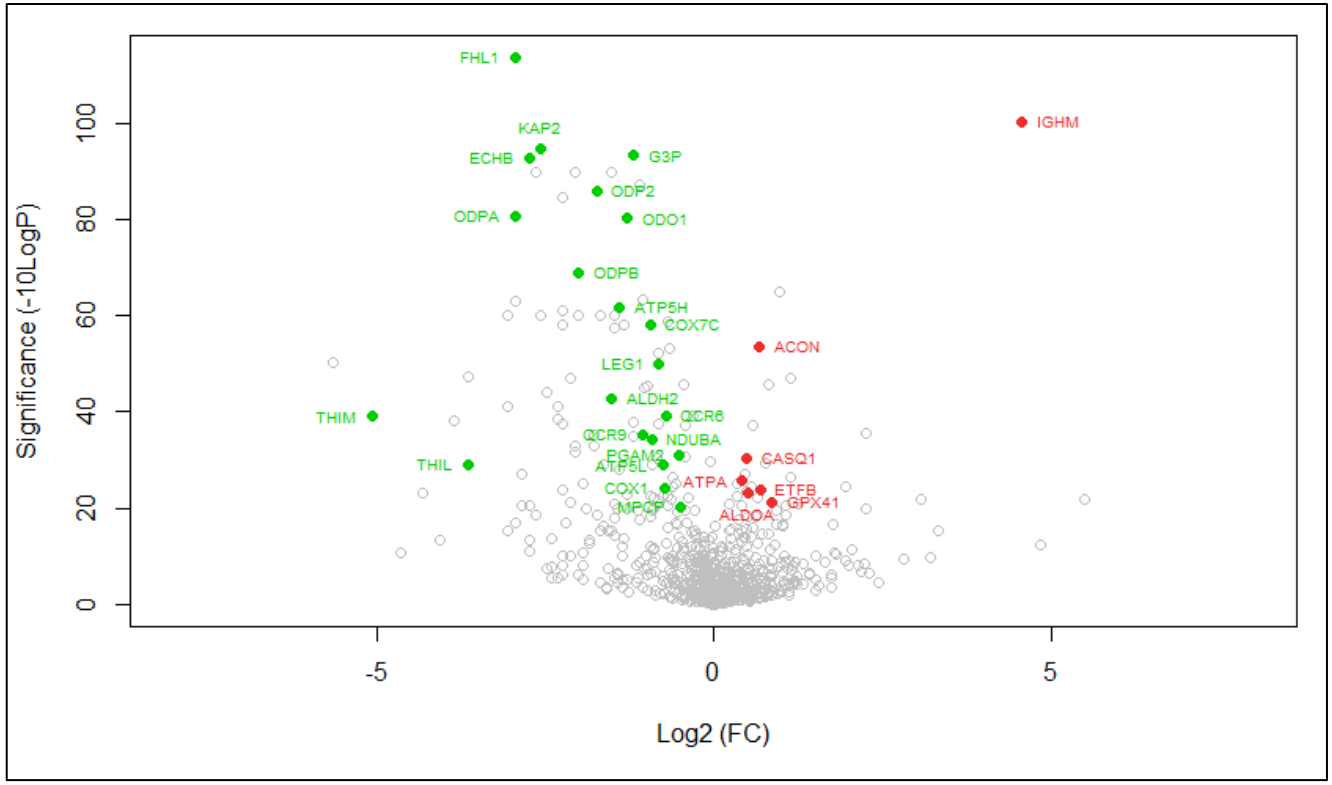

Figure 4.3.3.3 Volcano plot highlighting proteins from the global label free proteomics data for soleus muscle. The significantly down-regulated proteins highlighted in green are Four and a half LIM domains protein 1 (FHL1), cAMP-dependent protein kinase type II-α regulatory subunit (KAP2), Trifunctional enzyme subunit β (ECHB, mitochondrial), Glyceraldehyde-3-phosphate dehydrogenase (G3P), Pyruvate dehydrogenase E1 component subunit α (ODPA, mitochondrial), Dihydrolipoyllysine-residue acetyltransferase component of pyruvate dehydrogenase complex (ODP2, mitochondrial), 2-oxoglutarate dehydrogenase (ODO1, mitochondrial), Pyruvate dehydrogenase E1 component subunit β (ODPB, mitochondrial), ATP synthase subunit d (ATP5H, mitochondrial), Cytochrome c oxidase subunit 7C (COX7C, mitochondrial), Galectin-1 (LEG1), Aldehyde dehydrogenase (ALDH2, mitochondrial), 3-ketoacyl-CoA thiolase (THIM, mitochondrial), Acetyl-CoA acetyltransferase (THIL, mitochondrial), Cytochrome b-c1 complex subunit 6 (QCR6, mitochondrial), Cytochrome b-c1 complex subunit 9 (QCR9), NADH dehydrogenase 1 β subcomplex subunit 10 (NDUBA), Phosphoglycerate mutase 2 (PGAM2), ATP synthase subunit g (ATP5L, mitochondrial), Prostaglandin G/H synthase 1 (COX1), Phosphate carrier protein (MPCP, mitochondrial). The significantly up-regulated proteins highlighted in red are Ig μ chain C region (IGHM), Aconitate hydratase (ACON, mitochondrial), Calsequestrin-1 (CASQ1), ATP synthase subunit α (ATPA, mitochondrial), Electron transfer flavoprotein subunit β (ETFB), Fructose-bisphosphate aldolase A (ALDOA), Phospholipid hydroperoxide glutathione peroxidase (GPX41, mitochondrial). Significance is defined as a significance of –10 log P of >20 (equivalent to *p* value of 0.01), a fold change >1.5 and a peptide quality of 0.8.

4.3.4 Western Blotting and Enzyme Activity Assays

Western blotting complimented the label free proteomics analysis and where possible verified the observed results. Enzyme activities were included along-side the appropriate blots for Thioredoxin, Thioredoxin Reductase and Aconitase. Label free proteomics data was determined using a peptide quality of 0.8, a significance score of –10 log P of >20 (equivalent to *p* value of 0.01) and a fold change >1.5. Table 3 lists the primary antibodies used here.

The thioredoxin system proteins across 3, 12 and 24 months of age are shown in figure 4.3.4.1A-D demonstrating no significant change to Thioredoxin 1 abundance with age as was supported by the label free proteomics data. The enzyme activity assay for both Thioredoxin 1 and Thioredoxin Reductase 1 also showed no change with age in figures 4.3.4.1B and D respectively. Figure 4.3.4.1E shows a significant decrease in protein abundance for Thioredoxin Interacting Protein (TXNIP) with a significant decrease from 3 to 12 months (p <0.001) and from 3 to 24 months (p <0.001). Peroxiredoxin 1 showed a significant decrease (p <0.05) in protein abundance from 12 to 24 months in figure 4.3.4.1F. Peroxiredoxin 4 showed a significant increase in abundance from 3 to 24 (p <0.01) and 12 to 24 months (p <0.05) in figure 4.3.4.1G. Peroxiredoxin 6 (figure 4.3.4.1H) showed no significant change in abundance with age. In contrast the relative quantitation using global label free analysis demonstrated no significant changes to thioredoxin or any of the peroxiredoxins between adult and old soleus muscle samples (figures 4.3.4.1I and J). Note that the analysis was performed on two gels simultaneously, hence the two Ponceau stains (figures 4.3.4.1K and L). Thioredoxin 1, Thioredoxin Reductase 1 and Peroxiredoxin 6 were tested on the first gel and Peroxiredoxin 1, Peroxiredoxin 4 and Thioredoxin Interacting Protein tested on the second gel due to their respective molecular weights. Furthermore, as described later, Aconitase was tested using the same blot following stripping and re-probing of the membrane as described in the methods (p.52).

Table 3. Primary and Secondary Antibody List for Western Blotting

Name	Abbreviation	Mw	Company	Product Code	LOT #	Dilution	Blocking Agent	Secondary Reqd.
Aconitase	Acon.	86 kDa	Abcam	ab129069	GR81376-7	1:5000	3% Milk	Anti-Rabbit
AMP kinase alpha	AMPk	62 kDa	Cell Signalling Technology	-	#19	1:1000	3% BSA	Anti-Rabbit
Carbonylation	Anti-DNP	Full Blot	Invitrogen	713500	-	1:1000	5% Milk	Anti-Rabbit
Copper-Zinc Super Oxide Dismutase	SOD1	16 kDa	Enzo	ADI-SOD-100	1051228	1:1000	3% Milk	Anti-Rabbit
DJ-1/PARK7 - SO3H	DJ-1/PARK7-SO3H	20 kDa	Abcam	ab169520	GR121877-7	1:1000	3% Milk	Anti-Rabbit
Peroxiredoxin 1	Prdx1	22 kDa	Abcam	ab15571	GR49827-2	1:1000	3% Milk	Anti-Rabbit
Peroxiredoxin 3	Prdx3	27 kDa	Abcam	ab16751	GR40935-1	1:1000	3% Milk	Anti-Rabbit
Peroxiredoxin 4	Prdx4	29 kDa	Abcam	ab16943	GR140162-1	1:1000	3% Milk	Anti-Mouse
Peroxiredoxin 6	Prdx6	25 kDa	Abcam	ab133348	GR145006-1	1:1000	3% Milk	Anti-Rabbit
Peroxiredoxin-SO3H	Prx-SO3H	Full Blot	Abcam	ab16830	-	1:1000	3% Milk	Anti-Rabbit
Thioredoxin 1	Trx1	12 kDa	Abcam	ab86255	GR43357-5	1:1000	3% Milk	Anti-Rabbit
Thioredoxin Reductase 1	TXNRD1	55 kDa	Abcam	ab16840	GR172892-1	1:2000	3% BSA	Anti-Rabbit
Thioredoxin Interacting Protein	TXNIP	45 kDa	Abcam	ab86993	GR132784-1	1:1000	3% Milk	Anti-Mouse

Table 3. Primary and HRP-conjugated secondary antibodies used for soleus western blotting. N.B. “Full Blot” required the whole membrane for imaging.

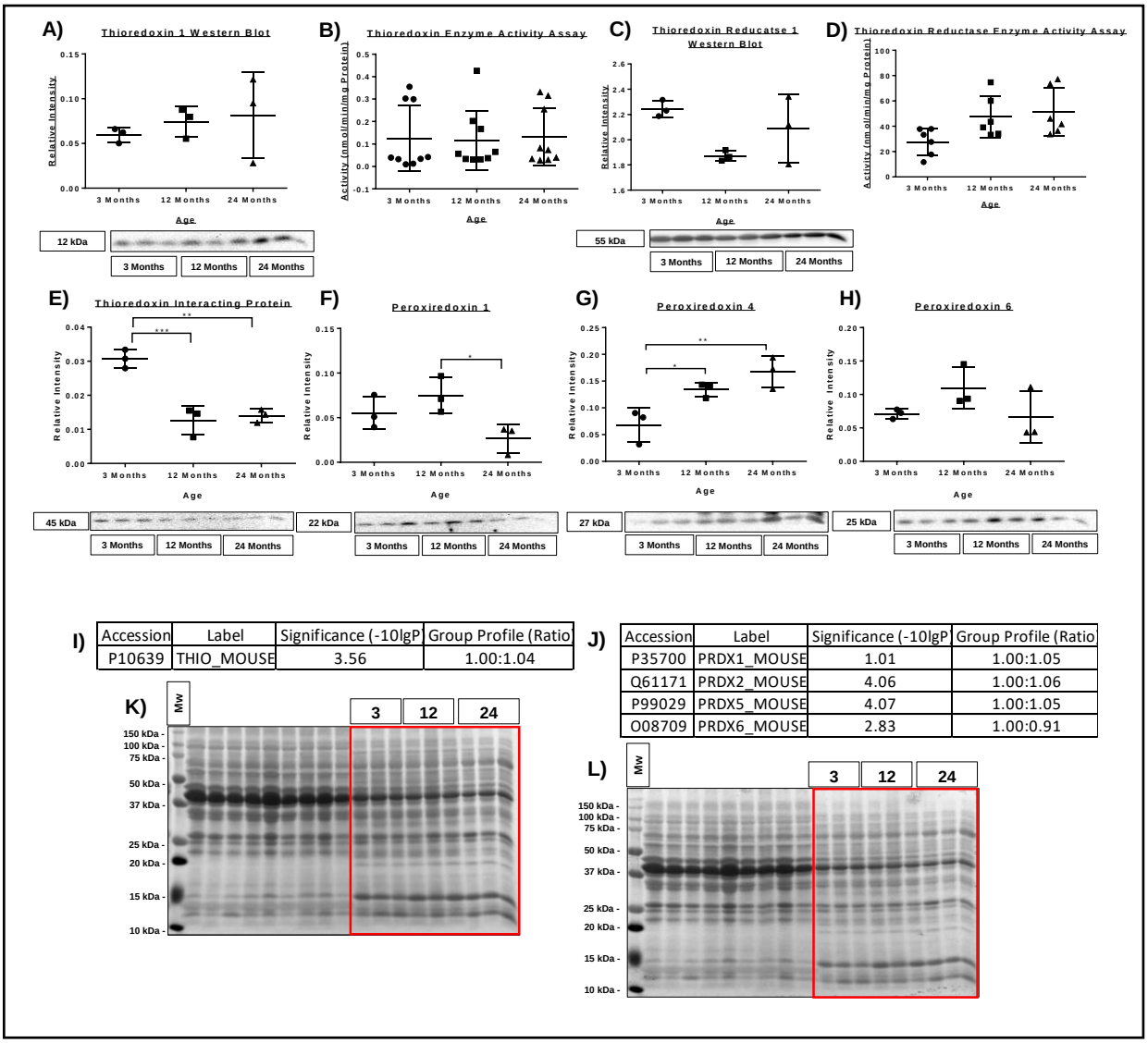

Figure 4.3.4.1. (A) Densiometric measurement for immunodetection by western blotting of Thioredoxin 1. (B) Enzyme activity assay performed for Thioredoxin (non-specific, detecting both TRX1 and TRX2). (C) Densiometric measurement for immunodetection by western blotting data for Thioredoxin Reductase 1 (TRXR1). (D) Enzyme activity assay performed for Thioredoxin Reductase (non-specific, detecting both TRXR1 and TRXR2). (E) Densiometric measurement for immunodetection by western blotting for Thioredoxin Interacting Protein (TXNIP), ** $p < 0.01$, *** $p < 0.001$. (F) Densiometric measurement for immunodetection by western blotting of Peroxiredoxins 1, * $p < 0.05$. (G) Densiometric measurement for immunodetection by western blotting of Peroxiredoxins 4. * $p < 0.05$, ** $p < 0.01$. (H) Densiometric measurement for immunodetection by western blotting of Peroxiredoxins 6. (I) Label free proteomics result for Thioredoxin 1 comparing 12 and 24 month old muscle. (J) Label free proteomics result for Peroxiredoxins 1, 2, 5 and 6, comparing 12 and 24 month old muscle. (K) The Ponceau S stain used for normalisation of (A, C & H) with the soleus section highlighted in red. (L) The Ponceau S stain used for normalisation of (E, F & G) with the soleus section highlighted in red. In all cases n=3 biological replicates. Short bars indicate upper and lower interquartile range while the middle represents the median value following statistical analysis using ANOVA with Tukey's post-hoc test.

Cu-Zn Superoxide Dismutase (SOD1) is shown in figure 4.3.4.2 and indicates a significant increase in protein abundance from 3 to 24 months of age although the proteomics result did not indicate a significant change from adult (12 months) to old (24 months).

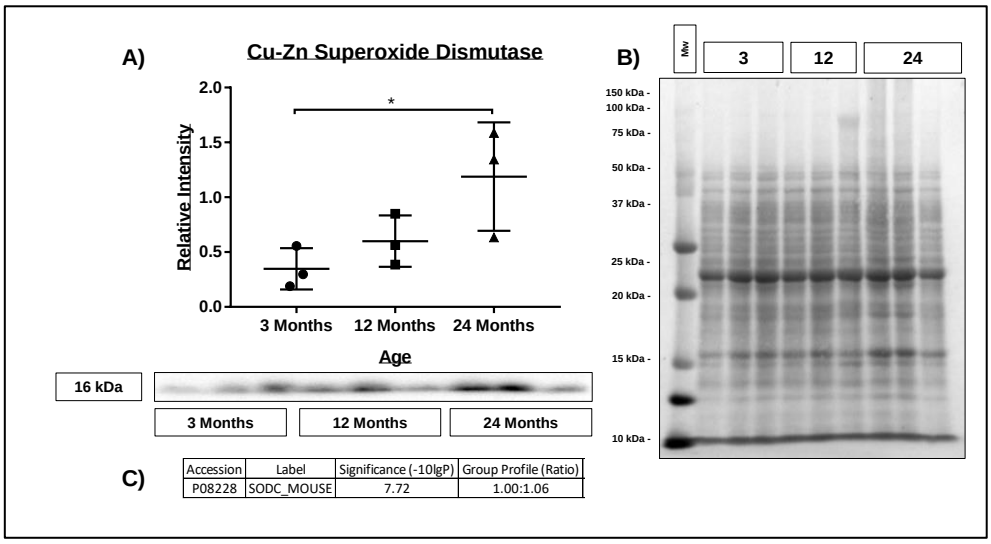

Figure 4.3.4.2. (A) Densiometric measurement for immunodetection by western blotting of Cu-Zn Superoxide Dismutase (SOD1). * $p < 0.05$. (B) Ponceau S stain used for normalisation. (C) Label free proteomics result for SOD1 in soleus muscle between adult and old mice. N=3 biological replicates. Short bars indicate upper and lower interquartile range while the middle represents the median value following statistical analysis using ANOVA with Tukey's post-hoc test.

Figure 4.3.4.3 shows sulphonylated peroxiredoxins in which the western blot demonstrated no significant changes with age. However, only one protein band out of three appeared for the 24 months samples and taking the sole protein sample at 24 months into account, there appears to be little change in protein abundance with age.

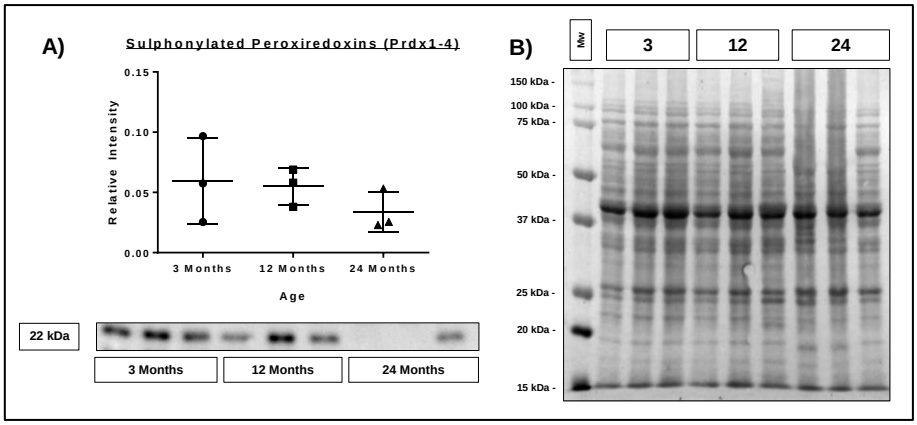

Figure 4.3.4.3. Sulphonylated Peroxiredoxins (Prdx-SO_3H) demonstrate sustained intracellular reactive oxygen species leading to irreversible modifications of Peroxiredoxins in soleus muscle. (A) The Densiometric measurement for immunodetection by western blotting antibody detected Peroxiredoxins 1-4 at 22 kDa. (B) Ponceau S stain used for normalisation. N=3 biological replicates. Short bars indicate upper and lower interquartile range while the middle represents the median value following statistical analysis using ANOVA with Tukey's post-hoc test.

Following the analysis of several redox sensitive proteins, energy metabolism proteins were then analysed. Figure 4.3.4.4 shows mitochondrial Aconitase protein abundance and the results show no significant change with age. The enzyme activity assay showed a significant increase (p <0.01) in activity with age from 3 to 12 months. In contrast the global label free proteomics analysis of Aconitase identified a significant increase in abundance with age from 12 to 24 months of age in soleus muscle. When conflicting results between western blot and mass spectrometry occur, we assume the mass spectrometry data takes precedence due to the increased sensitivity of the technique. This is discussed in detail in experimental considerations and limitations (p.221). Furthermore, this was performed on a stripped membrane following its prior use for protein abundances detailed in figure 4.3.4.1. The details of this method are described in methods (p.53).

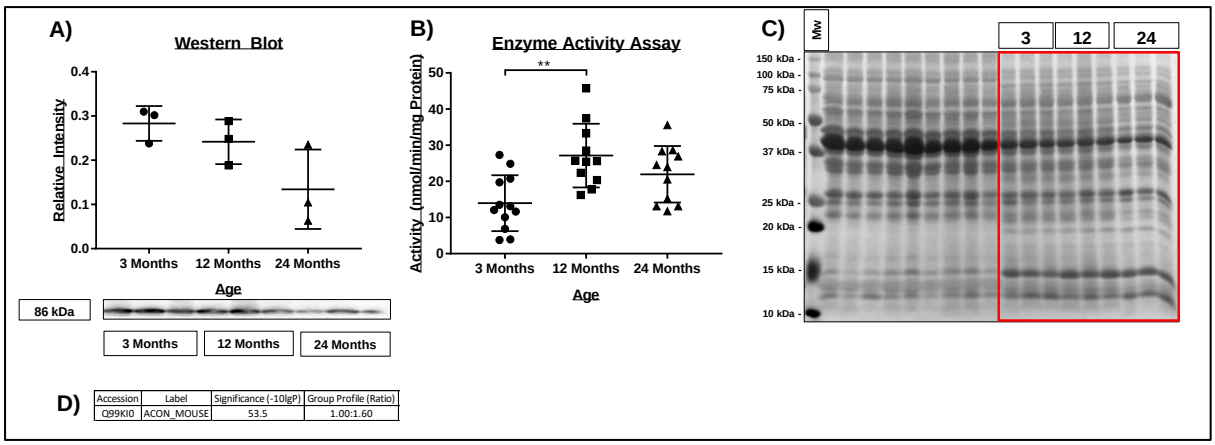

Figure 4.3.4.4. Aconitase (ACO2) in mouse soleus muscle. (A) Densiometric measurement for immunodetection by western blotting of 3, 12 and 24 month samples. (B) Enzyme activity assay performed for Aconitase. ** $p < 0.01$. (C) The Ponceau S stain used for normalisation of (A) with the relevant soleus samples highlighted in red. (D) Global label free proteomics result for Aconiotase. N=3 biological replicates. Short bars indicate upper and lower interquartile range while the middle represents the median value following statistical analysis using ANOVA with Tukey's post-hoc test.

Figure 4.3.4.5A shows the sulphonylated form of PARK7 (PARK7-SO_3H) and showed no significant change in protein abundance. However, two samples did not show any band anticipated for the 24 month samples. No significant difference was observed between 3 and 12 months. The global label free proteomics analysis (figure 4.3.4.5C) showed no significant change with age from 12 to 24 months in the mouse soleus. Additionally the energy metabolism protein Adenosine monophosphate kinase (AMPK) (figure 4.3.4.5B) was analysed. The western blot results showed no significant change to protein abundance with age if the single band present at 24 months is taken into consideration due to a similar issue as presented in figure 4.3.4.5A with only one of the three 24 month protein bands observable. The global label free proteomics results (figure 4.3.4.5D) identified the subunits of AMPK and showed no change to KAPCA (or PRKACA). However, KAP2 (or PRKAR2A) did show a significant decrease with age from 12 to 24 months.

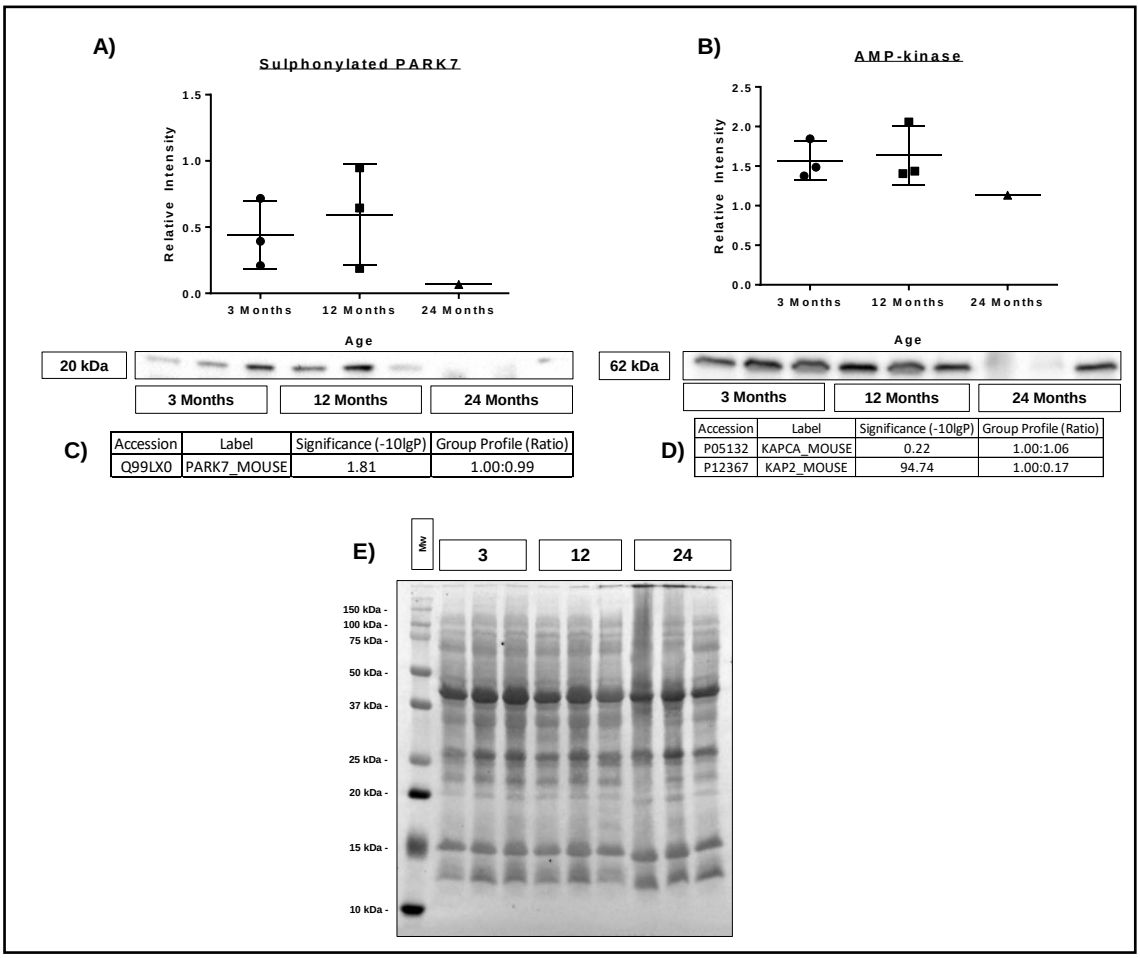

Figure 4.3.4.5. (A) Densiometric measurement for immunodetection by western blotting of sulphonylated Park7 (PARK7-SO_3H). (B) Densiometric measurement for immunodetection by western blotting of AMP-kinase. (C) Global label free proteomics result for PARK7-SO_3H. (D) Global label free proteomics results for two subunits of AMPK: KAPCA (or PRKACA) and Kap2 (PRKAR2A). (E) Ponceau S stain used for normalisation of both A and B. N=3 biological replicates. Short bars indicate upper and lower interquartile range while the middle represents the median value following statistical analysis using ANOVA with Tukey's post-hoc test.

Carbonylated proteins are those modified with a carbonyl group (C=O) and is another product of sustained increases in intracellular ROS concentrations with age. The data are shown in figure 4.3.4.6 and showed no significant change in protein carbonyl abundance with age.

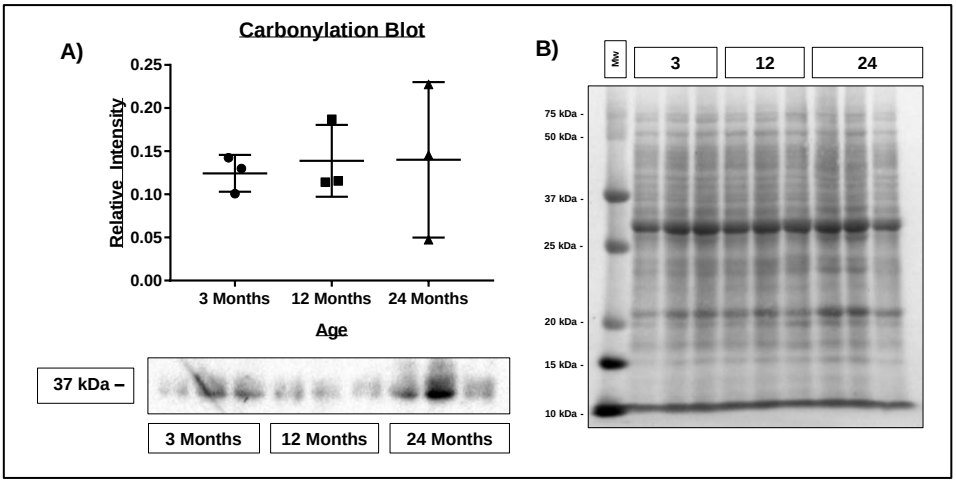

Figure 4.3.4.6. A Carbonyl blot used to identify carbonylated proteins in soleus muscle samples. (A) Densiometric measurement for immunodetection by western blotting of protein carbonylation in mouse soleus muscle at 3, 12 and 24 months. (B) Ponceau S stain used for normalisation of (A). N=3 biological replicates. Short bars indicate upper and lower interquartile range while the middle represents the median value following statistical analysis using ANOVA with Tukey's post-hoc test.

The results of various protein abundance changes in mouse soleus therefore showed a varied response to ageing. Significantly less protein was obtained due to the size of the mouse soleus compared with the quadriceps muscle, this was reflected in the number of western blots that could be performed compared to the quadriceps. This directly impacted the extent of the analysis of ageing using western blotting since several proteins were not detected and repeat blots unfeasible.

4.3.5 GOrilla Pathway Analysis

GOrilla analysis uses the global label free proteomics data to determine pathway relationships between ontological terms. In the soleus there was an emphasis on energy metabolism terms and this was reflected in the pathways highlighted with significance and includes mitochondrial components, metabolic proteins and oxido-reductase activity.

GOrilla analysis of biological processes highlighted a number of potential pathways from the initial label free proteomics dataset. Thioester metabolic process and Acyl Co-A

metabolic process; TCA metabolic process, Citrate metabolic process and TCA cycle; Acyl Co-A biosynthetic process from pyruvate and mitochondrial Acyl Co-A biosynthetic process from pyruvate. These pathways suggest a predominance of the metabolic pathway proteins identified in soleus muscle.

GOrilla analysis of cellular components highlights pyruvate dehydrogenase complex, mitochondrion, organelle inner membrane, mitochondrial membrane and mitochondrial inner membrane. As per the biological processes identified in figure 4.3.5.1, this suggests a predominance in energy metabolism, specifically of proteins located to the mitochondrial membrane.

Molecular function analysis via GOrilla highlighted a number of functions by identifying significant ontological changes to terms connected predominantly with mitochondrial metabolic processes including a number of oxido-reductase activities and certain energy metabolism pathways such as pyruvate dehydrogenase activities. This range of pathways identify coenzyme factor turnover in the soleus and overall the analysis highlights an emphasis on metabolic in activity in the soleus supported by previous global label free data such as the heat map and volcano plots of figures 4.3.3.1 and 4.3.3.2 respectively.

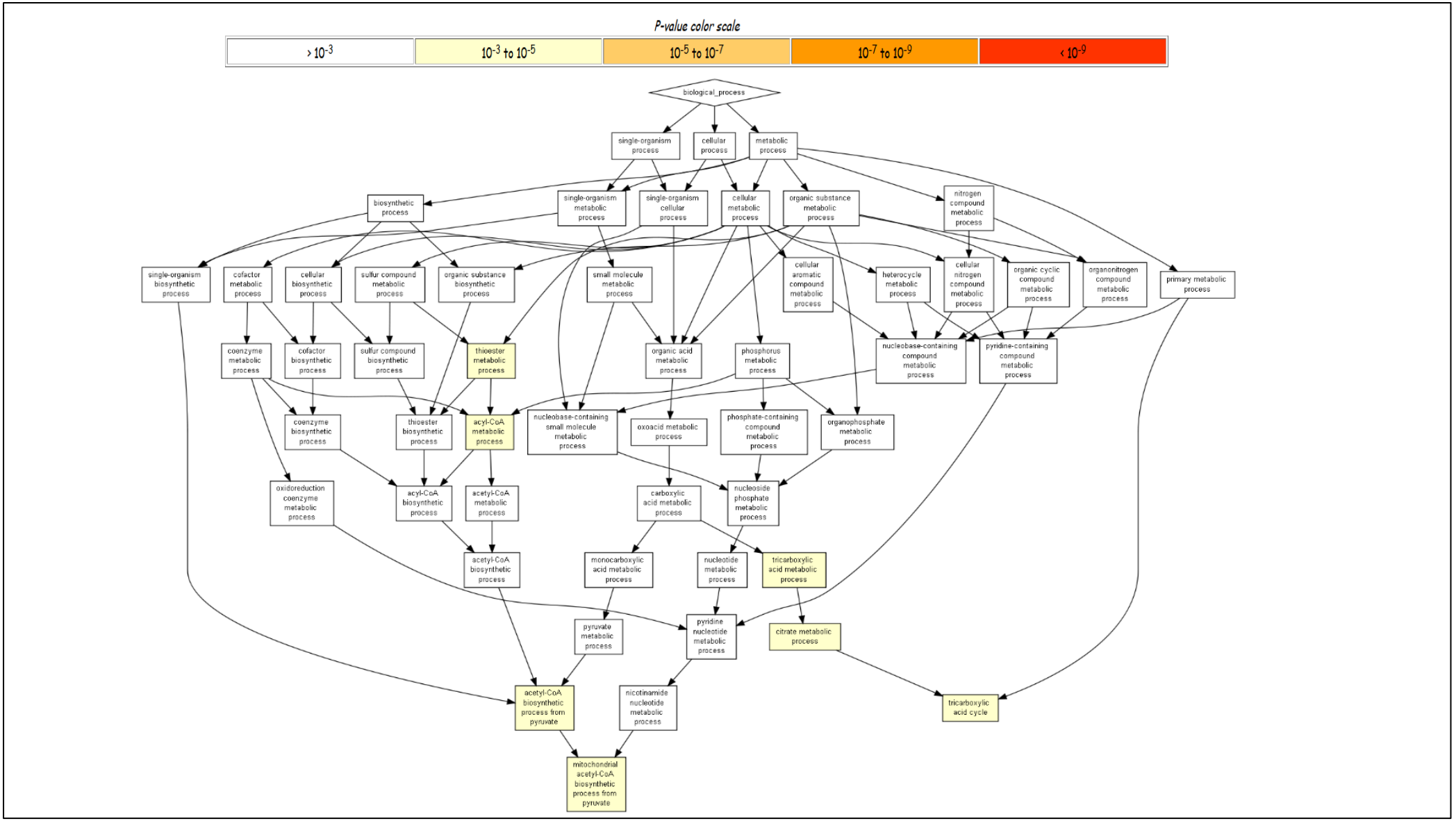

Figure 4.3.5.1 GOrilla analysis of biological process in soleus muscle. Highlighted terms were those determined to contain statistically significant relationships ($p \geq 10^{-3} \leq 10^{-5}$).

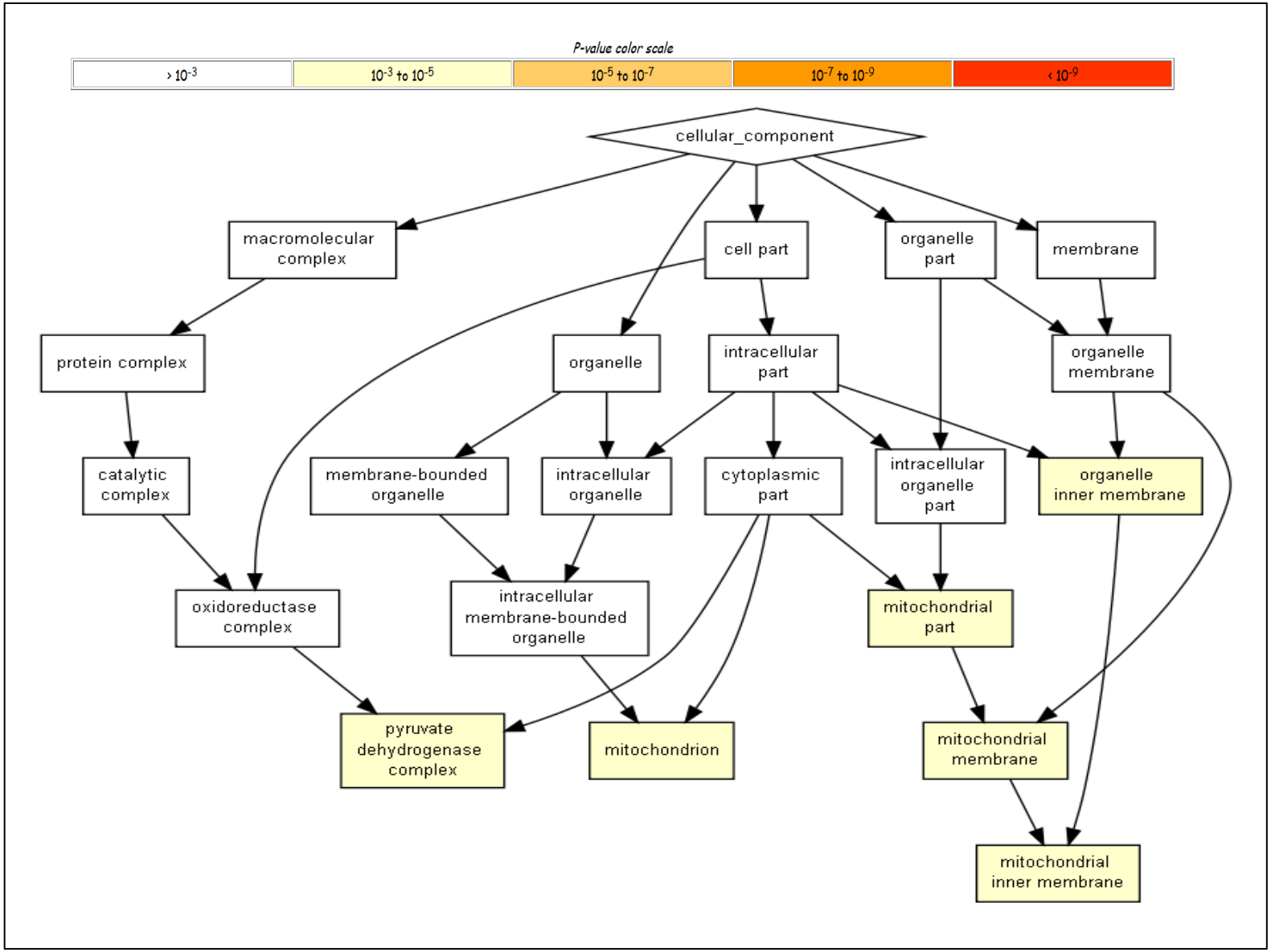

Figure 4.3.5.2 GOrilla cellular components in soleus muscle. Terms highlighted were those determined to contain statistically significant relationships ($p \geq 10^{-3} \leq 10^{-5}$).

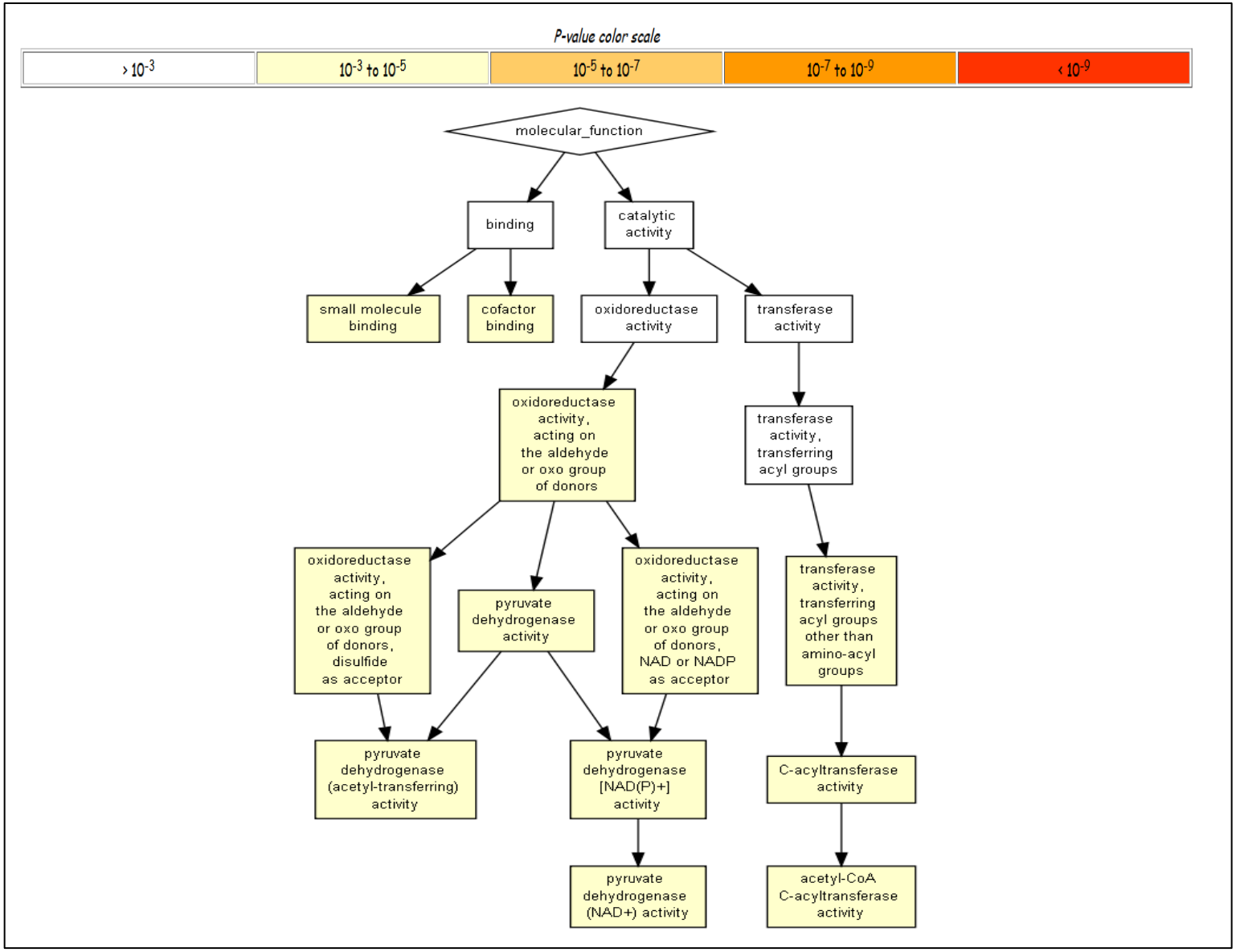

Figure 4.3.5.3 GOrilla analysis of soleus muscle molecular function. Terms highlighted were those determined to contain statistically significant relationships ($p \geq 10^{-3} \leq 10^{-5}$).

4.3.6 STRING Analysis of Significantly Changed Label Free Data

STRING (Search Tool for the Retrieval of Interacting Genes/Proteins) analysis highlights protein-protein interactions based on experimental evidence. The reference to gene ontologies enables the classification of groups of proteins from those detected in the mouse soleus label-free proteomics dataset. This enables identification of changes to protein-protein interactions within a group of similarly-functioning proteins. This was only performed on the significantly down regulated proteomics data as only a few proteins that were significantly up regulated were detected in the soleus muscle.

Figure 4.3.6.1 used the significantly down regulated dataset to highlight protein interactions for oxidation-reduction processes. This showed a large number of mitochondrial specific proteins involved in the electron transport chain such as subunits of Cytochrome b-c1 complex (UQCRH and UQCRC10) to three NADH dehydrogenases and GAPDH. The data presented here is detailed in table 4 which includes all proteins plus their associated label free proteomics data.

A)

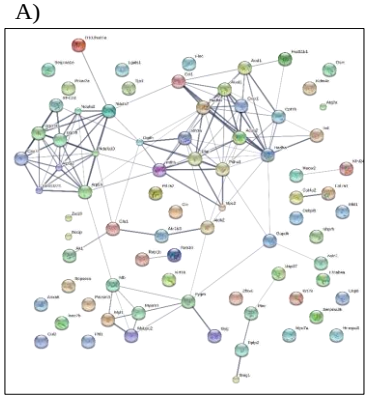

B)

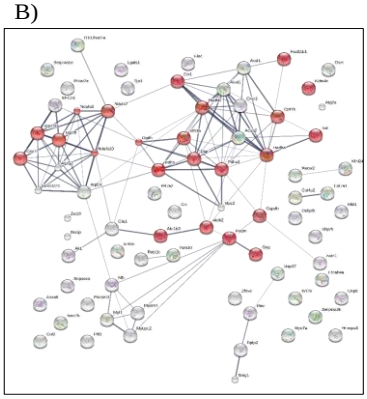

(C)

#pathway ID	pathway description	observed gene count	false discovery rate
GO.0055114	oxidation-reduction process	23	2.00E-11

Figure 4.3.6.1 Significantly down regulated proteins in the soleus muscle. (A) The whole dataset of 78 proteins. (B) Following enrichment for oxidation-reduction processes, 23 proteins are highlighted. (C) STRING data including the false detection rate for the interaction analysis.

Table 4 Significantly Down Regulated Proteins for STRING Analysis

Accession	Label	Significance (-10lgP)	Group Profile (Ratio)	Description
Q60597	ODO1	80.24	1.00:0.41	2-oxoglutarate dehydrogenase mitochondrial OS=Mus musculus GN=Ogdh PE=1 SV=3
P42125	D3D2	58.75	1.00:0.62	3 2-trans-enoyl-CoA isomerase mitochondrial OS=Mus musculus GN=Dci PE=2 SV=1
P47738	ALDH2	42.86	1.00:0.35	Aldehyde dehydrogenase mitochondrial OS=Mus musculus GN=Aldh2 PE=1 SV=1
P45376	ALDR	21.53	1.00:0.57	Aldose reductase OS=Mus musculus GN=Akr1b1 PE=1 SV=3
Q924X2	CPT1B	27.12	1.00:0.14	Carnitine O-palmitoyltransferase 1 muscle isoform OS=Mus musculus GN=Cpt1b PE=2 SV=1
P50172	DHI1	21.23	1.00:0.23	Corticosteroid 11-beta-dehydrogenase isozyme 1 OS=Mus musculus GN=Hsd11b1 PE=1 SV=3
P99028	QCR6	39.21	1.00:0.61	Cytochrome b-c1 complex subunit 6 mitochondrial OS=Mus musculus GN=Uqcrh PE=1 SV=2
Q8R1I1	QCR9	35.15	1.00:0.48	Cytochrome b-c1 complex subunit 9 OS=Mus musculus GN=Uqcr10 PE=1 SV=1
P17665	COX7C	58.1	1.00:0.52	Cytochrome c oxidase subunit 7C mitochondrial OS=Mus musculus GN=Cox7c PE=1 SV=1
Q8BMF4	ODP2	86.07	1.00:0.30	Dihydrolipoyllysine-residue acetyltransferase component of pyruvate dehydrogenase complex mitochondrial OS=Mus musculus GN=Dlat PE=1 SV=2
P16858	G3P	93.31	1.00:0.44	Glyceraldehyde-3-phosphate dehydrogenase OS=Mus musculus GN=Gapdh PE=1 SV=2
Q9WUB3	PYGM	22.63	1.00:0.59	Glycogen phosphorylase muscle form OS=Mus musculus GN=Pygm PE=1 SV=3
Q9R062	GLYG	20.45	1.00:0.62	Glycogenin-1 OS=Mus musculus GN=Gyg1 PE=2 SV=3
Q9D6R2	IDH3A	84.62	1.00:0.21	Isocitrate dehydrogenase [NAD] subunit alpha mitochondrial OS=Mus musculus GN=Idh3a PE=1 SV=1
Q9JHI5	IVD	33.04	1.00:0.29	Isovaleryl-CoA dehydrogenase mitochondrial OS=Mus musculus GN=Ivd PE=1 SV=1
Q8VCD7	KDM4C	89.79	1.00:0.24	Lysine-specific demethylase 4C OS=Mus musculus GN=Kdm4c PE=1 SV=1
Q9CQ91	NDUA3	22.19	1.00:0.54	NADH dehydrogenase [ubiquinone] 1 alpha subcomplex subunit 3 OS=Mus musculus GN=Ndufa3 PE=1 SV=1
Q9DCS9	NDUBA	34.34	1.00:0.53	NADH dehydrogenase [ubiquinone] 1 beta subcomplex subunit 10 OS=Mus musculus GN=Ndufb10 PE=1 SV=3
Q9DC70	NDUS7	21.78	1.00:0.64	NADH dehydrogenase [ubiquinone] iron-sulfur protein 7 mitochondrial OS=Mus musculus GN=Ndufs7 PE=1 SV=1
P35486	ODPA	80.8	1.00:0.13	Pyruvate dehydrogenase E1 component subunit alpha somatic form mitochondrial OS=Mus musculus GN=Pdha1 PE=1 SV=1
Q8BMS1	ECHA	50.21	1.00:0.02	Trifunctional enzyme subunit alpha mitochondrial OS=Mus musculus GN=Hadha PE=1 SV=1
Q99JY0	ECHB	92.84	1.00:0.15	Trifunctional enzyme subunit beta mitochondrial OS=Mus musculus GN=Hadhb PE=1 SV=1

Table 4. Global label free proteomics results for the significantly down regulated proteins used in figure 4.3.6.1 for STRING analysis.

A significant number of mitochondrial proteins were down regulated in the soleus with age. This highlights a distinct change to energy metabolism requirements in mouse soleus muscle as it ages.

4.3.7 Redox Changes in Mouse Soleus with Age

Redox cysteines were identified via differential labelling of soleus proteins using (*d*0-NEM and *d*5-NEM). It was postulated that a reduction in redox sensitive cysteines may impact the activity and therefore function of proteins.

Figure 4.3.7.1 indicates the numbers of redox, reduced and reversibly oxidised proteins in mouse soleus muscles for adult and old mice. The numbers indicate an overall increase in reversibly oxidised and reduced proteins in samples from old mice whereas a decrease in redox proteins was observed in adult mice. In the adult soleus, 173 proteins were detected and in the 24 month old, 174 were detected. Within the numbers of proteins detected there were a variety of differences between the different ages. The redox protein lists for adult and old soleus files archived as S7 – Soleus Adult Redox Proteins; S8 – Soleus Old Redox Proteins can be accessed at 10.17638/datacat.liverpool.ac.uk/437.

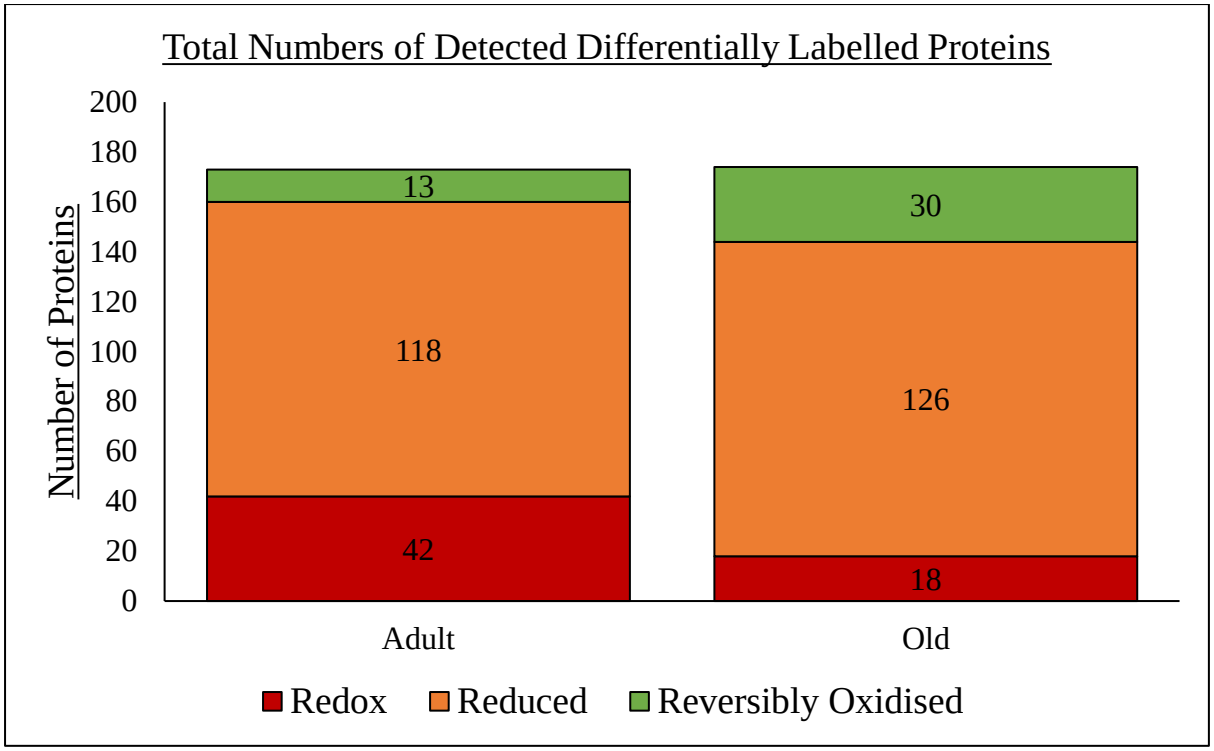

Figure 4.3.7.1 Numbers of proteins containing redox, reduced and reversibly oxidised cysteine-containing peptides in soleus muscle from adult and old mice.

The reduction in the number of redox sensitive cysteine containing proteins in soleus muscles of old mice may indicate a reduced flexibility in the protein to perform its function, or on a larger scale, a reduced ability of the cell to control or react to change in intracellular ROS concentrations.

Table 5 combines the global label free data on changes in protein significance with the group ratio difference of adult and old to indicate whether a protein changes its redox state with age. There was a significant representation of mitochondrial specific proteins as demonstrated by the proportion of energy metabolism proteins (e.g. cytochromes) relative to the number of cytoskeletal proteins when this data is compared to the quadriceps (see Chapter 5, p.184 for greater detail in comparing the muscles).

Table 5. Redox Cysteines in Soleus Muscle

Accession	Protein	Adult:Old	Significance (-10logP)	Peptide	Cysteine	Adult Red/Ox	Old Red/Ox
Q60597	**2-Oxoglutarate dehydrogenase (Mitochondrial)**	**1.00:0.41**	**80.24**	ICEEAFTR	566	4.02	21.91
Q99KI0	**Aconitate hydratase (Mitochondrial) (Aco2)**	**1.00:1.60**	**53.50**	DVGGIVLANACGPCIGQWDR	448/451*	3.18	8.43
				VGLIGSCTNSSYEDMGR	385	1.85	3.95
				VAVPSTIHCDHLIEAQVGGEK	126	4.35	11.59
O88990	Alpha-actinin-3 (Actn3)			CDIDIR	286	13.81	39.52
				LCYVALDFENEMATAASSSSLEK	218	11.14	16.23
P05202	Aspartate aminotransferase (Mitochondrial) (Got2)	1.00:1.02	7.39	VGAFTVVCK	295	1.90	13.05
Q9DCX2	**ATP synthase subunit d, mitochondrial (Fragment)(Atp5h)**	**1.00:0.38**	**61.87**	SCAEFVSGSQLR	101	24.99	129.81
P45591	Cofilin-2 (Cfl2)	1.00:1.43	18.30	LLPLNDCR	80	14.54	74.39
Q9CZ13	Cytochrome b-c1 complex subunit 1 (mitochondrial) (Uqcrc1)	1.00:0.89	8.96	LCTSATESEVTR	380	23.64	46.49
Q9DB77	Cytochrome b-c1 complex subunit 2 (mitochondrial) (Uqcrc2)	1.00:1.04	3.16	NALANPLYCPDYR	192	4833.44	90.84
P99028	**Cytochrome b-c1 complex subunit 6 (mitochondrial) (Uqcrh)**	**1.00:0.61**	**39.21**	ERLELCDNR	51	25.97	23.86
P21550	Beta-enolase (Eno3)	1.00:0.79	14.85	TGAPCR	399	8.89	22.85
				ACNCLLLK	337/339*	84.66	60.82
				VNQIGSVTESLQACK	357	7.14	20.73
P97447	**Four and a half LIM domains protein 1 (Fhl1)**	**1.00:0.13**	**113.70**	CSVNLANKR	255	476.66	99.38
P05064	**Fructose-bisphosphate aldolase A (Aldoa)**	**1.00:1.43**	**23.11**	ALANSLACQGK	339	21.69	53.27
P16858	**Glyceraldehyde-3-phosphate dehydrogenase (Gapdh)**	**1.00:0.44**	**93.31**	IVSNASCTTNCLAPLAK	150/154*	5524.28	278.52
P54071	Isocitrate dehydrogenase [NADP] (mitochondrial) (Idh2)	1.00:0.93	7.60	CATITPDEAR	113	0.02	0.01
P06151	L-Lactate dehydrogenase (Ldha)	1.00:0.68	25.24	VIGSGCNLDSAR	163	22.79	59.57
P51174	Long-chain specific acyl-CoA dehydrogenase (mitochondrial) (Acadl)	1.00:1.08	10.15	AFVDSCLQLHETK	351	2.73	23.99
				CIGAIAMTEPGAGSDLQGVR	166	7.54	14.97
P14152	Malate dehydrogenase (cytoplasmic) (Mdh1)	1.00:0.97	5.01	ENFSCLTR	154	8.23	43.95
				VIVVGNPANTNCLTASK	137	9.02	21.65
P08249	Malate dehydrogenase (mitochondrial) (Mdh2)	1.00:1.01	3.84	EGVVECSFVQSK	275	13.51	40.48
				ETECTYFSTPLLLGK	285	24.59	36.59
				GCDVVVIPAGVPR	93	4.48	16.30
				GYLGPEQLPDCLK	89	27.10	37.69
P13542	Myosin-8 (Myh8)			CNGVLEGIR	698	43.95	73.27
		1.00:1.22	3.97	HDCDLLR	1343	24.04	44.75
P09542	**Myosin light chain 3 (Myl3)**	**1.00:1.17**	**20.73**	ITYGQCGDVLR	85	54.39	67.53
				LMAGQEDSNGCINYEAFVK	191	15.56	27.26
P97457	Myosin regulatory light chain 2, skeletal muscle isoform (Mylpf)	1.00:0.73	45.56	NICYVITHGDAK	157	23.14	42.82
				QFLEELLTTQCDR	128	27.50	51.56
Q91YT0	NADH dehydrogenase [ubiquinone] flavoprotein 1, mitochondrial (Fragment) (Ndufv1)	1.00:1.01	5.73	YLVVNADEGEPGTCK	46	295.18	699.84
Q91VD9	NADH-ubiquinone oxidoreductase 75 kDa subunit (mitochondrial) (Ndufs1)	1.00:0.87	9.42	MCLVEIEK	78	115.96	3328.04
P07724	Serum albumin (Alb)	1.00:0.90	12.32	CSYDEHAK	58	3.83	4.87
P17751	Triosephosphate isomerase (Tpi1)	1.00:0.98	14.07	IIYGGSVTGATCK	268	19.41	45.36
		1.00:0.98	14.07	IAVAAQNCYK	117	731.14	1591.58
P13412	**Troponin I, fast skeletal muscle (Tnni2)**	**1.00:0.81**	**39.05**	VCMDLR	134	18.38	44.64
Q9WUZ5	Troponin I, slow skeletal muscle (Tnni1)	1.00:0.91	12.86	ECWEQEHEER	13	85.64	132.57
P58771	Tropomyosin 1, alpha, isoform CRA_i (Tpm1)	1.00:1.00	7.40	CAELEEELK	154	16.71	31.32
P21107	Tropomyosin alpha-3 chain (Tpm3)	1.00:1.19	13.81	CSELEEELK	154	55.27	76.49
Q6IRU2	Tropomyosin alpha-4 chain (Tpm4)	1.00:1.77	5.77	CGDLEEELK	154	14.01	36.23

Table 5. Redox-cysteine containing proteins detected via differential labelling. Significantly changed proteins are highlighted in **bold** and tryptic peptides are denoted with an asterisk (*).

Together these protein modifications, in addition to those tested using western blotting support the initial global proteomics data indicating ageing in mouse soleus muscle predominantly affects energy metabolism proteins by causing an increase in their reduced redox state.

Figure 4.3.7.2 shows redox peptides identified with both the *d*0-NEM and *d*5-NEM tags via tandem mass spectrometry and the figure reflects the data shown in Table 5. Several proteins are highlighted as increasing in their reduced state with age (suggesting a possible reduction in function) including a number of energy metabolism proteins such as NADH ubiquinone oxidoreductase (NDUFS1) Cys78 increasing 28.7 fold, Aspartate aminotransferase (GOT2) Cys295 6.86 fold, 2-oxoglutarate dehydrogenase (OGDH) Cys566 5.45 fold, ATP synthase subunit d (ATP5H) Cys101 5.19 fold, Cofilin-2 (CFL2) Cys80 5.12 fold and cytoplasmic Malate dehydrogenase (MDH1) Cys154 5.34 fold. Conversely Cytochrome b-c1 complex subunit 2 (UQCRC2) Cys192, Cytochrome b-c1 complex subunit 6 (UQCRH) Cys51, B-enolase (ENO3) 337/339*, Four and a half LIM domains proteins 1 (FHL1) Cys255 and Glyceraldehyde-3-phosphate dehydrogenase (GAPDH) Cys150/154* and Isocitrate dehydrogenase (IDH2) Cys113 all demonstrated becoming less reduced with age with Isocitrate dehydrogenase being reversibly oxidised in adult mice soleus muscle and becoming more reversibly oxidised in old mice soleus muscle.

Redox Cysteines in Adult and Old Mouse Soleus Muscle

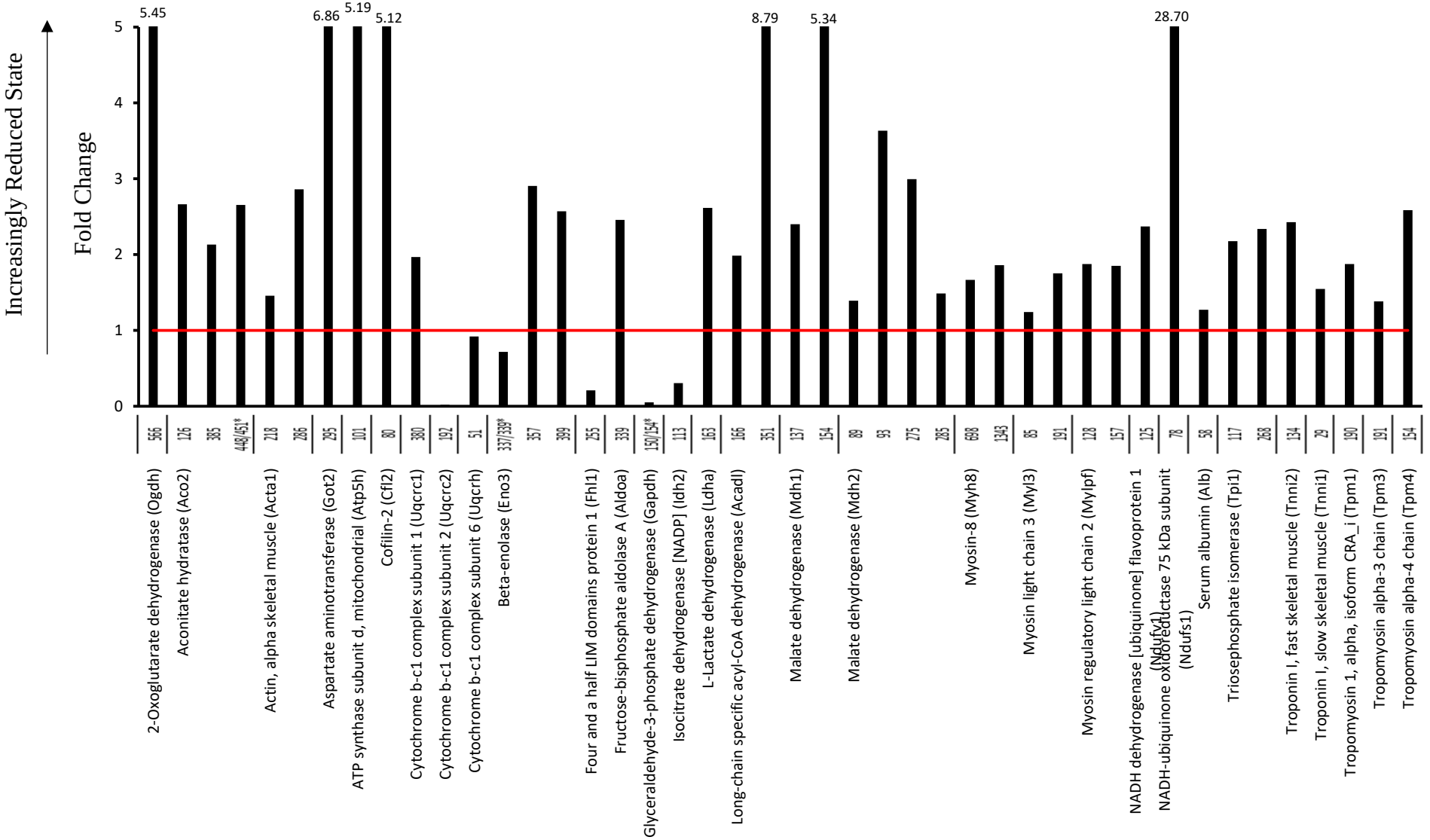

Figure 4.3.7.2 Redox-cysteine containing proteins including the specific redox-cysteine number, ratio change with age between adult and old mouse soleus muscle. Values > 1.0 indicate a reduced state, values < 1.0 indicate a reversibly oxidised state. Data are derived from Table 5.

4.3.8 Comparison of Differentially Labelled Proteins with Age

Venn diagrams of the redox, reduced and reversibly oxidised proteins were produced using VennDIS software to identify differences between the proteins in the label free proteomics data between soleus muscles of adult and old mice. In all diagrams, the colours of each slice are arbitrary. The data are subsequently used for STRING analysis in section 4.3.9. All tables listing individual proteins for each figure are located in supplementary information.

In figure 4.3.8.1 the redox, reduced and reversibly oxidised protein numbers were combined to consider overall differences between the soleus muscle of adult and old mice. Figure 4.3.8.1 highlights 46 proteins from the adult mouse soleus and includes energy metabolism proteins such as Aldehyde dehydrogenase (ALDH2) and Isocitrate dehydrogenase (IDH3A and IDH3G), Pyruvate dehydrogenase (PDHA1 and PDHB) and the cytosolic redox control protein Cu-Zn Superoxide Dismutase (SOD1). Proteins identified in samples of adult and old mice (127 proteins) in figure 4.3.8.1 include several energy metabolism proteins such as mitochondrial Aconitase (ACO2), various ATP synthases (ATP2A1, ATP2A3, ATP5A1, ATP5C1, ATP5E1 and ATP5H) and a number of NADH Oxidases. Data in figure 4.3.8.1 (containing 47 proteins) from old mice include the energy metabolism ATP synthase subunits ATP1A1 and ATP5F1, the H_2O_2 controlling PRDX6 and protein chaperones PARK7 and HSP1 (Chaperonin). The individual proteins identified are in the supplementary information (Table 4.3.8.1 A/B/C, p. 254-256).

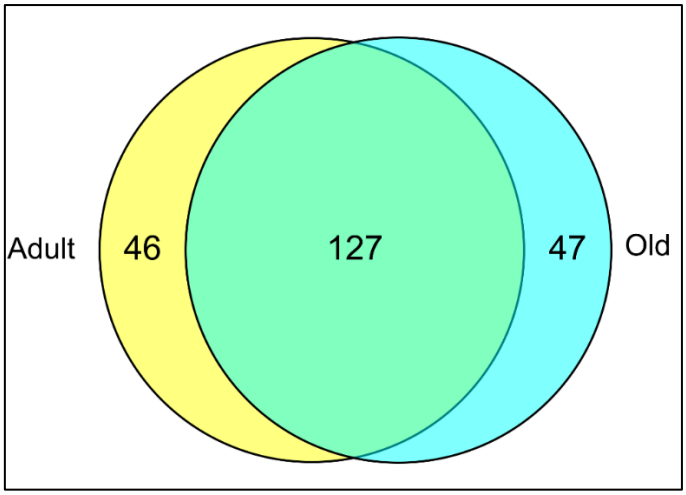

Figure 4.3.8.1 Venn diagram comparing differentially labelled proteins (redox, reduced and reversibly oxidised) from soleus muscle in adult and old mice identifying overall changes to differentially labelled proteins between the two groups. The individual protein lists are presented in the supplementary information (Table 4.3.8.1 A/B/C, p.254-256).

Figure 4.3.8.2 shows differentially labelled redox-only proteins (with both *d*0-NEM and *d*5-NEM) for adult mice (17 proteins). These highlight the redox control protein Cu-Zn Superoxide dismutase (SOD1) and a range of cellular energy metabolism proteins such as Glyceraldehyde 3-phosphate (GAPDH) and Isocitrate dehydrogenase 2 (IDH2). For proteins identified in soleus muscles for both adult and old mice (25 proteins) that were redox labelled, the list again included many energy metabolism proteins. Of note was Aconitase (ACO2). For proteins identified in the dataset for soleus muscle in old mice (5 proteins), of note was the ROS control protein Peroxiredoxin 6 (PRDX6). The individual proteins identified are presented in the supplementary information (Table 4.3.8.2 A/B/C, p.257-258).

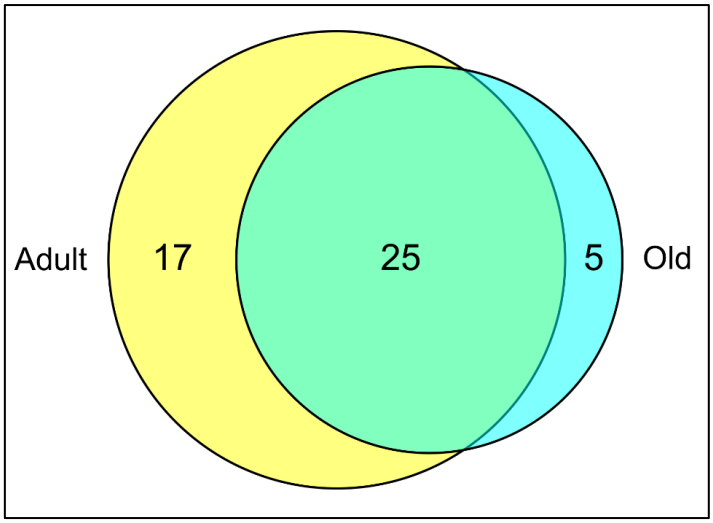

Figure 4.3.8.2 Venn diagram of redox proteins in the soleus muscle of adult and old mice from those identified as differentially labelled with both standard *N*-ethylmaleimide (*d*0-NEM) and heavy *N*-ethylmaleimide (*d*5-NEM). The individual proteins identified are presented in the supplementary information (Table 4.3.8.2 A/B/C, p.257-258).

The Venn diagram in figure 4.3.8.3 shows proteins that were only reduced, that is containing only the *d*5-NEM labelling. The list from adult mice (35 proteins) includes a number of proteins involved in glutathione metabolism such as Glutathione S-transferase κ and π, the chaperone and redox sensor protein PARK7 and energy metabolism proteins Isocitrate dehydrogenase 3 (IDH3A) and Aldehyde dehydrogenase (ALDH). For the central slice, containing proteins identified in soleus muscle for both adult and old mice (83 proteins), a range of energy metabolism proteins were identified in addition to Heat shock proteins 3, 4 and 6, and the mitochondrial ROS control protein Peroxiredoxin 3. In the soleus muscle from old mice (43 proteins), proteins of interest included the energy metabolism protein Glyceraldehyde 3-phosphate dehydrogenase (GAPDH), Protein disulphide isomerase (P4HB), involved in the formation and cleavage of disulphide bonds, and Glutathione peroxidase (GPX4). The individual proteins identified are presented in the supplementary information (Table 4.3.8.3 A/B/C, p.259-261).

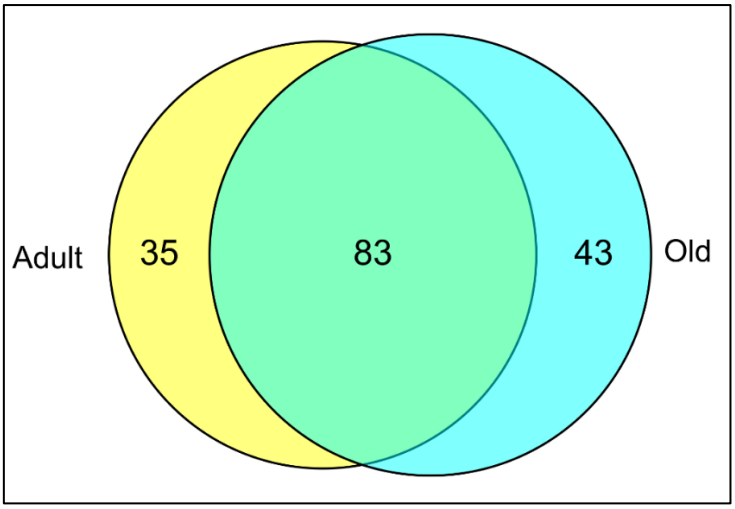

Figure 4.3.8.3 Venn diagram of reduced labelled proteins (*d*0-NEM) in soleus muscle between adult and old mice. The individual proteins are presented in the supplementary information (Table 4.3.8.3 A/B/C, p.259-261).

Figure 4.3.8.4 shows proteins that were reversibly oxidised (containing only *d*5-NEM labelling). This identifies 4 proteins for adult muscles, 9 identified in soleus muscle from both adult and old mice and 9 proteins in soleus muscle from old mice. No particular proteins of interest to skeletal muscle ageing were observed in this dataset. In the set for adult mice collagen binding proteins (such as Fibromodulin) were observed and Cytochrome c oxidase (COX6B) for energy metabolism in both ages of mice. Finally, three immunoglobulins were observed in the reversibly oxidised data set for old mice. The individual proteins identified are presented in the supplementary information (Table 4.3.8.4 A/B/C, p.262).

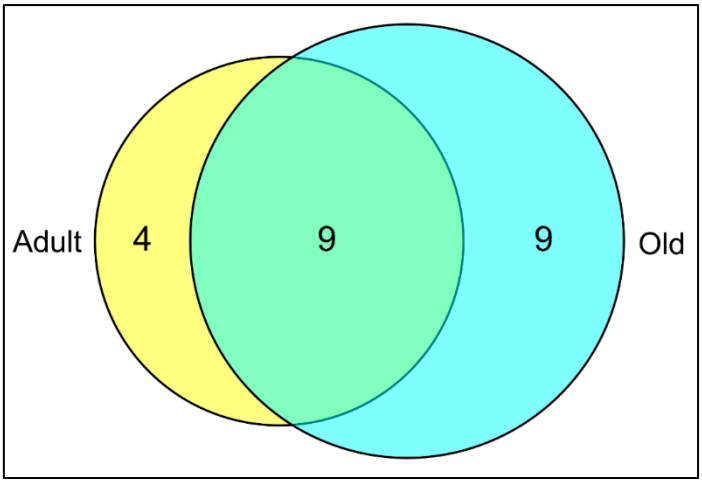

Figure 4.3.8.4 Venn diagram of reversibly oxidised proteins (labelled with only *d*5-NEM) in adult and old soleus muscle. The individual proteins identified are presented in the supplementary information (Table 4.3.8.4 A/B/C, p.262).

4.3.9 STRING Analysis of Differentially Labelled Proteins

STRING identifies protein-protein interactions between differentially labelled proteins of the soleus muscle. Following the differential labelling and mass spectrometry analysis indicating whether a protein is redox, reduced or reversibly oxidised, the data were then filtered using VennDIS to separate proteins observed in samples from either adult or old mice, or in both ages of mice. Due to the low number of redox proteins from old mice, they could not be analysed due to the statistical stringencies of the STRING algorithm.

The data in figure 4.3.9.1 shows protein interactions following enrichment for oxidation-reduction mechanisms in redox proteins of the soleus from adult mice. A strong link was observed between two mitochondrial Cytochrome b-c1 complex subunits (UQCRC1 and UQCRC2) and NADH dehydrogenase (NDUFV1). The energy metabolism protein Glyceraldehyde 3-phosphate dehydrogenase (GAPDH) appears to weakly link to Isocitrate dehydrogenase (IDH2) and Cu-Zn Superoxide dehydrogenase (SOD1) in addition to the Cytochrome b-c1 complex subunit (UQCRC1).

(A)

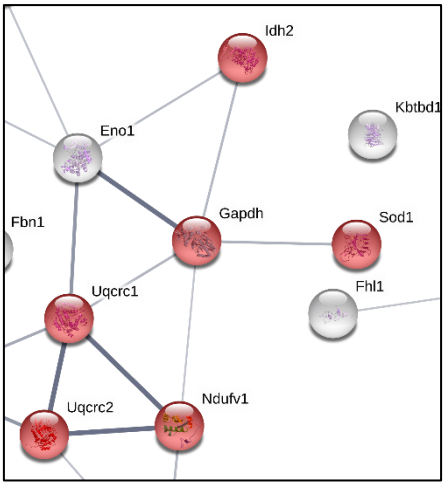

(B)

#pathway ID	pathway description	observed gene count	false discovery rate
GO.0055114	oxidation-reduction process	6	0.00861

(C)

Accession	Protein	Significance (-10lgP)	Group Profile (Ratio)	Description
Q9CZ13	QCR1_MOUSE	8.96	1.00:0.89	Cytochrome b-c1 complex subunit 1 mitochondrial OS=Mus musculus GN=Uqcrc1 PE=1 SV=1
Q9DB77	QCR2_MOUSE	3.16	1.00:1.04	Cytochrome b-c1 complex subunit 2 mitochondrial OS=Mus musculus GN=Uqcrc2 PE=1 SV=1
P16858	G3P_MOUSE	93.31	1.00:0.44	Glyceraldehyde-3-phosphate dehydrogenase OS=Mus musculus GN=Gapdh PE=1 SV=2
P54071	IDHP_MOUSE	7.6	1.00:0.93	Isocitrate dehydrogenase [NADP] mitochondrial OS=Mus musculus GN=Idh2 PE=1 SV=3
Q91YT0	NDUV1_MOUSE	5.73	1.00:1.01	NADH dehydrogenase [ubiquinone] flavoprotein 1 mitochondrial OS=Mus musculus GN=Ndufv1 PE=1 SV=1
P08228	SODC_MOUSE	7.72	1.00:1.06	Superoxide dismutase [Cu-Zn] OS=Mus musculus GN=Sod1 PE=1 SV=2

Figure 4.3.9.1 Soleus redox proteins from adult mice enriched for oxidation-reduction processes. (A) Visualisation of protein interactions. (B) GO Pathway ID and FDR for the observations. (C) Global label free results for the identified proteins in (A).

Figure 4.3.9.2 shows redox data enriched for oxidative phosphorylation from adult mice as this is a key metabolic process in soleus muscle. Protein interactions identified were between the energy metabolism proteins UQCRC1, UQCRC2, NDUFV1 and ATP synthase ε (mitochondrial) (ATP5E).

(A)

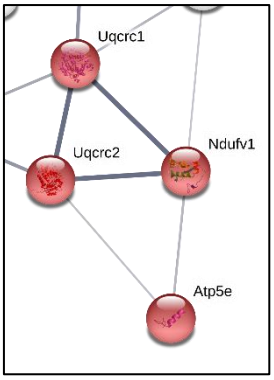

(B)

#pathway ID	pathway description	observed gene count	false discovery rate
190	Oxidative phosphorylation	4	0.000213

(C)

Accession	Significance (-10lgP)	Group Profile (Ratio)	Description
P56382	2.35	1.00:1.19	ATP synthase subunit epsilon mitochondrial OS=Mus musculus GN=Atp5e PE=2 SV=2
Q9CZ13	8.96	1.00:0.89	Cytochrome b-c1 complex subunit 1 mitochondrial OS=Mus musculus GN=Uqcrc1 PE=1 SV=1
Q9DB77	3.16	1.00:1.04	Cytochrome b-c1 complex subunit 2 mitochondrial OS=Mus musculus GN=Uqcrc2 PE=1 SV=1
Q91YT0	5.73	1.00:1.01	NADH dehydrogenase [ubiquinone] flavoprotein 1 mitochondrial OS=Mus musculus GN=Ndufv1 PE=1 SV=1

Figure 4.3.9.2 STRING analysis of soleus redox proteins enriched for oxidative phosphorylation from adult mice. (A) Visualisation of protein interactions. (B) GO Pathway ID and FDR for the observations. (C) Global label free results for the identified proteins in (A).

Data enriched for glycolysis and gluconeogenesis interactions from adult and old mice are shown in figure 4.3.9.3. These data highlight strong protein interactions between β-Enolase (ENO3), L-lactate dehydrogenase A chain (LDHA), L-lactate dehydrogenase B chain (LDHB), Triosephosphate isomerase (TPI1) and Fructose-bisphosphate aldolase A (ALDOA). The result highlights glycolytic proteins identified in soleus from adult and old mice while STRING analysis showed interactions between similar types of proteins. The global label free data showed only LDHA was significantly down regulated suggesting different extents of ageing affecting glycolytic systems in mouse soleus with age.

(A)

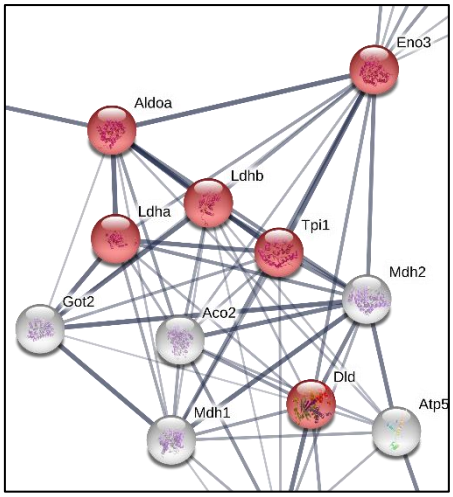

(B)

#pathway ID	pathway description	observed gene count	false discovery rate
10	Glycolysis / Gluconeogenesis	6	5.26E-09

(C)

Accession	Protein	Significance (-10lgP)	Group Profile (Ratio)	Description
P21550	ENOB_MOUSE	14.85	1.00:0.79	Beta-enolase OS=Mus musculus GN=Eno3 PE=1 SV=3
O08749	DLDH_MOUSE	6.88	1.00:1.07	Dihydrolipoyl dehydrogenase mitochondrial OS=Mus musculus GN=Dld PE=1 SV=2
P05064	ALDOA_MOUSE	23.11	1.00:1.43	Fructose-bisphosphate aldolase A OS=Mus musculus GN=Aldoa PE=1 SV=2
P06151	LDHA_MOUSE	25.24	1.00:0.68	L-lactate dehydrogenase A chain OS=Mus musculus GN=Ldha PE=1 SV=3
P16125	LDHB_MOUSE	19.42	1.00:0.82	L-lactate dehydrogenase B chain OS=Mus musculus GN=Ldhb PE=1 SV=2
P17751	TPIS_MOUSE	14.07	1.00:0.98	Triosephosphate isomerase OS=Mus musculus GN=Tpi1 PE=1 SV=3

Figure 4.3.9.3 (A) STRING analysis of redox proteins in the soleus from adult and old mice following enrichment for glycolysis/gluconeogenesis. (B) STRING pathway information. (C) Global label free proteomics data of proteins highlighted in (A).

Figure 4.3.9.4 shows the reduced proteins from soleus samples enriched for oxidative-phosphorylation from adult and old mice. This highlighted Acyl carrier protein (NDUFAB1), ATP synthase subunits (ATP5A1 and ATP5C1), Cytochrome c1 haeme protein (CYC1), NADH dehydrogenases (NDUFA7, NDUFA9, NDUFS2 and NDUFS6), NADH-ubiquinone subunit (MTND3) and Succinate dehydrogenase (SDHA), all were mitochondrial-based. The STRING pathway shows the global label free proteomics data but none of the proteins significantly changed in abundance with age. These results show the proteins in reduced form were involved in oxidative phosphorylation in soleus muscle of adult and old mice and highlighted interactions between a number of ATP synthases and NADH dehydrogenases for cellular energy metabolism.

(A)

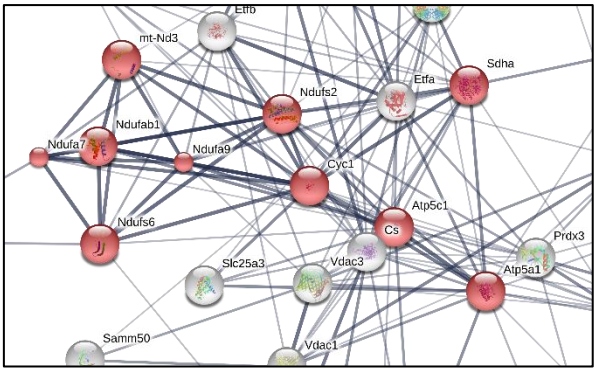

(B)

#pathway ID	pathway description	observed gene count	false discovery rate
190	Oxidative phosphorylation	10	2.43E-09

(C)

Accession	Protein	Significance (-10lgP)	Group Profile (Ratio)	Description
Q9CR21	ACPM_MOUSE	4.66	1.00:0.92	Acyl carrier protein mitochondrial OS=Mus musculus GN=Ndufab1 PE=1 SV=1
Q03265	ATPA_MOUSE	25.64	1.00:1.34	ATP synthase subunit alpha mitochondrial OS=Mus musculus GN=Atp5a1 PE=1 SV=1
Q91VR2	ATPG_MOUSE	6.91	1.00:1.09	ATP synthase subunit gamma mitochondrial OS=Mus musculus GN=Atp5c1 PE=1 SV=1
Q9D0M3	CY1_MOUSE	8.59	1.00:0.88	Cytochrome c1 heme protein mitochondrial OS=Mus musculus GN=Cyc1 PE=1 SV=1
Q9Z1P6	NDUA7_MOUSE	3.15	1.00:1.01	NADH dehydrogenase [ubiquinone] 1 alpha subcomplex subunit 7 OS=Mus musculus GN=Ndufa7 PE=1 SV=3
Q9DC69	NDUA9_MOUSE	3.58	1.00:1.12	NADH dehydrogenase [ubiquinone] 1 alpha subcomplex subunit 9 mitochondrial OS=Mus musculus GN=Ndufa9 PE=1 SV=1
Q91WD5	NDUS2_MOUSE	10.18	1.00:0.65	NADH dehydrogenase [ubiquinone] iron-sulfur protein 2 mitochondrial OS=Mus musculus GN=Ndufs2 PE=1 SV=1
P52503	NDUS6_MOUSE	4.29	1.00:0.94	NADH dehydrogenase [ubiquinone] iron-sulfur protein 6 mitochondrial OS=Mus musculus GN=Ndufs6 PE=1 SV=2
P03899	NU3M_MOUSE	3.89	1.00:0.73	NADH-ubiquinone oxidoreductase chain 3 OS=Mus musculus GN=Mtnd3 PE=3 SV=3
Q8K2B3	DHSA_MOUSE	10.12	1.00:0.91	Succinate dehydrogenase [ubiquinone] flavoprotein subunit mitochondrial OS=Mus musculus GN=Sdha PE=1 SV=1

Figure 4.3.9.4 STRING analysis of reduced proteins from soleus muscle in adult and old mice. (A) Protein interactions following enrichment for oxidative phosphorylation. (B) STRING pathway analysis information. (C) Global label free proteomics data for proteins highlighted in (A).

Figure 4.3.9.5 shows interactions between proteins with reduced cysteines following enrichment for oxidation-reduction processes in adult and old mice. This highlights 13 proteins in NADH dehydrogenases (NDUFV1, NDUFA12 and NDUFB9), Cytochrome b-c1 complexes (UQCRC1 and UQCRC2), the protein chaperone PARK7, Protein disulphide isomerase (P4HB), Δ(3,5)-Δ(2,4)-dienoyl-CoA isomerase (ECH1), 2-oxoglutarate dehydrogenase (OGDH), Glutamate dehydrogenase (GLUD1), Isocitrate dehydrogenase 2 (IDH2) and Glyceraldehyde 3-phosphate dehydrogenase (GAPDH). The result indicates a number of reduced proteins with age involved in oxidation-reduction reactions. Furthermore, the global label free result showed that two proteins were significantly decreased in protein abundance (OGDH and GAPDH). Together this information indicates the effect of ageing to different extents on proteins where many can be reduced with age thereby affecting their

performance as enzymes whilst only one or two demonstrate a change in abundance suggesting less of an effect on protein transcription.

(A)

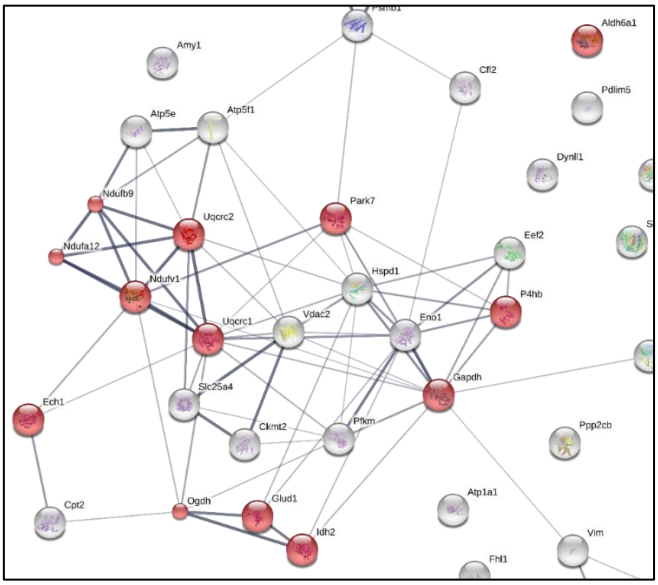

(B)

#pathway ID	pathway description	observed gene count	false discovery rate
GO.0055114	oxidation-reduction process	13	1.10E-06

(C)

Accession	Label	Significance (-10lgP)	Group Profile (Ratio)	Description
Q60597	ODO1_MOUSE	80.24	1.00:0.41	2-oxoglutarate dehydrogenase mitochondrial OS=Mus musculus GN=Ogdh PE=1 SV=3
Q9CZ13	QCR1_MOUSE	8.96	1.00:0.89	Cytochrome b-c1 complex subunit 1 mitochondrial OS=Mus musculus GN=Uqcrc1 PE=1 SV=1
Q9DB77	QCR2_MOUSE	3.16	1.00:1.04	Cytochrome b-c1 complex subunit 2 mitochondrial OS=Mus musculus GN=Uqcrc2 PE=1 SV=1
O35459	ECH1_MOUSE	15.72	1.00:1.20	Delta(3 5)-Delta(2 4)-dienoyl-CoA isomerase mitochondrial OS=Mus musculus GN=Ech1 PE=2 SV=1
P26443	DHE3_MOUSE	22.38	1.00:1.27	Glutamate dehydrogenase 1 mitochondrial OS=Mus musculus GN=Glud1 PE=1 SV=1
P16858	G3P_MOUSE	93.31	1.00:0.44	Glyceraldehyde-3-phosphate dehydrogenase OS=Mus musculus GN=Gapdh PE=1 SV=2
P54071	IDHP_MOUSE	7.6	1.00:0.93	Isocitrate dehydrogenase [NADP] mitochondrial OS=Mus musculus GN=Idh2 PE=1 SV=3
Q9EQ20	MMSA_MOUSE	3.13	1.00:1.36	Methylmalonate-semialdehyde dehydrogenase [acylating] mitochondrial OS=Mus musculus GN=Aldh6a1 PE=1 SV=1
Q7TMF3	NDUAC_MOUSE	11.61	1.00:0.69	NADH dehydrogenase [ubiquinone] 1 alpha subcomplex subunit 12 OS=Mus musculus GN=Ndufa12 PE=1 SV=2
Q9CQJ8	NDUB9_MOUSE	4.6	1.00:0.63	NADH dehydrogenase [ubiquinone] 1 beta subcomplex subunit 9 OS=Mus musculus GN=Ndufb9 PE=1 SV=3
Q91YT0	NDUV1_MOUSE	5.73	1.00:1.01	NADH dehydrogenase [ubiquinone] flavoprotein 1 mitochondrial OS=Mus musculus GN=Ndufv1 PE=1 SV=1
P09103	PDIA1_MOUSE	4.16	1.00:1.07	Protein disulfide-isomerase OS=Mus musculus GN=P4hb PE=1 SV=1
Q99LX0	PARK7_MOUSE	1.81	1.00:0.99	Protein DJ-1 OS=Mus musculus GN=Park7 PE=1 SV=1

Figure 4.3.9.5 STRING analysis of reduced proteins enriched for oxidation-reduction processes from soleus muscle in old mice. (A) Protein interactions following enrichment for oxidation-reduction processes. (B) STRING pathway information. (C) Global label free proteomics data for enriched proteins in (A).

Figure 4.3.9.6 shows the reduced cysteines from soleus muscle enriched for oxidative phosphorylation due to its prominence in soleus energy metabolism. This highlights seven proteins and includes the corresponding label free data from the global proteomics analysis. Interactions between ATP synthases (ATP5E, ATP5F1), NADH dehydrogenases (NDUFB9, NDUFA12, NDUFV1) and Cytochrome b-c1 complexes (UQCRC2 and UQCRC1) are apparent. These results showed fewer interactions between proteins in the soleus for oxidative

phosphorylation when compared to adult data in figure 4.3.9.4 suggesting a reduced demand for oxidative phosphorylation in the soleus as the cells age.

(A)

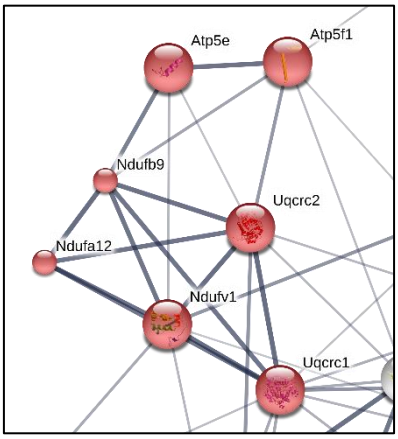

(B)

#pathway ID	pathway description	observed gene count	false discovery rate
190	Oxidative phosphorylation	7	2.23E-07

(C)

Accession	Label	Significance (-10lgP)	Group Profile (Ratio)	Description
Q9CQQ7	AT5F1_MOUSE	5.03	1.00:0.84	ATP synthase subunit b, mitochondrial OS=Mus musculus GN=Atp5f1 PE=1 SV=1
P56382	ATP5E_MOUSE	2.35	1.00:1.19	ATP synthase subunit epsilon, mitochondrial OS=Mus musculus GN=Atp5e PE=2 SV=2
Q9CZ13	QCR1_MOUSE	8.96	1.00:0.89	Cytochrome b-c1 complex subunit 1, mitochondrial OS=Mus musculus GN=Uqcrc1 PE=1 SV=1
Q9DB77	QCR2_MOUSE	3.16	1.00:1.04	Cytochrome b-c1 complex subunit 2, mitochondrial OS=Mus musculus GN=Uqcrc2 PE=1 SV=1
Q7TMF3	NDUAC_MOUSE	11.61	1.00:0.69	NADH dehydrogenase [ubiquinone] 1 alpha subcomplex subunit 12 OS=Mus musculus GN=Ndufa12 PE=1 SV=2
Q9CQJ8	NDUB9_MOUSE	4.6	1.00:0.63	NADH dehydrogenase [ubiquinone] 1 beta subcomplex subunit 9 OS=Mus musculus GN=Ndufb9 PE=1 SV=3
Q91YT0	NDUV1_MOUSE	5.73	1.00:1.01	NADH dehydrogenase [ubiquinone] flavoprotein 1, mitochondrial OS=Mus musculus GN=Ndufv1 PE=1 SV=1

Figure 4.3.9.6 STRING analysis of reduced proteins from soleus muscle in old mice. (A) protein interaction following enrichment for oxidative phosphorylation. (B) STRING pathway information. (C) Global label free proteomics data for proteins highlighted in (A).

Overall the STRING analysis of protein interactions from the lists produced from soleus muscle from adult, old and both ages of mice, indicate many links between energy metabolism proteins. This highlighted clusters of proteins involved in specific intracellular functions which enabled a focused evaluation of the global label free data combined with the lists of redox-cysteine containing proteins identified previously. Together, these data gave insight into the changing intracellular dynamic of energy metabolism via oxidation-reduction, oxidative phosphorylation and glycolysis.

4.3.10 Motif-X Analysis of the Cysteine Microenvironment

Motif-X enables identification of conserved sequence motifs across a sample of peptides. Soleus peptides were selected from the differentially labelled dataset with a central cysteine selected and the same parameters as used to analyse the quadriceps were followed. All parameters included a significance of $p \leq 0.01$.

Figure 4.3.10A shows glutamic acid was identified in soleus redox peptides from adult mice at +5 from the central cysteine. It contains an acidic side chain giving a negative overall charge to the molecule (Berg et al., 2002).

Isoleucine was detected (figure 4.3.10B) as being conserved at +4 from a central cysteine amino acid in proteins with reduced cysteines from adult mice. Isoleucine contains a chiral centre around which the other attached molecular groups can rotate leading to isomerisation however only one isomer is found in proteins. It is hydrophobic in nature due to its aliphatic side chain (Berg et al., 2002).

In figure 4.3.10C, at -4 from a central cysteine, Aspartate, the deprotonated form of Aspartic acid, was identified in soleus samples with reversibly oxidised cysteines from adult mice. It has an overall negative charge however in certain circumstances can accept a proton thereby affecting its conformation (Berg et al., 2002).

In soleus for old mice (figure 4.3.10D) Isoleucine was again identified as a conserved amino acid at +4 from the central cysteine. As previously described it contains a chiral centre although only one isomer is present in proteins. It is hydrophobic due to its aliphatic side chain (Berg et al., 2002).

Motif-X analysis of reduced soleus peptides from old mice in figure 4.3.10E identified a conserved glutamate at +2 from the central cysteine. Glutamate, as previously described, has

a negative charge due to its deprotonated form and in certain instances can accept protons. This enables important functionality in particular circumstances (Berg et al., 2002).

Analysis of reversibly oxidised peptides from old soleus of old mice in figure 4.3.10F identified an Aspartate at -4. As previously described, this amino acid is the deprotonated form of aspartic acid giving it a negative charge since it has a carboxylate side chain. In addition to this, changes to amino acids near to redox cysteine will also likely impact their pK_a and thereby affecting disulphide bond formation which in turn will affect protein function if the cysteine is located at an active site or structurally important location (Berg et al., 2002).

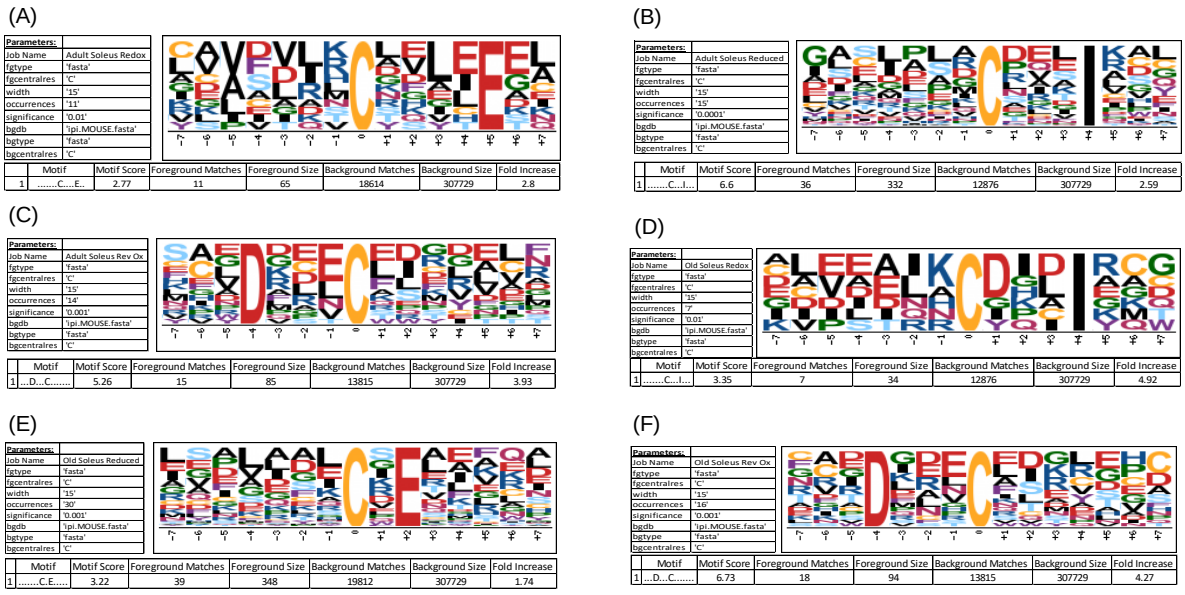

Parameters:	
Job Name	Adult Soleus Redox
fgtype	'fasta'
fgcentralres	'C'
width	'15'
occurrences	'11'
significance	'0.01'
bgdb	'ipi.MOUSE.fasta'
bgtype	'fasta'
bgcentralres	'C'

	Motif	Motif Score	Foreground Matches	Foreground Size	Background Matches	Background Size	Fold Increase
1	.....C....E..	2.77	11	65	18614	307729	2.8

Parameters:	
Job Name	Adult Soleus Reduced
fgtype	'fasta'
fgcentralres	'C'
width	'15'
occurrences	'15'
significance	'0.0001'
bgdb	'ipi.MOUSE.fasta'
bgtype	'fasta'
bgcentralres	'C'

	Motif	Motif Score	Foreground Matches	Foreground Size	Background Matches	Background Size	Fold Increase
1	.....C...I...	6.6	36	332	12876	307729	2.59

Parameters:	
Job Name	Adult Soleus Rev Ox
fgtype	'fasta'
fgcentralres	'C'
width	'15'
occurrences	'14'
significance	'0.001'
bgdb	'ipi.MOUSE.fasta'
bgtype	'fasta'
bgcentralres	'C'

	Motif	Motif Score	Foreground Matches	Foreground Size	Background Matches	Background Size	Fold Increase
1	...D...C.....	5.26	15	85	13815	307729	3.93

Parameters:	
Job Name	Old Soleus Redox
fgtype	'fasta'
fgcentralres	'C'
width	'15'
occurrences	'7'
significance	'0.01'
bgdb	'ipi.MOUSE.fasta'
bgtype	'fasta'
bgcentralres	'C'

	Motif	Motif Score	Foreground Matches	Foreground Size	Background Matches	Background Size	Fold Increase
1	.....C...I...	3.35	7	34	12876	307729	4.92

Parameters:	
Job Name	Old Soleus Reduced
fgtype	'fasta'
fgcentralres	'C'
width	'15'
occurrences	'30'
significance	'0.001'
bgdb	'ipi.MOUSE.fasta'
bgtype	'fasta'
bgcentralres	'C'

	Motif	Motif Score	Foreground Matches	Foreground Size	Background Matches	Background Size	Fold Increase
1	.....C.E.....	3.22	39	348	19812	307729	1.74

Parameters:	
Job Name	Old Soleus Rev Ox
fgtype	'fasta'
fgcentralres	'C'
width	'15'
occurrences	'16'
significance	'0.001'
bgdb	'ipi.MOUSE.fasta'
bgtype	'fasta'
bgcentralres	'C'

	Motif	Motif Score	Foreground Matches	Foreground Size	Background Matches	Background Size	Fold Increase
1	...D...C.....	6.73	18	94	13815	307729	4.27

Figure 4.3.10. Motif-X analysis of redox cysteine containing proteins. (A) Redox peptide from the soleus adult mice highlighting a conserved glutamic acid at +5 from the central cysteine. (B) Reduced peptides from soleus muscles in adult mice highlighting a conserved isoleucine at +4 from the central cysteine. (C) Reversibly oxidised cysteine in peptides isolated from soleus muscle in adult mice with a conserved aspartic acid at -4 from the central cysteine. (D) Soleus redox peptide sequences from old mice with an Isoleucine identified at +4 from the central cysteine. (E) Soleus reduced peptides from old mice with a conserved glutamic acid at +2 from the central cysteine. (F) Soleus reversibly oxidised peptides from old mice with a conserved aspartic acid at -4 from the central cysteine.

The Motif-X data showed changes to amino acid sequences within a specific vicinity of a central cysteine residue. Future work would consider how this affects protein structure and

function as highlighted in Table 5 (p.161) regarding redox state changes with age. In addition to this, proteomics work identifying changes to proteins and peptide sequences may help to elucidate age-related changes in the redox biochemistry of the soleus skeletal muscle (Berg et al., 2002).

4.4 Discussion

The soleus is a slow twitch muscle involved in longer term contractions such as distance running and posture control (Deldicque et al., 2010). I hypothesised that the redox state of intracellular proteins would change with age (see section 4.2, p.136) and the overall results of this chapter support this hypothesis and identified a number of changes to redox control proteins with age in the Soleus, in the addition to changes in redox state of proteins of interest.

Section 4.3.3 looked at the label free proteomics data using a volcano plot. Figure 4.3.3.3 indicates a range of significantly changed proteins identified via accession numbers between individual adult and old mouse muscle samples. Significantly decreased proteins included a number of mitochondria-based energy metabolism proteins such as Cytochrome c oxidase subunit 7C (COX7C), Glyceraldehyde-3-phosphate dehydrogenase (G3P/GAPDH) and ATP synthase subunit d (ATP5H) highlighting a reduction in oxidative energy metabolism in the mouse soleus. Conversely, significantly increased proteins included Aconitase (ACON), Glutathione Peroxidase 1 (GPX41) and Electron transfer flavoprotein (ETFB). Aconitase and Electron transfer flavoprotein are important energy metabolism enzymes involved in the citric acid cycle and electron transfers within the mitochondria respectively. Glutathione Peroxidase is an antioxidant enzyme that protects against lipid peroxidation (Yant et al., 2003, Seiler et al., 2008). This examination of the label free data from soleus muscle therefore indicates a reduction in energy metabolism with age which is in contrast to the changes observed in the quadriceps where cytoskeletal proteins were mainly affected. These changes suggest a disparity

between energy metabolism pathways within the cell during ageing which has been identified in other rodent studies (Garvey et al., 2014, Yarovaya et al., 2002). It may be an indication of effects seen relating to decreased muscle strength with age which may help to explain changes in posture observed with age given the function of the soleus in both rodents and humans (Goulart et al., 2000, Deldicque et al., 2011). In a more general context other studies have demonstrated the effect of increased ROS concentrations having a negative impact on muscle force generation (Reid, 2001, Jackson, 2008). The data presented here add to this body of increasing knowledge that changes to redox states of proteins, specifically in relation to energy metabolism, may eventually provide a direct link between intracellular ROS control and the physiological outcome of ageing in skeletal muscle.

Redox Ageing

This study assessed certain proteins of interest known to be involved in intracellular redox control. Data in figure 4.3.7.1 highlights a decrease in the number of redox-flexible proteins and shows an increase in the number of reduced proteins with age in mouse soleus muscle. Figure 4.7.3.2 shows the fold change of redox proteins identified via differential labelling. Several proteins are highlighted as increasing in their reduced state with age (suggesting a possible reduction in function) including a number of energy metabolism proteins such as NADH ubiquinone oxidoreductase (NDUFS1) Cys78 increasing by 28.7 fold, Aspartate aminotransferase (GOT2) Cys295 6.86 fold, 2-oxoglutarate dehydrogenase (OGDH) Cys566 by 5.45 fold, ATP synthase subunit d (ATP5H) Cys101 by 5.19 fold, Cofilin-2 (CFL2) Cys80 by 5.12 fold and cytoplasmic Malate dehydrogenase (MDH1) Cys154 by 5.34 fold. These all increased in reduced state with age suggesting a possible reduction in function. Conversely Cytochrome b-c1 complex subunit 2 (UQCRC2) Cys192, Cytochrome b-c1 complex subunit 6 (UQCRH) Cys51, B-enolase (ENO3) 337/339*, Four and a half LIM domains proteins 1 (FHL1) Cys255 and Glyceraldehyde-3-phosphate dehydrogenase (GAPDH) Cys150/154*

(containing a tryptic peptide) and Isocitrate dehydrogenase (IDH2) Cys113 all demonstrated becoming less reduced with age with Isocitrate dehydrogenase being reversibly oxidised in adult mice soleus muscle and becoming more reversibly oxidised in old mice soleus muscle. These changes in energy metabolism proteins with age correspond to another study which identified similar changes to energy metabolism proteins, specifically highlighting multiple modifications to NDUFS1 with age (Choksi et al., 2008).

Figure 4.3.4.1 presented western blot data for Thioredoxin 1 (A), Thioredoxin Reductase 1 (C), Thioredoxin interacting protein (TXNIP, E), Peroxiredoxins 1 (F), 4 (G) and 6 (H). The results showed no significant change in protein abundance for Thioredoxin 1, Thioredoxin Reductase 1 or Peroxiredoxin 6. The same was true for the enzyme activity tests for Thioredoxin and Thioredoxin Reductase, neither of which changed significantly with age. However, protein abundance significantly decreased for TXNIP from both 3 to 12 months (p <0.001) and 3 to 24 months (p <0.01). As this protein is involved in negative regulation of Thioredoxin, it is a part of the Thioredoxin system for maintenance of properly functioning Peroxiredoxins (Alhawiti et al., 2017). A significant decrease in protein abundance with no change in Thioredoxin 1 or Thioredoxin Reductase 1 may suggest a disconnection within the Thioredoxin system with age. Peroxiredoxin 1 (figure 4.3.4.1F) demonstrated a significant decrease in abundance from 12 to 24 months. Peroxiredoxin 4 (figure 4.3.4.1G) demonstrated a significant increase in abundance from both 3 to 24 (p <0.05) and 12 to 24 months (p <0.01). Peroxiredoxin 6 (4.3.4.1H) demonstrated no significant change in protein abundance with age. None exhibited a significant change in the global proteomics results (figure 4.3.4.1J). Peroxiredoxin 4 has been shown to regulate the transcription factor NF-kB linking intracellular redox changes and transcription (Jin et al., 1997). Peroxiredoxin 5 was also identified in the label free data but was unchanged with age. Sulphonylated peroxiredoxins (PRDX1-4) were also assessed but no significant change in protein abundance was observed.

Figure 4.3.4.4 shows Cu-Zn Superoxide Dismutase (SOD1) which demonstrated a significant increase in protein abundance with age from 3 to 24 months (p <0.05), however no significant change was observed in the global proteomics data. An increase in protein abundance may indicate an increased requirement for control of intracellular ROS as SOD1 mice knock out studies have shown this may lead to an increased rate of ageing and contribute to fibre loss (Sakellariou et al., 2011).

Protein carbonylation (figure 4.3.4.10) shows markers of long term intracellular reactive oxygen species stress. The blot showed no significant change with age to carbonylated protein abundance which is in contrast to a study that identified an increase in carbonylated soleus proteins with age. It was, however, performed on female mice where males were used in this study (Tohma et al., 2014).

Energy Metabolism and Ageing

To initially determine differences between adult and old soleus muscle tissue in relation to energy metabolism, Succinate dehydrogenase (SDH) staining was performed in figure 4.3.2.1 which highlighted an apparent reduction in oxidative capacity of the muscle cells with age. Other studies showed no significant change in SDH staining between adult and old soleus muscle cells (Leduc-Gaudet et al., 2015) or a significant loss of mouse soleus muscle fibre numbers with age (Sheard and Anderson, 2012).

Adenosine monophosphate kinase (AMPK) is involved in a range of roles from intracellular energy regulation to cytoskeletal adjustment and acts as an energy sensor for the cell by reacting to reductions in AMP/ADP concentrations (Treebak et al., 2006, Kahn et al., 2005). The data in figure 4.3.4.8 did not show any significant change in protein abundance, however the global label free data (figure 4.3.4.8C) identified two subunits of AMPK:

PRKACA (KAPCA) and PRKAR2A (KAP2) and of these only PRKAR2A/KAP2 were significantly reduced with age.

Aconitase (ACON, mitochondrial) data is shown in figure 4.3.4.7 where western blotting did not identify any significant change in protein abundance with age. The enzyme activity showed a significant increase from 3 months to 12 months (p <0.01) and global proteomics data showed a significant increase in abundance with age from adult to old. In Table 6, the redox assessment of Aconitase highlighted increases in the reduced state of Cys448/451 from 3.2 to 8.4, Cys385 from 1.9 to 4.0, and Cys126 from 4.3 to 11.6 with age. Interestingly, these changes, combined with the change in proteomics abundance and enzyme activity with age may all suggest an increased demand for this enzyme in energy metabolism which was not observed in the quadriceps.

A key protein in terms of a western blotting housekeeping is Glyceraldehyde 3-phosphate dehydrogenase and differential labelling identified the Cys150/154 (tryptic peptide) as decreased in its reduced state with age in the soleus of ageing mice. Cys150 has been identified as undergoing ADP-ribosylation by autocatalysis following irreversible inhibition (Mustafa et al., 2009, UniProt, 2017c). Additionally, the label free proteomics showed a significant decrease in abundance of the protein with age. Together, the change in redox state combined with the reduction in protein abundance may induce autophagy as previously demonstrated by Hara and Nakajima (Hara et al., 2005, Nakajima et al., 2007). Furthermore, this presents a physiological decline in soleus function with age.

Mitochondrial respiratory chain Complex III subunit Cytochrome b-c1 (UQCRH) Cys51 forms part of a disulphide bond between with Cys65. Changes to the redox state of this cysteine may affect protein function due to changes in conformation (UniProt, 2017b). Conversely NADH ubiquinone oxidoreductase (NDUFS1) became less reduced with age and its Cys78,

located in the metal ion binding site, may therefore directly affect protein functionality (UniProt, 2017e). The only reversibly oxidised cysteine detected in the soleus belonged to Isocitrate dehydrogenase 2 (IDH2) Cys113 which started at 0.023 in the adult form and became more reversibly oxidised in old soleus muscle to 0.007 (UniProt, 2017h). Cys113 itself has no defined function but is located near a substrate binding site.

These protein modifications along with those detailed in table 6, and together with western blotting data all support the initial global proteomics data in indicating that ageing in mouse soleus muscle predominantly affects energy metabolism proteins and their peptides.

Protein Folding Response to Ageing

Increases in sulphonylated PARK7 (PARK7-SO_3H) may reflect sustained intracellular ROS concentrations as PARK7 has a number of roles, most notably as a protein chaperone and redox sensor. The western blot data in fig. 4.3.4.9 demonstrated no significant change in protein abundance between 3 and 12 months suggesting PARK7 was not heavily modified in the soleus due to ROS. The standard PARK7 was identified in the relative quantification proteomics data and this also demonstrated no significant change from adult to old. There was a problem identifying bands in figure 4.3.4.9 with two of the three lanes apparently containing no protein in the soleus samples. Statistical analysis for western blotting of PARK7-SO_3H could not be performed between adult and old.

Comparison and STRING Analysis of Differentially Labelled Proteins

Differential labelling highlighted changes to the redox state of soleus muscle tissue with age. Figure 4.3.7.1 identified a decrease in the number of redox proteins and increases in the number of reduced and reversibly oxidised proteins with age. Furthermore, VennDIS then filtered the results into redox, reduced and reversibly oxidised proteins datasets enabling subsequent analysis with STRING to highlight specific interactions within certain protein

datasets. Of particular interest were proteins identified in the datasets from adult and old mice which highlighted age related changes to the redox state of particular proteins. Figures 4.3.8.1 to 4.3.8.4 used VennDIS to identify lists of proteins within the different sets of redox, reduced and reversibly oxidised proteins. The results highlighted in the label free proteomics results helps to build upon the current knowledge of age-related differences in skeletal muscle proteomes such as work by Chaves and Hansson (Chaves et al., 2013, Hansson et al., 2005).

Following identification of changes to specific cysteines, VennDIS highlighted which proteins of the differentially labelled dataset affected samples from adult, old or both ages of mice. These values were then fed into STRING for protein interaction analysis relating to the redox states of the proteins thereby highlighting age related redox changes to the soleus. The data in this section highlighted a range of interactions, many of which were to be expected within energy metabolism enrichments with a number of figures highlighting interesting results. Figure 4.3.9.1 highlighted a link between GAPDH and SOD1. The reduction in GAPDH protein abundance suggests a disconnect with age between energy metabolism and redox homeostasis may occur.

The results of the different STRING analyses help to highlight interactome properties identified in skeletal muscle ageing and effects encountered with different redox states. Other studies have considered skeletal muscle interactomes but in pig (Blandin et al., 2013) and humans (Cao et al., 2014) however it appears this is one of the first to perform it in mice.

Motif-X Analysis of Redox Proteins

Motif-X was performed on the differentially labelled data sets to identify any conserved amino acids in the redox, reduced or reversibly oxidised peptide sequences and the change with age. This analysis highlighted similar conserved amino acids in figures 4.3.10B (adult reduced data set) and 4.3.10D (old redox data set) with an Isoleucine at +4 from the central cysteine.

Previously described as having an involvement in skeletal muscle energy metabolism (Egan and Zierath, 2013), this result may indicate a change in energy metabolism pathways with age as cysteines' redox state change. In figure 4.3.10C (adult reversibly oxidised data set) and 4.3.10F (old reversibly oxidised) an Aspartic acid was highlighted at -4 from the central cysteine (Zurlo et al., 1990). It is postulated that the overall negative charge of this amino acid is required for a stable microenvironment for a conserved cysteine residue.

4.5 Conclusions

The results demonstrate that age-related changes to mouse soleus muscle primarily affect energy metabolism proteins. Global label free data highlighted a number of these proteins that changed in abundance with age which was supported by the differential labelling that showed redox changes to specific cysteine residues within proteins of interest. Many of these are significantly reduced in old tissue and an increasing number of cysteines appeared to be either reduced or reversibly oxidised reflecting a change from a responsive range of proteins for intracellular redox signalling to a more rigid system that cannot react as quickly to those changes. Finally, pathway analysis using GOrilla and STRING, combined with examination of any conserved sequence motifs via Motif-X provide a picture of a disparate system when aged. The next step will compare soleus and quadriceps muscle to consider how musculoskeletal ageing differentially affects these tissues.

CHAPTER 5

A COMPARISON OF THE QUADRICEPS AND SOLEUS MUSCLES

5.1 Introduction

Having looked at the quadriceps and soleus in isolation, here they are compared to highlight differences between them as they age. A major difference between quadriceps and soleus is their primary energy production mechanism due to differences in fibre types (see section 1.3, p.29). The soleus contains predominantly slow twitch, type I fibres and is involved in posture and walking. It primarily produces its energy via oxidative phosphorylation which enables longer lasting energy production for prolonged use. Conversely, the quadriceps contain predominantly type II, fast twitch fibres and is used for rapid explosive force such as sprinting. This is reflected in the energy metabolism of the fibres within the quadriceps where they predominantly use glycolysis to ensure a rapid production and delivery of energy in the form of ATP to the actin-myosin complex (Chakkalakal et al., 2012, Kammoun et al., 2014, Barclay et al., 1993, Crow and Kushmerick, 1982, Barclay, 1982).

In relation to ageing the quadriceps appear more susceptible than the soleus given their predominance of fast twitch type II fibres (Lexell, 1995, Larsson and Salviati, 1989). This may reflect the fibre types of each muscle and therefore the energy metabolism of each may lend to increased susceptibility of atrophy within a tissue (Fitts et al., 1984, Larsson and Edstrom, 1986, Lowe et al., 2000).

One study analysed the differences between fibre types following incomplete spinal cord injury on muscle regeneration. Surprisingly, they observed a significant increase in the predominantly type I fibre soleus regeneration compared to the type II Tibialis anterior (Jayaraman et al., 2013). In a study by Girgenrath *et al.* Myostatin expression was demonstrated to affect fibre type distribution in fast and slow fibre types and that a loss of Myostatin expression causes an increase in type II fibres (Girgenrath et al., 2005). These studies briefly highlight the plasticity of skeletal muscle both in terms of regeneration and during formation.

Comparisons in this chapter will predominantly consider the label free proteomics data using pathway and STRING protein-protein interaction analysis before considering the redox differences between the muscles. This will allow identification of age-related changes to thiol signalling in the two mouse skeletal muscles as they age.

5.2 Aim

The aim of this chapter is to identify similarities and differences between quadriceps and soleus in their proteomics data to better understand how different types of skeletal muscles age.

5.3 The Quadriceps versus the Soleus Muscle with Age

Label free proteomics identified 946 proteins in adult and old quadriceps and soleus muscles combined. In figure 5.3.1 VennDIS was used to determine which proteins occurred in each muscle (amalgamating both adult and old data). This shows 205 proteins were detected only in the quadriceps, 307 only in the soleus and 434 in both tissues. The individual data used in figure 5.3.1 are presented in the supplementary information, Table 5.3.1 (p.263-267).

The quadriceps data highlighted proteins such as Frataxin (FXN), a protein involved in iron-sulphur cluster assembly and maintenance and possible oxidative stress protector (Huang et al., 2009), protein disulphide isomerase A6 (PDIA6) which works as a protein chaperone (Vekich et al., 2012, UniProt, 2017g) and the cytoskeletal proteins β-actin (ACTNB) and α-actin 3 (ACTN3) and the redox control protein Peroxiredoxin 4 (PRDX4) (Tasaki et al., 2017). Conversely the soleus highlighted a range of metabolomic proteins such as the complex I subunit NADH dehydrogenase (NDUFS7), Cytochrome b (MT-CYB), ATP synthase subunits (ATPAF2, ATP4A). Glutaredoxin 5, involved in iron-sulphur cluster and regeneration (Linares et al., 2009, UniProt, 2017f).

The redox control proteins Peroxiredoxin 1-3, 5 & 6, Thioredoxin 1 and heat shock proteins (HSP90A1, HSPA1A, HSPB6, HSPA8), the striated muscle function protein β-enolase (ENO3) and Annexin A6 (ANXA6), potentially involved in Calcium release were detected in both muscles at both ages. These are only a small sample of the 434 proteins detected, it indicates their importance to skeletal muscle functionality throughout life and across the two tissues.

The combined proteomics data of soleus proteins from adult and old mice showed several involved in energy metabolism such as Cytochrome b (MT-CYB), ATP synthase (ATPAF2), several of NADH dehydrogenases and their associated subcomplexes (e.g. NDUFA2-9, NDUFB1-9, NDUFS1-4 etc.), the Calcium binding protein Calsequestrin 2 (CASQ2), the Glutathione conjugation proteins Glutathione S-transferase κ-1 (GSTK1) and Glutathione S-transferase α-4 (GSTA4) and the cytoplasmic iron-sensing protein Aconitase 1 (ACO1) (Pickova et al., 2003, Xiao et al., 1999).

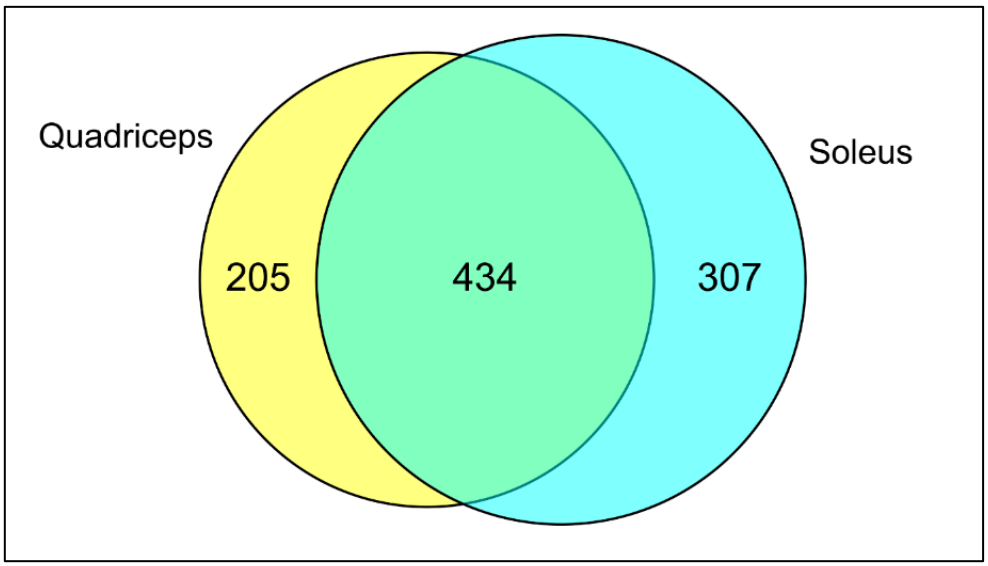

Figure 5.3.1. Venn diagram comparing total detected protein numbers between quadriceps and soleus muscle in adult and old mice (see supplementary information Table 5.3.1, p. 263-267).

Following a brief consideration of the global proteomics results for the tissues, PathVisio (v. 3.2.3) was used to highlight changes observed in individual proteins involved in specific pathways of interest. The data in figure 5.3.2 shows sarcomeric proteins identified in the global label free proteomics dataset for quadriceps. Red indicates proteins significantly increased with age while green is significantly decreased with age and yellow indicates no change. The graphic indicates that those proteins involved in sarcomeric function in mouse quadriceps were predominantly decreased with age such as the Actins, Myosin heavy and light chains, Tropomyosins and Troponins. Further to this, soleus sarcomeric proteins were then considered using PathVisio to compare changes to those found in quadriceps. Figure 5.3.3 indicates that some sarcomeric proteins were down regulated with age in the soleus, but not to the same extent as observed in the quadriceps with several Troponins, Tropomyosin and Myosin heavy chain protein isoforms being unchanged with age. Myosin light chain 1 was up regulated with age, whereas the opposite was observed in the quadriceps. Electron transport chain proteins in quadriceps are shown in figure 5.3.4 and highlighted several proteins that were either unchanged or slightly up regulated in complex I. Only the Succinate dehydrogenase subunit (SDHB) was increased with age in complex II. Complex III was predominantly down regulated with age and Complex IV was largely unchanged although some specific proteins such as COX1 and COX7C were up regulated with age. Complex V showed some up regulated proteins such as the ATP synthase subunits Atp5e, ATP5H and ATP5I. The Adenine nucleotide translocator showed a down regulation in quadriceps with age for SLC25A4 and SLC25A5. The soleus electron transport chain proteins are shown in figure 5.3.5 and the results showed an overall down regulation of proteins with age. The few proteins up regulated with age include complex I proteins Ndufb2, Ndufs6 and Ndufs8. Complex V highlighted several ATP synthase subunits along with the Adenine nucleotide translocator protein SLC25A5 which was up regulated in the quadriceps was found to be down regulated in the soleus with age.

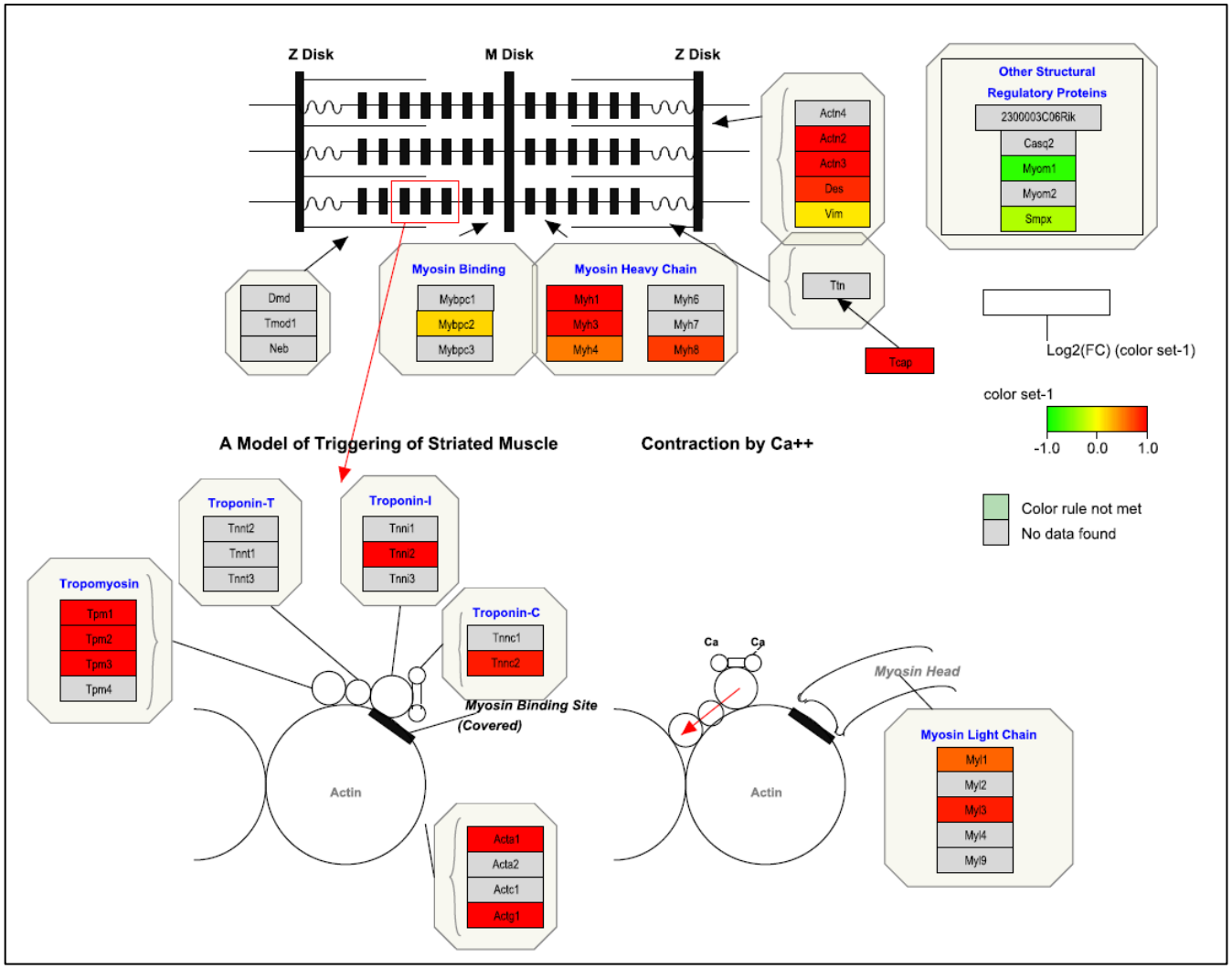

Figure 5.3.2 PathVisio analysis of quadriceps sarcomeric proteins using the global label free proteomics data. Red indicates an up regulation with age, green a down regulation on a sliding scale though yellow which indicates no change.

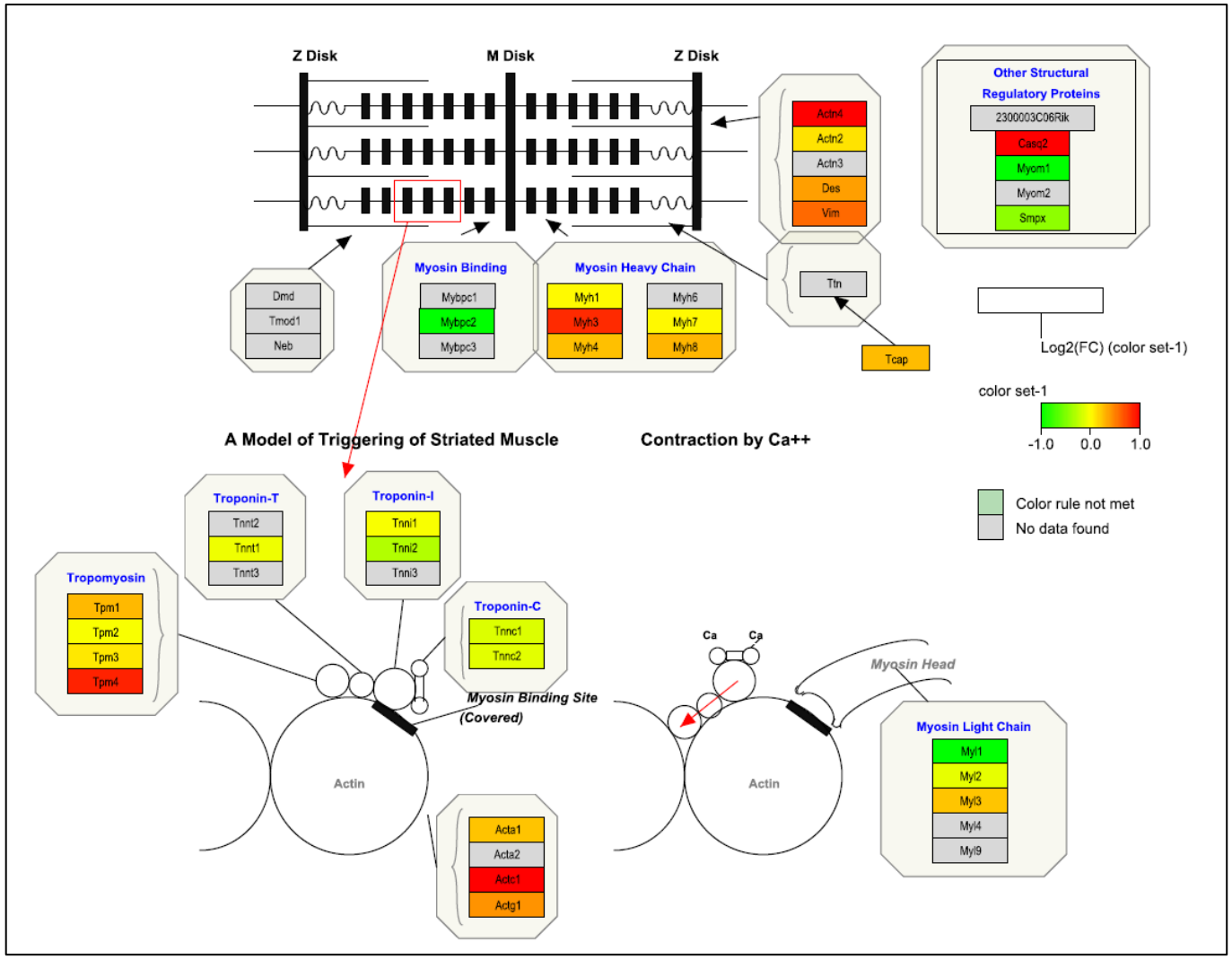

Figure 5.3.3 PathVisio analysis of soleus sarcomeric proteins using the global label free proteomics data. Red indicates an up regulation with age, green a down regulation on a sliding scale though yellow which indicates no change.

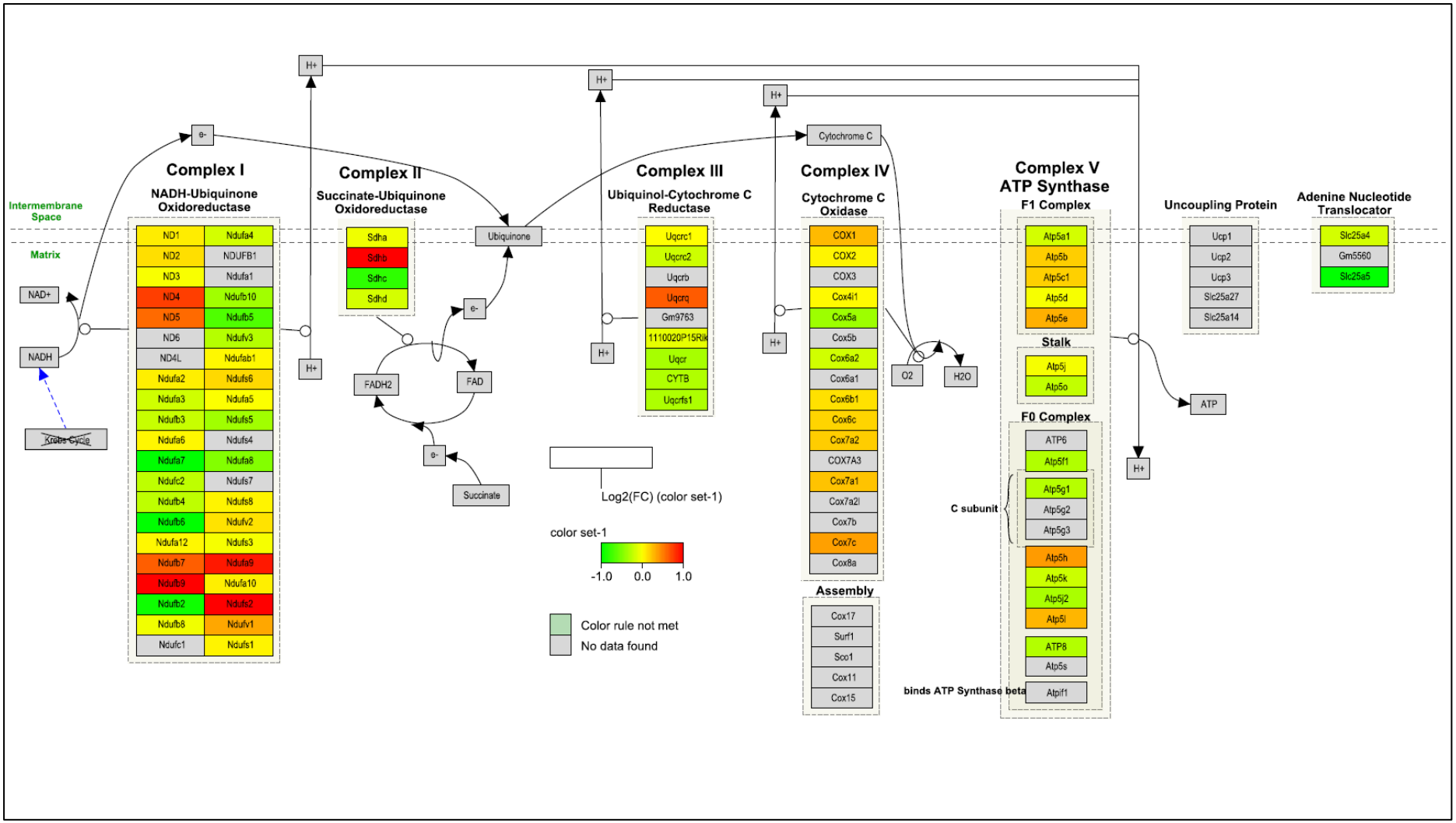

Figure 5.3.4 PathVisio analysis of electron transport chain proteins in the quadriceps using global label free proteomics data. Red indicates an up regulation with age, green a down regulation on a sliding scale though yellow which indicates no change.

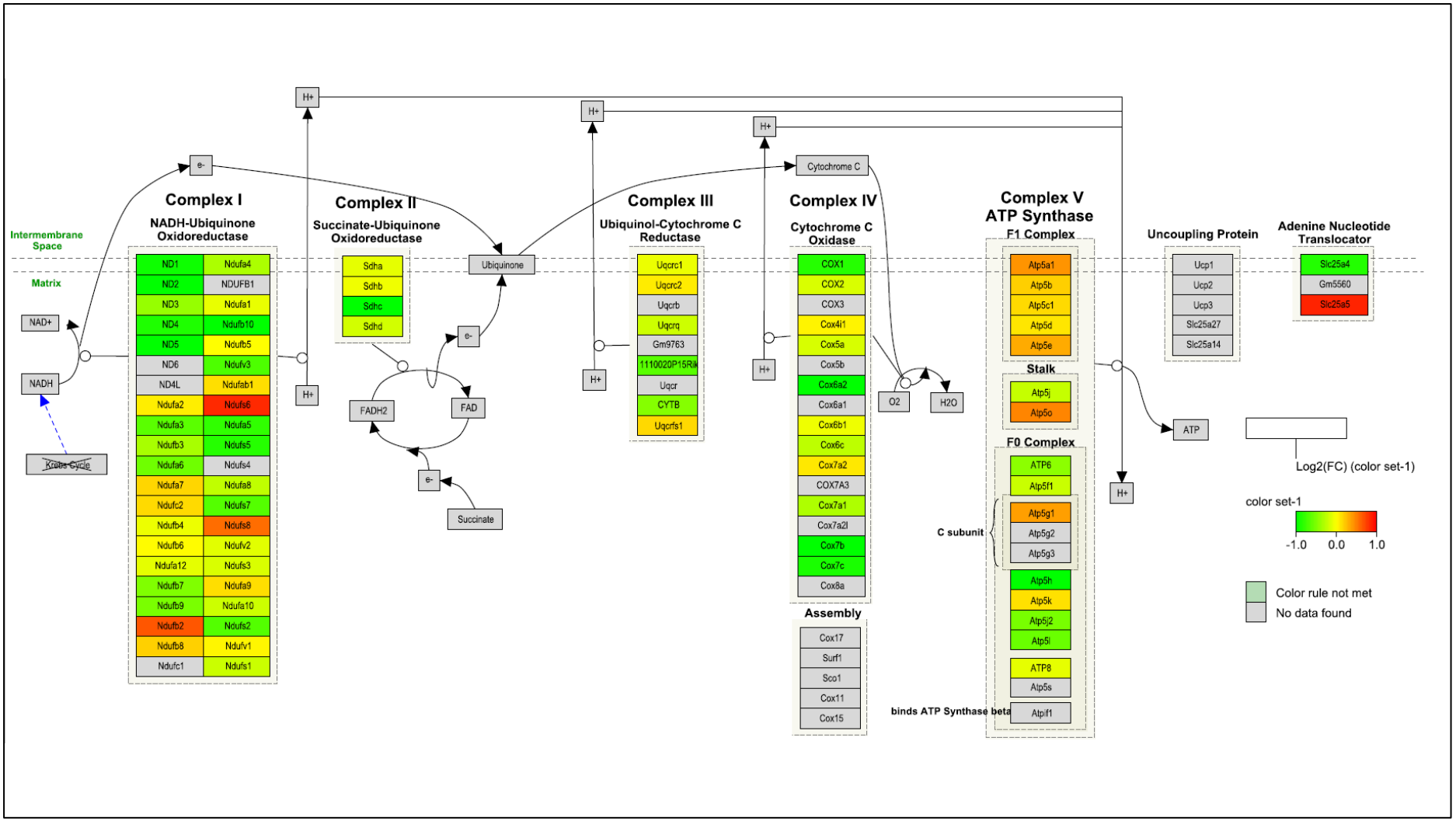

Figure 5.3.5 PathVisio analysis of the soleus electron transport chain proteins using the global label free proteomics data. Red indicates an up regulation with age, green a down regulation on a sliding scale though yellow which indicates no change.

The PathVisio assessment of the quadriceps and soleus global proteomics data helped to indicate clear differences between the two muscles as they age. Both sarcomeric proteins and those involved in the electron transport chain appears to change in abundance with age but to differing extents in each muscle.

5.4 Redox Comparisons of the Quadriceps and Soleus Muscles

Thiol signalling in skeletal muscle ageing requires redox flexible proteins to enable a reaction to changing intracellular ROS concentrations. This is performed via a redox cysteine amino acid conserved in crucial locations throughout the protein. When comparing how quadriceps and soleus muscles age, examination of changes in numbers of differentially labelled proteins helped to clarify the extent of changes in the redox state of protein in each muscle.

Figure 5.4.1 shows a decrease in the numbers of redox-labelled (*d*0-NEM + *d*5-NEM) proteins with age in both the quadriceps and soleus muscles.

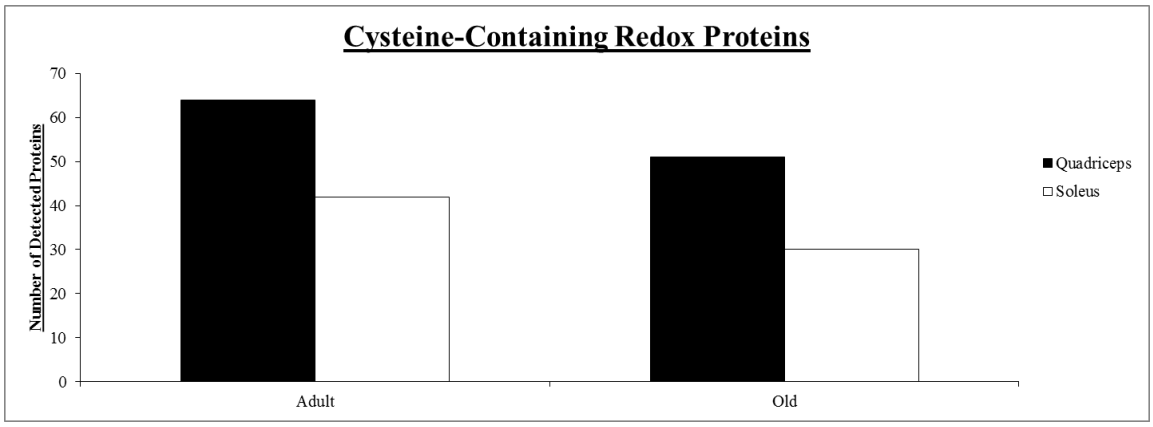

Figure 5.4.1 Cysteine containing redox (*d*0-NEM + *d*5-NEM) labelled proteins in quadriceps and soleus between adult and old tissue. Sample size data are n=5 in adult and n=6 in old quadriceps while int the soleus dataset n=5 in both adult and old.

Figure 5.4.2 shows the reduced (*d*0-NEM) labelled proteins. In both quadriceps and soleus muscles they demonstrated an increase in the numbers of these proteins with age.

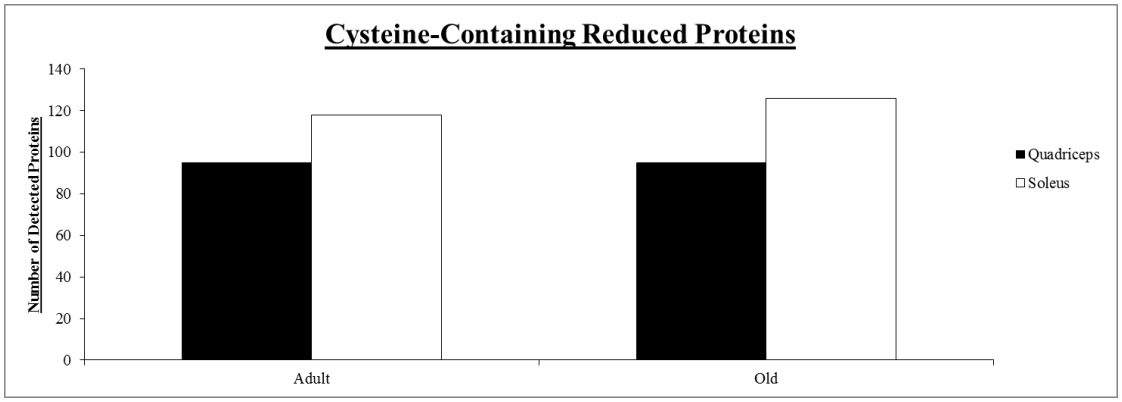

Figure 5.4.2 Cysteine containing reduced (*d*0-NEM) labelled proteins in quadriceps and soleus between adult and old tissue. Sample sizes data are n=5 in adult and n=6 in old quadriceps while int the soleus dataset n=5 in both adult and old.

Figure 5.4.3 shows reversibly oxidised (*d*5-NEM) labelled proteins and highlighted decreases in the number of proteins in both quadriceps and soleus muscles with age.

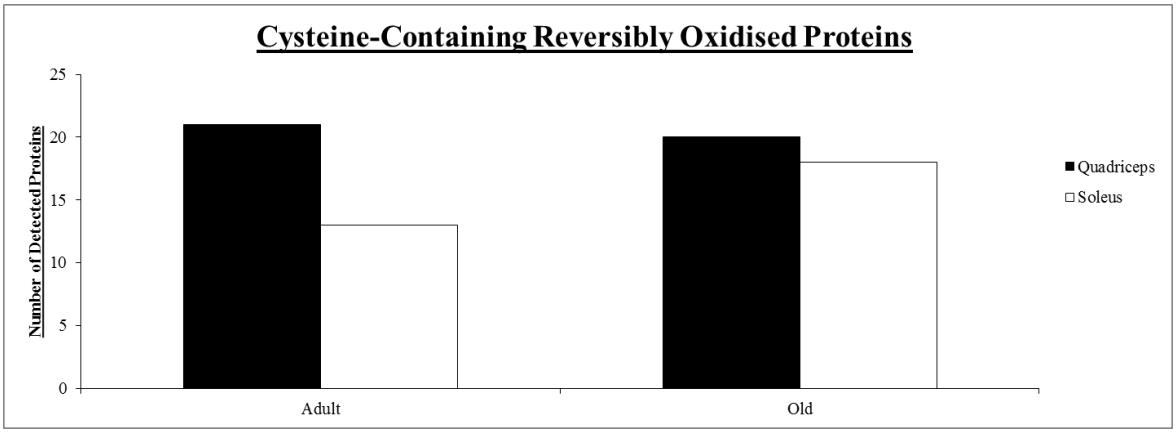

Figure 5.4.3 Cysteine containing reversibly oxidised (*d*5-NEM) labelled proteins in quadriceps and soleus from adult and old mice. Sample size data are n=5 in adult and n=6 in old quadriceps while int the soleus dataset n=5 in both adult and old.

The above figures were tabulated below in table 7, highlighting the changes in differentially labelled protein numbers with age.

		Redox (D5NEM+NEM)	Reduced (NEM)	(Reversibly) Oxidised (D5-NEM)	**Total**
Quadriceps	Adult	64	95	21	**180**
	Old	51	95	20	**166**
		Redox (D5NEM+NEM)	Reduced (NEM)	(Reversibly) Oxidised (D5-NEM)	**Total**
Soleus	Adult	42	118	13	**173**
	Old	30	126	18	**174**

Table 6. Numbers of differentially labelled proteins in quadriceps and soleus muscles indicating redox (*d*0-NEM + *d*5-NEM), reduced (*d*0-NEM) and reversibly oxidised (*d*5-NEM) numbers.

After describing the changes in differentially labelled protein numbers with age in each muscle, VennDIS was employed to highlight proteins found in the adult or old mice in both muscles. The data tables are presented in the supplementary data (see Table 5.4.4, p.268-278). Figure 5.4.4A shows the muscle in adult mice for redox-labelled proteins and a total of 81 proteins were highlighted. In figure 5.4.4A, the thirty-nine proteins from adult mice that were classed as redox proteins in the quadriceps included the redox sensor and chaperone protein PARK7, the heat shock/chaperone HSPA8 (HSC71) and cytoskeletal proteins Myomesin 2, Myosin binding protein and Myosin heavy polypeptide proteins (Auerbach et al., 1999). In the seventeen redox proteins from soleus in the adult mice highlighted, they also included Myosin heavy polypeptide 2 and 7 in addition to many energy metabolism proteins such as Lactate dehydrogenase and NADHG dehydrogenase. Of the twenty-five proteins identified in both muscles, these included mitochondrial Aconitase, Glyceraldehyde-3-phosphate dehydrogenase and Superoxide dismutase 1 (Cu-Zn Superoxide dismutase) in addition to Tropomyosin 1-α, Tropomyosin 4 and Troponin 1.

In figure 5.4.4B quadriceps from old mice, thirty-three redox proteins highlighted included ATP synthases, Creatine kinases, Glyceraldehyde-3-phosphate dehydrogenase, Heat

shock protein 8 and Superoxide dismutase 1 (Cu-Zn Superoxide dismutase). Whereas in the soleus muscle from old mice, those highlighted included Peroxiredoxin 6 along with an ATP synthase subunit, Lactate dehydrogenase B and NADH dehydrogenase. Of the eighteen proteins identified in both muscles, they included mitochondrial Aconitase along with the energy metabolism Lactate dehydrogenase A and Malate dehydrogenase 1 and 2 and structural proteins Myosin heavy polypeptide 2 and 4 and Tropomyosin 1-α.

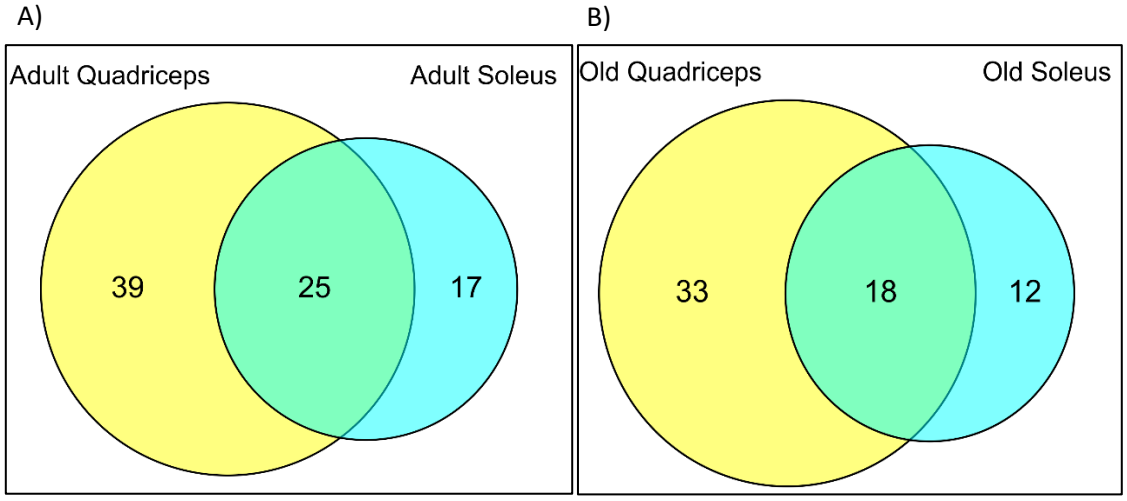

Figure 5.4.4. Venn diagram of differentially labelled redox proteins in quadriceps and soleus muscles from adult and old mice (see supplementary information Table 5.4.4, p.268-278).

Subsequent to the VennDIS analysis, STRING was used to assess protein-protein interactions in quadriceps and soleus from adult and old mice. This enabled a cross-comparison of interacting proteins that may be significantly changed with age and allowing analysis of specific pathways or mechanisms. GOrilla was not used here as the number of proteins from the redox datasets were too few to perform a pathway analysis.

Figure 5.4.5A shows analysis using STRING to examine differentially labelled proteomics data for quadriceps and soleus from adult mice to identify any protein interactions that occur in both tissues at 12 months of age. Enrichment for glycolysis proteins highlighted interactions between mitochondrial Dihydrolipoyl dehydrogenase (DLD), β-enolase (ENO3),

α-enolase (ENO1), Triosephosphate isomerase (TPI1) and Fructose bisphosphate aldolase A (ALDOA). The data in table 7 highlights the associated proteins in the label free proteomics data although none were significantly changed in abundance with age. This result shows basic interactions between only a few proteins for glycolysis occur in both quadriceps and soleus adult tissues.

A)

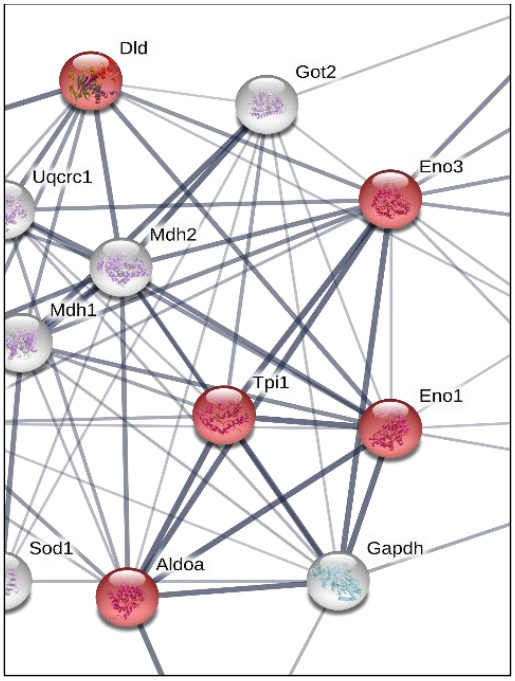

B)

#pathway ID	pathway description	observed gene count	false discovery rate
10	Glycolysis / Gluconeogenesis	5	3.76E-07

Figure 5.4.5 (A) STRING analysis of redox proteins detected in both quadriceps and soleus muscles from adult mice enriched for Glycolysis/gluconeogenesis. (B) STRING analysis information and FDR.

	Accession	Labels	Significance (-10lgP)	Group Profile (Ratio)	Description
Q	P17182	ENOA_MOUSE	1.46	1.00:1.32	Alpha-enolase OS=Mus musculus GN=Eno1 PE=1 SV=3
Q	P21550	ENOB_MOUSE	5.88	1.00:0.89	Beta-enolase OS=Mus musculus GN=Eno3 PE=1 SV=3
Q	O08749	DLDH_MOUSE	4.49	1.00:1.99	Dihydrolipoyl dehydrogenase mitochondrial OS=Mus musculus GN=Dld PE=1 SV=2
Q	P05064	ALDOA_MOUSE	2.12	1.00:1.04	Fructose-bisphosphate aldolase A OS=Mus musculus GN=Aldoa PE=1 SV=2
Q	P17751	TPIS_MOUSE	8.68	1.00:0.84	Triosephosphate isomerase OS=Mus musculus GN=Tpi1 PE=1 SV=3

	Accession	Label	Significance (-10lgP)	Group Profile (Ratio)	Description
S	P17182	ENOA_MOUSE	5.8	1.00:1.10	Alpha-enolase OS=Mus musculus GN=Eno1 PE=1 SV=3
S	P21550	ENOB_MOUSE	14.85	1.00:0.79	Beta-enolase OS=Mus musculus GN=Eno3 PE=1 SV=3
S	O08749	DLDH_MOUSE	6.88	1.00:1.07	Dihydrolipoyl dehydrogenase mitochondrial OS=Mus musculus GN=Dld PE=1 SV=2
S	P05064	ALDOA_MOUSE	23.11	1.00:1.43	Fructose-bisphosphate aldolase A OS=Mus musculus GN=Aldoa PE=1 SV=2
S	P17751	TPIS_MOUSE	14.07	1.00:0.98	Triosephosphate isomerase OS=Mus musculus GN=Tpi1 PE=1 SV=3

Table 7. Quadriceps (Q) and soleus (S) global label free proteomics data for the associated proteins highlighted in figure 5.4.5.

An equivalent study was performed for quadriceps and soleus muscles of old mice. Figure 5.4.5 shows four proteins involved in interactions for glycolysis which were Fructose bisphosphate aldolase A (ALDOA), Triosephosphate isomerase (TPI1), β-enolase (Eno3) and Dihydrolipoyl dehydrogenase (DLD). Table 9 gives the associated label free proteomics data for the proteins in figure 5.4.6A, but none were significantly changed in abundance with age. This result highlights a lack of α-enolase (ENO1) when compared with the adult samples.

A)

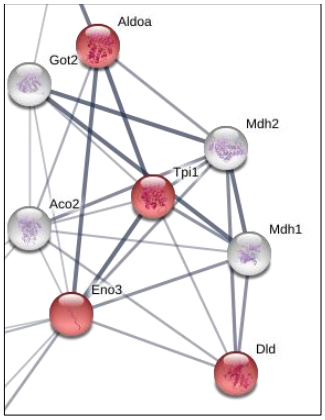

B)

#pathway ID	pathway description	observed gene count	false discovery rate
10	Glycolysis / Gluconeogenesis	4	3.20E-06

Figure 5.4.6 (A) STRING analysis of quadriceps and soleus redox proteins from old mice enriched for glycolysis/gluconeogenesis protein interactions. (B) STRING analysis information and FDR.

	Accession	Labels	Significance (-10lgP)	Group Profile (Ratio)	Description
Q	P21550	ENOB_MOUSE	5.88	1.00:0.89	Beta-enolase OS=Mus musculus GN=Eno3 PE=1 SV=3
Q	O08749	DLDH_MOUSE	4.49	1.00:1.99	Dihydrolipoyl dehydrogenase mitochondrial OS=Mus musculus GN=Dld PE=1 SV=2
Q	P05064	ALDOA_MOUSE	2.12	1.00:1.04	Fructose-bisphosphate aldolase A OS=Mus musculus GN=Aldoa PE=1 SV=2
Q	P17751	TPIS_MOUSE	8.68	1.00:0.84	Triosephosphate isomerase OS=Mus musculus GN=Tpi1 PE=1 SV=3

	Accession	Labels	Significance (-10lgP)	Group Profile (Ratio)	Description
S	P21550	ENOB_MOUSE	14.85	1.00:0.79	Beta-enolase OS=Mus musculus GN=Eno3 PE=1 SV=3
S	O08749	DLDH_MOUSE	6.88	1.00:1.07	Dihydrolipoyl dehydrogenase mitochondrial OS=Mus musculus GN=Dld PE=1 SV=2
S	P05064	ALDOA_MOUSE	23.11	1.00:1.43	Fructose-bisphosphate aldolase A OS=Mus musculus GN=Aldoa PE=1 SV=2
S	P17751	TPIS_MOUSE	14.07	1.00:0.98	Triosephosphate isomerase OS=Mus musculus GN=Tpi1 PE=1 SV=3

Table 8. Quadriceps (Q) and soleus (S) global label free proteomics information for the associated proteins in figure 5.4.6.

Figure 5.4.6A shows data for STRING analysis to consider quadriceps and soleus muscles from adult mice following enrichment for protein-protein interactions in metabolic

pathways. The results highlighted thirteen proteins: α-enolase (ENO1), β-enolase (ENO3), Aspartate aminotransferase (GOT2), Creatine kinase (CKMT2), Cytochrome b-c1 complex subunit 1 and 2 (UQCRC1 & UQCRC2), Dihydrolipoyl dehydrogenase (DLD), Fructose bisphosphate aldolase A (ALDOA), Malate dehydrogenase 1 and 2 (MDH1 & MDH2). Table 9 shows the label free proteomics data for the proteins in figure 5.4.6A, none were significantly changed in abundance with age. This result demonstrated a number of protein interactions that occur for metabolic pathways in quadriceps and soleus muscles from adult mice.

A)

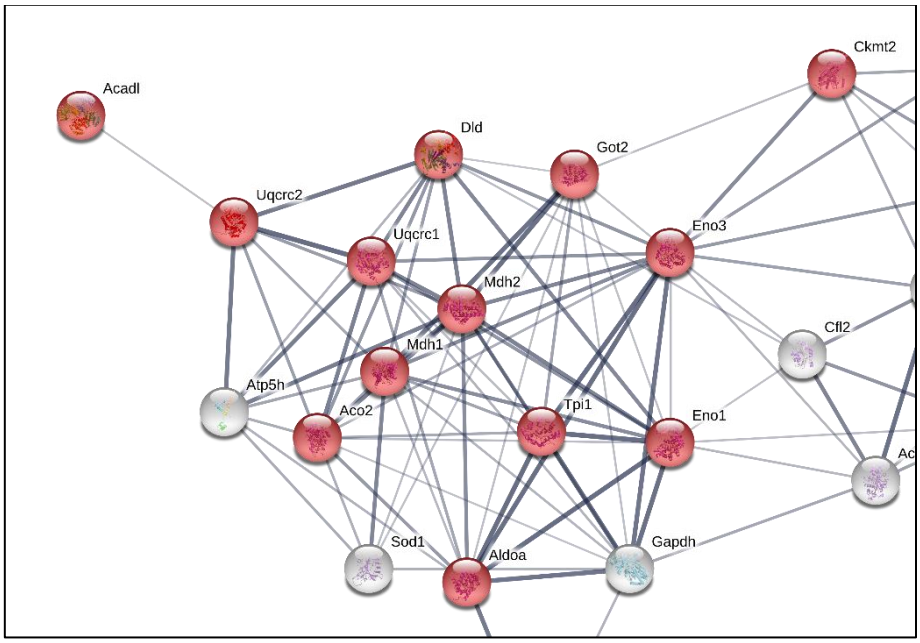

B)

#pathway ID	pathway description	observed gene count	false discovery rate
1100	Metabolic pathways	13	7.62E-09

Figure 5.4.7 (A) STRING analysis of quadriceps and soleus redox proteins from adult mice following enrichment for proteins involved in metabolic pathways. (B) STRING analysis data and FDR.

	Accession	Labels	Significance (-10lgP)	Group Profile (Ratio)	Description
Q	P17182	ENOA_MOUSE	1.46	1.00:1.32	Alpha-enolase OS=Mus musculus GN=Eno1 PE=1 SV=3
Q	P05202	AATM_MOUSE	1.89	1.00:1.13	Aspartate aminotransferase mitochondrial OS=Mus musculus GN=Got2 PE=1 SV=1
Q	P21550	ENOB_MOUSE	5.88	1.00:0.89	Beta-enolase OS=Mus musculus GN=Eno3 PE=1 SV=3
Q	Q6P8J7	KCRS_MOUSE	5.14	1.00:0.95	Creatine kinase S-type mitochondrial OS=Mus musculus GN=Ckmt2 PE=1 SV=1
Q	Q9CZ13	QCR1_MOUSE	4.09	1.00:0.92	Cytochrome b-c1 complex subunit 1 mitochondrial OS=Mus musculus GN=Uqcrc1 PE=1 SV=1
Q	Q9DB77	QCR2_MOUSE	1.29	1.00:1.09	Cytochrome b-c1 complex subunit 2 mitochondrial OS=Mus musculus GN=Uqcrc2 PE=1 SV=1
Q	O08749	DLDH_MOUSE	4.49	1.00:1.99	Dihydrolipoyl dehydrogenase mitochondrial OS=Mus musculus GN=Dld PE=1 SV=2
Q	P05064	ALDOA_MOUSE	2.12	1.00:1.04	Fructose-bisphosphate aldolase A OS=Mus musculus GN=Aldoa PE=1 SV=2
Q	P14152	MDHC_MOUSE	2.06	1.00:1.06	Malate dehydrogenase cytoplasmic OS=Mus musculus GN=Mdh1 PE=1 SV=3
Q	P08249	MDHM_MOUSE	10.78	1.00:0.76	Malate dehydrogenase mitochondrial OS=Mus musculus GN=Mdh2 PE=1 SV=3

	Accession	Labels	Significance (-10lgP)	Group Profile (Ratio)	Description
S	P17182	ENOA_MOUSE	5.8	1.00:1.10	Alpha-enolase OS=Mus musculus GN=Eno1 PE=1 SV=3
S	P05202	AATM_MOUSE	7.39	1.00:1.02	Aspartate aminotransferase mitochondrial OS=Mus musculus GN=Got2 PE=1 SV=1
S	P21550	ENOB_MOUSE	14.85	1.00:0.79	Beta-enolase OS=Mus musculus GN=Eno3 PE=1 SV=3
S	Q6P8J7	KCRS_MOUSE	25.16	1.00:1.26	Creatine kinase S-type mitochondrial OS=Mus musculus GN=Ckmt2 PE=1 SV=1
S	Q9CZ13	QCR1_MOUSE	8.96	1.00:0.89	Cytochrome b-c1 complex subunit 1 mitochondrial OS=Mus musculus GN=Uqcrc1 PE=1 SV=1
S	Q9DB77	QCR2_MOUSE	3.16	1.00:1.04	Cytochrome b-c1 complex subunit 2 mitochondrial OS=Mus musculus GN=Uqcrc2 PE=1 SV=1
S	O08749	DLDH_MOUSE	6.88	1.00:1.07	Dihydrolipoyl dehydrogenase mitochondrial OS=Mus musculus GN=Dld PE=1 SV=2
S	P05064	ALDOA_MOUSE	23.11	1.00:1.43	Fructose-bisphosphate aldolase A OS=Mus musculus GN=Aldoa PE=1 SV=2
S	P14152	MDHC_MOUSE	5.01	1.00:0.97	Malate dehydrogenase cytoplasmic OS=Mus musculus GN=Mdh1 PE=1 SV=3
S	P08249	MDHM_MOUSE	3.84	1.00:1.01	Malate dehydrogenase mitochondrial OS=Mus musculus GN=Mdh2 PE=1 SV=3

Table 9. Quadriceps (Q) and soleus (S) global label free proteomics data for the proteins highlighted in figure 5.4.7.

STRING analysis was also performed on the quadriceps and soleus muscle combined redox data from old muscle to identify changes to protein-protein interactions following enrichment for metabolic pathways. Figure 5.4.7A shows fewer interactions when compared with figure 5.4.6A. The proteins involved here were Fructose bisphosphate aldolase A (ALDOA), mitochondrial Aconitase (ACO2), Aspartate aminotransferase (GOT2), β-enolase (ENO3), Dihydrolipoyl dehydrogenase (DLD), and Malate dehydrogenase 1 and 2 (MDH1 & MDH2). Table 11 shows the label free proteomics data for the associated proteins and demonstrated no significant changes in protein abundance with age. This result demonstrated a reduction in the number of protein interactions in both quadriceps and soleus muscles that occur with age.

A)

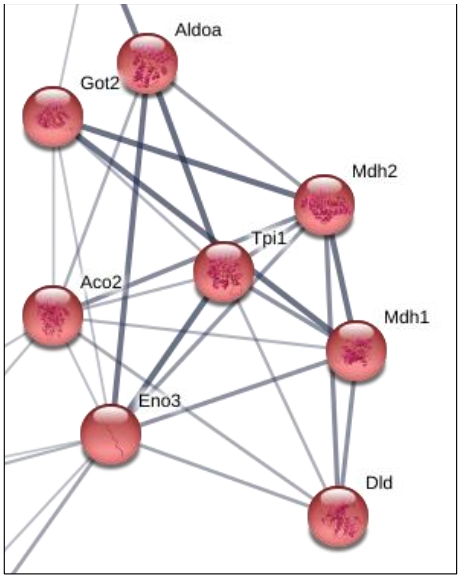

B)

#pathway ID	pathway description	observed gene count	false discovery rate
1100	Metabolic pathways	9	7.52E-07

Figure 5.4.8 (A) STRING analysis of old redox proteins in quadriceps and soleus muscles following enrichment for metabolic pathway protein interactions. (B) STRING analysis information and FDR.

	Accession	Labels	Significance (-10lgP)	Group Profile (Ratio)	Description
Q	Q99KI0	ACON_MOUSE	1.85	1.00:1.00	Aconitate hydratase mitochondrial OS=Mus musculus GN=Aco2 PE=1 SV=1
Q	P05202	AATM_MOUSE	1.89	1.00:1.13	Aspartate aminotransferase mitochondrial OS=Mus musculus GN=Got2 PE=1 SV=1
Q	P21550	ENOB_MOUSE	5.88	1.00:0.89	Beta-enolase OS=Mus musculus GN=Eno3 PE=1 SV=3
Q	O08749	DLDH_MOUSE	4.49	1.00:1.99	Dihydrolipoyl dehydrogenase mitochondrial OS=Mus musculus GN=Dld PE=1 SV=2
Q	P05064	ALDOA_MOUSE	2.12	1.00:1.04	Fructose-bisphosphate aldolase A OS=Mus musculus GN=Aldoa PE=1 SV=2
Q	P14152	MDHC_MOUSE	2.06	1.00:1.06	Malate dehydrogenase cytoplasmic OS=Mus musculus GN=Mdh1 PE=1 SV=3
Q	P08249	MDHM_MOUSE	10.78	1.00:0.76	Malate dehydrogenase mitochondrial OS=Mus musculus GN=Mdh2 PE=1 SV=3

	Accession	Labels	Significance (-10lgP)	Group Profile (Ratio)	Description
S	Q99KI0	ACON_MOUSE	53.5	1.00:1.60	Aconitate hydratase mitochondrial OS=Mus musculus GN=Aco2 PE=1 SV=1
S	P05202	AATM_MOUSE	7.39	1.00:1.02	Aspartate aminotransferase mitochondrial OS=Mus musculus GN=Got2 PE=1 SV=1
S	P21550	ENOB_MOUSE	14.85	1.00:0.79	Beta-enolase OS=Mus musculus GN=Eno3 PE=1 SV=3
S	O08749	DLDH_MOUSE	6.88	1.00:1.07	Dihydrolipoyl dehydrogenase mitochondrial OS=Mus musculus GN=Dld PE=1 SV=2
S	P05064	ALDOA_MOUSE	23.11	1.00:1.43	Fructose-bisphosphate aldolase A OS=Mus musculus GN=Aldoa PE=1 SV=2
S	P14152	MDHC_MOUSE	5.01	1.00:0.97	Malate dehydrogenase cytoplasmic OS=Mus musculus GN=Mdh1 PE=1 SV=3
S	P08249	MDHM_MOUSE	3.84	1.00:1.01	Malate dehydrogenase mitochondrial OS=Mus musculus GN=Mdh2 PE=1 SV=3

Table 10. Quadriceps (Q) and soleus (S) global label free proteomics information for associated proteins in figure 5.4.8.

These results help to highlight differences in protein-protein interactions between the quadriceps and soleus muscles. In both cases comparisons of interactions in glycolysis and metabolic pathways demonstrated fewer interactions with age.

5.5 Discussion

This chapter compared the quadriceps and soleus muscles following analysis of them individually in chapters three and four respectively. The aim (as stated on p.206) was to identify the similarities and differences between quadriceps and soleus muscles seen in proteomics to better understand how different types of skeletal muscle age.

The initial comparisons used PathVisio to place proteins identified from the global label free proteomics data into two systems of interest.

The PathVisio analysis of the label free proteomics data visualised changes to quadriceps and soleus proteins with age. Figures 5.3.2 and 5.3.3 looked at the sarcomeric proteins involved in skeletal muscle contraction in the quadriceps and soleus respectively. The results showed more up-regulated proteins in the quadriceps with age, potentially reflecting an increased demand with age. When compared with the soleus results, this showed many of the same proteins were either up regulated to a lesser extent or in some cases were down regulated in the soleus. This increased requirement for sarcomeric proteins in quadriceps mouse muscle with age is reflected by other literature that determined age-related changes to cytoskeletal proteins in ageing human muscle related to specific fibre types (Lexell, 1995, Jakobsson et al., 1990, Fazelzadeh et al., 2016, Chopard et al., 2001, Koh and Escobedo, 2004). The soleus data highlights an increase in energy metabolism requirements. Much of the previous literature has focused on mitochondrial involvement and specific metabolism effects during ageing rather than using a global proteomic view of these changes (Lopez-Lluch et al., 2008, Dirks et al., 2006, Ramsey et al., 2000). Interestingly skeletal muscle filament regulatory proteins myomesin (MYOM1) and small muscular protein (SMPX) were down regulated. When taken together the up-regulation of cytoskeleton and myofibrillar proteins and down regulation of their associated regulatory proteins points to a potential dysregulation of the muscle fibre. This

may contribute to the increased stiffness and loss of muscle force associated with age. These changes were in the mitochondrial rich soleus muscle and this generally supports other studies that have highlighted how type I slow twitch fibres age more slowly than type II fast twitch fibres (Jacobs et al., 2013, Gonzalez et al., 2000).

The electron transport chain was studied in the quadriceps (figure 5.3.4) and the soleus (figure 5.3.5). The quadriceps data indicates many proteins were unchanged whereas the soleus demonstrated a number of down-regulated proteins. The soleus data also highlighted NADH dehydrogenases as being up regulated with age. This supports a study that reported the down regulation of the electron transport chain in mouse skeletal muscle with age, although they considered the effects in gastrocnemius and vastus lateralis muscles (Mercken et al., 2017, Boengler et al., 2017).

Following the label free comparison of the tissues, the redox data was also examined using STRING. Following the use of VennDIS shown in figure 5.3.1 to filter the adult quadriceps and soleus redox proteins and old quadriceps and soleus proteins where each dataset was previously described in the individual muscle chapters, here it is presented together as a comparison between the quadriceps and soleus muscles. The results highlighted a decrease in redox protein numbers (figure 5.4.1) with age for quadriceps from 64 to 51 and soleus from 42 to 30. The numbers of reduced proteins (figure 5.4.2) increased for the soleus from 118 to 126, but there was no effect in the quadriceps, which remained unchanged at 95. Numbers of reversibly oxidised proteins (figure 5.4.3) decreased for quadriceps from 21 to 20 with age and increased in the soleus from 13 to 18. Previous studies have measured changes to the redox environment in mouse skeletal muscle with age, but none have previously gone into this depth using differential labelling to identify changes to specific cysteine residues of particular proteins (Vasilaki et al., 2006a, Le Moal et al., 2017, Claflin et al., 2015, Lee et al., 2015, Ji, 2008).

VennDIS was again used to separate the data into requisite categories to analyse protein-protein interactions via STRING (figure 5.4.4). Only redox proteins were considered as these are the primary focus of this thesis. The initial consideration was given to glycolysis, the crucial energy metabolism pathway in skeletal muscle. Figure 5.4.5 shows proteins from the adult dataset and figure 5.4.6, the proteins from the old dataset. Comparing the results of adult and old tissues, and between quadriceps and soleus glycolytic protein interactions showed no difference between groups. A recent proteomics study on human vastus lateralis identified a reduction in glycolysis for slow twitch muscles and an increase in glycolysis for fast twitch muscles, as they age (Murgia et al., 2015, Ohlendieck, 2010). The differences to our data on mouse muscle ageing may relate to the different species or it may serve to further highlight how tissues age differently since I compared two muscles of predominantly different fibre types.

General metabolism protein interactions were also considered to clarify whether the differences in ageing of each muscle reflected changes in protein interactions via different pathways. Figure 5.4.7 shows quadriceps and soleus protein interactions from adult mice and figure 5.4.8 shows protein interaction of the two muscles from old mice. The results identified no marked difference between the tissues regarding protein interactions. The result of both the glycolytic and metabolic pathways provided an interesting insight into protein interactions with age. In mouse skeletal muscle it appears these protein-protein interactions do not change, despite data in previous chapters highlighting changes to protein abundance or their redox state with age.

5.6 Conclusion

In conclusion, this chapter set out to consider differences and similarities between the quadriceps and soleus muscles as they age. The results demonstrated clear differences in the

quadriceps and soleus as they age in relation to sarcomeric and electron transport chain proteins. Furthermore, changes to the redox states of proteins showed some similarities between muscles in the age-related effects on redox states of proteins whereas protein-protein interactions did not appear to be affected. Together these results identified how different muscle types can age to differing extents, even within the same crucial systems such as energy production. The next stage of this analysis would be to consider other pathways such as autophagy, protein folding response and chaperones, and protein-DNA interactions to further elucidate how these crucial processes change with age and how these differ in the two different forms of skeletal muscle.

CHAPTER 6

CELL STRETCHING STUDY

6.1 Introduction

Thiol signalling in skeletal muscle is reliant on ROS and is required for normal homeostasis of skeletal muscle. ROS are recognised as crucial messengers for relaying changes to the intracellular redox state. This is facilitated by cysteine residues that are evolutionarily conserved at specific locations since they can form disulphide bonds, amongst other covalent linkages, that affect protein conformation or interactions with other proteins or molecules. As previously demonstrated, ageing of quadriceps and soleus muscles in mice leads to a discordant change to redox control systems such as Thioredoxins, Peroxiredoxins and Superoxide dismutases. Reactive oxygen species (ROS) are produced under normal conditions during skeletal muscle contractions. Further to previous work that addressed the characterisation of ageing in two types of mouse skeletal muscle, the next step was to assess ROS induction following contractions. After considering several techniques (Kamotani et al., 2008, Wang et al., 2014, Kurazumi et al., 2011), an *in vitro* method was established that would enable three time-points of data collection using C2C12 myotubes. The experiment was explained in detail in section 2.10, p.59. Briefly, the FlexCell method utilised 6-well plates containing a stretchable plastic membrane enabling induced contractions of the C2C12 myotubes via a vacuum pump attached to the incubator. The cells were then isolated via scraping and western blotting performed to identify any initial differences in protein content as a proof of principle prior to a proteomic assessment of changes to C2C12 myotubes following contractions.

The C2C12 myocytes used were from in-house stocks although the cell line originates from a female mouse at 2 months of age in which cells were isolated 70 hrs after a crush injury (Yaffe and Saxel, 1977). The purpose of using cells for this work was to use an accessible technique for assessing proteomic changes to skeletal muscle for preliminary experiments.

The aim of this chapter is to assess the viability of the cell-stretch technique on C2C12 myotubes prior to a full analysis of intracellular proteomics before and after stretching. It was envisaged that this will enable an *in vitro* model for assessment of redox responses by skeletal muscle cells following bidirectional stimulation.

6.2 Results

C2C12 cells were grown from liquid nitrogen stocks and once confluent in T75s were seeded onto stretch plates. Figure 6.2.1 shows the seeding of myocytes (A) and differentiation of the cells into myotubes (B) after four days growth on standard 6-well plates.

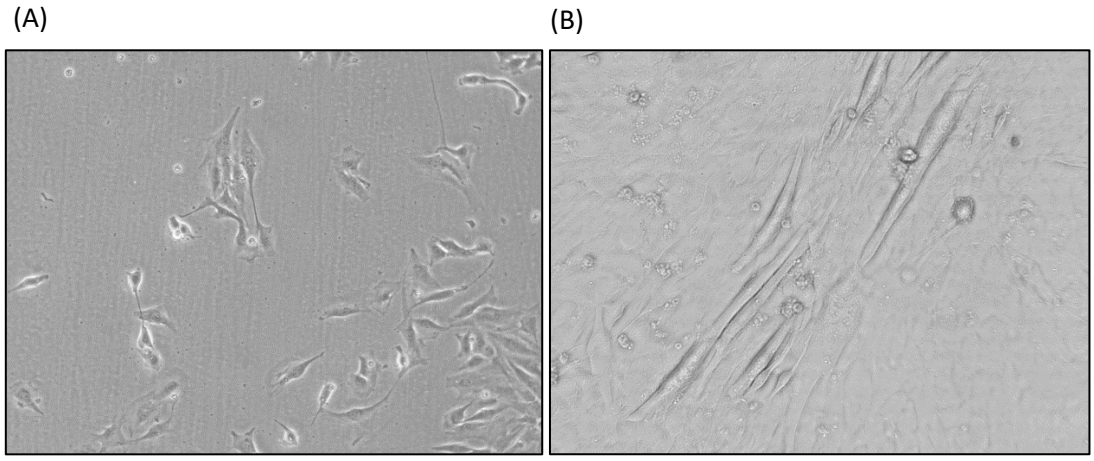

Figure 6.2.1 (A) Undifferentiated C2C12 myocytes. (B) Differentiated C2C12 myotubes following 4 days growth in differentiation media. Both images are of cells cultured on standard 6-well plates.

After preparation the cells were seeded on stretch plates and cyclically stretched at 12% for zero minutes (control), 15 minutes or 2 hours. Figure 6.2.2 shows an example image of the cells on the plate. The focus appears slightly off due to the custom plate size which did not fit plate holders available and the inverted microscopes were at their maximum focal length at this point.

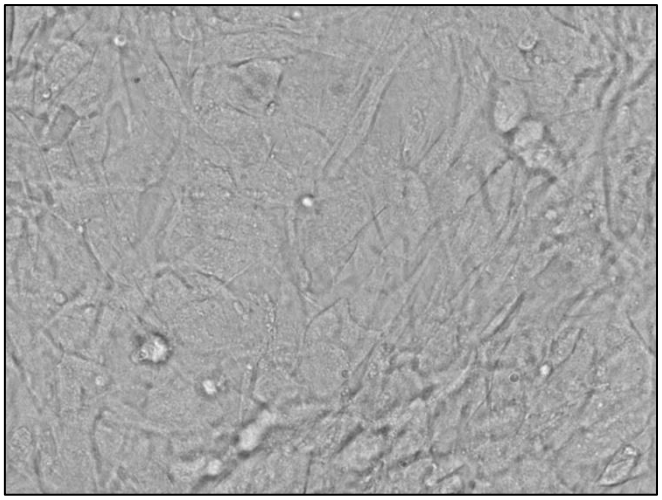

Figure 6.2.2 Differentiated C2C12 cells on 6-well stretch plate. The focus was limited by the different depth of the wells compared to standard 6-well plates.

Sample Label	Conc. (ug/ul)
Ctrl 1	1.02
Ctrl 2	1.07
Ctrl 3	1.17
Ctrl 4	1.11
Ctrl 5	0.80
Ctrl 6	0.98
30 mins 1	1.24
30 mins 2	1.23
30 mins 3	1.45
30 mins 4	1.59
30 mins 5	1.24
30 mins 6	1.13
2 hrs 1	1.33
2 hrs 2	1.07
2 hrs 3	1.10
2 hrs 4	0.98
2 hrs 5	1.23
2 hrs 6	1.00

Table 11. Protein content results for the samples determined following a Bradford Assay of whole cell protein content.

Western blots in figure 6.2.3 studied the effects of stretch and used antibodies to the protein chaperone and redox sensor PARK7 (figure 6.2.3A) involved in oxidative signalling in addition to chaperone activities. The content did not change with the stretching protocol and neither did P62 (figure 6.2.3B), a nucleoporin protein involved in autophagy as a receptor and mTOR signalling (Andres-Mateos et al., 2007, Sugiyama et al., 2016). Finally, ULK1 (figure

6.2.3C), a serine/threonine kinase also involved in autophagy (Loffler et al., 2011) was studied and demonstrated a significant increase in protein abundance following two hours of stretching. These proteins were selected as it was thought autophagy might be implicated in a cellular response to stretching due to the physical changes occurring to the cells over the different times.

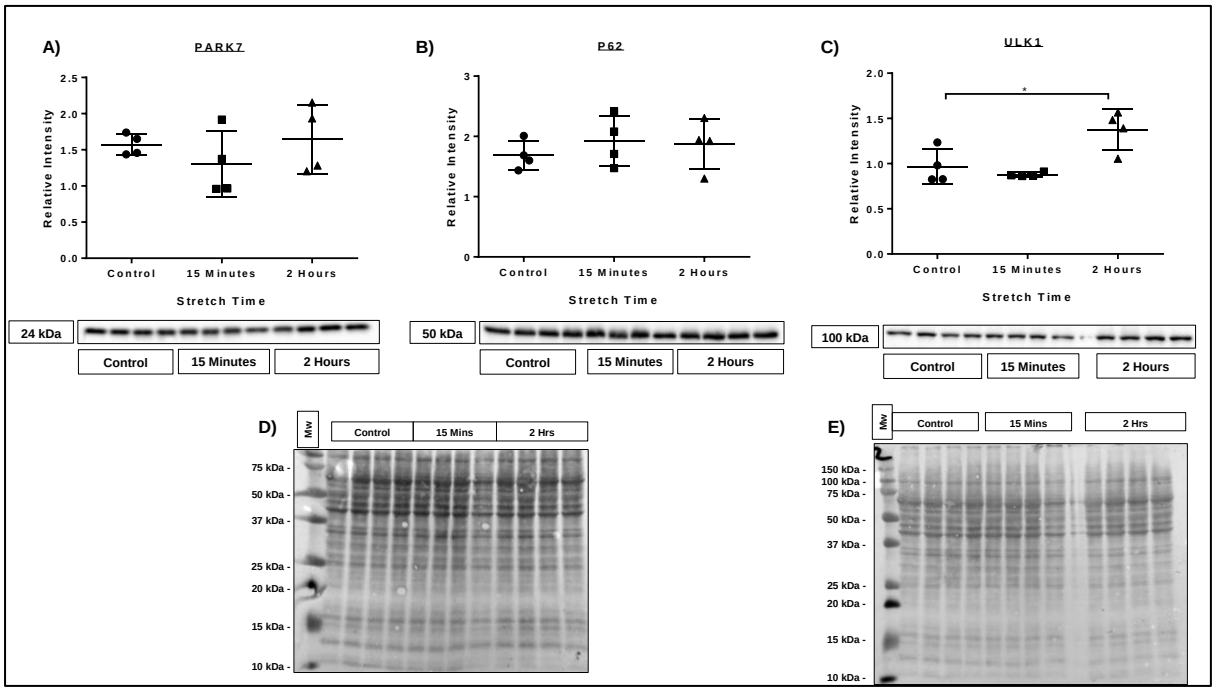

Figure 6.2.3. Densiometric measurement for immunodetection by western blotting data following 0 minutes (control), 15 minutes and 2 hours of cyclical stretching of C2C12 myotubes. Change in protein abundance was measured for (A) PARK7, (B) P62 and (C) ULK1, $*p < 0.05$. (D) Ponceau S stain used for normalisation of the PARK7 and P62 blots. (E) Ponceau S stain used for normalisation of the ULK1 blot. N=3 biological replicates. Short bars indicate upper and lower interquartile range while the middle represents the median value following statistical analysis using ANOVA with Tukey's post-hoc test.

6.3 Discussion and Conclusion

This experiment was undertaken to enable a preliminary look at an experimental protocol for myotube stretching and to optimise the equipment and software. Successful implementation of the protocol would enable future experiments to take an *in vitro* approach to examine the effect of mechanical stress on myotubes. Although these cells are being

stretched, rather than contracted, the physical change to the cell may cause changes that are closer to physiological conditions than cells maintained at rest.

Takemoto *et al.* used a 12% stretch intensity which appeared potentially sufficient to induce a redox response in the cells without causing excessive damage (Takemoto et al., 2012). Other work by Deshmukh *et al.* compared C2C12 cells and skeletal muscle tissue. They highlighted a 44% (significant) difference between proteomes of mouse skeletal muscle (triceps) and C2C12 cells (Deshmukh et al., 2015).

The Western blot of PARK7, P62 and ULK1 provide a brief insight into potential changes occurring following cell stretching. The results showed no significant change in P62 and PARK7 after 2 hours stretching. Given PARK7's role in protein folding amongst other abilities, it was surprising to see it unchanged following cell stretching while in previous chapters, PARK7 increased in abundance with age in quadriceps. This may suggest a difference in protein control mechanisms between the short and the long term. A significant increase in the autophagy protein ULK1 was observed and is supported by Moller *et al.*'s work in humans that identified an increase in ULK1 following exercise (Moller et al., 2015).

While differences in the methodology are acknowledged, the data from quadriceps and soleus muscles can be briefly considered as it aids our understanding as an alternative perspective on ageing skeletal muscle. The results in figure 6.2.3 (A) identified no change to PARK7 following induced physical stress on the cells, this contrasts with the quadriceps results which identified an increase in PARK7 abundance with age through western blotting. As this was not observed following stretching of the cells, it raises interesting questions regarding the duration and intensity of the stretching. The quadriceps label free analysis identified p62 but not ULK1 in the dataset although it was not significantly changed with age. Neither p62 nor ULK1 were detected in the soleus label free dataset. It should be noted, however, that the

C2C12 cells were taken from female mice and therefore the differences may be subject to sex differences rather than ageing or physical stretching.

Although brief, the aim of this chapter was to identify an experimental protocol that would be suitable for further studies and provide enough protein for western blots which was achieved. This sets in place the potential for future experiments to assess proteomic changes in myotubes and other cell types following stretching. This outcome also supports the three R's to replace, reduce or refine experiments involving animal models. Although this protocol does not contract the cells, the physical stress may induce further changes to the cellular proteome and transcriptome that have not yet been identified *in vitro.*

CHAPTER 7

GENERAL DISCUSSIONS

The work in this thesis aimed to improve understanding of how mouse skeletal muscle ages in two metabolically distinct muscles at both the global proteomic scale and specific redox changes in individual amino acids. The quadriceps and soleus muscles were examined in adult and old mice. The data are novel since no other study has used differential labelling combined with label free proteomics to analyse changes in redox state and protein abundance simultaneously. The global label free results highlighted changes to predominantly cytoskeletal proteins in the quadriceps with age whilst the metabolic machinery of the soleus appeared susceptible to age-related changes.

Overall, the work in this thesis supports other studies in demonstrating the importance of understanding changes to the intracellular redox state in relation to changes in cysteine amino acids with age. The importance of cysteine as a conserved amino acid in strategic locations such as in redox enzyme's active sites also, in a wider context of understanding how skeletal muscle ages (Klitgaard et al., 1990, Yang et al., 2016). In a broader context still, this work supports developments in the field of ROS biochemistry in ageing skeletal muscle by combining two proteomics techniques to elucidate both global changes to two different types of muscle as well as identifying changes to the redox proteome for individual cysteines amino acids (Ferreira and Reid, 2008).

It was hypothesised that the two muscles would age differently based on their metabolic and functional backgrounds and the data presented in this thesis supports this. It was also hypothesised that we would observe changes to redox proteins with age, however it was unclear how exactly these changes would manifest in the two different forms of ageing muscle.

Thiol signalling in skeletal muscle during ageing looked at the effect of changes to the intracellular redox environment and how this affected the mouse skeletal muscle. A number of studies have compared fast and slow twitch skeletal muscle ageing, however they used either

different species or muscle types (Demontis et al., 2013, Johnson et al., 2013, Leduc-Gaudet et al., 2015, Zhang and Gao, 2014). This study primarily used mass spectrometry to obtain a high-resolution assessment of the global proteome of quadriceps and soleus muscle. Differential labelling of individual cysteine amino acids was used to allow assessment of changes to the intracellular redox state of specific proteins with age. This approach also used a range of techniques such as western blotting to determine changes to protein abundance with age and enzyme activity assays to assess whether those changes in abundance were reflected in enzymic activity changes. Histological analysis of the muscles showed a reduction in oxidative phosphorylation energy metabolism via succinate dehydrogenase for both quadriceps and soleus as they age. In addition to the label free proteomic analysis, pathway analysis in GOrilla and STRING protein-protein interactions were also performed on the label free dataset to highlight how ageing impacted intracellular pathways or interactions.

This section aims to highlight key changes seen in ageing skeletal muscle and to put the results into the wider context of the scientific literature, setting the scene for future work and discussing experimental limitations before outlining the conclusions of the thesis.

Overall Comparisons of the Quadriceps and Soleus Data

The quadriceps and soleus muscles were found to age in different ways as determined by the label free proteomics and differential labelling data. In the quadriceps, ageing predominantly affected cytoskeletal proteins suggesting a possible increase in cellular stiffness relating to increased abundance of cytoskeletal proteins with age. In contrast, ageing in the soleus predominantly affected energy metabolism proteins. In addition to this, the number of redox sensitive proteins was also reduced with age in both muscles together with an increase in the number of reduced proteins with age.

Redox Changes to the Skeletal Muscle Proteome

We hypothesised that changes to the redox proteome would be observed with age, however the detected changes were not consistent across the different muscle types.

Ageing in the quadriceps identified an increased abundance of cytoskeletal proteins with age such as troponins (TNNI2 and TNNT3) and actin (ACTS) while protein chaperones HSP70 and HSPB6 were down regulated with age. Interestingly none of the peroxiredoxins or thioredoxin proteins were changed in abundance with age which was unexpected given the previous suggestions of the free radical theory of ageing. In contrast, the soleus demonstrated a down regulation of a large number of energy metabolism proteins or their subunits with age. It was interesting to note that this was not straight forward though as aconitase, fructose bisphosphate aldolase, electron transfer flavoprotein subunit α and ATP synthase subunit α was all significantly up regulated with age in the soleus. This soleus data is supported by an earlier study that observed similar changes in adult and old skeletal muscle fibres (O'Connell et al., 2007).

The redox cysteine results identified differences in changes to the redox state of specific proteins however the differences between muscles was less pronounced. In the quadriceps cofilin-2 (Cys80) changed in its redox state by increasing in reduced form 7.21-fold. Interestingly, the next two highest changing proteins changed from being reversibly oxidised forms in adult quadriceps to becoming very reduced in old muscle. They were glucose 6-phosphate isomerase (Cys321) and malate dehydrogenase (Cys154) increasing by 6.06 and 6.80-fold respectively. The changes to cofilin-2 and malate dehydrogenase were also observed in another study that looked at rat skeletal muscle ageing (Donoghue et al., 2010).

In the soleus a number of energy metabolism proteins were affected by changes to their redox states such as NADH ubiquinone (Ndufs1; Cys78) which saw a 28.7-fold increase in its

reduced state. Interestingly, two proteins identified as having significantly changed redox states in the quadriceps were also identified in the soleus. They were cofilin-2 (Cys80) with a 5.12-fold increase and malate dehydrogenase 1 (Cys154) which had a 5.34-fold increase in reduced redox states.

Thioredoxin 1 and Thioredoxin Reductase 1 are cytosol-based proteins and Thioredoxin 2 and Thioredoxin Reductase 2 are their mitochondrial equivalents, with a redox active cysteine at their active sites. This enables them to respond to changes in intracellular ROS concentrations by a change in oxidation state which affects the active site. Results from chapters 3 and 4 showed no change in abundance with age for either variant of Thioredoxin or Thioredoxin Reductase and no change was seen in either of their enzyme activities with age. The protein abundance result agrees with a study by Can *et al.* which analysed human serum levels of Thioredoxin 1 and also observed no change in old (Can et al., 2017). Several other studies have considered redox modifications to Thioredoxin or its effect in other organs (Dimauro et al., 2012, Kim et al., 2003), however none have looked at intracellular changes to protein abundance between fast and slow twitch muscles, and with age.

Peroxiredoxins showed very different responses in abundance in the quadriceps and soleus to ageing. Western blotting of quadriceps muscle identified no changes to protein abundance for Peroxiredoxins 1, 4 or 6, whereas the soleus demonstrated a significant decrease in Peroxiredoxin 1 and an increase in Peroxiredoxin 4 protein abundance with age. Peroxiredoxin 3 and 4 were not detected in the global label free proteomics data for the soleus due to limitations of detection, although in the quadriceps all six peroxiredoxins were detected. Other studies have examined Peroxiredoxins in a range of different species and systems, for example reporting a reduction in Peroxiredoxin 1 gene expression levels in the ageing human and its secretion in response to inflammation inducing production of inflammatory cytokines (Mullen et al., 2015). Peroxiredoxin 4 overexpression in *Drosophila* has been shown to

increase the inflammatory response and lead to an increase in longevity (Klichko et al., 2016). Studies of Peroxiredoxin 6 in neuronal Nitric Oxide Synthase knock-out mouse showed an up regulation of PRDX6 (Da Silva-Azevedo et al., 2009).

This study is the first to demonstrate protein abundance changes in fast and slow twitch skeletal muscles and how they differ with age. Additionally this information builds upon previous studies from our lab that determined how changes to the Peroxiredoxin 6 redox state within the sciatic nerve might lead to a change in Peroxiredoxin 6 signalling (McDonagh et al., 2016). Peroxiredoxins 2 (cytosolic), 3 and 5 (both mitochondrial) were only detected in quadriceps at 12 and 24 months. The results showed significant increases in mitochondrial Peroxiredoxin 3 and 5 with age. Studies have suggested Peroxiredoxin 3 may provide an 'anti-ageing' effect by controlling mitochondrial homeostasis and removal of the protein has been demonstrated to reduce contractile force of skeletal muscle (Lee et al., 2014, Zhang et al., 2016b). Peroxiredoxin 5 which is also mitochondrial, has not been described in detail in mouse skeletal muscle other than a single study describing its general function as a peroxynitrite reductase (Dubuisson et al., 2004). The speed of reactivity of Peroxiredoxin 2 and 3 were determined by Peskin *et al.* indicating that following hyperoxidation (which leads to inactivation of peroxiredoxins), Peroxiredoxin 3 had approximately a 10-fold higher rate constant for disulphide formation when compared to Peroxiredoxin 2 (Peskin et al., 2013). Hyperoxidation is described in detail in figure 1.4.1 (p.36). Briefly, hyperoxidation of peroxiredoxins occur where the first reactive cysteine reacts with H_2O_2 forming a sulphenic acid, this then condenses and a second H_2O_2 reacts with the (second) resolving cysteine on the protein. At this point the peroxiredoxin is said to be hyperoxidised (Peskin et al., 2013). The increased rate by which Peroxiredoxin 3 can form disulphide bonds when hyperoxidised may reflect higher requirement for control within the mitochondria, compared with the cytoplasm.

In addition to assessing individual peroxiredoxins, their sulphonylated forms (Peroxiredoxin-SO_3H, for peroxiredoxins 1-4) were assessed in quadriceps and soleus muscle to determine the extent of post-translational modifications with age. Data for the quadriceps revealed a significant increase with age whereas the soleus showed no change. No other published studies appear to specifically describe the effect of mouse skeletal muscle ageing and its relation to sulphonylated proteins, although one study reported sulphonylated proteins in rats following X-ray irradiation at a single age point (Fedorova et al., 2010).

Carbonylated proteins were assessed in both muscles with age and the quadriceps demonstrated a decease while no change was observed in the soleus. This was unexpected as it was assumed that ageing would cause an increase in reactive oxygen species and therefore an increase in carbonylated proteins with age. A number of other studies have identified carbonylated proteins in rat or mouse models (Meany et al., 2007, Radak et al., 2002, Carpentieri et al., 2016). Our data are in agreement with another study that demonstrated changes to carbonylated proteins in the mouse electron transport chain in mice with age (Choksi et al., 2008) but they examined quadriceps and pectoralis muscles.

Glutathionylation was also examined in the quadriceps. This is another measurement which can indicate sustained intracellular ROS concentrations and a range of studies have highlighted its specific effects on skeletal muscle proteins such as Creatine kinase (Reddy et al., 2000), Sodium-Potassium ATPase pump activity (Juel, 2014) and Myosin and Actin (Passarelli et al., 2008, Moen et al., 2014, Dalle-Donne et al., 2003). The data obtained here showed a significant increase in glutathionylated proteins between muscle from adult and old mice. Further work is discussed below which will consider potential, specific targets following this initial observation.

Antioxidant proteins control reactive oxygen species and maintain redox homeostasis within skeletal muscle fibres. The work reported here examined both the cytosolic Cu-Zn superoxide dismutase (SOD1) and the mitochondrial Mn-Superoxide dismutase (SOD2). SOD1 was examined in both quadriceps and soleus while SOD2 was only tested in the quadriceps. A number of studies have tested SOD1 or SOD2 knock out mouse models to elucidate the importance of SOD activity in skeletal muscle and ageing (Nagahisa et al., 2016, Masser et al., 2016, McArdle et al., 2004b, Zhang et al., 2013). One study reported significant increases in SOD1 and SOD2 with age (Pietrangelo et al., 2015). The western blot results showed here showed a significant increase in SOD1 content in quadriceps from 3 to 12 months while the soleus content increased from 3 to 24 months of age. SOD2 did not change in protein abundance with age in the quadriceps. The SOD1 results broadly support the proposal that with age comes an increasing demand for ROS control in the cytoplasm for both muscle types. However, the lack of change in SOD2 in quadriceps may also reflect the reduction in mitochondria numbers as observed in ageing skeletal muscle (Alnaqeeb and Goldspink, 1987, Peterson et al., 2012).

Experimental Considerations and Limitations

Mass spectrometry is a very useful technique for assessing changes to proteins, either through their abundance using global analysis of a sample, or via differential labelling of specific amino acids to identify changes to their oxidation state. Mass spectrometry analysis is often supported by western blotting. This combination of the two methods has enabled a verification system that has yet to be surpassed, although it is not without limitations. In this thesis a number of experiments included information of the same protein from both techniques. Where they do not agree with each other, the data are assessed in the respective discussion chapter. Western blotting offers high specificity for a particular sequence, but mass

spectrometry is highly sensitive to detecting protein in a mixture. It is this combination that enabled a detailed analysis of protein changes skeletal muscle as it ages.

Limitations of the Western blotting technique are that it is semi-quantitative, such that the results, whilst highly specific, only indicate a change in arbitrary units against a normalised background based on the amount of chemiluminescence detected. As previously described, normalisation of proteins utilised multiple bands from a Ponceau S stain which helped to indicate both equal protein loading across all lanes. Laboratory limitations include labour intensiveness since it requires multiple steps of membrane washing, multiple buffers and incubation with both a blocking agent and with the respective antibodies. Specificities of these steps such as wash time, buffer production methods and incubation time may vary from lab to lab and produce variables that must be accounted for (Anderson et al., 2011, Kurien and Scofield, 2006). The antibodies used, although highly specific, are often proprietary meaning that the actual sequence detected is not always public knowledge and therefore an antibody from different companies may produce different results (Gilda et al., 2015). The Western blots performed for this thesis all used exactly the same method for buffer preparation, antibody dilutions and blot image analysis. Western blot analysis of the soleus proved particularly difficult due to the limited amount of protein available from the small muscle.

The mass spectrometry experiment analysed six adult and five old samples of muscle from individual mice whereas for western blotting only three biological samples from muscle at 3, 12 and 24 months of age were examined. The extra time point used in the western blot data was due to its timely availability during this study. The samples were from the same strains of mice, housed under the same conditions and no outliers were removed from the western blot plots as shown by the individual data-points. Although the blot data is interesting in demonstrating changes in peroxiredoxins, the mass spectrometry results are likely to be a more accurate picture of changes in protein abundance with age due to the increased sensitivity. It

should be noted that the confidence in the proteins detected is dependent upon the percentage of those detected. Therefore, proteins with only a single peptide detected would yield a very low confidence compared to proteins with many peptide strands identified.

The limitations of mass spectrometry are changing rapidly due to improved techniques for sample preparation, protein fractionation, the mass spectrometers' ability to quantitate detected proteins and bioanalytics software with improving search algorithms for matching detected sequences of peptides to protein databases for individual species (Deshmukh, 2016).

The technique employed in this thesis was a data-dependent acquisition (DDA) which relied on detection of peptide sequences which were then compared to a known database of sequences to identify peptides and subsequently proteins (Egertson et al., 2015). This utilises consecutive time windows to fill the ion trap with the 10 most abundant ions fragmented by MS/MS, these ions are discarded, and the subsequent most abundant ions are fragmented until the dwell time has passed and the trap fills with a new set of ions. The clear drawback to this method is that it relies on peptide abundance during the initial run for subsequent detections with many low abundant ions failing to be fragmented by MS/MS and hence detected. This means highly abundant peptide sequences can overshadow those with a lower abundance in a given sample and as the skeletal muscle proteome contains over 50% contractile proteins, this is likely to skew the results of those proteins detected within samples (Deshmukh, 2016, Deshmukh et al., 2015, Ohlendieck, 2011). Alternatives to this limitation include high-fractionation of protein samples to ensure separation and detection of very low abundance peptides. Another approach is to analyse single muscle fibres to ensure peptide quantitation is directly linked to approximate abundance within a muscle fibre type (Deshmukh et al., 2015). It is due to these limitations of the mass spectrometry technique that western blotting was also employed here as this enables detection of proteins of interest with high specificity (Ohlendieck, 2013).

As an alternative to the limitations of DDA, there is data independent analysis (DIA). An example of this is selective reaction monitoring (SRM) also referred to as multiple reaction monitoring (MRM) when scaled up. This identifies peptides via a unique fingerprint of the parent ion and the subsequent product ion, matching them and enabling an exact quantification of individual peptides from a sample (Aebersold et al., 2013, Gillet et al., 2012). SRM is hypothesis driven and relies on knowing which peptides to search for prior to the experiment. When targets of interest are defined then specific pathways or systems can be further quantified using this technique (Thomas and Zhang, 2016). However, SRM still has some limitations as it requires internal standards for quantification which need to be well characterised and calibrated, a lack of high throughput meaning only select peptides can be measured and reproducibility due to varying experimental methods and sample preparation (Gallien et al., 2013).

Another alternative mass spectrometry technique is SWATH-MS or sequential window of all theoretical fragment ion spectra mass spectrometry which analyses all detected peptide fragments in a mass range (Krisp and Molloy, 2017). This enables identification of peptides within a specific mass range and the data can be reprocessed at a later stage should new evidence come to light (Zhang et al., 2015).

As a more general limitation of mass spectrometry the proposed peptides need to be analysable via mass spectrometry which immediately precludes a variety of potential targets from analysis or quantification via any current mass spectrometric method (Gallien et al., 2013, Xiao et al., 2012).

Future Work

Various additional experiments could add to the data obtained and further improve the understanding of ageing skeletal muscle. One example is the mass spectrometric analysis of S-

sulphonylated proteins specifically, to understand these irreversible modifications in skeletal muscle. It would be interesting to see if the changes correlate to ageing muscle or specific conditions (Borotto et al., 2017). Next steps would include testing of different stretch conditions to see if there is a 'sweet spot' for stretching of myotubes followed by developing the cell stretch methodology to include the contraction phase. Subsequently changes to redox proteins following the increasingly physiologically relevant protocol would be a natural next step. Finally, a proteomic analysis of the cells before and after stretching would provide much needed insight into the effect of mechanical stretching on myotubes and determine whether any similarities to *in vivo* mechanisms exist. Furthermore, it would be building on the initial C2C12 proteomics work performed by Deshmukh *et al.*(Deshmukh et al., 2015).

Thesis Conclusions

This thesis has added to knowledge in the field of skeletal muscle ageing by assessing differences in two forms of muscle: the quadriceps, a predominantly fast twitch, Type II muscle and the soleus, a predominantly slow twitch, type I muscle and across three ages. The global label free proteomics assessment has showed a number of age-related changes not previously described and the differential labelling of specific cysteine residues gave an important insight into which proteins are susceptible to changes in the intracellular redox state. The data combined also showed how although certain proteins are susceptible to change with age, this may not affect their enzymatic activity.

In conclusion this thesis has demonstrated that ageing affects thiol signalling in skeletal muscle ageing in a number of different ways. The global proteome analysis paints the two muscles as distinct and changing in clearly different ways with age however, the redox changes observed are far more conservative.

and relating to muscle fibre type. This proves the overall hypothesis correct: that the two muscles will age differently due to their metabolic and functional backgrounds. The novel approach in the thesis combined label free relative quantitation of the global proteome with differential labelling for each muscle and between adult and old muscle samples to identify a range of age-associated changes for each muscle.

It is hoped that this data may go some way to understanding the complexities of how different types of skeletal muscle age by providing a foundation for further research to understand why sarcopenia occurs and in time mitigate its outcomes.

BIBLIOGRAPHY:

<Free radical generation by skeletal muscle of adult and old mice - effect of contractile activity. Vasilaki A et al., 2006.pdf>.

ACHTEN, J., GLEESON, M. & JEUKENDRUP, A. E. 2002. Determination of the exercise intensity that elicits maximal fat oxidation. *Med Sci Sports Exerc,* 34**,** 92-7.

AEBERSOLD, R., BURLINGAME, A. L. & BRADSHAW, R. A. 2013. Western blots versus selected reaction monitoring assays: time to turn the tables? *Mol Cell Proteomics,* 12**,** 2381-2.

ALHAWITI, N. M., AL MAHRI, S., AZIZ, M. A., MALIK, S. S. & MOHAMMAD, S. 2017. TXNIP in Metabolic Regulation: Physiological Role and Therapeutic Outlook. *Curr Drug Targets,* 18**,** 1095-1103.

ALLEN, R. G. & TRESINI, M. 2000. Oxidative stress and gene regulation. *Free Radic Biol Med,* 28**,** 463-99.

ALNAQEEB, M. A. & GOLDSPINK, G. 1987. Changes in fibre type, number and diameter in developing and ageing skeletal muscle. *J Anat,* 153**,** 31-45.

ANDERSON, G. J., C, M. C. & KENNEDY, R. T. 2011. Western blotting using capillary electrophoresis. *Anal Chem,* 83**,** 1350-5.

ANDRES-MATEOS, E., PERIER, C., ZHANG, L., BLANCHARD-FILLION, B., GRECO, T. M., THOMAS, B., KO, H. S., SASAKI, M., ISCHIROPOULOS, H., PRZEDBORSKI, S., DAWSON, T. M. & DAWSON, V. L. 2007. DJ-1 gene deletion reveals that DJ-1 is an atypical peroxiredoxin-like peroxidase. *Proc Natl Acad Sci U S A,* 104**,** 14807-12.

ARNER, E. S., ZHONG, L. & HOLMGREN, A. 1999. Preparation and assay of mammalian thioredoxin and thioredoxin reductase. *Methods Enzymol,* 300**,** 226-39.

ASEA, A., KRAEFT, S. K., KURT-JONES, E. A., STEVENSON, M. A., CHEN, L. B., FINBERG, R. W., KOO, G. C. & CALDERWOOD, S. K. 2000. HSP70 stimulates cytokine production through a CD14-dependant pathway, demonstrating its dual role as a chaperone and cytokine. *Nat Med,* 6**,** 435-42.

ATKINS, P. W. & DE PAULA, J. 2010. *Physical chemistry,* New York, W. H. Freeman and Co.

AUERBACH, D., BANTLE, S., KELLER, S., HINDERLING, V., LEU, M., EHLER, E. & PERRIARD, J. C. 1999. Different domains of the M-band protein myomesin are involved in myosin binding and M-band targeting. *Mol Biol Cell,* 10**,** 1297-308.

BARBIERI, E. & SESTILI, P. 2012. Reactive oxygen species in skeletal muscle signaling. *J Signal Transduct,* 2012**,** 982794.

BARCLAY, C. J., CONSTABLE, J. K. & GIBBS, C. L. 1993. Energetics of fast- and slow-twitch muscles of the mouse. *J Physiol,* 472**,** 61-80.

BARCLAY, J. K. 1982. Energetics of mammalian fast and slow twitch muscles. *Fed Proc,* 41**,** 189-91.

BASAIAWMOIT, R. V. & RATTAN, S. I. 2010. Cellular stress and protein misfolding during aging. *Methods Mol Biol,* 648**,** 107-17.

BATINIC-HABERLE, I., TOVMASYAN, A. & SPASOJEVIC, I. 2015. An educational overview of the chemistry, biochemistry and therapeutic aspects of Mn porphyrins--From superoxide dismutation to H2O2-driven pathways. *Redox Biol,* 5**,** 43-65.

BEDARD, K. & KRAUSE, K. H. 2007. The NOX family of ROS-generating NADPH oxidases: physiology and pathophysiology. *Physiol Rev,* 87**,** 245-313.

BERG, J. M., TYMOCZKO, J. L. & STRYER, L. 2002. *Biochemistry,* New York, W.H. Freeman.

BHABAK, K. P. & MUGESH, G. 2010. Functional mimics of glutathione peroxidase: bioinspired synthetic antioxidants. *Acc Chem Res,* 43**,** 1408-19.

BI, S., HONG, P. W., LEE, B. & BAUM, L. G. 2011. Galectin-9 binding to cell surface protein disulfide isomerase regulates the redox environment to enhance T-cell migration and HIV entry. *Proc Natl Acad Sci U S A,* 108**,** 10650-5.

BIZZOZERO, O. A., ZIEGLER, J. L., DE JESUS, G. & BOLOGNANI, F. 2006. Acute depletion of reduced glutathione causes extensive carbonylation of rat brain proteins. *J Neurosci Res,* 83**,** 656-67.

BLANDIN, G., MARCHAND, S., CHARTON, K., DANIELE, N., GICQUEL, E., BOUCHETEIL, J. B., BENTAIB, A., BARRAULT, L., STOCKHOLM, D., BARTOLI, M. & RICHARD, I. 2013. A human skeletal muscle interactome centered on proteins involved in muscular dystrophies: LGMD interactome. *Skelet Muscle,* 3**,** 3.

BLOEMBERG, D. & QUADRILATERO, J. 2012. Rapid determination of myosin heavy chain expression in rat, mouse, and human skeletal muscle using multicolor immunofluorescence analysis. *PLoS One,* 7**,** e35273.

BOENGLER, K., KOSIOL, M., MAYR, M., SCHULZ, R. & ROHRBACH, S. 2017. Mitochondria and ageing: role in heart, skeletal muscle and adipose tissue. *J Cachexia Sarcopenia Muscle,* 8**,** 349-369.

BOFFOLI, D., SCACCO, S. C., VERGARI, R., PERSIO, M. T., SOLARINO, G., LAFORGIA, R. & PAPA, S. 1996. Ageing is associated in females with a decline in the content and activity on the b-c1 complex in skeletal muscle mitochondria. *Biochim Biophys Acta,* 1315**,** 66-72.

BOHNERT, K. R., MCMILLAN, J. D. & KUMAR, A. 2018. Emerging roles of ER stress and unfolded protein response pathways in skeletal muscle health and disease. *J Cell Physiol,* 233**,** 67-78.

BOOTH, F. W. & THOMASON, D. B. 1991. Molecular and cellular adaptation of muscle in response to exercise: perspectives of various models. *Physiol Rev,* 71**,** 541-85.

BOROTTO, N. B., MCCLORY, P. J., MARTIN, B. R. & HAKANSSON, K. 2017. Targeted Annotation of S-Sulfonylated Peptides by Selective Infrared Multiphoton Dissociation Mass Spectrometry. *Anal Chem,* 89**,** 8304-8310.

BRANCO, V., COPPO, L., SOLA, S., LU, J., RODRIGUES, C. M. P., HOLMGREN, A. & CARVALHO, C. 2017. Impaired cross-talk between the thioredoxin and glutathione systems is related to ASK-1 mediated apoptosis in neuronal cells exposed to mercury. *Redox Biol,* 13**,** 278-287.

BRANDES, R. P., WEISSMANN, N. & SCHRODER, K. 2014. Nox family NADPH oxidases: Molecular mechanisms of activation. *Free Radic Biol Med,* 76**,** 208-26.

BRASH, A. R. 1999. Lipoxygenases: occurrence, functions, catalysis, and acquisition of substrate. *J Biol Chem,* 274**,** 23679-82.

BRIGELIUS, R., MUCKEL, C., AKERBOOM, T. P. & SIES, H. 1983. Identification and quantitation of glutathione in hepatic protein mixed disulfides and its relationship to glutathione disulfide. *Biochem Pharmacol,* 32**,** 2529-34.

BROOK, M. S., WILKINSON, D. J., PHILLIPS, B. E., PEREZ-SCHINDLER, J., PHILP, A., SMITH, K. & ATHERTON, P. J. 2016. Skeletal muscle homeostasis and plasticity in youth and ageing: impact of nutrition and exercise. *Acta Physiol (Oxf),* 216**,** 15-41.

BROOKS, S. V. & FAULKNER, J. A. 1988. Contractile properties of skeletal muscles from young, adult and aged mice. *J Physiol,* 404**,** 71-82.

CAMPBELL, N. A. & REECE, J. B. 2005. *Biology,* San Francisco, Pearson, Benjamin Cummings.

CAN, B., KARA, O., KIZILARSLANOGLU, M. C., ARIK, G., AYCICEK, G. S., SUMER, F., CIVELEK, R., DEMIRTAS, C. & ULGER, Z. 2017. Serum markers of inflammation and oxidative stress in sarcopenia. *Aging Clin Exp Res,* 29**,** 745-752.

CANET-AVILES, R. M., WILSON, M. A., MILLER, D. W., AHMAD, R., MCLENDON, C., BANDYOPADHYAY, S., BAPTISTA, M. J., RINGE, D., PETSKO, G. A. & COOKSON, M. R. 2004. The Parkinson's disease protein DJ-1 is neuroprotective due to cysteine-sulfinic acid-driven mitochondrial localization. *Proc Natl Acad Sci U S A,* 101**,** 9103-8.

CAO, J., HUANG, T., LI, X. & ZHAO, S. 2014. Interactome mapping reveals important pathways in skeletal muscle development of pigs. *Int J Mol Sci,* 15**,** 21788-802.

CARPENTIERI, A., GAMBERI, T., MODESTI, A., AMORESANO, A., COLOMBINI, B., NOCELLA, M., BAGNI, M. A., FIASCHI, T., BAROLO, L., GULISANO, M. & MAGHERINI, F. 2016. Profiling Carbonylated Proteins in Heart and Skeletal Muscle Mitochondria from Trained and Untrained Mice. *J Proteome Res,* 15**,** 3666-3678.

CHAKKALAKAL, J. V., KUANG, S., BUFFELLI, M., LICHTMAN, J. W. & SANES, J. R. 2012. Mouse transgenic lines that selectively label Type I, Type IIA, and Types IIX+B skeletal muscle fibers. *Genesis,* 50**,** 50-8.

CHAVES, D. F., CARVALHO, P. C., LIMA, D. B., NICASTRO, H., LORENZETI, F. M., SIQUEIRA-FILHO, M., HIRABARA, S. M., ALVES, P. H., MORESCO, J. J., YATES, J. R., 3RD & LANCHA, A. H., JR. 2013. Comparative proteomic analysis of the aging soleus and extensor digitorum longus rat muscles using TMT labeling and mass spectrometry. *J Proteome Res,* 12**,** 4532-46.

CHENG, G., CAO, Z., XU, X., VAN MEIR, E. G. & LAMBETH, J. D. 2001. Homologs of gp91phox: cloning and tissue expression of Nox3, Nox4, and Nox5. *Gene,* 269**,** 131-40.

CHO, C. S., YOON, H. J., KIM, J. Y., WOO, H. A. & RHEE, S. G. 2014. Circadian rhythm of hyperoxidized peroxiredoxin II is determined by hemoglobin autoxidation and the 20S proteasome in red blood cells. *Proc Natl Acad Sci U S A,* 111**,** 12043-8.

CHOKSI, K. B., NUSS, J. E., DEFORD, J. H. & PAPACONSTANTINOU, J. 2008. Age-related alterations in oxidatively damaged proteins of mouse skeletal muscle mitochondrial electron transport chain complexes. *Free Radic Biol Med,* 45**,** 826-38.

CHOPARD, A., PONS, F. & MARINI, J. F. 2001. Cytoskeletal protein contents before and after hindlimb suspension in a fast and slow rat skeletal muscle. *Am J Physiol Regul Integr Comp Physiol,* 280**,** R323-30.

CHOU, M. F. & SCHWARTZ, D. 2011. Biological sequence motif discovery using motif-x. *Curr Protoc Bioinformatics,* Chapter 13**,** Unit 13 15-24.

CHU, P. H., RUIZ-LOZANO, P., ZHOU, Q., CAI, C. & CHEN, J. 2000. Expression patterns of FHL/SLIM family members suggest important functional roles in skeletal muscle and cardiovascular system. *Mech Dev,* 95**,** 259-65.

CHUNG, H. S., WANG, S. B., VENKATRAMAN, V., MURRAY, C. I. & VAN EYK, J. E. 2013. Cysteine oxidative posttranslational modifications: emerging regulation in the cardiovascular system. *Circ Res,* 112**,** 382-92.

CLAFLIN, D. R., JACKSON, M. J. & BROOKS, S. V. 2015. Age affects the contraction-induced mitochondrial redox response in skeletal muscle. *Front Physiol,* 6**,** 21.

CLEMENTS, C. M., MCNALLY, R. S., CONTI, B. J., MAK, T. W. & TING, J. P. 2006. DJ-1, a cancer- and Parkinson's disease-associated protein, stabilizes the antioxidant transcriptional master regulator Nrf2. *Proc Natl Acad Sci U S A,* 103**,** 15091-6.

COLLINS, Y., CHOUCHANI, E. T., JAMES, A. M., MENGER, K. E., COCHEME, H. M. & MURPHY, M. P. 2012. Mitochondrial redox signalling at a glance. *J Cell Sci,* 125**,** 801-6.

CROFTS, A. R. 2004. The cytochrome bc1 complex: function in the context of structure. *Annu Rev Physiol,* 66**,** 689-733.

CROW, M. T. & KUSHMERICK, M. J. 1982. Chemical energetics of slow- and fast-twitch muscles of the mouse. *J Gen Physiol,* 79**,** 147-66.

D'AUTREAUX, B. & TOLEDANO, M. B. 2007. ROS as signalling molecules: mechanisms that generate specificity in ROS homeostasis. *Nat Rev Mol Cell Biol,* 8**,** 813-24.

DA SILVA-AZEVEDO, L., JAHNE, S., HOFFMANN, C., STALDER, D., HELLER, M., PRIES, A. R., ZAKRZEWICZ, A. & BAUM, O. 2009. Up-regulation of the peroxiredoxin-6 related metabolism of reactive oxygen species in skeletal muscle of mice lacking neuronal nitric oxide synthase. *J Physiol,* 587**,** 655-68.

DALLE-DONNE, I., ROSSI, R., GIUSTARINI, D., COLOMBO, R. & MILZANI, A. 2003. Actin S-glutathionylation: evidence against a thiol-disulphide exchange mechanism. *Free Radic Biol Med,* 35**,** 1185-93.

DARNOLD, J. R., VORBECK, M. L. & MARTIN, A. P. 1990. Effect of aging on the oxidative phosphorylation pathway. *Mech Ageing Dev,* 53**,** 157-67.

DASGUPTA, A., ZHENG, J. & BIZZOZERO, O. A. 2012. Protein carbonylation and aggregation precede neuronal apoptosis induced by partial glutathione depletion. *ASN Neuro,* 4.

DAVIES, K. J., QUINTANILHA, A. T., BROOKS, G. A. & PACKER, L. 1982. Free radicals and tissue damage produced by exercise. *Biochem Biophys Res Commun,* 107**,** 1198-205.

DE PALMA, C., MORISI, F., PAMBIANCO, S., ASSI, E., TOUVIER, T., RUSSO, S., PERROTTA, C., ROMANELLO, V., CARNIO, S., CAPPELLO, V., PELLEGRINO, P., MOSCHENI, C., BASSI, M. T.,

SANDRI, M., CERVIA, D. & CLEMENTI, E. 2014. Deficient nitric oxide signalling impairs skeletal muscle growth and performance: involvement of mitochondrial dysregulation. *Skelet Muscle,* 4**,** 22.

DEEPA, S. S., BHASKARAN, S., ESPINOZA, S., BROOKS, S. V., MCARDLE, A., JACKSON, M. J., VAN REMMEN, H. & RICHARDSON, A. 2017. A new mouse model of frailty: the Cu/Zn superoxide dismutase knockout mouse. *Geroscience,* 39**,** 187-198.

DELDICQUE, L., CANI, P. D., PHILP, A., RAYMACKERS, J. M., MEAKIN, P. J., ASHFORD, M. L., DELZENNE, N. M., FRANCAUX, M. & BAAR, K. 2010. The unfolded protein response is activated in skeletal muscle by high-fat feeding: potential role in the downregulation of protein synthesis. *Am J Physiol Endocrinol Metab,* 299**,** E695-705.

DELDICQUE, L., VAN PROEYEN, K., FRANCAUX, M. & HESPEL, P. 2011. The unfolded protein response in human skeletal muscle is not involved in the onset of glucose tolerance impairment induced by a fat-rich diet. *Eur J Appl Physiol,* 111**,** 1553-8.

DEMONTIS, F., PICCIRILLO, R., GOLDBERG, A. L. & PERRIMON, N. 2013. Mechanisms of skeletal muscle aging: insights from Drosophila and mammalian models. *Dis Model Mech,* 6**,** 1339-52.

DESHMUKH, A. S. 2016. Proteomics of Skeletal Muscle: Focus on Insulin Resistance and Exercise Biology. *Proteomes,* 4.

DESHMUKH, A. S., MURGIA, M., NAGARAJ, N., TREEBAK, J. T., COX, J. & MANN, M. 2015. Deep proteomics of mouse skeletal muscle enables quantitation of protein isoforms, metabolic pathways, and transcription factors. *Mol Cell Proteomics,* 14**,** 841-53.

DEVASAGAYAM, T. P., TILAK, J. C., BOLOOR, K. K., SANE, K. S., GHASKADBI, S. S. & LELE, R. D. 2004. Free radicals and antioxidants in human health: current status and future prospects. *J Assoc Physicians India,* 52**,** 794-804.

DI MEO, S. & VENDITTI, P. 2001. Mitochondria in exercise-induced oxidative stress. *Biol Signals Recept,* 10**,** 125-40.

DIMAURO, I., PEARSON, T., CAPOROSSI, D. & JACKSON, M. J. 2012. In vitro susceptibility of thioredoxins and glutathione to redox modification and aging-related changes in skeletal muscle. *Free Radic Biol Med,* 53**,** 2017-27.

DIRKS, A. J., HOFER, T., MARZETTI, E., PAHOR, M. & LEEUWENBURGH, C. 2006. Mitochondrial DNA mutations, energy metabolism and apoptosis in aging muscle. *Ageing Res Rev,* 5**,** 179-95.

DONOGHUE, P., STAUNTON, L., MULLEN, E., MANNING, G. & OHLENDIECK, K. 2010. DIGE analysis of rat skeletal muscle proteins using nonionic detergent phase extraction of young adult versus aged gastrocnemius tissue. *J Proteomics,* 73**,** 1441-53.

DUBUISSON, M., VANDER STRICHT, D., CLIPPE, A., ETIENNE, F., NAUSER, T., KISSNER, R., KOPPENOL, W. H., REES, J. F. & KNOOPS, B. 2004. Human peroxiredoxin 5 is a peroxynitrite reductase. *FEBS Lett,* 571**,** 161-5.

DUMONT, N. A., WANG, Y. X. & RUDNICKI, M. A. 2015. Intrinsic and extrinsic mechanisms regulating satellite cell function. *Development,* 142**,** 1572-81.

EDEN, E., LIPSON, D., YOGEV, S. & YAKHINI, Z. 2007. Discovering motifs in ranked lists of DNA sequences. *Plos Computational Biology,* 3**,** 508-522.

EDEN, E., NAVON, R., STEINFELD, I., LIPSON, D. & YAKHINI, Z. 2009. GOrilla: a tool for discovery and visualization of enriched GO terms in ranked gene lists. *BMC Bioinformatics,* 10**,** 48.

EGAN, B. & ZIERATH, J. R. 2013. Exercise metabolism and the molecular regulation of skeletal muscle adaptation. *Cell Metab,* 17**,** 162-84.

EGERTSON, J. D., MACLEAN, B., JOHNSON, R., XUAN, Y. & MACCOSS, M. J. 2015. Multiplexed peptide analysis using data-independent acquisition and Skyline. *Nat Protoc,* 10**,** 887-903.

ESPINOSA, A., HENRIQUEZ-OLGUIN, C. & JAIMOVICH, E. 2016. Reactive oxygen species and calcium signals in skeletal muscle: A crosstalk involved in both normal signaling and disease. *Cell Calcium,* 60**,** 172-9.

FAZELZADEH, P., HANGELBROEK, R. W., TIELAND, M., DE GROOT, L. C., VERDIJK, L. B., VAN LOON, L. J., SMILDE, A. K., ALVES, R. D., VERVOORT, J., MULLER, M., VAN DUYNHOVEN, J. P. &

BOEKSCHOTEN, M. V. 2016. The Muscle Metabolome Differs between Healthy and Frail Older Adults. *J Proteome Res,* 15**,** 499-509.

FEDOROVA, M., KULEVA, N. & HOFFMANN, R. 2010. Identification of cysteine, methionine and tryptophan residues of actin oxidized in vivo during oxidative stress. *J Proteome Res,* 9**,** 1598-609.

FERNANDES, A. P. & HOLMGREN, A. 2004. Glutaredoxins: glutathione-dependent redox enzymes with functions far beyond a simple thioredoxin backup system. *Antioxid Redox Signal,* 6**,** 63-74.

FERRARO, E., GIAMMARIOLI, A. M., CHIANDOTTO, S., SPOLETINI, I. & ROSANO, G. 2014. Exercise-induced skeletal muscle remodeling and metabolic adaptation: redox signaling and role of autophagy. *Antioxid Redox Signal,* 21**,** 154-76.

FERREIRA, L. F. & LAITANO, O. 2016. Regulation of NADPH oxidases in skeletal muscle. *Free Radic Biol Med,* 98**,** 18-28.

FERREIRA, L. F. & REID, M. B. 2008. Muscle-derived ROS and thiol regulation in muscle fatigue. *J Appl Physiol (1985),* 104**,** 853-60.

FERRUCCI, L., PENNINX, B. W., VOLPATO, S., HARRIS, T. B., BANDEEN-ROCHE, K., BALFOUR, J., LEVEILLE, S. G., FRIED, L. P. & MD, J. M. 2002. Change in muscle strength explains accelerated decline of physical function in older women with high interleukin-6 serum levels. *J Am Geriatr Soc,* 50**,** 1947-54.

FITTS, R. H., TROUP, J. P., WITZMANN, F. A. & HOLLOSZY, J. O. 1984. The effect of ageing and exercise on skeletal muscle function. *Mech Ageing Dev,* 27**,** 161-72.

FORMAN, H. J., URSINI, F. & MAIORINO, M. 2014. An overview of mechanisms of redox signaling. *J Mol Cell Cardiol,* 73**,** 2-9.

FRATELLI, M., DEMOL, H., PUYPE, M., CASAGRANDE, S., EBERINI, I., SALMONA, M., BONETTO, V., MENGOZZI, M., DUFFIEUX, F., MICLET, E., BACHI, A., VANDEKERCKHOVE, J., GIANAZZA, E. & GHEZZI, P. 2002. Identification by redox proteomics of glutathionylated proteins in oxidatively stressed human T lymphocytes. *Proc Natl Acad Sci U S A,* 99**,** 3505-10.

FRIEDKIN, M. & LEHNINGER, A. L. 1949. Esterification of inorganic phosphate coupled to electron transport between dihydrodiphosphopyridine nucleotide and oxygen. *J Biol Chem,* 178**,** 611-44.

FRONTERA, W. R., HUGHES, V. A., FIELDING, R. A., FIATARONE, M. A., EVANS, W. J. & ROUBENOFF, R. 2000. Aging of skeletal muscle: a 12-yr longitudinal study. *J Appl Physiol (1985),* 88**,** 1321-6.

GALLIEN, S., DURIEZ, E., DEMEURE, K. & DOMON, B. 2013. Selectivity of LC-MS/MS analysis: implication for proteomics experiments. *J Proteomics,* 81**,** 148-58.

GARCIA, S. M., TAMAKI, S., XU, X. & POMERANTZ, J. H. 2017. Human Satellite Cell Isolation and Xenotransplantation. *Methods Mol Biol,* 1668**,** 105-123.

GARVEY, S. M., DUGLE, J. E., KENNEDY, A. D., MCDUNN, J. E., KLINE, W., GUO, L., GUTTRIDGE, D. C., PEREIRA, S. L. & EDENS, N. K. 2014. Metabolomic profiling reveals severe skeletal muscle group-specific perturbations of metabolism in aged FBN rats. *Biogerontology,* 15**,** 217-32.

GILDA, J. E., GHOSH, R., CHEAH, J. X., WEST, T. M., BODINE, S. C. & GOMES, A. V. 2015. Western Blotting Inaccuracies with Unverified Antibodies: Need for a Western Blotting Minimal Reporting Standard (WBMRS). *PLoS One,* 10**,** e0135392.

GILLET, L. C., NAVARRO, P., TATE, S., ROST, H., SELEVSEK, N., REITER, L., BONNER, R. & AEBERSOLD, R. 2012. Targeted data extraction of the MS/MS spectra generated by data-independent acquisition: a new concept for consistent and accurate proteome analysis. *Mol Cell Proteomics,* 11**,** O111 016717.

GILLETT, G. T., FOX, M. F., ROWE, P. S., CASIMIR, C. M. & POVEY, S. 1996. Mapping of human non-muscle type cofilin (CFL1) to chromosome 11q13 and muscle-type cofilin (CFL2) to chromosome 14. *Ann Hum Genet,* 60**,** 201-11.

GIRGENRATH, S., SONG, K. & WHITTEMORE, L. A. 2005. Loss of myostatin expression alters fiber-type distribution and expression of myosin heavy chain isoforms in slow- and fast-type skeletal muscle. *Muscle Nerve,* 31**,** 34-40.

GOLJANEK-WHYSALL, K., IWANEJKO, L. A., VASILAKI, A., PEKOVIC-VAUGHAN, V. & MCDONAGH, B. 2016. Ageing in relation to skeletal muscle dysfunction: redox homoeostasis to regulation of gene expression. *Mamm Genome,* 27**,** 341-57.

GONZALEZ-MORALES, N., HOLENKA, T. K. & SCHOCK, F. 2017. Filamin actin-binding and titin-binding fulfill distinct functions in Z-disc cohesion. *PLoS Genet,* 13**,** e1006880.

GONZALEZ, E., MESSI, M. L. & DELBONO, O. 2000. The specific force of single intact extensor digitorum longus and soleus mouse muscle fibers declines with aging. *J Membr Biol,* 178**,** 175-83.

GOULART, F., VALLS-SOLE, J. & ALVAREZ, R. 2000. Posture-related changes of soleus H-reflex excitability. *Muscle Nerve,* 23**,** 925-32.

HALLIWELL, B. 1994. Free radicals and antioxidants: a personal view. *Nutr Rev,* 52**,** 253-65.

HAMRICK, M. W., DING, K. H., PENNINGTON, C., CHAO, Y. J., WU, Y. D., HOWARD, B., IMMEL, D., BORLONGAN, C., MCNEIL, P. L., BOLLAG, W. B., CURL, W. W., YU, J. & ISALES, C. M. 2006. Age-related loss of muscle mass and bone strength in mice is associated with a decline in physical activity and serum leptin. *Bone,* 39**,** 845-53.

HAN, D., CANALI, R., GARCIA, J., AGUILERA, R., GALLAHER, T. K. & CADENAS, E. 2005. Sites and mechanisms of aconitase inactivation by peroxynitrite: modulation by citrate and glutathione. *Biochemistry,* 44**,** 11986-96.

HANSSON, O., DONSMARK, M., LING, C., NEVSTEN, P., DANFELTER, M., ANDERSEN, J. L., GALBO, H. & HOLM, C. 2005. Transcriptome and proteome analysis of soleus muscle of hormone-sensitive lipase-null mice. *J Lipid Res,* 46**,** 2614-23.

HARA, M. R., AGRAWAL, N., KIM, S. F., CASCIO, M. B., FUJIMURO, M., OZEKI, Y., TAKAHASHI, M., CHEAH, J. H., TANKOU, S. K., HESTER, L. D., FERRIS, C. D., HAYWARD, S. D., SNYDER, S. H. & SAWA, A. 2005. S-nitrosylated GAPDH initiates apoptotic cell death by nuclear translocation following Siah1 binding. *Nat Cell Biol,* 7**,** 665-74.

HARDIE, D. G. & SAKAMOTO, K. 2006. AMPK: a key sensor of fuel and energy status in skeletal muscle. *Physiology (Bethesda),* 21**,** 48-60.

HARMAN, D. 1956. Aging: a theory based on free radical and radiation chemistry. *J Gerontol,* 11**,** 298-300.

HAZELTON, G. A. & LANG, C. A. 1980. Glutathione contents of tissues in the aging mouse. *Biochem J,* 188**,** 25-30.

HESS, D. T., MATSUMOTO, A., KIM, S. O., MARSHALL, H. E. & STAMLER, J. S. 2005. Protein S-nitrosylation: purview and parameters. *Nat Rev Mol Cell Biol,* 6**,** 150-66.

HIONA, A. & LEEUWENBURGH, C. 2008. The role of mitochondrial DNA mutations in aging and sarcopenia: implications for the mitochondrial vicious cycle theory of aging. *Exp Gerontol,* 43**,** 24-33.

HOLMGREN, A. 1988. Thioredoxin and glutaredoxin: small multi-functional redox proteins with active-site disulphide bonds. *Biochem Soc Trans,* 16**,** 95-6.

HORN, A., VAN DER MEULEN, J. H., DEFOUR, A., HOGARTH, M., SREETAMA, S. C., REED, A., SCHEFFER, L., CHANDEL, N. S. & JAISWAL, J. K. 2017. Mitochondrial redox signaling enables repair of injured skeletal muscle cells. *Sci Signal,* 10.

HUANG, M. L., BECKER, E. M., WHITNALL, M., SURYO RAHMANTO, Y., PONKA, P. & RICHARDSON, D. R. 2009. Elucidation of the mechanism of mitochondrial iron loading in Friedreich's ataxia by analysis of a mouse mutant. *Proc Natl Acad Sci U S A,* 106**,** 16381-6.

HUXLEY, A. F. & NIEDERGERKE, R. 1954. Structural changes in muscle during contraction; interference microscopy of living muscle fibres. *Nature,* 173**,** 971-3.

HUXLEY, H. & HANSON, J. 1954. Changes in the cross-striations of muscle during contraction and stretch and their structural interpretation. *Nature,* 173**,** 973-6.

IGNATCHENKO, V., IGNATCHENKO, A., SINHA, A., BOUTROS, P. C. & KISLINGER, T. 2015. VennDIS: a JavaFX-based Venn and Euler diagram software to generate publication quality figures. *Proteomics,* 15**,** 1239-44.

IMAMURA, H., NHAT, K. P., TOGAWA, H., SAITO, K., IINO, R., KATO-YAMADA, Y., NAGAI, T. & NOJI, H. 2009. Visualization of ATP levels inside single living cells with fluorescence resonance energy transfer-based genetically encoded indicators. *Proc Natl Acad Sci U S A,* 106**,** 15651-6.

ITO, G., ARIGA, H., NAKAGAWA, Y. & IWATSUBO, T. 2006. Roles of distinct cysteine residues in S-nitrosylation and dimerization of DJ-1. *Biochem Biophys Res Commun,* 339**,** 667-72.

ITOH, H., TAKAHASHI, A., ADACHI, K., NOJI, H., YASUDA, R., YOSHIDA, M. & KINOSITA, K. 2004. Mechanically driven ATP synthesis by F1-ATPase. *Nature,* 427**,** 465-8.

JACKSON, M. J. 2008. Redox regulation of skeletal muscle. *IUBMB Life,* 60**,** 497-501.

JACKSON, M. J. 2009. Redox regulation of adaptive responses in skeletal muscle to contractile activity. *Free Radic Biol Med,* 47**,** 1267-75.

JACKSON, M. J. 2013. Interactions between reactive oxygen species generated by contractile activity and aging in skeletal muscle? *Antioxid Redox Signal,* 19**,** 804-12.

JACKSON, M. J. 2016a. Reactive oxygen species in sarcopenia: Should we focus on excess oxidative damage or defective redox signalling? *Mol Aspects Med,* 50**,** 33-40.

JACKSON, M. J. 2016b. Reactive oxygen species in sarcopenia: Should we focus on excess oxidative damage or defective redox signalling? *Mol Aspects Med*.

JACKSON, M. J., PYE, D. & PALOMERO, J. 2007. The production of reactive oxygen and nitrogen species by skeletal muscle. *J Appl Physiol (1985),* 102**,** 1664-70.

JACOBS, R. A., DIAZ, V., SOLDINI, L., HAIDER, T., THOMASSEN, M., NORDSBORG, N. B., GASSMANN, M. & LUNDBY, C. 2013. Fast-twitch glycolytic skeletal muscle is predisposed to age-induced impairments in mitochondrial function. *J Gerontol A Biol Sci Med Sci,* 68**,** 1010-22.

JAKOBSSON, F., BORG, K. & EDSTROM, L. 1990. Fibre-type composition, structure and cytoskeletal protein location of fibres in anterior tibial muscle. Comparison between young adults and physically active aged humans. *Acta Neuropathol,* 80**,** 459-68.

JANG, Y. C., PEREZ, V. I., SONG, W., LUSTGARTEN, M. S., SALMON, A. B., MELE, J., QI, W., LIU, Y., LIANG, H., CHAUDHURI, A., IKENO, Y., EPSTEIN, C. J., VAN REMMEN, H. & RICHARDSON, A. 2009. Overexpression of Mn superoxide dismutase does not increase life span in mice. *J Gerontol A Biol Sci Med Sci,* 64**,** 1114-25.

JANISZEWSKI, M., LOPES, L. R., CARMO, A. O., PEDRO, M. A., BRANDES, R. P., SANTOS, C. X. & LAURINDO, F. R. 2005. Regulation of NAD(P)H oxidase by associated protein disulfide isomerase in vascular smooth muscle cells. *J Biol Chem,* 280**,** 40813-9.

JANSSEN, I., HEYMSFIELD, S. B., WANG, Z. M. & ROSS, R. 2000. Skeletal muscle mass and distribution in 468 men and women aged 18-88 yr. *J Appl Physiol (1985),* 89**,** 81-8.

JAYARAMAN, A., LIU, M., YE, F., WALTER, G. A. & VANDENBORNE, K. 2013. Regenerative responses in slow- and fast-twitch muscles following moderate contusion spinal cord injury and locomotor training. *Eur J Appl Physiol,* 113**,** 191-200.

JEON, J. H., LEE, K. N., HWANG, C. Y., KWON, K. S., YOU, K. H. & CHOI, I. 2005. Tumor suppressor VDUP1 increases p27(kip1) stability by inhibiting JAB1. *Cancer Res,* 65**,** 4485-9.

JEONG, W., BAE, S. H., TOLEDANO, M. B. & RHEE, S. G. 2012. Role of sulfiredoxin as a regulator of peroxiredoxin function and regulation of its expression. *Free Radic Biol Med,* 53**,** 447-56.

JI, L. L. 2008. Modulation of skeletal muscle antioxidant defense by exercise: Role of redox signaling. *Free Radic Biol Med,* 44**,** 142-52.

JIN, D. Y., CHAE, H. Z., RHEE, S. G. & JEANG, K. T. 1997. Regulatory role for a novel human thioredoxin peroxidase in NF-kappaB activation. *J Biol Chem,* 272**,** 30952-61.

JIN, S., DAI, Y., LI, C., FANG, X., HAN, H. & WANG, D. 2016. MicroRNA-544 inhibits glioma proliferation, invasion and migration but induces cell apoptosis by targeting PARK7. *Am J Transl Res,* 8**,** 1826-37.

JOHNSON, M. L., ROBINSON, M. M. & NAIR, K. S. 2013. Skeletal muscle aging and the mitochondrion. *Trends Endocrinol Metab,* 24**,** 247-56.

JUEL, C. 2014. Oxidative stress (glutathionylation) and Na,K-ATPase activity in rat skeletal muscle. *PLoS One,* 9**,** e110514.

KAHN, B. B., ALQUIER, T., CARLING, D. & HARDIE, D. G. 2005. AMP-activated protein kinase: ancient energy gauge provides clues to modern understanding of metabolism. *Cell Metab,* 1**,** 15-25.
KALCKAR, H. M. 1974. Origins of the concept oxidative phosphorylation. *Mol Cell Biochem,* 5**,** 55-63.
KALCKAR, H. M. 1991. 50 years of biological research--from oxidative phosphorylation to energy requiring transport regulation. *Annu Rev Biochem,* 60**,** 1-37.
KALININA, E. V., CHERNOV, N. N. & SAPRIN, A. N. 2008. Involvement of thio-, peroxi-, and glutaredoxins in cellular redox-dependent processes. *Biochemistry (Mosc),* 73**,** 1493-510.
KAMI, K. & SENBA, E. 2005. Galectin-1 is a novel factor that regulates myotube growth in regenerating skeletal muscles. *Curr Drug Targets,* 6**,** 395-405.
KAMMOUN, M., CASSAR-MALEK, I., MEUNIER, B. & PICARD, B. 2014. A simplified immunohistochemical classification of skeletal muscle fibres in mouse. *Eur J Histochem,* 58**,** 2254.
KAMOTANI, Y., BERSANO-BEGEY, T., KATO, N., TUNG, Y. C., HUH, D., SONG, J. W. & TAKAYAMA, S. 2008. Individually programmable cell stretching microwell arrays actuated by a Braille display. *Biomaterials,* 29**,** 2646-55.
KEE, A. J., SCHEVZOV, G., NAIR-SHALLIKER, V., ROBINSON, C. S., VRHOVSKI, B., GHODDUSI, M., QIU, M. R., LIN, J. J., WEINBERGER, R., GUNNING, P. W. & HARDEMAN, E. C. 2004. Sorting of a nonmuscle tropomyosin to a novel cytoskeletal compartment in skeletal muscle results in muscular dystrophy. *J Cell Biol,* 166**,** 685-96.
KELDER, T., VAN IERSEL, M. P., HANSPERS, K., KUTMON, M., CONKLIN, B. R., EVELO, C. T. & PICO, A. R. 2012. WikiPathways: building research communities on biological pathways. *Nucleic Acids Res,* 40**,** D1301-7.
KENNEDY, M. C., SPOTO, G., EMPTAGE, M. H. & BEINERT, H. 1988. The active site sulfhydryl of aconitase is not required for catalytic activity. *J Biol Chem,* 263**,** 8190-3.
KENT-BRAUN, J. A., NG, A. V. & YOUNG, K. 2000. Skeletal muscle contractile and noncontractile components in young and older women and men. *J Appl Physiol (1985),* 88**,** 662-8.
KHODABUKUS, A. & BAAR, K. 2015. Contractile and metabolic properties of engineered skeletal muscle derived from slow and fast phenotype mouse muscle. *J Cell Physiol,* 230**,** 1750-7.
KIM, H. G., HONG, S. M., KIM, S. J., PARK, H. J., JUNG, H. I., LEE, Y. Y., MOON, J. S., LIM, H. W., PARK, E. H. & LIM, C. J. 2003. Age-related changes in the activity of antioxidant and redox enzymes in rats. *Mol Cells,* 16**,** 278-84.
KLICHKO, V. I., ORR, W. C. & RADYUK, S. N. 2016. The role of peroxiredoxin 4 in inflammatory response and aging. *Biochim Biophys Acta,* 1862**,** 265-73.
KLITGAARD, H., ZHOU, M., SCHIAFFINO, S., BETTO, R., SALVIATI, G. & SALTIN, B. 1990. Ageing alters the myosin heavy chain composition of single fibres from human skeletal muscle. *Acta Physiol Scand,* 140**,** 55-62.
KOH, T. J. & ESCOBEDO, J. 2004. Cytoskeletal disruption and small heat shock protein translocation immediately after lengthening contractions. *Am J Physiol Cell Physiol,* 286**,** C713-22.
KORNBERG, M. D., SEN, N., HARA, M. R., JULURI, K. R., NGUYEN, J. V., SNOWMAN, A. M., LAW, L., HESTER, L. D. & SNYDER, S. H. 2010. GAPDH mediates nitrosylation of nuclear proteins. *Nat Cell Biol,* 12**,** 1094-100.
KOZLOV, A. V., SZALAY, L., UMAR, F., KROPIK, K., STANIEK, K., NIEDERMULLER, H., BAHRAMI, S. & NOHL, H. 2005. Skeletal muscles, heart, and lung are the main sources of oxygen radicals in old rats. *Biochim Biophys Acta,* 1740**,** 382-9.
KREBIEHL, G., RUCKERBAUER, S., BURBULLA, L. F., KIEPER, N., MAURER, B., WAAK, J., WOLBURG, H., GIZATULLINA, Z., GELLERICH, F. N., WOITALLA, D., RIESS, O., KAHLE, P. J., PROIKAS-CEZANNE, T. & KRUGER, R. 2010. Reduced basal autophagy and impaired mitochondrial dynamics due to loss of Parkinson's disease-associated protein DJ-1. *PLoS One,* 5**,** e9367.
KREBS, H. A. & HOLZACH, O. 1952. The conversion of citrate into cis-aconitate and isocitrate in the presence of aconitase. *Biochem J,* 52**,** 527-8.

KRISP, C. & MOLLOY, M. P. 2017. SWATH Mass Spectrometry for Proteomics of Non-Depleted Plasma. *Methods Mol Biol,* 1619**,** 373-383.

KURAZUMI, H., KUBO, M., OHSHIMA, M., YAMAMOTO, Y., TAKEMOTO, Y., SUZUKI, R., IKENAGA, S., MIKAMO, A., UDO, K., HAMANO, K. & LI, T. S. 2011. The effects of mechanical stress on the growth, differentiation, and paracrine factor production of cardiac stem cells. *PLoS One,* 6**,** e28890.

KURIEN, B. T. & SCOFIELD, R. H. 2006. Western blotting. *Methods,* 38**,** 283-93.

KURODA, J., NAKAGAWA, K., YAMASAKI, T., NAKAMURA, K., TAKEYA, R., KURIBAYASHI, F., IMAJOH-OHMI, S., IGARASHI, K., SHIBATA, Y., SUEISHI, K. & SUMIMOTO, H. 2005. The superoxide-producing NAD(P)H oxidase Nox4 in the nucleus of human vascular endothelial cells. *Genes Cells,* 10**,** 1139-51.

KUTMON, M., RIUTTA, A., NUNES, N., HANSPERS, K., WILLIGHAGEN, E. L., BOHLER, A., MELIUS, J., WAAGMEESTER, A., SINHA, S. R., MILLER, R., COORT, S. L., CIRILLO, E., SMEETS, B., EVELO, C. T. & PICO, A. R. 2016. WikiPathways: capturing the full diversity of pathway knowledge. *Nucleic Acids Res,* 44**,** D488-94.

KUTMON, M., VAN IERSEL, M. P., BOHLER, A., KELDER, T., NUNES, N., PICO, A. R. & EVELO, C. T. 2015. PathVisio 3: an extendable pathway analysis toolbox. *PLoS Comput Biol,* 11**,** e1004085.

LARSEN, F. J., SCHIFFER, T. A., ORTENBLAD, N., ZINNER, C., MORALES-ALAMO, D., WILLIS, S. J., CALBET, J. A., HOLMBERG, H. C. & BOUSHEL, R. 2016. High-intensity sprint training inhibits mitochondrial respiration through aconitase inactivation. *FASEB J,* 30**,** 417-27.

LARSSON, L. & EDSTROM, L. 1986. Effects of age on enzyme-histochemical fibre spectra and contractile properties of fast- and slow-twitch skeletal muscles in the rat. *J Neurol Sci,* 76**,** 69-89.

LARSSON, L. & SALVIATI, G. 1989. Effects of age on calcium transport activity of sarcoplasmic reticulum in fast- and slow-twitch rat muscle fibres. *J Physiol,* 419**,** 253-64.

LAY, A. J., JIANG, X. M., DALY, E., SUN, L. & HOGG, P. J. 2002. Plasmin reduction by phosphoglycerate kinase is a thiol-independent process. *J Biol Chem,* 277**,** 9062-8.

LE MOAL, E., PIALOUX, V., JUBAN, G., GROUSSARD, C., ZOUHAL, H., CHAZAUD, B. & MOUNIER, R. 2017. Redox Control of Skeletal Muscle Regeneration. *Antioxid Redox Signal,* 27**,** 276-310.

LEDUC-GAUDET, J. P., PICARD, M., ST-JEAN PELLETIER, F., SGARIOTO, N., AUGER, M. J., VALLEE, J., ROBITAILLE, R., ST-PIERRE, D. H. & GOUSPILLOU, G. 2015. Mitochondrial morphology is altered in atrophied skeletal muscle of aged mice. *Oncotarget,* 6**,** 17923-37.

LEE, K. P., SHIN, Y. J., CHO, S. C., LEE, S. M., BAHN, Y. J., KIM, J. Y., KWON, E. S., JEONG, D. Y., PARK, S. C., RHEE, S. G., WOO, H. A. & KWON, K. S. 2014. Peroxiredoxin 3 has a crucial role in the contractile function of skeletal muscle by regulating mitochondrial homeostasis. *Free Radic Biol Med,* 77**,** 298-306.

LEE, S. R., KHAMOUI, A. V., JO, E., PARK, B. S., ZOURDOS, M. C., PANTON, L. B., ORMSBEE, M. J. & KIM, J. S. 2015. Effects of chronic high-fat feeding on skeletal muscle mass and function in middle-aged mice. *Aging Clin Exp Res,* 27**,** 403-11.

LEIJENDEKKER, W. J. & ELZINGA, G. 1990. Metabolic recovery of mouse extensor digitorum longus and soleus muscle. *Pflugers Arch,* 416**,** 22-7.

LENART, P. & KREJCI, L. 2016. Reprint of "DNA, the central molecule of aging". *Mutat Res,* 788**,** 25-31.

LEXELL, J. 1995. Human aging, muscle mass, and fiber type composition. *J Gerontol A Biol Sci Med Sci,* 50 Spec No**,** 11-6.

LEXELL, J., DOWNHAM, D. & SJOSTROM, M. 1984. Distribution of different fibre types in human skeletal muscles. A statistical and computational study of the fibre type arrangement in m. vastus lateralis of young, healthy males. *J Neurol Sci,* 65**,** 353-65.

LEXELL, J., DOWNHAM, D. & SJOSTROM, M. 1986. Distribution of different fibre types in human skeletal muscles. Fibre type arrangement in m. vastus lateralis from three groups of healthy men between 15 and 83 years. *J Neurol Sci,* 72**,** 211-22.

LEXELL, J., TAYLOR, C. C. & SJOSTROM, M. 1988. What is the cause of the ageing atrophy? Total number, size and proportion of different fiber types studied in whole vastus lateralis muscle from 15- to 83-year-old men. *J Neurol Sci,* 84**,** 275-94.

LINARES, G. R., XING, W., GOVONI, K. E., CHEN, S. T. & MOHAN, S. 2009. Glutaredoxin 5 regulates osteoblast apoptosis by protecting against oxidative stress. *Bone,* 44**,** 795-804.

LINSLEY, J. W., HSU, I. U., WANG, W. & KUWADA, J. Y. 2017. Transport of the α subunit of the voltage gated L-type calcium channel through the sarcoplasmic reticulum occurs prior to localization to triads and requires the β subunit but not Stac3 in skeletal muscles. *Traffic,* 18**,** 622-632.

LIOCHEV, S. I. & FRIDOVICH, I. 1999. Superoxide and iron: partners in crime. *IUBMB Life,* 48**,** 157-61.

LO CONTE, M. & CARROLL, K. S. 2013. The redox biochemistry of protein sulfenylation and sulfinylation. *J Biol Chem,* 288**,** 26480-8.

LOFFLER, A. S., ALERS, S., DIETERLE, A. M., KEPPELER, H., FRANZ-WACHTEL, M., KUNDU, M., CAMPBELL, D. G., WESSELBORG, S., ALESSI, D. R. & STORK, B. 2011. Ulk1-mediated phosphorylation of AMPK constitutes a negative regulatory feedback loop. *Autophagy,* 7**,** 696-706.

LOPEZ-LLUCH, G., IRUSTA, P. M., NAVAS, P. & DE CABO, R. 2008. Mitochondrial biogenesis and healthy aging. *Exp Gerontol,* 43**,** 813-9.

LOWE, D. A., DEGENS, H., CHEN, K. D. & ALWAY, S. E. 2000. Glyceraldehyde-3-phosphate dehydrogenase varies with age in glycolytic muscles of rats. *J Gerontol A Biol Sci Med Sci,* 55**,** B160-4.

LUMB, R. A. & BULLEID, N. J. 2002. Is protein disulfide isomerase a redox-dependent molecular chaperone? *EMBO J,* 21**,** 6763-70.

LYONS, C. N., MATHIEU-COSTELLO, O. & MOYES, C. D. 2006. Regulation of skeletal muscle mitochondrial content during aging. *J Gerontol A Biol Sci Med Sci,* 61**,** 3-13.

MACLEAN, B., TOMAZELA, D. M., SHULMAN, N., CHAMBERS, M., FINNEY, G. L., FREWEN, B., KERN, R., TABB, D. L., LIEBLER, D. C. & MACCOSS, M. J. 2010. Skyline: an open source document editor for creating and analyzing targeted proteomics experiments. *Bioinformatics,* 26**,** 966-8.

MANABE, Y., TAKAGI, M., NAKAMURA-YAMADA, M., GOTO-INOUE, N., TAOKA, M., ISOBE, T. & FUJII, N. L. 2014. Redox proteins are constitutively secreted by skeletal muscle. *J Physiol Sci,* 64**,** 401-9.

MARABITA, M., BARALDO, M., SOLAGNA, F., CEELEN, J. J., SARTORI, R., NOLTE, H., NEMAZANYY, I., PYRONNET, S., KRUGER, M., PENDE, M. & BLAAUW, B. 2016. S6K1 Is Required for Increasing Skeletal Muscle Force during Hypertrophy. *Cell Rep,* 17**,** 501-513.

MARCHI, S., GIORGI, C., SUSKI, J. M., AGNOLETTO, C., BONONI, A., BONORA, M., DE MARCHI, E., MISSIROLI, S., PATERGNANI, S., POLETTI, F., RIMESSI, A., DUSZYNSKI, J., WIECKOWSKI, M. R. & PINTON, P. 2012. Mitochondria-ros crosstalk in the control of cell death and aging. *J Signal Transduct,* 2012**,** 329635.

MARINO, S. M. & GLADYSHEV, V. N. 2012. Analysis and functional prediction of reactive cysteine residues. *J Biol Chem,* 287**,** 4419-25.

MARTYN, K. D., KIM, M. J., QUINN, M. T., DINAUER, M. C. & KNAUS, U. G. 2005. p21-activated kinase (Pak) regulates NADPH oxidase activation in human neutrophils. *Blood,* 106**,** 3962-9.

MASSER, D. R., CLARK, N. W., VAN REMMEN, H. & FREEMAN, W. M. 2016. Loss of the antioxidant enzyme CuZnSOD (Sod1) mimics an age-related increase in absolute mitochondrial DNA copy number in the skeletal muscle. *Age (Dordr),* 38**,** 323-333.

MCARDLE, A., DILLMANN, W. H., MESTRIL, R., FAULKNER, J. A. & JACKSON, M. J. 2004a. Overexpression of HSP70 in mouse skeletal muscle protects against muscle damage and age-related muscle dysfunction. *FASEB J,* 18**,** 355-7.

MCARDLE, A., PATTWELL, D., VASILAKI, A., GRIFFITHS, R. D. & JACKSON, M. J. 2001. Contractile activity-induced oxidative stress: cellular origin and adaptive responses. *Am J Physiol Cell Physiol,* 280**,** C621-7.

MCARDLE, A., VAN DER MEULEN, J., CLOSE, G. L., PATTWELL, D., VAN REMMEN, H., HUANG, T. T., RICHARDSON, A. G., EPSTEIN, C. J., FAULKNER, J. A. & JACKSON, M. J. 2004b. Role of mitochondrial superoxide dismutase in contraction-induced generation of reactive oxygen species in skeletal muscle extracellular space. *Am J Physiol Cell Physiol,* 286**,** C1152-8.

MCDONAGH, B., SAKELLARIOU, G. K. & JACKSON, M. J. 2014a. Application of redox proteomics to skeletal muscle aging and exercise. *Biochem Soc Trans,* 42**,** 965-70.

MCDONAGH, B., SAKELLARIOU, G. K., SMITH, N. T., BROWNRIDGE, P. & JACKSON, M. J. 2014b. Differential cysteine labeling and global label-free proteomics reveals an altered metabolic state in skeletal muscle aging. *J Proteome Res,* 13**,** 5008-21.

MCDONAGH, B., SCULLION, S. M., VASILAKI, A., POLLOCK, N., MCARDLE, A. & JACKSON, M. J. 2016. Ageing-induced changes in the redox status of peripheral motor nerves imply an effect on redox signalling rather than oxidative damage. *Free Radic Biol Med,* 94**,** 27-35.

MEANY, D. L., XIE, H., THOMPSON, L. V., ARRIAGA, E. A. & GRIFFIN, T. J. 2007. Identification of carbonylated proteins from enriched rat skeletal muscle mitochondria using affinity chromatography-stable isotope labeling and tandem mass spectrometry. *Proteomics,* 7**,** 1150-63.

MERCKEN, E. M., CAPRI, M., CARBONEAU, B. A., CONTE, M., HEIDLER, J., SANTORO, A., MARTIN-MONTALVO, A., GONZALEZ-FREIRE, M., KHRAIWESH, H., GONZALEZ-REYES, J. A., MOADDEL, R., ZHANG, Y., BECKER, K. G., VILLALBA, J. M., MATTISON, J. A., WITTIG, I., FRANCESCHI, C. & DE CABO, R. 2017. Conserved and species-specific molecular denominators in mammalian skeletal muscle aging. *NPJ Aging Mech Dis,* 3**,** 8.

MITCHELL, P. 1961. Coupling of phosphorylation to electron and hydrogen transfer by a chemi-osmotic type of mechanism. *Nature,* 191**,** 144-8.

MOEN, R. J., CORNEA, S., OSEID, D. E., BINDER, B. P., KLEIN, J. C. & THOMAS, D. D. 2014. Redox-sensitive residue in the actin-binding interface of myosin. *Biochem Biophys Res Commun,* 453**,** 345-9.

MOLLER, A. B., VENDELBO, M. H., CHRISTENSEN, B., CLASEN, B. F., BAK, A. M., JORGENSEN, J. O., MOLLER, N. & JESSEN, N. 2015. Physical exercise increases autophagic signaling through ULK1 in human skeletal muscle. *J Appl Physiol (1985),* 118**,** 971-9.

MONTEIRO, G., HORTA, B. B., PIMENTA, D. C., AUGUSTO, O. & NETTO, L. E. 2007. Reduction of 1-Cys peroxiredoxins by ascorbate changes the thiol-specific antioxidant paradigm, revealing another function of vitamin C. *Proc Natl Acad Sci U S A,* 104**,** 4886-91.

MOTOHASHI, N. & ASAKURA, A. 2012. Molecular Regulation of Muscle Satellite Cell Self-Renewal. *J Stem Cell Res Ther,* Suppl 11.

MULLEN, L., HANSCHMANN, E. M., LILLIG, C. H., HERZENBERG, L. A. & GHEZZI, P. 2015. Cysteine Oxidation Targets Peroxiredoxins 1 and 2 for Exosomal Release through a Novel Mechanism of Redox-Dependent Secretion. *Mol Med,* 21**,** 98-108.

MUNRO, D. & TREBERG, J. R. 2017. A radical shift in perspective: mitochondria as regulators of reactive oxygen species. *J Exp Biol,* 220**,** 1170-1180.

MURGIA, M., NAGARAJ, N., DESHMUKH, A. S., ZEILER, M., CANCELLARA, P., MORETTI, I., REGGIANI, C., SCHIAFFINO, S. & MANN, M. 2015. Single muscle fiber proteomics reveals unexpected mitochondrial specialization. *EMBO Rep,* 16**,** 387-95.

MURPHY, M. E. & KEHRER, J. P. 1986. Activities of antioxidant enzymes in muscle, liver and lung of chickens with inherited muscular dystrophy. *Biochem Biophys Res Commun,* 134**,** 550-6.

MUSTAFA, A. K., GADALLA, M. M., SEN, N., KIM, S., M, W., GAZI, S. K., BARROW, R. K., YANG, G., WANG, R. & SNYDER, S. H. 2009. H2S signals through protein S-sulfhydration. *Sci Signal,* 2**,** ra72.

NAGAHISA, H., OKABE, K., IUCHI, Y., FUJII, J. & MIYATA, H. 2016. Characteristics of Skeletal Muscle Fibers of SOD1 Knockout Mice. *Oxid Med Cell Longev,* 2016**,** 9345970.

NAKAJIMA, H., AMANO, W., FUJITA, A., FUKUHARA, A., AZUMA, Y. T., HATA, F., INUI, T. & TAKEUCHI, T. 2007. The active site cysteine of the proapoptotic protein glyceraldehyde-3-phosphate

dehydrogenase is essential in oxidative stress-induced aggregation and cell death. *J Biol Chem,* 282**,** 26562-74.

NATHAN, C. & CUNNINGHAM-BUSSEL, A. 2013. Beyond oxidative stress: an immunologist's guide to reactive oxygen species. *Nat Rev Immunol,* 13**,** 349-61.

NORRGARD, M. A., IVARSSON, Y., TARS, K. & MANNERVIK, B. 2006. Alternative mutations of a positively selected residue elicit gain or loss of functionalities in enzyme evolution. *Proc Natl Acad Sci U S A,* 103**,** 4876-81.

O'CONNELL, K., GANNON, J., DORAN, P. & OHLENDIECK, K. 2007. Proteomic profiling reveals a severely perturbed protein expression pattern in aged skeletal muscle. *Int J Mol Med,* 20**,** 145-53.

O'LEARY, M. F., VAINSHTEIN, A., IQBAL, S., OSTOJIC, O. & HOOD, D. A. 2013. Adaptive plasticity of autophagic proteins to denervation in aging skeletal muscle. *Am J Physiol Cell Physiol,* 304**,** C422-30.

O'NEILL, H. M. 2013. AMPK and Exercise: Glucose Uptake and Insulin Sensitivity. *Diabetes Metab J,* 37**,** 1-21.

OBERG, A. L. & MAHONEY, D. W. 2012. Statistical methods for quantitative mass spectrometry proteomic experiments with labeling. *BMC Bioinformatics,* 13 Suppl 16**,** S7.

OHLENDIECK, K. 2010. Proteomics of skeletal muscle glycolysis. *Biochim Biophys Acta,* 1804**,** 2089-101.

OHLENDIECK, K. 2011. Skeletal muscle proteomics: current approaches, technical challenges and emerging techniques. *Skelet Muscle,* 1**,** 6.

OHLENDIECK, K. 2013. Proteomic identification of biomarkers of skeletal muscle disorders. *Biomark Med,* 7**,** 169-86.

OLIVEIRA-PAULA, G. H., LACCHINI, R. & TANUS-SANTOS, J. E. 2014. Inducible nitric oxide synthase as a possible target in hypertension. *Curr Drug Targets,* 15**,** 164-74.

PALMER, T. B. & THOMPSON, B. J. 2016. Influence of age on passive stiffness and size, quality, and strength characteristics. *Muscle Nerve*.

PAN, J. & CARROLL, K. S. 2014. Chemical biology approaches to study protein cysteine sulfenylation. *Biopolymers,* 101**,** 165-72.

PARK, C. Y., PIERCE, S. A., VON DREHLE, M., IVEY, K. N., MORGAN, J. A., BLAU, H. M. & SRIVASTAVA, D. 2010. skNAC, a Smyd1-interacting transcription factor, is involved in cardiac development and skeletal muscle growth and regeneration. *Proc Natl Acad Sci U S A,* 107**,** 20750-5.

PASSARELLI, C., PETRINI, S., PASTORE, A., BONETTO, V., SALE, P., GAETA, L. M., TOZZI, G., BERTINI, E., CANEPARI, M., ROSSI, R. & PIEMONTE, F. 2008. Myosin as a potential redox-sensor: an in vitro study. *J Muscle Res Cell Motil,* 29**,** 119-26.

PAULSEN, C. E. & CARROLL, K. S. 2013. Cysteine-mediated redox signaling: chemistry, biology, and tools for discovery. *Chem Rev,* 113**,** 4633-79.

PESKIN, A. V., DICKERHOF, N., POYNTON, R. A., PATON, L. N., PACE, P. E., HAMPTON, M. B. & WINTERBOURN, C. C. 2013. Hyperoxidation of peroxiredoxins 2 and 3: rate constants for the reactions of the sulfenic acid of the peroxidatic cysteine. *J Biol Chem,* 288**,** 14170-7.

PETERSON, C. M., JOHANNSEN, D. L. & RAVUSSIN, E. 2012. Skeletal muscle mitochondria and aging: a review. *J Aging Res,* 2012**,** 194821.

PICKOVA, A., PAUL, J., PETRUZZELLA, V. & HOUSTEK, J. 2003. Differential expression of ATPAF1 and ATPAF2 genes encoding F(1)-ATPase assembly proteins in mouse tissues. *FEBS Lett,* 551**,** 42-6.

PIETRANGELO, L., D'INCECCO, A., AINBINDER, A., MICHELUCCI, A., KERN, H., DIRKSEN, R. T., BONCOMPAGNI, S. & PROTASI, F. 2015. Age-dependent uncoupling of mitochondria from Ca2(+) release units in skeletal muscle. *Oncotarget,* 6**,** 35358-71.

POOLE, L. B. 2015. The basics of thiols and cysteines in redox biology and chemistry. *Free Radic Biol Med,* 80**,** 148-57.

POWERS, S. K. & JACKSON, M. J. 2008. Exercise-induced oxidative stress: cellular mechanisms and impact on muscle force production. *Physiol Rev,* 88**,** 1243-76.

POWERS, S. K., JI, L. L., KAVAZIS, A. N. & JACKSON, M. J. 2011. Reactive oxygen species: impact on skeletal muscle. *Compr Physiol,* 1**,** 941-69.

PRIGGE, J. R., ERIKSSON, S., IVERSON, S. V., MEADE, T. A., CAPECCHI, M. R., ARNER, E. S. & SCHMIDT, E. E. 2012. Hepatocyte DNA replication in growing liver requires either glutathione or a single allele of txnrd1. *Free Radic Biol Med,* 52**,** 803-10.

RABEK, J. P., BOYLSTON, W. H., 3RD & PAPACONSTANTINOU, J. 2003. Carbonylation of ER chaperone proteins in aged mouse liver. *Biochem Biophys Res Commun,* 305**,** 566-72.

RADAK, Z., TAKAHASHI, R., KUMIYAMA, A., NAKAMOTO, H., OHNO, H., OOKAWARA, T. & GOTO, S. 2002. Effect of aging and late onset dietary restriction on antioxidant enzymes and proteasome activities, and protein carbonylation of rat skeletal muscle and tendon. *Exp Gerontol,* 37**,** 1423-30.

RADAK, Z., TAYLOR, A. W., OHNO, H. & GOTO, S. 2001. Adaptation to exercise-induced oxidative stress: from muscle to brain. *Exerc Immunol Rev,* 7**,** 90-107.

RAMSEY, J. J., HARPER, M. E. & WEINDRUCH, R. 2000. Restriction of energy intake, energy expenditure, and aging. *Free Radic Biol Med,* 29**,** 946-68.

RAY, P. D., HUANG, B. W. & TSUJI, Y. 2012. Reactive oxygen species (ROS) homeostasis and redox regulation in cellular signaling. *Cell Signal,* 24**,** 981-90.

REDDY, S., JONES, A. D., CROSS, C. E., WONG, P. S. & VAN DER VLIET, A. 2000. Inactivation of creatine kinase by S-glutathionylation of the active-site cysteine residue. *Biochem J,* 347 Pt 3**,** 821-7.

REID, M. B. 2001. Nitric oxide, reactive oxygen species, and skeletal muscle contraction. *Med Sci Sports Exerc,* 33**,** 371-6.

RHEE, S. G., KANG, S. W., CHANG, T. S., JEONG, W. & KIM, K. 2001. Peroxiredoxin, a novel family of peroxidases. *IUBMB Life,* 52**,** 35-41.

RICHARME, G., MIHOUB, M., DAIROU, J., BUI, L. C., LEGER, T. & LAMOURI, A. 2015. Parkinsonism-associated protein DJ-1/Park7 is a major protein deglycase that repairs methylglyoxal- and glyoxal-glycated cysteine, arginine, and lysine residues. *J Biol Chem,* 290**,** 1885-97.

ROACH, P. J. 2002. Glycogen and its metabolism. *Curr Mol Med,* 2**,** 101-20.

ROMANICK, M., THOMPSON, L. V. & BROWN-BORG, H. M. 2013. Murine models of atrophy, cachexia, and sarcopenia in skeletal muscle. *Biochim Biophys Acta,* 1832**,** 1410-20.

ROOS, G., FOLOPPE, N. & MESSENS, J. 2013. Understanding the pK(a) of redox cysteines: the key role of hydrogen bonding. *Antioxid Redox Signal,* 18**,** 94-127.

RSTUDIO TEAM (2015). *RStudio: Integrated Development for R. RStudio, Inc.,* [Online]. Available: http://www.rstudio.com/ [Accessed 25/05/2016 2016].

SAEY, D., LEMIRE, B. B., GAGNON, P., BOMBARDIER, E., TUPLING, A. R., DEBIGARE, R., COTE, C. H. & MALTAIS, F. 2011. Quadriceps metabolism during constant workrate cycling exercise in chronic obstructive pulmonary disease. *J Appl Physiol (1985),* 110**,** 116-24.

SAKELLARIOU, G. K., JACKSON, M. J. & VASILAKI, A. 2014. Redefining the major contributors to superoxide production in contracting skeletal muscle. The role of NAD(P)H oxidases. *Free Radic Res,* 48**,** 12-29.

SAKELLARIOU, G. K., MCDONAGH, B., PORTER, H., GIAKOUMAKI, II, EARL, K. E., NYE, G. A., VASILAKI, A., BROOKS, S. V., RICHARDSON, A., VAN REMMEN, H., MCARDLE, A. & JACKSON, M. J. 2018. Comparison of Whole Body SOD1 Knockout with Muscle-Specific SOD1 Knockout Mice Reveals a Role for Nerve Redox Signaling in Regulation of Degenerative Pathways in Skeletal Muscle. *Antioxid Redox Signal,* 28**,** 275-295.

SAKELLARIOU, G. K., PEARSON, T., LIGHTFOOT, A. P., NYE, G. A., WELLS, N., GIAKOUMAKI, II, VASILAKI, A., GRIFFITHS, R. D., JACKSON, M. J. & MCARDLE, A. 2016. Mitochondrial ROS regulate oxidative damage and mitophagy but not age-related muscle fiber atrophy. *Sci Rep,* 6**,** 33944.

SAKELLARIOU, G. K., PYE, D., VASILAKI, A., ZIBRIK, L., PALOMERO, J., KABAYO, T., MCARDLE, F., VAN REMMEN, H., RICHARDSON, A., TIDBALL, J. G., MCARDLE, A. & JACKSON, M. J. 2011. Role of superoxide-nitric oxide interactions in the accelerated age-related loss of muscle mass in mice lacking Cu,Zn superoxide dismutase. *Aging Cell,* 10**,** 749-60.

SALMONS, S. 2017. The adaptive response of skeletal muscle: What is the evidence? *Muscle Nerve*.
SALMONS, S. & SRETER, F. A. 1976. Significance of impulse activity in the transformation of skeletal muscle type. *Nature,* 263**,** 30-4.
SALVADOR, A., SOUSA, J. & PINTO, R. E. 2001. Hydroperoxyl, superoxide and pH gradients in the mitochondrial matrix: a theoretical assessment. *Free Radic Biol Med,* 31**,** 1208-15.
SANDSTROM, M. E., ZHANG, S. J., BRUTON, J., SILVA, J. P., REID, M. B., WESTERBLAD, H. & KATZ, A. 2006. Role of reactive oxygen species in contraction-mediated glucose transport in mouse skeletal muscle. *J Physiol,* 575**,** 251-62.
SANTULLI, G. & MARKS, A. R. 2015. Essential Roles of Intracellular Calcium Release Channels in Muscle, Brain, Metabolism, and Aging. *Curr Mol Pharmacol,* 8**,** 206-22.
SASAGAWA, I., MATSUKI, S., SUZUKI, Y., IUCHI, Y., TOHYA, K., KIMURA, M., NAKADA, T. & FUJII, J. 2001. Possible involvement of the membrane-bound form of peroxiredoxin 4 in acrosome formation during spermiogenesis of rats. *Eur J Biochem,* 268**,** 3053-61.
SCHAUER, M., KOTTEK, T., SCHONHERR, M., BHATTACHARYA, A., IBRAHIM, S. M., HIROSE, M., KOHLING, R., FUELLEN, G., SCHMITZ, U. & KUNZ, M. 2015. A mutation in the NADH-dehydrogenase subunit 2 suppresses fibroblast aging. *Oncotarget,* 6**,** 8552-66.
SCHIAFFINO, S., DYAR, K. A., CICILIOT, S., BLAAUW, B. & SANDRI, M. 2013. Mechanisms regulating skeletal muscle growth and atrophy. *FEBS J,* 280**,** 4294-314.
SCHIAFFINO, S. & REGGIANI, C. 2011. Fiber types in mammalian skeletal muscles. *Physiol Rev,* 91**,** 1447-531.
SCHIEBER, M. & CHANDEL, N. S. 2014. ROS function in redox signaling and oxidative stress. *Curr Biol,* 24**,** R453-62.
SCHWARTZ, D. & GYGI, S. P. 2005. An iterative statistical approach to the identification of protein phosphorylation motifs from large-scale data sets. *Nat Biotechnol,* 23**,** 1391-8.
SCIOTE, J. J. & MORRIS, T. J. 2000. Skeletal muscle function and fibre types: the relationship between occlusal function and the phenotype of jaw-closing muscles in human. *J Orthod,* 27**,** 15-30.
SEIFERT, F., CISZAK, E., KOROTCHKINA, L., GOLBIK, R., SPINKA, M., DOMINIAK, P., SIDHU, S., BRAUER, J., PATEL, M. S. & TITTMANN, K. 2007. Phosphorylation of serine 264 impedes active site accessibility in the E1 component of the human pyruvate dehydrogenase multienzyme complex. *Biochemistry,* 46**,** 6277-87.
SEILER, A., SCHNEIDER, M., FORSTER, H., ROTH, S., WIRTH, E. K., CULMSEE, C., PLESNILA, N., KREMMER, E., RADMARK, O., WURST, W., BORNKAMM, G. W., SCHWEIZER, U. & CONRAD, M. 2008. Glutathione peroxidase 4 senses and translates oxidative stress into 12/15-lipoxygenase dependent- and AIF-mediated cell death. *Cell Metab,* 8**,** 237-48.
SELKOE, D. J. 2004. Cell biology of protein misfolding: the examples of Alzheimer's and Parkinson's diseases. *Nat Cell Biol,* 6**,** 1054-61.
SHEARD, P. W. & ANDERSON, R. D. 2012. Age-related loss of muscle fibres is highly variable amongst mouse skeletal muscles. *Biogerontology,* 13**,** 157-67.
SHER, J. & CARDASIS, C. 1976. Skeletal muscle fiber types in the adult mouse. *Acta Neurol Scand,* 54**,** 45-56.
SHERWOOD, R. I., CHRISTENSEN, J. L., CONBOY, I. M., CONBOY, M. J., RANDO, T. A., WEISSMAN, I. L. & WAGERS, A. J. 2004. Isolation of adult mouse myogenic progenitors: functional heterogeneity of cells within and engrafting skeletal muscle. *Cell,* 119**,** 543-54.
SHTIFMAN, A., ZHONG, N., LOPEZ, J. R., SHEN, J. & XU, J. 2011. Altered Ca2+ homeostasis in the skeletal muscle of DJ-1 null mice. *Neurobiol Aging,* 32**,** 125-32.
SILVEIRA, L. R., PEREIRA-DA-SILVA, L., JUEL, C. & HELLSTEN, Y. 2003. Formation of hydrogen peroxide and nitric oxide in rat skeletal muscle cells during contractions. *Free Radic Biol Med,* 35**,** 455-64.
SMITH, M. A. & REID, M. B. 2006. Redox modulation of contractile function in respiratory and limb skeletal muscle. *Respir Physiol Neurobiol,* 151**,** 229-41.

SOBOTTA, M. C., LIOU, W., STOCKER, S., TALWAR, D., OEHLER, M., RUPPERT, T., SCHARF, A. N. & DICK, T. P. 2015. Peroxiredoxin-2 and STAT3 form a redox relay for H2O2 signaling. *Nat Chem Biol,* 11**,** 64-70.

SPUDICH, J. A. & WATT, S. 1971. The regulation of rabbit skeletal muscle contraction. I. Biochemical studies of the interaction of the tropomyosin-troponin complex with actin and the proteolytic fragments of myosin. *J Biol Chem,* 246**,** 4866-71.

STAMLER, J. S. & MEISSNER, G. 2001. Physiology of nitric oxide in skeletal muscle. *Physiol Rev,* 81**,** 209-237.

SUGIYAMA, M., YOSHIZUMI, T., YOSHIDA, Y., BEKKI, Y., MATSUMOTO, Y., YOSHIYA, S., TOSHIMA, T., IKEGAMI, T., ITOH, S., HARIMOTO, N., OKANO, S., SOEJIMA, Y., SHIRABE, K. & MAEHARA, Y. 2016. p62 Promotes Amino Acid Sensitivity of mTOR Pathway and Hepatic Differentiation in Adult Liver Stem/Progenitor Cells. *J Cell Physiol*.

SZKLARCZYK, D., FRANCESCHINI, A., WYDER, S., FORSLUND, K., HELLER, D., HUERTA-CEPAS, J., SIMONOVIC, M., ROTH, A., SANTOS, A., TSAFOU, K. P., KUHN, M., BORK, P., JENSEN, L. J. & VON MERING, C. 2015. STRING v10: protein-protein interaction networks, integrated over the tree of life. *Nucleic Acids Res,* 43**,** D447-52.

TAKEMOTO, K., MIZUTANI, T., TAMURA, K., TAKEDA, K., HAGA, H. & KAWABATA, K. 2012. The Number of Cyclic Stretch Regulates Cellular Elasticity in C2C12 Myoblasts. *CellBio,* 01**,** 1-10.

TALIB, J. & DAVIES, M. J. 2016. Exposure of aconitase to smoking-related oxidants results in iron loss and increased iron response protein-1 activity: potential mechanisms for iron accumulation in human arterial cells. *J Biol Inorg Chem,* 21**,** 305-17.

TASAKI, E., MATSUMOTO, S., TADA, H., KURAHASHI, T., ZHANG, X., FUJII, J., UTSUMI, T. & IUCHI, Y. 2017. Protective role of testis-specific peroxiredoxin 4 against cellular oxidative stress. *J Clin Biochem Nutr,* 60**,** 156-161.

THOMAS, S. N. & ZHANG, H. 2016. Targeted proteomic assays for the verification of global proteomics insights. *Expert Rev Proteomics***,** 1-3.

TING, L., COWLEY, M. J., HOON, S. L., GUILHAUS, M., RAFTERY, M. J. & CAVICCHIOLI, R. 2009. Normalization and statistical analysis of quantitative proteomics data generated by metabolic labeling. *Mol Cell Proteomics,* 8**,** 2227-42.

TOHMA, H., EL-SHAFEY, A. F., CROFT, K., SHAVLAKADZE, T., GROUNDS, M. D. & ARTHUR, P. G. 2014. Protein thiol oxidation does not change in skeletal muscles of aging female mice. *Biogerontology,* 15**,** 87-98.

TREEBAK, J. T., GLUND, S., DESHMUKH, A., KLEIN, D. K., LONG, Y. C., JENSEN, T. E., JORGENSEN, S. B., VIOLLET, B., ANDERSSON, L., NEUMANN, D., WALLIMANN, T., RICHTER, E. A., CHIBALIN, A. V., ZIERATH, J. R. & WOJTASZEWSKI, J. F. 2006. AMPK-mediated AS160 phosphorylation in skeletal muscle is dependent on AMPK catalytic and regulatory subunits. *Diabetes,* 55**,** 2051-8.

TRIFUNOVIC, A., WREDENBERG, A., FALKENBERG, M., SPELBRINK, J. N., ROVIO, A. T., BRUDER, C. E., BOHLOOLY, Y. M., GIDLOF, S., OLDFORS, A., WIBOM, R., TORNELL, J., JACOBS, H. T. & LARSSON, N. G. 2004. Premature ageing in mice expressing defective mitochondrial DNA polymerase. *Nature,* 429**,** 417-23.

TYANOVA, S., TEMU, T., SINITCYN, P., CARLSON, A., HEIN, M. Y., GEIGER, T., MANN, M. & COX, J. 2016. The Perseus computational platform for comprehensive analysis of (prote)omics data. *Nat Methods*.

UNIPROT. 2017a. *B-enolase* [Online]. Available: http://www.uniprot.org/uniprot/P13929 [Accessed 03/08/2017 2017].

UNIPROT. 2017b. *Cytochrome b-c1 complex subunit 6, mitochondrial* [Online]. Available: http://www.uniprot.org/uniprot/P99028 [Accessed 03/08/2017 2017].

UNIPROT. 2017c. *Glyceraldehyde-3-phosphate dehydrogenase* [Online]. Available: http://www.uniprot.org/uniprot/P16858 [Accessed 03/08/2017 2017].

UNIPROT. 2017d. *Heat shock cognate 71 kDa protein* [Online]. Available: http://www.uniprot.org/uniprot/P63017 [Accessed 03/08/2017 2017].
UNIPROT. 2017e. *NADH-ubiquinone oxidoreductase 75 kDa subunit, mitochondrial* [Online]. Available: http://www.uniprot.org/uniprot/Q91VD9 [Accessed 03/08/2017 2017].
UNIPROT. 2017f. *NADH dehydrogenase [ubiquinone] iron-sulfur protein 7, mitochondrial* [Online]. Available: http://www.uniprot.org/uniprot/Q9DC70 [Accessed 03/09/2017 2017].
UNIPROT. 2017g. *Protein disulfide-isomerase A6* [Online]. Available: http://www.uniprot.org/uniprot/Q922R8 [Accessed 03/09/2017 2017].
UNIPROT. 2017h. *Tropomyosin α-4 chain* [Online]. Available: http://www.uniprot.org/uniprot/Q6IRU2 [Accessed 03/08/2017 2017].
VABULAS, R. M., AHMAD-NEJAD, P., GHOSE, S., KIRSCHNING, C. J., ISSELS, R. D. & WAGNER, H. 2002. HSP70 as endogenous stimulus of the Toll/interleukin-1 receptor signal pathway. *J Biol Chem,* 277**,** 15107-12.
VAN IERSEL, M. P., KELDER, T., PICO, A. R., HANSPERS, K., COORT, S., CONKLIN, B. R. & EVELO, C. 2008. Presenting and exploring biological pathways with PathVisio. *BMC Bioinformatics,* 9**,** 399.
VASILAKI, A., MANSOURI, A., VAN REMMEN, H., VAN DER MEULEN, J. H., LARKIN, L., RICHARDSON, A. G., MCARDLE, A., FAULKNER, J. A. & JACKSON, M. J. 2006a. Free radical generation by skeletal muscle of adult and old mice: effect of contractile activity. *Aging Cell,* 5**,** 109-17.
VASILAKI, A., MCARDLE, F., IWANEJKO, L. M. & MCARDLE, A. 2006b. Adaptive responses of mouse skeletal muscle to contractile activity: The effect of age. *Mech Ageing Dev,* 127**,** 830-9.
VASILAKI, A., RICHARDSON, A., VAN REMMEN, H., BROOKS, S. V., LARKIN, L., MCARDLE, A. & JACKSON, M. J. 2017. Role of nerve-muscle interactions and reactive oxygen species in regulation of muscle proteostasis with ageing. *J Physiol*.
VEKICH, J. A., BELMONT, P. J., THUERAUF, D. J. & GLEMBOTSKI, C. C. 2012. Protein disulfide isomerase-associated 6 is an ATF6-inducible ER stress response protein that protects cardiac myocytes from ischemia/reperfusion-mediated cell death. *J Mol Cell Cardiol,* 53**,** 259-67.
VENDROV, A. E., VENDROV, K. C., SMITH, A., YUAN, J., SUMIDA, A., ROBIDOUX, J., RUNGE, M. S. & MADAMANCHI, N. R. 2015. NOX4 NADPH Oxidase-Dependent Mitochondrial Oxidative Stress in Aging-Associated Cardiovascular Disease. *Antioxid Redox Signal,* 23**,** 1389-409.
VIGELSO, A., DYBBOE, R., HANSEN, C. N., DELA, F., HELGE, J. W. & GUADALUPE GRAU, A. 2015. GAPDH and β-actin protein decreases with aging, making Stain-Free technology a superior loading control in Western blotting of human skeletal muscle. *J Appl Physiol (1985),* 118**,** 386-94.
VINA, J., BORRAS, C., ABDELAZIZ, K. M., GARCIA-VALLES, R. & GOMEZ-CABRERA, M. C. 2013. The free radical theory of aging revisited: the cell signaling disruption theory of aging. *Antioxid Redox Signal,* 19**,** 779-87.
WANG, B., CAI, Z., TAO, K., ZENG, W., LU, F., YANG, R., FENG, D., GAO, G. & YANG, Q. 2016. Essential control of mitochondrial morphology and function by chaperone-mediated autophagy through degradation of PARK7. *Autophagy,* 12**,** 1215-28.
WANG, D., ZHENG, W., XIE, Y., GONG, P., ZHAO, F., YUAN, B., MA, W., CUI, Y., LIU, W., SUN, Y., PIEL, M., ZHANG, W. & JIANG, X. 2014. Tissue-specific mechanical and geometrical control of cell viability and actin cytoskeleton alignment. *Sci Rep,* 4**,** 6160.
WANG, L. C. & KERNELL, D. 2001. Fibre type regionalisation in lower hindlimb muscles of rabbit, rat and mouse: a comparative study. *J Anat,* 199**,** 631-43.
WATT, M. J. & CHENG, Y. 2017. Triglyceride metabolism in exercising muscle. *Biochim Biophys Acta,* 1862**,** 1250-1259.
WESTERBLAD, H., BRUTON, J. D. & KATZ, A. 2010. Skeletal muscle: energy metabolism, fiber types, fatigue and adaptability. *Exp Cell Res,* 316**,** 3093-9.
WILSON, M. A. 2011. The role of cysteine oxidation in DJ-1 function and dysfunction. *Antioxid Redox Signal,* 15**,** 111-22.

WOO, C. H., LEE, Z. W., KIM, B. C., HA, K. S. & KIM, J. H. 2000. Involvement of cytosolic phospholipase A2, and the subsequent release of arachidonic acid, in signalling by rac for the generation of intracellular reactive oxygen species in rat-2 fibroblasts. *Biochem J,* 348 Pt 3**,** 525-30.

XIAO, B., SINGH, S. P., NANDURI, B., AWASTHI, Y. C., ZIMNIAK, P. & JI, X. 1999. Crystal structure of a murine glutathione S-transferase in complex with a glutathione conjugate of 4-hydroxynon-2-enal in one subunit and glutathione in the other: evidence of signaling across the dimer interface. *Biochemistry,* 38**,** 11887-94.

XIAO, J. F., ZHOU, B. & RESSOM, H. W. 2012. Metabolite identification and quantitation in LC-MS/MS-based metabolomics. *Trends Analyt Chem,* 32**,** 1-14.

YAFFE, D. & SAXEL, O. 1977. Serial passaging and differentiation of myogenic cells isolated from dystrophic mouse muscle. *Nature,* 270**,** 725-7.

YANG, J., CARROLL, K. S. & LIEBLER, D. C. 2016. The Expanding Landscape of the Thiol Redox Proteome. *Mol Cell Proteomics,* 15**,** 1-11.

YANT, L. J., RAN, Q., RAO, L., VAN REMMEN, H., SHIBATANI, T., BELTER, J. G., MOTTA, L., RICHARDSON, A. & PROLLA, T. A. 2003. The selenoprotein GPX4 is essential for mouse development and protects from radiation and oxidative damage insults. *Free Radic Biol Med,* 34**,** 496-502.

YARIAN, C. S., REBRIN, I. & SOHAL, R. S. 2005. Aconitase and ATP synthase are targets of malondialdehyde modification and undergo an age-related decrease in activity in mouse heart mitochondria. *Biochem Biophys Res Commun,* 330**,** 151-6.

YARIAN, C. S., TOROSER, D. & SOHAL, R. S. 2006. Aconitase is the main functional target of aging in the citric acid cycle of kidney mitochondria from mice. *Mech Ageing Dev,* 127**,** 79-84.

YAROVAYA, N. O., KRAMAROVA, L., BORG, J., KOVALENKO, S. A., CARAGOUNIS, A. & LINNANE, A. W. 2002. Age-related atrophy of rat soleus muscle is accompanied by changes in fibre type composition, bioenergy decline and mtDNA rearrangements. *Biogerontology,* 3**,** 25-7.

YOTOV, W. V. & ST-ARNAUD, R. 1996. Differential splicing-in of a proline-rich exon converts αNAC into a muscle-specific transcription factor. *Genes Dev,* 10**,** 1763-72.

YU, H., WADDELL, J. N., KUANG, S. & BIDWELL, C. A. 2014. Park7 expression influences myotube size and myosin expression in muscle. *PLoS One,* 9**,** e92030.

ZHANG, C. & GAO, Y. 2014. Effects of aging on the lateral transmission of force in rat skeletal muscle. *J Biomech,* 47**,** 944-8.

ZHANG, J., XIN, L., SHAN, B., CHEN, W., XIE, M., YUEN, D., ZHANG, W., ZHANG, Z., LAJOIE, G. A. & MA, B. 2012. PEAKS DB: de novo sequencing assisted database search for sensitive and accurate peptide identification. *Mol Cell Proteomics,* 11**,** M111 010587.

ZHANG, Y., BILBAO, A., BRUDERER, T., LUBAN, J., STRAMBIO-DE-CASTILLIA, C., LISACEK, F., HOPFGARTNER, G. & VARESIO, E. 2015. The Use of Variable Q1 Isolation Windows Improves Selectivity in LC-SWATH-MS Acquisition. *J Proteome Res,* 14**,** 4359-71.

ZHANG, Y., DAVIS, C., SAKELLARIOU, G. K., SHI, Y., KAYANI, A. C., PULLIAM, D., BHATTACHARYA, A., RICHARDSON, A., JACKSON, M. J., MCARDLE, A., BROOKS, S. V. & VAN REMMEN, H. 2013. CuZnSOD gene deletion targeted to skeletal muscle leads to loss of contractile force but does not cause muscle atrophy in adult mice. *FASEB J,* 27**,** 3536-48.

ZHANG, Y., YU, B., HE, J. & CHEN, D. 2016a. From Nutrient to MicroRNA: a Novel Insight into Cell Signaling Involved in Skeletal Muscle Development and Disease. *Int J Biol Sci,* 12**,** 1247-1261.

ZHANG, Y. G., WANG, L., KAIFU, T., LI, J., LI, X. & LI, L. 2016b. Featured Article: Accelerated decline of physical strength in peroxiredoxin-3 knockout mice. *Exp Biol Med (Maywood),* 241**,** 1395-400.

ZIERATH, J. R. & HAWLEY, J. A. 2004. Skeletal muscle fiber type: influence on contractile and metabolic properties. *PLoS Biol,* 2**,** e348.

ZUO, L., CHRISTOFI, F. L., WRIGHT, V. P., BAO, S. & CLANTON, T. L. 2004. Lipoxygenase-dependent superoxide release in skeletal muscle. *J Appl Physiol (1985),* 97**,** 661-8.

ZURLO, F., LARSON, K., BOGARDUS, C. & RAVUSSIN, E. 1990. Skeletal muscle metabolism is a major determinant of resting energy expenditure. *J Clin Invest,* 86**,** 1423-7.

Supplementary Information

Table 3.3.8.1 A The 44 proteins identified by differential labelling for redox, reduced and reversibly oxidised proteins detected in adult mouse quadriceps.

F8WGM8	Actg1 - actin, gamma, cytoplasmic 1
F8VPN4	Agl - amylo-1,6-glucosidase, 4-alpha-glucanotransferase
Q9EQ20	Aldh6a1 - aldehyde dehydrogenase family 6, subfamily A1
D3Z7U0	Anxa11 - annexin A11
Q9CWJ9	Atic - 5-aminoimidazole-4-carboxamide ribonucleotide formyltransferase/IMP cyclohydrolase
D3YYN7	Atp1a2 - ATPase, Na+/K+ transporting, alpha 2 polypeptide
A2AKV0	Atp5c1 - ATP synthase, H+ transporting, mitochondrial F1 complex, gamma polypeptide 1
Q9CQQ7	Atp5f1 - ATP synthase, H+ transporting, mitochondrial F0 complex, subunit B1
O88374	Bcat2 - branched chain aminotransferase 2, mitochondrial
Q8R4N0	Clybl - citrate lyase beta like protein
Q8R1G2	Cmbl - carboxymethylenebutenolidase-like (Pseudomonas)
P19536	Cox5b - cytochrome c oxidase, subunit Vb
D6RIN4	Dynll2 - dynein light chain LC8-type 2
O70251	Eef1b2 - eukaryotic translation elongation factor 1 beta 2
D3YY68	Eef1d - eukaryotic translation elongation factor 1 delta (guanine nucleotide exchange protein)
Q3UGC7	Eif3j1 - eukaryotic translation initiation factor 3, subunit J1
Q8BTU6	Eif4a2 - eukaryotic translation initiation factor 4A2
P97807	Fh1 - fumarate hydratase 1
Q9CPU0	Glo1 - glyoxalase 1
D3YUM8	Gm4950 - predicted pseudogene 4950
S4R1E5	Gpx4 - Glutathione peroxidase
E9Q5B5	Hk2 - hexokinase 2
Q61696	Hspa1a - heat shock protein 1A;
Q5EBG6	Hspb6 - heat shock protein, alpha-crystallin-related, B6
Q9D6R2	Idh3a - isocitrate dehydrogenase 3 (NAD+) alpha
Q80ZJ2	Impa1 - inositol (myo)-1(or 4)-monophosphatase 1
H3BLD4	Kdm2a - lysine (K)-specific demethylase 2A
P06151	Ldha - lactate dehydrogenase A
A2AMM0	Murc - muscle-related coiled-coil protein
P13542	Myh8 - myosin, heavy polypeptide 8, skeletal muscle, perinatal
Q9CPP6	Ndufa5 - NADH dehydrogenase (ubiquinone) 1 alpha subcomplex, 5
F6ZFT1	Ndufab1 - NADH dehydrogenase (ubiquinone) 1, alpha/beta subcomplex, 1
E9QQ96	Obscn - obscurin, cytoskeletal calmodulin and titin-interacting RhoGEF
P62962	Pfn1 - profilin 1
D6RG50	Prkab2 - protein kinase, AMP-activated, beta 2 non-catalytic subunit
P12367	Prkar2a - protein kinase, cAMP dependent regulatory, type II alpha
A2AWQ9	Scrn3 - secernin 3
Q8BH59	Slc25a12 - solute carrier family 25 (mitochondrial carrier, Aralar), member 12
P48962	Slc25a4 - solute carrier family 25 (mitochondrial carrier, adenine nucleotide translocator), member 4
Q8JZR6	Slc4a8 - solute carrier family 4 (anion exchanger), member 8
P10639	Txn1 - thioredoxin 1
D3YZS3	Ube2l3 - ubiquitin-conjugating enzyme E2L 3
Q64727	Vcl - vinculin
P20152	Vim - vimentin

Table 3.3.8.1 B The 133 proteins identified by differential labelling as redox, reduced and reversibly oxidised proteins detected in adult and old mouse quadriceps.

P51174	Acadl - acyl-Coenzyme A dehydrogenase, long-chain
Q07417	Acads - acyl-Coenzyme A dehydrogenase, short chain
B1AR28	Acadvl - acyl-Coenzyme A dehydrogenase, very long chain
Q99KI0	Aco2 - aconitase 2, mitochondrial
P63268	Actg2 - actin, gamma 2, smooth muscle, enteric
O88990	Actn3 - actinin alpha 3
P28650	Adssl1 - adenylosuccinate synthetase like 1
P29699	Ahsg - alpha-2-HS-glycoprotein
Q9R0Y5	Ak1 - adenylate kinase 1
P45376	Akr1b3 - aldo-keto reductase family 1, member B3 (aldose reductase)
P07724	Alb - albumin
P47738	Aldh2 - aldehyde dehydrogenase 2, mitochondrial
P05064	Aldoa - aldolase A, fructose-bisphosphate
Q3V1D3	Ampd1 - adenosine monophosphate deaminase 1
F8WIT2	Anxa6 - annexin A6
Q8C0M9	Asrgl1 - asparaginase like 1
Q8R429	Atp2a1 - ATPase, Ca++ transporting, cardiac muscle, fast twitch 1
D3Z6F5	Atp5a1 - ATP synthase, H+ transporting, mitochondrial F1 complex, alpha subunit 1
B1ASE2	Atp5h - ATP synthase, H+ transporting, mitochondrial F0 complex, subunit d
Q6P1B9	Bin1 - bridging integrator 1
P14211	Calr - calreticulin
P16015	Car3 - carbonic anhydrase 3
P45591	Cfl2 - cofilin 2, muscle
P07310	Ckm - creatine kinase, muscl
Q6P8J7	Ckmt2 - creatine kinase, mitochondrial 2
P56391	Cox6b1 - cytochrome c oxidase, subunit Vlb polypeptide 1
Q9CZU6	Cs - citrate synthase
O08749	Dld - dihydrolipoamide dehydrogenase
Q9D2G2	Dlst - dihydrolipoamide S-succinyltransferase (E2 component of 2-oxo-glutarate complex)
Q8BK84	Dupd1 - dual specificity phosphatase and pro isomerase domain containing 1
F6T930	Echs1 - enoyl Coenzyme A hydratase, short chain, 1, mitochondrial
P58252	Eef2 - eukaryotic translation elongation factor 2
Q6PHC1	Eno1 - enolase 1, alpha non-neuron
B0QZL1	Eno1 - enolase 1, alpha non-neuron
P21550	Eno3 - enolase 3, beta muscle
Q99LC5	Etfa - electron transferring flavoprotein, alpha polypeptide
Q9DCW4	Etfb - electron transferring flavoprotein, beta polypeptide
P04117	Fabp4 - fatty acid binding protein 4, adipocyte
D3Z100	Fam98c - family with sequence similarity 98, member C
Q61554	Fbn1 - fibrillin 1
Q5STE3	Fstl4 - follistatin-like 4
P16858	Gapdh - glyceraldehyde-3-phosphate dehydrogenase
O55126	Gbas - glioblastoma amplified sequence
P05201	Got1 - glutamate oxaloacetate transaminase 1, soluble
P05202	Got2 - glutamate oxaloacetate transaminase 2, mitochondrial
E0CXN5	Gpd1 - glycerol-3-phosphate dehydrogenase 1 (soluble)
P06745	Gpi1 - glucose phosphate isomerase 1
P10649	Gstm1 - glutathione S-transferase, mu 1
D3YX76	Gstm2 - glutathione S-transferase, mu 2
E9Q024	Gstm5 - glutathione S-transferase, mu 5
Q61425	Hadh - hydroxyacyl-Coenzyme A dehydrogenase
A8DUK4	Hbb-b1 - hemoglobin, beta adult major chain
P70349	Hint1 - histidine triad nucleotide binding protein 1
Q91X72	Hpx - hemopexin
Q61316	Hspa4 - heat shock protein 4
Q504P4	Hspa8 - heat shock protein 8
P38647	Hspa9 - heat shock protein 9
P63038	Hspd1 - heat shock protein 1 (chaperonin)
P70404	Idh3g - isocitrate dehydrogenase 3 (NAD+), gamma
P01867	Igh3 - Ig gamma-2B chain C region
F6TQW2	Ighg2c - immunoglobulin heavy constant gamma 2C
A2AUC9	Kbtbd10 - kelch repeat and BTB (POZ) domain containing 10
D3YTY9	Kng1 - kininogen 1
P16045	Lgals1 - lectin, galactose binding, soluble 1

P04247	Mb - myoglobin
P14152	Mdh1 - malate dehydrogenase 1, NAD (soluble)
P08249	Mdh2 - malate dehydrogenase 2, NAD (mitochondrial)
P34884	Mif - macrophage migration inhibitory factor
P03899	mt-Nd3 - mitochondrially encoded NADH dehydrogenase 3
Q6P6L5	Mybpc1 - myosin binding protein C, slow-type
Q5XKE0	Mybpc2 - myosin binding protein C, fast-type
P70402	Mybph - myosin binding protein H
Q5SX39	Myh4 - myosin, heavy polypeptide 4, skeletal muscle
P05977	Myl1 - myosin, light polypeptide 1
P09542	Myl3 - myosin, light polypeptide 3
Q8VCR8	Mylk2 - myosin, light polypeptide kinase 2, skeletal muscle
P97457	Mylpf - myosin light chain, phosphorylatable, fast skeletal muscle
Q62234	Myom1 - myomesin 1
Q14BI5	Myom2 - myomesin 2
Q9QYG0	Ndrg2 - N-myc downstream regulated gene 2
Q99LC3	Ndufa10 - NADH dehydrogenase (ubiquinone) 1 alpha subcomplex 10
Q9CR61	Ndufb7 - NADH dehydrogenase (ubiquinone) 1 beta subcomplex, 7
D3YXX5	Ndufv1 - NADH dehydrogenase (ubiquinone) flavoprotein 1
Q01768	Nme2 - NME/NM23 nucleoside diphosphate kinase 2
P61971	Nutf2-ps1 - nuclear transport factor 2, pseudogene 1
Q60597	Ogdh - oxoglutarate dehydrogenase (lipoamide)
P09103	P4hb - prolyl 4-hydroxylase, beta polypeptide
A2A817	Park7 - Parkinson disease (autosomal recessive, early onset) 7
P35486	Pdha1 - pyruvate dehydrogenase E1 alpha 1
Q9D051	Pdhb - pyruvate dehydrogenase (lipoamide) beta
P70296	Pebp1 - phosphatidylethanolamine binding protein 1
P47857	Pfkm - phosphofructokinase, muscle
O70250	Pgam2 - phosphoglycerate mutase 2
P09411	Pgk1-rs7 - phosphoglycerate kinase-1, related sequence-7
Q9D0F9	Pgm2 - phosphoglucomutase 2
P52480	Pkm - pyruvate kinase, muscle
P17742	Ppia - peptidylprolyl isomerase A
P63330	Ppp2ca - protein phosphatase 2 (formerly 2A), catalytic subunit, alpha isoform
P35700	Prdx1 - peroxiredoxin 1
P20108	Prdx3 - peroxiredoxin 3
G3UZJ4	Prdx5 - peroxiredoxin 5
Q9WUB3	Pygm - muscle glycogen phosphorylase
Q9DD03	Rab13 - RAB13, member RAS oncogene family
Q9CQ09	Rpl3l - ribosomal protein L3-like
Q3V1Z5	Rps4y2 - ribosomal protein S4, Y-linked 2
Q8K2B3	Sdha - succinate dehydrogenase complex, subunit A, flavoprotein (Fp
Q9CQA3	Sdhb - succinate dehydrogenase complex, subunit B, iron sulfur (Ip)
F8WGB3	Sdhc - succinate dehydrogenase complex, subunit C
P07759	Serpina3k - serine (or cysteine) peptidase inhibitor, clade A, member 3K
Q60854	Serpinb6a - serine (or cysteine) peptidase inhibitor, clade B, member 6a
Q8VEM8	Slc25a3 - solute carrier family 25 (mitochondrial carrier, phosphate carrier), member 3
P08228	Sod1 - superoxide dismutase 1, soluble
Q7TQ48	Srl - sarcalumenin
Q9Z2I9	Sucla2 - succinate-Coenzyme A ligase, ADP-forming, beta subunit
Q923W1	Tgs1 - trimethylguanosine synthase homolog (S. cerevisiae)
P20801	Tnnc2 - troponin C2, fast
P13412	Tnni2 - troponin I, skeletal, fast 2
P17751	Tpi1 - triosephosphate isomerase 1
G5E8R0	Tpm1 - tropomyosin 1, alpha
Q6IRU2	Tpm4 - tropomyosin 4
P63028	Tpt1 - tumor protein, translationally-controlled 1
Q921I1	Trf - transferrin
D3YXQ9	Ttll13 - tubulin tyrosine ligase-like family, member 13
P61089	Ube2n - ubiquitin-conjugating enzyme E2N
Q91ZJ5	Ugp2 - UDP-glucose pyrophosphorylase 2
Q9CZ13	Uqcrc1 - ubiquinol-cytochrome c reductase core protein 1
Q9DB77	Uqcrc2 - ubiquinol cytochrome c reductase core protein 2
P99028	Uqcrh - ubiquinol-cytochrome c reductase hinge protein
Q01853	Vcp - valosin containing protein
Q60932	Vdac1 - voltage-dependent anion channel 1
D6REF3	Ywhae - tyrosine 3-monooxygenase/tryptophan 5-monooxygenase activation protein, epsilon polypeptide
P61982	Ywhag - tyrosine 3-monooxygenase/tryptophan 5-monooxygenase activation protein, gamma polypeptide
P63101	Ywhaz - tyrosine 3-monooxygenase/tryptophan 5-monooxygenase activation protein, zeta polypeptide

Table 3.3.8.1 C The 33 proteins identified by differential labelling for redox, reduced and reversibly oxidised proteins detected in old mouse quadriceps.

E9Q1F2	Actg1 - actin, gamma, cytoplasmic 1
P28474	Adh5 - alcohol dehydrogenase 5 (class III), chi polypeptide
D3YVX6	Atp1a2 - ATPase, Na+/K+ transporting, alpha 2 polypeptide
P56382	Atp5e - ATP synthase, H+ transporting, mitochondrial F1 complex, epsilon subunit
J3QP71	Bsg - basigin
F6QJN8	Capzb - capping protein (actin filament) muscle Z-line, beta
P10605	Ctsb - cathepsin B
F6Y6L6	Ctsd - cathepsin D
Q9CQ62	Decr1 - 2,4-dienoyl CoA reductase 1, mitochondrial
P62631	Eef1a2 - eukaryotic translation elongation factor 1 alpha 2
P70695	Fbp2 - fructose bisphosphatase 2
P50396	Gdi1 - guanosine diphosphate (GDP) dissociation inhibitor 1
Q61598	Gdi2 - guanosine diphosphate (GDP) dissociation inhibitor 2
Q64521	Gpd2 - glycerol phosphate dehydrogenase 2, mitochondrial
Q8BUV3	Gphn - gephyrin
P19157	Gstp1 - glutathione S-transferase, pi 1
E9Q5B6	Hnrnpd - heterogeneous nuclear ribonucleoprotein D
P06330	Ig heavy chain V region AC38 205.12
P01649	Ig kappa chain V-V regions
D3Z736	Ldha - lactate dehydrogenase A
D3Z6D8	Mapk3 - mitogen-activated protein kinase 3
F6Q3K8	Mpi - mannose phosphate isomerase
G3UW82	Myh2 - myosin, heavy polypeptide 2, skeletal muscle, adult
Q9CQ75	Ndufa2 - NADH dehydrogenase (ubiquinone) 1 alpha subcomplex, 2
P29758	Oat - ornithine aminotransferase
F6V9F1	Pcmt1 - protein-L-isoaspartate (D-aspartate) O-methyltransferase 1
Q9CRA2	Pdlim5 - PDZ and LIM domain 5
D3Z0Y2	Prdx6 - peroxiredoxin 6
G3UXL2	Prps1l3 - phosphoribosyl pyrophosphate synthetase 1-like 3
P62889	Rpl30 - ribosomal protein L30
D3YV43	Rps3 - ribosomal protein S3
Q7TMY4	Thoc7 - THO complex 7 homolog (Drosophila)
P68037	Ube2l3 - ubiquitin-conjugating enzyme E2L 3

Table 3.3.8.2 A The 21 redox proteins identified in adult mouse quadriceps.

P28650	Adssl1 - adenylosuccinate synthetase like 1
F8VPN4	Agl - amylo-1,6-glucosidase, 4-alpha-glucanotransferase
P45376	Akr1b3 - aldo-keto reductase family 1, member B3 (aldose reductase)
Q3V1D3	Ampd1 - adenosine monophosphate deaminase 1
B1ASE2	Atp5h - ATP synthase, H+ transporting, mitochondrial F0 complex, subunit d
Q9CZU6	Cs - citrate synthase
Q60854	erpinb6a - serine (or cysteine) peptidase inhibitor, clade B, member 6a
Q99LC5	Etfa - electron transferring flavoprotein, alpha polypeptide
P97807	Fh1 - fumarate hydratase 1
A8DUK4	Hbb-b1 - hemoglobin, beta adult major chain
A2AUC9	Kbtbd10 - kelch repeat and BTB (POZ) domain containing 10
P06151	Ldha - lactate dehydrogenase A
Q5XKE0	Mybpc2 - myosin binding protein C, fast-type
P13542	Myh8 - myosin, heavy polypeptide 8, skeletal muscle, perinatal
Q9QYG0	Ndrg2 - N-myc downstream regulated gene 2
A2A817	Park7 - Parkinson disease (autosomal recessive, early onset) 7
P70296	Pebp1 - phosphatidylethanolamine binding protein 1
P09411	Pgk1-rs7 - phosphoglycerate kinase-1, related sequence-7
Q9D0F9	Pgm2 - phosphoglucomutase 2
P17742	Ppia - peptidylprolyl isomerase A
Q7TQ48	Srl - sarcalumenin

Table 3.3.8.2 B The 43 redox proteins identified in both adult and old mouse quadriceps.

P51174	Acadl - acyl-Coenzyme A dehydrogenase, long-chain
Q99KI0	Aco2 - aconitase 2, mitochondrial
P63268	Actg2 - actin, gamma 2, smooth muscle, enteric
P07724	Alb - albumin
P05064	Aldoa - aldolase A, fructose-bisphosphate
Q8R429	Atp2a1 - ATPase, Ca++ transporting, cardiac muscle, fast twitch 1
P45591	Cfl2 - cofilin 2, muscle
P07310	Ckm - creatine kinase, muscle
Q6P8J7	Ckmt2 - creatine kinase, mitochondrial 2
O08749	Dld - dihydrolipoamide dehydrogenase
P58252	Eef2 - eukaryotic translation elongation factor 2
B0QZL1	Eno1 - enolase 1, alpha non-neuron
Q6PHC1	Eno1 - enolase 1, alpha non-neuron
P21550	Eno3 - enolase 3, beta muscle
D3Z100	Fam98c - family with sequence similarity 98, member C
P16858	Gapdh - glyceraldehyde-3-phosphate dehydrogenase
P05201	Got1 - glutamate oxaloacetate transaminase 1, soluble
P05202	Got2 - glutamate oxaloacetate transaminase 2, mitochondria
P06745	Gpi1 - glucose phosphate isomerase 1
Q504P4	Hspa8 - heat shock protein 8
P14152	Mdh1 - malate dehydrogenase 1, NAD (soluble)
P08249	Mdh2 - malate dehydrogenase 2, NAD (mitochondrial)
Q5SX39	Myh4 - myosin, heavy polypeptide 4, skeletal muscle
P97457	Mylpf - myosin light chain, phosphorylatable, fast skeletal muscle
Q14BI5	Myom2 - myomesin 2
D3YXX5	Ndufv1 - NADH dehydrogenase (ubiquinone) flavoprotein 1
Q01768	Nme2 - NME/NM23 nucleoside diphosphate kinase 2
P61971	Nutf2-ps1 - nuclear transport factor 2, pseudogene 1
Q60597	Ogdh - oxoglutarate dehydrogenase (lipoamide)
Q9D051	Pdhb - pyruvate dehydrogenase (lipoamide) beta
P47857	Pfkm - phosphofructokinase, muscle
O70250	Pgam2 - phosphoglycerate mutase 2
P52480	Pkm - pyruvate kinase, muscle
Q9WUB3	Pygm - muscle glycogen phosphorylase
P08228	superoxide dismutase 1, soluble
P13412	Tnni2 - troponin I, skeletal, fast 2
P17751	Tpi1 - triosephosphate isomerase 1
G5E8R0	Tpm1 - tropomyosin 1, alpha
Q6IRU2	Tpm4 - tropomyosin 4
Q9CZ13	Uqcrc1 - ubiquinol-cytochrome c reductase core protein 1
Q9DB77	Uqcrc2 - ubiquinol cytochrome c reductase core protein 2
D6REF3	Ywhae - tyrosine 3-monooxygenase/tryptophan 5-monooxygenase activation protein, epsilon polypeptide
P61982	Ywhag - tyrosine 3-monooxygenase/tryptophan 5-monooxygenase activation protein, gamma polypeptide

Table 3.3.8.2 C The 8 redox proteins identified in adult mouse quadriceps.

P56382	Atp5e - ATP synthase, H+ transporting, mitochondrial F1 complex, epsilon subunit
P62631	Eef1a2 - eukaryotic translation elongation factor 1 alpha 2
P70349	Hint1 - histidine triad nucleotide binding protein 1
D3Z736	Ldha - lactate dehydrogenase A
G3UW82	Myh2 - myosin, heavy polypeptide 2, skeletal muscle, adult
F6V9F1	Pcmt1 - protein-L-isoaspartate (D-aspartate) O-methyltransferase 1
P07759	Serpina3k - serine (or cysteine) peptidase inhibitor, clade A, member 3K
P63101	Ywhaz - tyrosine 3-monooxygenase/tryptophan 5-monooxygenase activation protein, zeta polypeptide

Table 3.3.8.3 A The 37 reduced proteins identified in adult mouse quadriceps.

F8WGM8	Actg1 - actin, gamma, cytoplasmic 1
Q9EQ20	Aldh6a1 - aldehyde dehydrogenase family 6, subfamily A1
D3Z7U0	Anxa11 - annexin A11
D3YYN7	Atp1a2 - ATPase, Na+/K+ transporting, alpha 2 polypeptide
A2AKV0	Atp5c1 - ATP synthase, H+ transporting, mitochondrial F1 complex, gamma polypeptide 1
Q9CQQ7	Atp5f1 - ATP synthase, H+ transporting, mitochondrial F0 complex, subunit B1
O88374	Bcat2 - branched chain aminotransferase 2, mitochondrial
Q8R4N0	Clybl - citrate lyase beta like
Q8R1G2	Cmbl - carboxymethylenebutenolidase-like (Pseudomonas)
D6RIN4	Dynll2 - dynein light chain LC8-type 2
O70251	Eef1b2 - eukaryotic translation elongation factor 1 beta 2
D3YY68	Eef1d - eukaryotic translation elongation factor 1 delta (guanine nucleotide exchange protein)
Q3UGC7	Eif3j1 - eukaryotic translation initiation factor 3, subunit J1
Q8BTU6	Eif4a2 - eukaryotic translation initiation factor 4A2
Q9CPU0	Glo1 - glyoxalase 1
D3YUM8	Gm4950 - predicted pseudogene 4950
S4R1E5	Gpx4 - Glutathione peroxidase
E9Q5B5	Hk2 - hexokinase 2
Q5EBG6	Hspb6 - heat shock protein, alpha-crystallin-related, B6
Q9D6R2	Idh3a - isocitrate dehydrogenase 3 (NAD+) alpha
Q80ZJ2	Impa1 - inositol (myo)-1(or 4)-monophosphatase 1
H3BLD4	Kdm2a - lysine (K)-specific demethylase 2A
A2AMM0	Murc - muscle-related coiled-coil protein
Q9CPP6	Ndufa5 - NADH dehydrogenase (ubiquinone) 1 alpha subcomplex, 5
F6ZFT1	Ndufab1 - NADH dehydrogenase (ubiquinone) 1, alpha/beta subcomplex, 1
E9QQ96	Obscn - obscurin, cytoskeletal calmodulin and titin-interacting RhoGEF
P62962	Pfn1 - profilin 1
D6RG50	Prkab2 - protein kinase, AMP-activated, beta 2 non-catalytic subunit
P12367	Prkar2a - protein kinase, cAMP dependent regulatory, type II alpha
A2AWQ9	Scrn3 - secernin 3
Q8BH59	Slc25a12 - solute carrier family 25 (mitochondrial carrier, Aralar), member 12
P48962	Slc25a4 - solute carrier family 25 (mitochondrial carrier, adenine nucleotide translocator), member 4
Q8JZR6	Slc4a8 - solute carrier family 4 (anion exchanger), member 8
P10639	Txn1 - thioredoxin 1
D3YZS3	Ube2l3 - ubiquitin-conjugating enzyme E2L 3
Q64727	Vcl - vinculin
P20152	Vim - vimentin

Table 3.3.8.3 B The 57 reduced proteins identified in both adult and old mouse quadriceps.

Q07417	Acads - acyl-Coenzyme A dehydrogenase, short chain
B1AR28	Acadvl - acyl-Coenzyme A dehydrogenase, very long chain
O88990	Actn3 - actinin alpha
Q9R0Y5	Ak1 - adenylate kinase 1
P47738	Aldh2 - aldehyde dehydrogenase 2, mitochondrial
F8WIT2	Anxa6 - annexin A6
Q8C0M9	Asrgl1 - asparaginase like 1
D3Z6F5	Atp5a1 - ATP synthase, H+ transporting, mitochondrial F1 complex, alpha subunit 1
Q6P1B9	Bin1 - bridging integrator 1
P16015	Car3 - carbonic anhydrase 3
Q9D2G2	Dlst - dihydrolipoamide S-succinyltransferase (E2 component of 2-oxo-glutarate complex)
Q8BK84	Dupd1 - dual specificity phosphatase and pro isomerase domain containing 1
F6T930	Echs1 - Enoyl-CoA hydratase, mitochondrial
Q9DCW4	Etfb - electron transferring flavoprotein, beta polypeptide
P04117	Fabp4 - fatty acid binding protein 4, adipocyte
O55126	Gbas - glioblastoma amplified sequence
E0CXN5	Gpd1 - glycerol-3-phosphate dehydrogenase 1 (soluble)
P10649	Gstm1 - glutathione S-transferase, mu 1
D3YX76	Gstm2 - glutathione S-transferase, mu 2
E9Q024	Gstm5 - glutathione S-transferase, mu 5
Q61425	Hadh - hydroxyacyl-Coenzyme A dehydrogenase
Q61316	Hspa4 - heat shock protein 4
P38647	Hspa9 - heat shock protein 9
P63038	Hspd1 - heat shock protein 1 (chaperonin)
P70404	Idh3g - isocitrate dehydrogenase 3 (NAD+), gamma
P16045	Lgals1 - lectin, galactose binding, soluble 1
P04247	Mb - myoglobin
P34884	Mif - macrophage migration inhibitory factor
P03899	mt-Nd3 - mitochondrially encoded NADH dehydrogenase 3
Q6P6L5	Mybpc1 - myosin binding protein C, slow-type
P70402	Mybph - myosin binding protein H
P05977	Myl1 - myosin, light polypeptide 1
P09542	Myl3 - myosin, light polypeptide 3
Q8VCR8	Mylk2 - myosin, light polypeptide kinase 2, skeletal muscle
Q62234	Myom1 - myomesin 1
Q99LC3	Ndufa10 - NADH dehydrogenase (ubiquinone) 1 alpha subcomplex 10
P09103	P4hb - prolyl 4-hydroxylase, beta polypeptide
P35486	Pdha1 - pyruvate dehydrogenase E1 alpha
P63330	Ppp2ca - protein phosphatase 2 (formerly 2A), catalytic subunit, alpha isoform
P35700	Prdx1 - peroxiredoxin 1
P20108	Prdx3 - peroxiredoxin 3
G3UZJ4	Prdx5 - peroxiredoxin 5
Q9DD03	Rab13 - RAB13, member RAS oncogene family
Q9CQ09	Rpl3l - ribosomal protein L3-like
Q3V1Z5	Rps4y2 - ribosomal protein S4, Y-linked 2
Q8K2B3	Sdha - succinate dehydrogenase complex, subunit A, flavoprotein (Fp)
Q9CQA3	Sdhb - succinate dehydrogenase complex, subunit B, iron sulfur (Ip)
F8WGB3	Sdhc - succinate dehydrogenase complex, subunit C, integral membrane protein
Q8VEM8	Slc25a3 - solute carrier family 25 (mitochondrial carrier, phosphate carrier), member 3
Q9Z2I9	Sucla2 - succinate-Coenzyme A ligase, ADP-forming, beta subunit
Q923W1	Tgs1 - trimethylguanosine synthase homolog (S. cerevisiae)
P20801	Tnnc2 - troponin C2, fast
P63028	Tpt1 - tumor protein, translationally-controlled 1
P61089	Ube2n - ubiquitin-conjugating enzyme E2N
Q91ZJ5	Ugp2 - UDP-glucose pyrophosphorylase
Q01853	Vcp - valosin containing protein
Q60932	Vdac1 - voltage-dependent anion channel

Table 3.3.8.3 C The 38 reduced proteins identified in old mouse quadriceps.

E9Q1F2	Actg1 - actin, gamma, cytoplasmic 1
P28474	Adh5 - alcohol dehydrogenase 5 (class III), chi polypeptide
P28650	Adssl1 - adenylosuccinate synthetase like 1
P45376	Akr1b3 - aldo-keto reductase family 1, member B3 (aldose reductase)
Q3V1D3	Ampd1 - adenosine monophosphate deaminase 1
D3YVX6	Atp1a2 - ATPase, Na+/K+ transporting, alpha 2 polypeptide
B1ASE2	Atp5h - ATP synthase, H+ transporting, mitochondrial F0 complex, subunit d
F6QJN8	Capzb - capping protein (actin filament) muscle Z-line, beta
Q9CZU6	Cs - citrate synthase
Q9CQ62	Decr1 - 2,4-dienoyl CoA reductase 1, mitochondrial
Q99LC5	Etfa - electron transferring flavoprotein, alpha polypeptide
P70695	Fbp2 - fructose bisphosphatase 2
P50396	Gdi1 - guanosine diphosphate (GDP) dissociation inhibitor 1
Q61598	Gdi2 - guanosine diphosphate (GDP) dissociation inhibitor 2
Q64521	Gpd2 - glycerol phosphate dehydrogenase 2, mitochondrial
Q8BUV3	Gphn - gephyrin
P19157	Gstp1 - glutathione S-transferase, pi 1
A8DUK4	Hbb-b1 - hemoglobin, beta adult major chain
E9Q5B6	Hnrnpd - heterogeneous nuclear ribonucleoprotein D
A2AUC9	Kbtbd10 - kelch repeat and BTB (POZ) domain containing 10
D3Z6D8	Mapk3 - mitogen-activated protein kinase 3
F6Q3K8	Mpi - mannose phosphate isomerase
Q5XKE0	Mybpc2 - myosin binding protein C, fast-type
Q9QYG0	Ndrg2 - N-myc downstream regulated gene
Q9CQ75	Ndufa2 - NADH dehydrogenase (ubiquinone) 1 alpha subcomplex,
P29758	Oat - ornithine aminotransferase
A2A817	Park7 - Parkinson disease (autosomal recessive, early onset) 7
Q9CRA2	Pdlim5 - PDZ and LIM domain 5
P70296	Pebp1 - phosphatidylethanolamine binding protein 1
P09411	Pgk1-rs7 - phosphoglycerate kinase-1, related sequence-7
Q9D0F9	Pgm2 - phosphoglucomutase 2
P17742	Ppia - peptidylprolyl isomerase A
G3UXL2	Prps1l3 - phosphoribosyl pyrophosphate synthetase 1-like 3
P62889	Rpl30 - ribosomal protein L30
D3YV43	Rps3 - ribosomal protein S3
Q60854	Serpinb6a - serine (or cysteine) peptidase inhibitor, clade B, member 6a
Q7TMY4	Thoc7 - THO complex 7 homolog (Drosophila)
P68037	Ube2l3 - ubiquitin-conjugating enzyme E2L 3

Table 3.3.8.4 A The 7 reversibly oxidised proteins identified in adult mouse quadriceps.

P07724	Alb - albumin
Q9CWJ9	Atic - 5-aminoimidazole-4-carboxamide ribonucleotide formyltransferase/IMP cyclohydrolase
P19536	Cox5b - cytochrome c oxidase, subunit Vb
P70349	Hint1 - histidine triad nucleotide binding protein 1
Q61696	Hspa1a - heat shock protein 1A
P07759	Serpina3k - serine (or cysteine) peptidase inhibitor, clade A, member 3K
P63101	Ywhaz - tyrosine 3-monooxygenase/tryptophan 5-monooxygenase activation protein, zeta polypeptide

Table 3.3.8.4 B The 14 reversibly oxidised proteins identified in both adult and old mouse quadriceps.

P29699	Ahsg - alpha-2-HS-glycoprotein
P14211	Calr - calreticulin
P56391	Cox6b1 - cytochrome c oxidase, subunit VIb polypeptide 1
Q61554	Fbn1 - fibrillin 1
Q5STE3	Fstl4 - follistatin-like 4
Q91X72	Hpx - hemopexin
P01867	Igh3 - Ig gamma-2B chain C region
F6TQW2	Ighg2c - immunoglobulin heavy constant gamma 2C
D3YTY9	Kng1 - kininogen 1
Q9CR61	Ndufb7 - NADH dehydrogenase (ubiquinone) 1 beta subcomplex, 7
Q7TQ48	Srl - sarcalumenin
Q921I1	Trf - transferrin
D3YXQ9	Ttll13 - tubulin tyrosine ligase-like family, member 13
P99028	Uqcrh - ubiquinol-cytochrome c reductase hinge protein

Table 3.3.8.4 C The 6 reversibly oxidised proteins identified in only old mouse quadriceps.

J3QP71	Bsg - basigin
P10605	Ctsb - cathepsin B
F6Y6L6	Ctsd - cathepsin D
P06330	Ig heavy chain V region AC38 205.12
P01649	Ig kappa chain V-V regions
D3Z0Y2	Prdx6 - peroxiredoxin 6

Table 4.3.8.1 A The 46 differentially labelled proteins of redox, reduced and reversibly oxidised proteins detected in adult mouse soleus muscle.

F7B1B6	Adck3 - aarF domain containing kinase 3
Q9R0Y5	Ak1 - adenylate kinase 1
P45376	Akr1b3 - aldo-keto reductase family 1, member B3 (aldose reductase)
P47738	Aldh2 - aldehyde dehydrogenase 2, mitochondrial
F8WIT2	Anxa6 - annexin A6
D3YYN7	Atp1a2 - ATPase, Na+/K+ transporting, alpha 2 polypeptide
Q6IRU5	Cltb - clathrin, light polypeptide (Lcb)
Q924X2	Cpt1b - carnitine palmitoyltransferase 1b, muscle
Q8BMF4	Dlat - dihydrolipoamide S-acetyltransferase (E2 component of pyruvate dehydrogenase complex)
F7B227	Ech1 - enoyl coenzyme A hydratase 1, peroxisomal
P97447	Fhl1 - four and a half LIM domains 1
P50608	Fmod - fibromodulin
Q9DCM2	Gstk1 - glutathione S-transferase kappa 1
P19157	Gstp1 - glutathione S-transferase, pi 1
Q8BMS1	Hadha - hydroxyacyl-Coenzyme A dehydrogenase/3-ketoacyl-Coenzyme A thiolase/enoyl-Coenzyme A hydratase (trifunctional protein), alpha subunit
Q99JY0	Hadhb - hydroxyacyl-Coenzyme A dehydrogenase/3-ketoacyl-Coenzyme A thiolase/enoyl-Coenzyme A hydratase (trifunctional protein), beta subunit
O88569	Hnrnpa2b1 - heterogeneous nuclear ribonucleoprotein A2/B1
Q61646	Hp - haptoglobin
P54071	Idh2 - isocitrate dehydrogenase 2 (NADP+), mitochondrial
Q9D6R2	Idh3a - isocitrate dehydrogenase 3 (NAD+) alpha
P70404	Idh3g - isocitrate dehydrogenase 3 (NAD+), gamma
A2AUC9	Kbtbd10 - kelch repeat and BTB (POZ) domain containing 10
P13542	Myh8 - myosin, heavy polypeptide 8, skeletal muscle, perinatal
Q62234	Myom1 - myomesin 1
Q9CQ75	Ndufa2 - NADH dehydrogenase (ubiquinone) 1 alpha subcomplex, 2
Q9DCJ5	Ndufa8 - NADH dehydrogenase (ubiquinone) 1 alpha subcomplex, 8
A2A813	Park7 - Parkinson disease (autosomal recessive, early onset) 7
P35486	Pdha1 - pyruvate dehydrogenase E1 alpha 1
Q9D051	Pdhb - pyruvate dehydrogenase (lipoamide) beta
O70400	Pdlim1 - PDZ and LIM domain 1 (elfin)
Q8CI51	Pdlim5 - PDZ and LIM domain 5
P17742	Ppia - peptidylprolyl isomerase A
P63330	Ppp2ca - protein phosphatase 2 (formerly 2A), catalytic subunit, alpha isoform
P61027	Rab10 - RAB10, member RAS oncogene family
E9PZM7	Scaf11 - SR-related CTD-associated factor 11
Q9CQA3	Sdhb - succinate dehydrogenase complex, subunit B, iron sulfur (Ip)
F8WGB3	Sdhc - succinate dehydrogenase complex, subunit C, integral membrane protein
Q9Z2Z6	Slc25a20 - solute carrier family 25 (mitochondrial carnitine/acylcarnitine translocase), member 20
P08228	Sod1 - superoxide dismutase 1, soluble
Q9Z2I9	Sucla2 - succinate-Coenzyme A ligase, ADP-forming, beta subunit
Q9WUM5	Suclg1 - succinate-CoA ligase, GDP-forming, alpha subunit
Q6IRU2	Tpm4 - tropomyosin 4
Q8BFR5	Tufm - Tu translation elongation factor, mitochondrial
F6T930	Unkown - entry obsolete in Uniprot as of October 2016
D6REF3	Ywhae - tyrosine 3-monooxygenase/tryptophan 5-monooxygenase activation protein, epsilon polypeptide
E9QMD3	Zfhx3 - zinc finger homeobox 3

Table 4.3.8.1 B The 127 differentially labelled proteins of redox, reduced and reversibly oxidised proteins detected in both adult and old mouse soleus muscle.

P51174	Acadl - acyl-Coenzyme A dehydrogenase, long-chain
Q07417	Acads - acyl-Coenzyme A dehydrogenase, short chain
B1AR28	Acadvl - acyl-Coenzyme A dehydrogenase, very long chain
Q99KI0	Aco2 - aconitase 2, mitochondrial
O55137	Acot1 - acyl-CoA thioesterase 1
D3Z041	Acsl1 - acyl-CoA synthetase long-chain family member 1
Q8BFZ3	Actbl2 - actin, beta-like 2
P63268	Actg2 - actin, gamma 2, smooth muscle, enteric
Q9JI91	Actn2 - actinin alpha 2
P07724	Alb - albumin
P05064	Aldoa - aldolase A, fructose-bisphosphate
Q9WV06	Ankrd2 - ankyrin repeat domain 2 (stretch responsive muscle)
Q8R429	Atp2a1 - ATPase, Ca++ transporting, cardiac muscle, fast twitch 1
B1ATS4	Atp2a3 - ATPase, Ca++ transporting, ubiquitous
D3Z6F5	Atp5a1 - ATP synthase, H+ transporting, mitochondrial F1 complex, alpha subunit 1
A2AKV0	Atp5c1 - ATP synthase, H+ transporting, mitochondrial F1 complex, gamma polypeptide 1
P56382	Atp5e - ATP synthase, H+ transporting, mitochondrial F1 complex, epsilon subunit
B1ASE2	Atp5h - ATP synthase, H+ transporting, mitochondrial F0 complex, subunit d
D3Z2Y8	Bdh1 - 3-hydroxybutyrate dehydrogenase, type 1
Q6P1B9	Bin1 - bridging integrator 1
P14211	Calr - calreticulin
F6QJN8	Capzb - capping protein (actin filament) muscle Z-line, beta
P16015	Car3 - carbonic anhydrase 3
P24270	Cat - catalase
Q08857	Cd36 - CD36 antigen
P45591	Cfl2 - cofilin 2, muscle
P07310	Ckm - creatine kinase, muscle
Q6P8J7	Ckmt2 - creatine kinase, mitochondrial 2
Q9R0G6	Comp - cartilage oligomeric matrix protein
P56391	Cox6b1 - cytochrome c oxidase, subunit VIb polypeptide 1
Q9CZU6	Cs - citrate synthase
Q9D0M3	Cyc1 - cytochrome c-1
O35215	Ddt - D-dopachrome tautomerase
O08749	Dld - dihydrolipoamide dehydrogenase
Q9D2G2	Dlst - dihydrolipoamide S-succinyltransferase (E2 component of 2-oxo-glutarate complex)
P62631	Eef1a2 - eukaryotic translation elongation factor 1 alpha 2
O70251	Eef1b2 - eukaryotic translation elongation factor 1 beta 2
B0QZL1	Eno1 - enolase 1, alpha non-neuron
P21550	Eno3 - enolase 3, beta muscle
Q99LC5	Etfa - electron transferring flavoprotein, alpha polypeptide
Q9DCW4	Etfb - electron transferring flavoprotein, beta polypeptide
Q921G7	Etfdh - electron transferring flavoprotein, dehydrogenase
P04117	Fabp4 - fatty acid binding protein 4, adipocyte
A2AQ53	Fbn1 - fibrillin 1
D3YW87	Flnc - filamin C, gamma
P16858	Gapdh - glyceraldehyde-3-phosphate dehydrogenase
O55126	Gbas - glioblastoma amplified sequence
Q9CPU0	Glo1 - glyoxalase 1
P05201	Got1 - glutamate oxaloacetate transaminase 1, soluble
P05202	Got2 - glutamate oxaloacetate transaminase 2, mitochondrial
P06745	Gpi1 - glucose phosphate isomerase 1
Q61425	Hadh - hydroxyacyl-Coenzyme A dehydrogenase
A8DUK4	Hbb-b1 - hemoglobin, beta adult major chain
Q91X72	Hpx - hemopexin
Q61316	Hspa4 - heat shock protein 4
Q504P4	Hspa8 - heat shock protein 8
P38647	Hspa9 - heat shock protein 9
Q9QZ57	Hspb3 - heat shock protein 3
P35385	Hspb7 - heat shock protein family, member 7 (cardiovascular)

D3Z736	Ldha - lactate dehydrogenase A
P16125	Ldhb - lactate dehydrogenase B
P48678	Lmna - lamin A
P04247	Mb - myoglobin
P14152	Mdh1 - malate dehydrogenase 1, NAD (soluble)
P08249	Mdh2 - malate dehydrogenase 2, NAD (mitochondrial)
P03899	mt-Nd3 - mitochondrially encoded NADH dehydrogenase 3
P16332	Mut - methylmalonyl-Coenzyme A mutase
Q6P6L5	Mybpc1 - myosin binding protein C, slow-type
G3UW82	Myh2 - myosin, heavy polypeptide 2, sk
Q91Z83	Myh7 - myosin, heavy polypeptide 7, cardiac muscle, beta
P05977	Myl1 - myosin, light polypeptide 1
P09542	Myl3 - myosin, light polypeptide 3
Q60605	Myl6 - myosin, light polypeptide 6, alkali, smooth muscle and non-muscle
Q8CI43	Myl6b - myosin, light polypeptide 6B
P97457	Mylpf - myosin light chain, phosphorylatable, fast
Q14BI5	Myom2 - myomesin 2
A2ABU4	Myom3 - myomesin family, member 3
Q9JIF9	Myot - myotilin
Q9CYG0	Ndrg2 - N-myc downstream regulated gene 2
Q9Z1P6	Ndufa7 - NADH dehydrogenase (ubiquinone) 1 alpha subcomplex, 7 (B14.5a)
Q9DC69	Ndufa9 - NADH dehydrogenase (ubiquinone) 1 alpha subcomplex, 9
F6ZFT1	Ndufab1 - NADH dehydrogenase (ubiquinone) 1, alpha/beta subcomplex, 1
Q9CR61	Ndufb7 - NADH dehydrogenase (ubiquinone) 1 beta subcomplex, 7
Q91VD9	Ndufs1 - NADH dehydrogenase (ubiquinone) Fe-S protein 1
F6RJ83	Ndufs2 - NADH dehydrogenase (ubiquinone) Fe-S protein 2
B1ARW4	Ndufs5 - NADH dehydrogenase (ubiquinone) Fe-S protein 5
P52503	Ndufs6 - NADH dehydrogenase (ubiquinone) Fe-S protein 6
D3Z0K1	Ndufv1 - NADH dehydrogenase (ubiquinone) flavoprotein 1
Q01768	Nme2 - NME/NM23 nucleoside diphosphate kinase 2
Q3UJQ9	Oxct1 - 3-oxoacid CoA transferase 1
Q5EBG6	Oxct1 - 3-oxoacid CoA transferase 1
P70296	Pebp1 - phosphatidylethanolamine binding protein 1
O70250	Pgam2 - phosphoglycerate mutase 2
Q9D0F9	Pgm2 - phosphoglucomutase 2
Q9DAX9	Phpt1 - phosphohistidine phosphatase 1
P52480	Pkm - pyruvate kinase, muscle
P20108	Prdx3 - peroxiredoxin 3
E9PUM3	Pygm - muscle glycogen phosphorylase
Q9DD03	Rab13 - RAB13, member RAS oncogene family
Q8BGH2	Samm50 - sorting and assembly machinery component 50 homolog (S. cerevisiae)
Q8K2B3	Sdha - succinate dehydrogenase complex, subunit A, flavoprotein (Fp)
D6RHN2	Selenbp1 - selenium binding protein 1
Q5SX46	Slc25a11 - solute carrier family 25 (mitochondrial carrier oxoglutarate carrier), member 11
Q8BH59	Slc25a12 - solute carrier family 25 (mitochondrial carrier, Aralar), member 12
Q8VEM8	Slc25a3 - solute carrier family 25 (mitochondrial carrier, phosphate carrier), member 3
P48962	Slc25a4 - solute carrier family 25 (mitochondrial carrier, adenine nucleotide translocator), member 4
P09671	Sod2 - superoxide dismutase 2, mitochondrial
O70548	Tcap - titin-cap
Q9Z1T2	Thbs4 - thrombospondin 4
E9Q8P0	Tnnc1 - troponin C, cardiac/slow skeletal
P20801	Tnnc2 - troponin C2, fast
D3YUN3	Tnni1 - troponin I, skeletal, slow 1
P13412	Tnni2 - troponin I, skeletal, fast 2
P17751	Tpi1 - triosephosphate isomerase 1
G5E8R0	Tpm1 - tropomyosin 1, alpha
D3Z6I8	Tpm3 - tropomyosin 3, gamma
P63028	Tpt1 - tumor protein, translationally-controlled 1
Q921I1	Trf - transferrin
Q91ZJ5	Ugp2 - UDP-glucose pyrophosphorylase 2
Q9CZ13	Uqcrc1 - ubiquinol-cytochrome c reductase core protein 1
Q9DB77	Uqcrc2 - ubiquinol cytochrome c reductase core protein 2
P99028	Uqcrh - ubiquinol-cytochrome c reductase hinge protein
Q01853	Vcp - valosin containing protein
Q60932	Vdac1 - voltage-dependent anion channel 1
Q60931	Vdac3 - voltage-dependent anion channel 3
P61982	Ywhag - tyrosine 3-monooxygenase/tryptophan 5-monooxygenase activation protein, gamma polypeptide
P63101	Ywhaz - tyrosine 3-monooxygenase/tryptophan 5-monooxygenase activation protein, zeta polypeptide

Table 4.3.8.1 C The 47 differentially labelled proteins of redox, reduced and reversibly oxidised proteins detected in old mouse soleus muscle.

Q9EQ20	Aldh6a1 - aldehyde dehydrogenase family 6, subfamily A1
D3YYQ5	Amy1 - amylase 1, salivary
Q8VDN2	Atp1a1 - ATPase, Na+/K+ transporting, alpha 1 polypeptide
Q9CQQ7	Atp5f1 - ATP synthase, H+ transporting, mitochondrial F0 complex, subunit B1
E9PY34	Cdc6 - cell division cycle 6
P52825	Cpt2 - carnitine palmitoyltransferase 2
P10605	Ctsb - cathepsin B
P97465	Dok1 - docking protein 1
P63168	Dynll1 - dynein light chain LC8-type 1
O35459	Ech1 - enoyl coenzyme A hydratase 1, peroxisomal
P58252	Eef2 - eukaryotic translation elongation factor 2
Q6PHC1	Eno1 - enolase 1
A2AEX7	Fhl1 - four and a half LIM domains 1
P26443	Glud1 - glutamate dehydrogenase 1
F8VPN3	Gm5160 - predicted gene 5160
D3YX79	Gm8394 - predicted gene 8394
S4R1E5	Gpx4 - Glutathione peroxidase
P63038	Hspd1 - heat shock protein 1 (chaperonin)
D6RIL6	Idh2 - isocitrate dehydrogenase 2 (NADP+), mitochondrial
P06330	Ig heavy chain V region AC38 205.12
P01644	Ig kappa chain V-V region HP R16.7
P01649	Ig kappa chain V-V regions
P01867	Igh3 - Ig gamma-2B chain C region
P16045	Lgals1 - lectin, galactose binding, soluble 1
Q5SX39	Myh4 - myosin, heavy polypeptide 4, skeletal muscle
Q7TMF3	Ndufa12 - NADH dehydrogenase (ubiquinone) 1 alpha subcomplex, 12
Q9CQJ8	Ndufb9 - NADH dehydrogenase (ubiquinone) 1 beta subcomplex, 9
Q60597	Ogdh - oxoglutarate dehydrogenase (lipoamide)
P09103	P4hb - prolyl 4-hydroxylase, beta polypeptide
A2A817	Park7 - Parkinson disease (autosomal recessive, early onset) 7
Q9CRA2	Pdlim5 - PDZ and LIM domain 5
S4R1V0	PDZ and LIM domain protein 1
P47857	Pfkm - phosphofructokinase, muscle
P62715	Ppp2cb - protein phosphatase 2 (formerly 2A), catalytic subunit, beta isoform
D3Z0Y2	Prdx6 - peroxiredoxin 6
O09061	Psmb1 - proteasome (prosome, macropain) subunit, beta type 1
Q9R1P3	Psmb2 - proteasome (prosome, macropain) subunit, beta type 2
P08207	S100a10 - S100 calcium binding protein A10 (calpactin)
Q9D451	Sept12 - septin 12
P07759	Serpina3k - serine (or cysteine) peptidase inhibitor, clade A, member 3K
Q60854	Serpinb6a - serine (or cysteine) peptidase inhibitor, clade B, member 6a
Q91WK1	Spryd4 - SPRY domain containing 4
Q7TQ48	Srl - sarcalumenin
P58774	Tpm2 - tropomyosin 2, beta
D3YZT5	Vdac2 - voltage-dependent anion channel 2
P20152	Vim - vimentin
Q9CWQ3	Xrcc6bp1 - XRCC6 binding protein 1

Table 4.3.8.2.A The 17 redox proteins identified in adult mouse soleus muscle.

P97447	Fhl1 - four and a half LIM domains 1
P16858	Gapdh - glyceraldehyde-3-phosphate dehydrogenase
D3Z0K1	Ndufv1 - NADH dehydrogenase (ubiquinone) flavoprotein 1
Q6P8J7	Ckmt2 - creatine kinase, mitochondrial
P13542	Myh8 - myosin, heavy polypeptide 8, skeletal muscle, perinatal
A2AUC9	Kbtbd10 - kelch repeat and BTB (POZ) domain containing 10
A2AQ53	Fbn1 - fibrillin 1
B0QZL1	Eno1 - enolase 1, alpha non-neuron
Q9CZ13	Uqcrc1 - ubiquinol-cytochrome c reductase core protein
P48962	Slc25a4 - solute carrier family 25 (mitochondrial carrier, adenine nucleotide translocator), member 4
P56382	Atp5e - ATP synthase, H+ transporting, mitochondrial F1 complex, epsilon subunit
Q9DB77	Uqcrc2 - ubiquinol cytochrome c reductase core protein 2
O70400	Pdlim1 - PDZ and LIM domain 1 (elfin)
P08228	Sod1 - superoxide dismutase 1, soluble
P45591	Cfl2 - cofilin 2, muscle
Q6IRU2	Tpm4 - tropomyosin 4
P54071	Idh2 - isocitrate dehydrogenase 2 (NADP+), mitochondrial

Table 4.3.8.2.B The 25 redox proteins identified in both adult and old mouse soleus muscle.

P07724	Alb - albumin
P99028	Uqcrh - ubiquinol-cytochrome c reductase hinge protein
O08749	Dld - dihydrolipoamide dehydrogenase
G5E8R0	Tpm1 - tropomyosin 1, alpha
P17751	Tpi1 - triosephosphate isomerase 1
P16125	Ldhb - lactate dehydrogenase B
P63268	Actg2 - actin, gamma 2, smooth muscle, enteric
D3Z6I8	Tpm3 - tropomyosin 3, gamma
P08249	Mdh2 - malate dehydrogenase 2, NAD (mitochondrial)
B1ASE2	Atp5h - ATP synthase, H+ transporting, mitochondrial F0 complex, subunit
Q921G7	Etfdh - electron transferring flavoprotein, dehydrogenase
P51174	Acadl - acyl-Coenzyme A dehydrogenase, long-chain
P97457	Mylpf - myosin light chain, phosphorylatable, fast skeletal muscle
P13412	Tnni2 - troponin I, skeletal, fast 2
D3Z736	Ldha - lactate dehydrogenase A
Q91VD9	Ndufs1 - NADH dehydrogenase (ubiquinone) Fe-S protein
D3YUN3	Tnni1 - troponin I, skeletal, slow 1
P14152	Mdh1 - malate dehydrogenase 1, NAD (soluble)
G3UW82	Myh2 - myosin, heavy polypeptide 2, skeletal muscle, adult
Q99KI0	Aco2 - aconitase 2, mitochondrial
P09542	Myl3 - myosin, light polypeptide 3
P05064	Aldoa - aldolase A, fructose-bisphosphate
P21550	Eno3 - enolase 3, beta muscle
P05202	Got2 - glutamate oxaloacetate transaminase 2, mitochondria
Q91Z83	Myh7 - myosin, heavy polypeptide 7, cardiac muscle, beta; Muscle contraction

Table 4.3.8.2.C The 5 redox proteins identified in old mouse soleus muscle.

Q5SX39	Myh4 - myosin, heavy polypeptide 4, skeletal muscle
P58774	Tpm2 - tropomyosin 2, beta
Q6PHC1	Eno1 - enolase 1, alpha non-neuron
E9PY34	Cdc6 - cell division cycle 6
D3Z0Y2	Prdx6 - peroxiredoxin 6

Table 4.3.8.3.A The 35 reduced proteins identified in adult mouse soleus muscle.

F8WGB3	Sdhc - succinate dehydrogenase complex, subunit C, integral membrane protein
E9QMD3	Zfhx3 - zinc finger homeobox 3
P61027	Rab10 - RAB10, member RAS oncogene family
Q9R0Y5	Ak1 - adenylate kinase 1
P35486	Pdha1 - pyruvate dehydrogenase E1 alpha 1
Q9DCM2	Gstk1 - glutathione S-transferase kappa 1
O88569	Hnrnpa2b1 - heterogeneous nuclear ribonucleoprotein A2/B1
P63330	Ppp2ca - protein phosphatase 2 (formerly 2A), catalytic subunit, alpha isoform
Q8BMS1	Hadha - hydroxyacyl-Coenzyme A dehydrogenase/3-ketoacyl-Coenzyme A thiolase/enoyl-Coenzyme A hydratase (trifunctional protein), alpha subunit
F7B227	Ech1 - enoyl coenzyme A hydratase 1, peroxisomal
P19157	Gstp1 - glutathione S-transferase, pi 1
F7B1B6	Adck3 - aarF domain containing kinase 3
P47738	Aldh2 - aldehyde dehydrogenase 2, mitochondrial
Q9D6R2	Idh3a - isocitrate dehydrogenase 3 (NAD+) alpha
Q8CI51	Pdlim5 - PDZ and LIM domain 5
Q9WUM5	Suclg1 - succinate-CoA ligase, GDP-forming, alpha subunit
Q9D051	Pdhb - pyruvate dehydrogenase (lipoamide) bet
Q62234	Myom1 - myomesin 1
Q9CQA3	Sdhb - succinate dehydrogenase complex, subunit B, iron sulfur (Ip)
Q8BFR5	Tufm - Tu translation elongation factor, mitochondrial
Q99JY0	Hadhb - hydroxyacyl-Coenzyme A dehydrogenase/3-ketoacyl-Coenzyme A thiolase/enoyl-Coenzyme A hydratase (trifunctional protein), beta subunit
P45376	Akr1b3 - aldo-keto reductase family 1, member B3 (aldose reductase)
F6T930	Akr1b1 - aldose reductase
Q8BMF4	Dlat - dihydrolipoamide S-acetyltransferase (E2 component of pyruvate dehydrogenase complex)
Q9CQ75	Ndufa2 - NADH dehydrogenase (ubiquinone) 1 alpha subcomplex,
Q9Z2I9	Sucla2 - succinate-Coenzyme A ligase, ADP-forming, beta subuni
Q9Z2Z6	Slc25a20 - solute carrier family 25 (mitochondrial carnitine/acylcarnitine translocase), member 20
D6REF3	Ywhae - tyrosine 3-monooxygenase/tryptophan 5-monooxygenase activation protein, epsilon polypeptide
D3YYN7	Atp1a2 - ATPase, Na+/K+ transporting, alpha 2 polypeptide
Q6IRU5	Cltb - clathrin, light polypeptide (Lcb); Clathrin is the major protein of the polyhedral coat of coated pits and vesicles
A2A813	Park7 - Parkinson disease (autosomal recessive, early onset) 7
P70404	Idh3g - isocitrate dehydrogenase 3 (NAD+), gamma
F8WIT2	Anxa6 - annexin A6; May associate with CD21. May regulate the release of Ca(2+) from intracellular stores
Q924X2	Cpt1b - carnitine palmitoyltransferase 1b, muscle
P17742	Ppia - peptidylprolyl isomerase A

Table 4.3.8.3.B The 83 reduced proteins identified in both adult and old mouse soleus muscle.

Q6P6L5	Mybpc1 - myosin binding protein C, slow-type
P04117	Fabp4 - fatty acid binding protein 4, adipocyte
D3Z041	Acsl1 - acyl-CoA synthetase long-chain family member 1
Q8R429	Atp2a1 - ATPase, Ca++ transporting, cardiac muscle, fast twitch 1
Q61316	Hspa4 - heat shock protein 4
D3Z2Y8	Bdh1 - 3-hydroxybutyrate dehydrogenase, type 1
P38647	Hspa9 - heat shock protein 9
O70250	Pgam2 - phosphoglycerate mutase 2
O70251	Eef1b2 - eukaryotic translation elongation factor 1 beta 2
Q6P1B9	Bin1 - bridging integrator 1
A8DUK4	Hbb-b1 - hemoglobin, beta adult major chain
Q9QZ57	Hspb3 - heat shock protein 3
B1ATS4	Atp2a3 - ATPase, Ca++ transporting, ubiquitous
Q01768	Nme2 - NME/NM23 nucleoside diphosphate kinase 2
O55137	Acot1 - acyl-CoA thioesterase 1
P35385	Hspb7 - heat shock protein family, member 7 (cardiovascular)
Q14BI5	Myom2 - myomesin 2
Q8BGH2	Samm50 - sorting and assembly machinery component 50 homolog (S. cerevisiae)
P62631	Eef1a2 - eukaryotic translation elongation factor 1 alpha 2
A2AKV0	Atp5c1 - ATP synthase, H+ transporting, mitochondrial F1 complex, gamma polypeptide 1
P04247	Mb - myoglobin
P05977	Myl1 - myosin, light polypeptide
P48678	Lmna - lamin A
Q9CZU6	Cs - citrate synthase
A2ABU4	Myom3 - myomesin family, member 3
Q9JIF9	Myot - myotilin
Q8K2B3	Sdha - succinate dehydrogenase complex, subunit A, flavoprotein (F
Q91ZJ5	Ugp2 - UDP-glucose pyrophosphorylase 2
P63101	Ywhaz - tyrosine 3-monooxygenase/tryptophan 5-monooxygenase activation protein, zeta polypeptide
Q60605	Myl6 - myosin, light polypeptide 6, alkali, smooth muscle and non-muscle
Q9D0F9	Pgm2 - phosphoglucomutase 2
Q61425	Hadh - hydroxyacyl-Coenzyme A dehydrogenase
P03899	mt-Nd3 - mitochondrially encoded NADH dehydrogenase 3
P52503	Ndufs6 - NADH dehydrogenase (ubiquinone) Fe-S protein 6
Q01853	Vcp - valosin containing protein
F6RJ83	Ndufs2 - NADH dehydrogenase (ubiquinone) Fe-S protein 2
Q3UJQ9	Oxct1 - 3-oxoacid CoA transferase 1
P16332	Mut - methylmalonyl-Coenzyme A mutase
Q5EBG6	Hspb6 - heat shock protein, alpha-crystallin-related, B6
Q8VEM8	Slc25a3 - solute carrier family 25 (mitochondrial carrier, phosphate carrier), member 3
O55126	Gbas - glioblastoma amplified sequence
Q9QYG0	Ndrg2 - N-myc downstream regulated gene 2
P05201	Got1 - glutamate oxaloacetate transaminase 1, soluble
Q9D0M3	Cyc1 - cytochrome c-1
Q8CI43	Myl6b - myosin, light polypeptide 6B
Q8BFZ3	Actbl2 - actin, beta-like 2
D3YW87	Flnc - filamin C, gamma
B1AR28	Acadvl - acyl-Coenzyme A dehydrogenase, very long chain
P52480	Pkm - pyruvate kinase, muscle
P07310	Ckm - creatine kinase, muscle
P61982	Ywhag - tyrosine 3-monooxygenase/tryptophan 5-monooxygenase activation protein, gamma polypeptide
Q8BH59	Slc25a12 - solute carrier family 25 (mitochondrial carrier, Aralar), member 1
F6QJN8	Capzb - capping protein (actin filament) muscle Z-line, beta
P06745	Gpi1 - glucose phosphate isomerase 1
P70296	Pebp1 - phosphatidylethanolamine binding protein 1
Q9WV06	Ankrd2 - ankyrin repeat domain 2 (stretch responsive muscle)
F6ZFT1	Ndufab1 - NADH dehydrogenase (ubiquinone) 1, alpha/beta subcomplex, 1
P20801	Tnnc2 - troponin C2, fast
Q07417	Acads - acyl-Coenzyme A dehydrogenase, short chain
Q9D2G2	Dlst - dihydrolipoamide S-succinyltransferase (E2 component of 2-oxo-glutarate complex)
D3Z6F5	Atp5a1 - ATP synthase, H+ transporting, mitochondrial F1 complex, alpha subunit
Q99LC5	Etfa - electron transferring flavoprotein, alpha polypeptide
E9Q8P0	Tnnc1 - troponin C, cardiac/slow skeletal
Q9Z1P6	Ndufa7 - NADH dehydrogenase (ubiquinone) 1 alpha subcomplex, 7 (B14.5a)
Q9CPU0	Glo1 - glyoxalase 1
P09671	Sod2 - superoxide dismutase 2, mitochondrial
Q504P4	Hspa8 - heat shock protein 8
E9PUM3	Pygm - muscle glycogen phosphorylas
P63028	Tpt1 - tumor protein, translationally-controlled 1
Q9JI91	Actn2 - actinin alpha 2
Q5SX46	Slc25a11 - solute carrier family 25 (mitochondrial carrier oxoglutarate carrier), member 11
D6RHN2	Selenbp1 - selenium binding protein 1
Q60931	Vdac3 - voltage-dependent anion channel 3
P24270	Cat - catalase
Q60932	Vdac1 - voltage-dependent anion channel 1
Q9DAK9	Phpt1 - phosphohistidine phosphatase
P16015	Car3 - carbonic anhydrase 3
Q9DD03	Rab13 - RAB13, member RAS oncogene family
Q9DC69	Ndufa9 - NADH dehydrogenase (ubiquinone) 1 alpha subcomplex, 9
P20108	Prdx3 - peroxiredoxin 3
O35215	Ddt - D-dopachrome tautomerase
O70548	Tcap - titin-cap
Q9DCW4	Etfb - electron transferring flavoprotein, beta polypeptide

Table 4.3.8.3.C The 43 reduced proteins identified in old mouse soleus muscle.

P97465	Dok1 - docking protein 1
P16858	Gapdh - glyceraldehyde-3-phosphate dehydrogenase
D3YYQ5	Amy1 - amylase 1, salivary
P63168	Dynll1 - dynein light chain LC8-type 1
S4R1E5	Gpx4 - Glutathione peroxidase
B0QZL1	Eno1 - enolase 1, alpha non-neuron
P20152	Vim - vimentin
P48962	Slc25a4 - solute carrier family 25 (mitochondrial carrier, adenine nucleotide translocator), member 4
S4R1V0	Pdlim1 - PDZ and LIM domain protein 1
Q60597	Ogdh - oxoglutarate dehydrogenase (lipoamide)
F8VPN3	Gm5160 - predicted gene 5160; PPIases accelerate the folding of proteins
P08207	S100a10 - S100 calcium binding protein A10 (calpactin)
P07759	Serpina3k - serine (or cysteine) peptidase inhibitor, clade A, member 3K
Q8VDN2	Atp1a1 - ATPase, Na+/K+ transporting, alpha 1 polypeptide
D3YX79	Gm8394 - predicted gene 8394
D3YZT5	Vdac2 - voltage-dependent anion channel 2
P16045	Lgals1 - lectin, galactose binding, soluble 1
P56382	Atp5e - ATP synthase, H+ transporting, mitochondrial F1 complex, epsilon subunit
P47857	Pfkm - phosphofructokinase, muscle
A2AEX7	Fhl1 - four and a half LIM domains 1
Q9CQJ8	Ndufb9 - NADH dehydrogenase (ubiquinone) 1 beta subcomplex,
Q60854	Serpinb6a - serine (or cysteine) peptidase inhibitor, clade B, member 6a
Q91WK1	Spryd4 - SPRY domain containing 4
D6RIL6	Idh2 - isocitrate dehydrogenase 2 (NADP+), mitochondrial
Q9CQQ7	Atp5f1 - ATP synthase, H+ transporting, mitochondrial F0 complex, subunit B1
Q7TMF3	Ndufa12 - NADH dehydrogenase (ubiquinone) 1 alpha subcomplex, 1
Q9EQ20	Aldh6a1 - aldehyde dehydrogenase family 6, subfamily A1
Q9CZ13	Uqcrc1 - ubiquinol-cytochrome c reductase core protein 1
P62715	Ppp2cb - protein phosphatase 2 (formerly 2A), catalytic subunit, beta isoform
Q9DB77	Uqcrc2 - ubiquinol cytochrome c reductase core protein 2
Q9CRA2	Pdlim5 - PDZ and LIM domain 5
P09103	P4hb - prolyl 4-hydroxylase, beta polypeptide
P26443	Glud1 - glutamate dehydrogenase 1
A2A817	Park7 - Parkinson disease (autosomal recessive, early onset) 7
D3Z0K1	Ndufv1 - NADH dehydrogenase (ubiquinone) flavoprotein 1
Q9R1P3	Psmb2 - proteasome (prosome, macropain) subunit, beta type 2
Q6P8J7	Ckmt2 - creatine kinase, mitochondrial 2
O09061	Psmb1 - proteasome (prosome, macropain) subunit, beta type 1
P45591	Cfl2 - cofilin 2, muscle
P52825	Cpt2 - carnitine palmitoyltransferase 2
O35459	Ech1 - enoyl coenzyme A hydratase 1, peroxisomal
P58252	Eef2 - eukaryotic translation elongation factor 2
P63038	Hspd1 - heat shock protein 1 (chaperonin)

Table 4.3.8.4.A The 4 reversibly oxidised proteins identified in adult mouse soleus muscle.

Q61646	Hp - haptoglobin
Q9DCJ5	Ndufa8 - NADH dehydrogenase (ubiquinone) 1 alpha subcomplex, 8
E9PZM7	Scaf11 - SR-related CTD-associated factor 11
P50608	Fmod - fibromodulin

Table 4.3.8.4.B The 9 reversibly oxidised proteins identified in both adult and old mouse soleus muscle.

Q9CR61	Ndufb7 - NADH dehydrogenase (ubiquinone) 1 beta subcomplex, 7
B1ARW4	Ndufs5 - NADH dehydrogenase (ubiquinone) Fe-S protein 5
P14211	Calr - calreticulin
Q9R0G6	Comp - cartilage oligomeric matrix protein
Q08857	Cd36 - CD36 antigen
Q9Z1T2	Thbs4 - thrombospondin 4
Q91X72	Hpx - hemopexin
Q921I1	Trf - transferrin
P56391	Cox6b1 - cytochrome c oxidase, subunit VIb polypeptide 1

Table 4.3.8.4.C The 9 reversibly oxidised proteins identified in old mouse soleus muscle.

P10605	Ctsb - cathepsin B
Q7TQ48	Srl - sarcalumenin
Q9CWQ3	Xrcc6bp1 - XRCC6 binding protein 1
Q9D451	Sept12 - septin 12
A2AQ53	Fbn1 - fibrillin 1
P01649	Ig kappa chain V-V-region
P01867	Igh-3 - Ig gamma-2B chain C region
P01644	Ig kappa chain V-V-region HP R16.7
P06330	Ig heavy chain V region AC38 205.12

Table 5.3.1 Quadriceps Adult and Old Label Free VennDIS Tables

Accession Number	Protein
P70170	Abcc9 - ATP-binding cassette, sub-family C (CFTR/MRP), member
P60710	Actb - actin, β
O88990	Actn3 - actinin α 3
Q4VC17	Adamts18 - a disintegrin-like and metallopeptidase (reprolysin type) with thrombospondin type 1 motif, 18
Q3U4G3	AI480653 - expressed sequence AI480653
O88987	Akap3 - A kinase (PRKA) anchor protein 3
P24549	Aldh1a1 - aldehyde dehydrogenase family 1, subfamily A
Q8K009	Aldh1l2 - aldehyde dehydrogenase 1 family, member L2
Q9DBF1	Aldh7a1 - aldehyde dehydrogenase family 7, member A1
Q91Y97	Aldob - aldolase B, fructose-bisphosphate
Q3V1D3	Ampd1 - adenosine monophosphate deaminase
Q9DBT5	Ampd2 - adenosine monophosphate deaminase
Q07076	Anxa7 - annexin A7
Q8R146	Apeh - acylpeptide hydrolase
Q8K4Z3	Apoa1bp - apolipoprotein A-I binding protein
P06728	Apoa4 - apolipoprotein A-IV
P84078	Arf1 - ADP-ribosylation factor 1
Q80Y19	Arhgap11a - Rho GTPase activating protein 11A
Q8R2G4	Art3 - ADP-ribosyltransferase 3
Q7SIG6	Asap2 - ArfGAP with SH3 domain, ankyrin repeat and PH domain 2
Q8BSY0	Asph - aspartate-β-hydroxylase
O08997	Atox1 - ATX1 (antioxidant protein 1) homolog 1 (yeas
Q64518	Atp2a3 - ATPase, Ca++ transporting, ubiquitous
O35855	Bcat2 - branched chain aminotransferase 2, mitochondri
Q8R164	Bphl - biphenyl hydrolase-like (serine hydrolase, breast epithelial mucin-associated antigen)
P62960	bx1 - Y box protein
P01027	C3 - complement component 3
Q8K182	C8a - complement component 8, α polypeptide
Q8R3Z5	Cacnb1 - calcium channel, voltage-dependent, β 1 subunit
P54285	Cacnb3 - calcium channel, voltage-dependent, β 3 subunit
Q9WUF3	Casp8ap2 - caspase 8 associated protein 2
P08074	Cbr2 - carbonyl reductase 2
Q8CII2	Cdc123 - cell division cycle 123
Q8CC36	Cdnf - cerebral dopamine neurotrophic factor
Q66K08	Cilp - cartilage intermediate layer protein, nucleotide pyrophosphohydrol
Q9Z0H8	Clip2 - CAP-GLY domain containing linker protein
Q8R4N0	Clybl - citrate lyase β like
Q9D1A2	Cndp2 - CNDP dipeptidase 2 (metallopeptidase M20 family
Q9CXX9	Cuedc2 - CUE domain containing 2
Q9D8X1	Cutc - cutC copper transporter homolog (E.coli)

Q571I4	D8Ertd82e - DNA segment, Chr 8, ERATO Doi 82, expressed
Q3U1J4	Ddb1 - damage specific DNA binding protein 1
Q9DBB8	Dhdh - dihydrodiol dehydrogenase (dimeric)
Q99PU8	Dhx30 - DEAH (Asp-Glu-Ala-His) box polypeptide 30
Q8K1M6	Dnm1l - dynamin 1-like
P59764	Dock4 - dedicator of cytokinesis 4
P97399	Dspp - dentin sialophosphoprotein
Q8BK84	Dupd1 - dual specificity phosphatase and pro isomerase domain containing 1
Q9D8N0	Eef1g - eukaryotic translation elongation factor 1 γ
Q9D485	Efhc2 - EF-hand domain (C-terminal) containing 2
P10630	Eif4a2 - eukaryotic translation initiation factor 4A2
Q80Y81	Elac2 - elaC homolog 2 (E. coli)
Q80UY1	ENSMUSG00000024726 - RIKEN cDNA 2410127L17 gene
Q8R0W0	Eppk1 - Epiplakin
Q8CGC7	Eprs - glutamyl-prolyl-tRNA synthetase
Q9D9R9	Fam186a - family with sequence similarity 186, member A
Q8BR27	Fam214b - RIKEN cDNA B230312A22 gene
Q9DCV4	Fam82b - family with sequence similarity 82, member B
P70695	Fbp2 - fructose bisphosphatase 2
Q9ESL9	Fgf20 - fibroblast growth factor 20
Q9JJ28	Flii - flightless I homolog (Drosophila)
A2AAE1	FSA - RIKEN cDNA 4932438A13 gene
O35943	Fxn - frataxin
Q9CZD3	Gars - glycyl-tRNA synthetase
Q64737	Gart - phosphoribosylglycinamide formyltransferase
Q8C494	Gm14492 - predicted gene 14492
P50247	Gm4737 - predicted gene 4737
P14115	Gm7536 - predicted gene 7536
P13707	Gpd1 - glycerol-3-phosphate dehydrogenase 1 (soluble)
Q64521	Gpd2 - glycerol phosphate dehydrogenase 2, mitochondrial
Q8BUV3	Gphn - gephyrin
Q61627	Grid1 - glutamate receptor, ionotropic, δ 1
P15626	Gstm2 - glutathione S-transferase, μ 2
P48774	Gstm5 - glutathione S-transferase, μ 5
Q8K284	Gtf3c1 - general transcription factor III C 1
P10922	H1f0 - H1 histone family, member 0
O35668	Hap1 - huntingtin-associated protein 1
P02089	Hbb-b2 - hemoglobin, β adult minor chai
P84228	Hist2h3b - histone cluster 2, H3b
O08528	Hk2 - hexokinase 2
P06330	Ig heavy chain V region AC38 205.12
Q07113	Igf2r - insulin-like growth factor 2 receptor
O55023	Impa1 - inositol (myo)-1(or 4)-monophosphatase 1
Q8CDK3	Iqub - IQ motif and ubiquitin domain containing

Q9Z329	Itpr2 - inositol 1,4,5-triphosphate receptor
Q9Z351	Kcnq2 - potassium voltage-gated channel, subfamily Q, member 2
Q6ZQ06	Kiaa1009 - RIKEN cDNA 4922501C03 gene
Q8R0W1	Kiaa1737 - RIKEN cDNA 2310044G17 gene
A2AJB1	Kiaa1984 - RIKEN cDNA 4921530D09 gene
Q99PT9	Kif19a - kinesin family member 19A
Q9QXL2	Kif21a - kinesin family member 21A
Q9Z320	Krt27 - keratin 27
B1AQ75	Krt36 - keratin 36
Q6IMF0	Krt83 - keratin 83
P48356	Lepr - leptin receptor
Q9Z0S2	Lhx2 - LIM homeobox protein 2
P37913	Lig1 - ligase I, DNA, ATP-dependent
P55302	Lrpap1 - low density lipoprotein receptor-related protein associated protein 1
Q8CI70	Lrrc20 - leucine rich repeat containing 20
Q60767	Ly75 - lymphocyte antigen 75
P70218	Map4k1 - mitogen-activated protein kinase kinase kinase kinase 1
P47811	Mapk14 - mitogen-activated protein kinase 14
Q3THS6	Mat2a - methionine adenosyltransferase II, alph
P34884	Mif - macrophage migration inhibitory factor
Q8BMD7	Morc4 - microrchidia 4
P00158	mt-Cytb - mitochondrially encoded cytochrome b
P04938	Mup11 - major urinary protein 11
Q99JI1	Mustn1 - musculoskeletal, embryonic nuclear protein 1
P70402	Mybph - myosin binding protein
O08638	Myh11 - myosin, heavy polypeptide 11, smooth muscle
Q8VDD5	Myh9 - myosin, heavy polypeptide 9, non-muscle
Q6PDN3	Mylk - myosin, light polypeptide kinase
Q8VCR8	Mylk2 - myosin, light polypeptide kinase 2, skeletal muscle
P19246	Nefh - neurofilament, heavy polypeptide
P08551	Nefl - neurofilament, light polypeptide
Q9CQ45	Nenf - neuron derived neurotrophic factor
P46662	Nf2 - neurofibromatosis 2
Q9D1X0	Nol3 - nucleolar protein 3 (apoptosis repressor with CARD domain
Q63850	Nup62 - nucleoporin 62
P61971	Nutf2-ps1 - nuclear transport factor 2, pseudogene
Q9CZ30	Ola1 - Obg-like ATPase 1
Q9ESF1	Otof - otoferlin
Q9DCL9	Paics - phosphoribosylaminoimidazole carboxylase, phosphoribosylaminoribosylaminoimidazole, succinocarboxamide synthetase
Q91ZA3	Pcca - propionyl-Coenzyme A carboxylase, α polypeptide
Q922R8	Pdia6 - protein disulfide isomerase associate
P09041	Pgk2 - phosphoglycerate kinase 2
Q8BZF8	Pgm5 - phosphoglucomutase
P18826	Phka1 - phosphorylase kinase α 1

Q3TCV3	Pion - pigeon homolog (Drosophila)
Q62028	Pla2r1 - phospholipase A2 receptor 1
Q9Z1B3	Plcb1 - phospholipase C, β 1
A2AP18	Plch2 - phospholipase C, η 2
Q3USB7	Plcl1 - phospholipase C-like 1
Q9R269	Ppl - periplakin
Q62415	Ppp1r13b - protein phosphatase 1, regulatory (inhibitor) subunit 13B
Q6R891	Ppp1r9b - protein phosphatase 1, regulatory subunit 9B
P63328	Ppp3ca - protein phosphatase 3, catalytic subunit, α isoform
P48453	Ppp3cb - protein phosphatase 3, catalytic subunit, β isoform
O08807	PRDX4 - peroxiredoxin 4
Q9DBC7	Prkar1a - protein kinase, cAMP dependent regulatory, type I, α
O08795	Prkcsh - protein kinase C substrate 80K-H
Q8BZ03	Prkd2 - protein kinase D2
Q9D7G0	Prps1 - phosphoribosyl pyrophosphate synthetase 1
Q8CI94	Pygb - brain glycogen phosphorylas
Q9ET01	Pygl - liver glycogen phosphorylase
Q8BVI4	Qdpr - quinoid dihydropteridine reductase
P34057	Rcvrn - recoverin
Q9EPQ2	Rpgrip1 - retinitis pigmentosa GTPase regulator interacting protein 1
Q9CXW4	Rpl11 - ribosomal protein L11
P47963	Rpl13 - ribosomal protein L13
Q9CR57	Rpl14 - ribosomal protein L14
P35980	Rpl18 - ribosomal protein L18
P62830	Rpl23 - ribosomal protein L23
P62889	Rpl30 - ribosomal protein L30
Q6ZWV7	Rpl35 - ribosomal protein L35
Q9D8E6	Rpl4 - ribosomal protein L4
P12970	Rpl7a - ribosomal protein L7A
P14869	Rplp0 - ribosomal protein, large, P0
P62270	Rps18 - ribosomal protein S18
P60867	Rps20 - ribosomal protein S20
P62855	Rps26-ps1 - ribosomal protein S26, pseudogene 1
P62908	Rps3 - ribosomal protein S3
P97351	Rps3a - ribosomal protein S3A
P62702	Rps4x - ribosomal protein S4, X-linked
P62754	Rps6 - ribosomal protein S6
P62082	Rps7 - ribosomal protein S7
Q01730	Rsu1 - Ras suppressor protein 1
O70622	Rtn2 - reticulon 2 (Z-band associated protein)
Q9CQC9	Sar1b - SAR1 gene homolog B (S. cerevisiae
Q64519	Sdc3 - syndecan 3
Q9D665	Sdr42e1 - short chain dehydrogenase/reductase family 42E, member 1
O70456	Sfn - stratifin

P82348	Sgcg - sarcoglycan, γ (dystrophin-associated glycoprote
Q8CFH6	Sik2 - salt inducible kinase 2
Q9QXX4	Slc25a13 - solute carrier family 25 (mitochondrial carrier, adenine nucleotide translocator), member 13
Q922R5	Smek2 - SMEK homolog 2, suppressor of mek1 (Dictyostelium)
Q8CI12	Smtnl2 - smoothelin-like 2
P97443	Smyd1 - SET and MYND domain containing 1
Q9CWR2	Smyd3 - SET and MYND domain containing 3
Q8BK63	snk1a1 - casein kinase 1, α 1
Q9QX47	Son - Son DNA binding protein
Q9D2H6	Sp2 - Sp2 transcription factor
Q80YT5	Spata20 - spermatogenesis associated 20
P08032	Spna1 - spectrin α
Q64105	Spr - sepiapterin reductase
Q924W7	St5 - suppression of tumorigenicity 5
Q9Z1Z2	Strap - serine/threonine kinase receptor associated protei
Q8BJS4	Sun2 - Sad1 and UNC84 domain containing 2
Q4FZC9	Syne3 - RIKEN cDNA 4831426I19 gene
Q64729	Tgfbr1 - transforming growth factor, β receptor
P39447	Tjp1 - tight junction protein 1
Q64511	Top2b - topoisomerase (DNA) II bet
Q8BV79	Trank1 - tetratricopeptide repeat and ankyrin repeat containing 1
Q9CQN1	Trap1 - TNF receptor-associated protein 1
Q80UG8	Ttll4 - tubulin tyrosine ligase-like family, member 4
Q02053	Uba1 - ubiquitin-like modifier activating enzyme 1
P61087	Ube2k - ubiquitin-conjugating enzyme E2K
Q9CZY3	Ube2v1 - ubiquitin-conjugating enzyme E2 variant 1
Q9D2M8	Ube2v2 - ubiquitin-conjugating enzyme E2 variant
Q9CPX8	Uqcr11 - ubiquinol-cytochrome c reductase, complex III subunit X
B1AY13	Usp24 - ubiquitin specific peptidase 24
Q99MX1	Usp26 - ubiquitin specific peptidase 2
Q91WQ3	Yars - tyrosyl-tRNA synthetase
Q0P5X5	Zbbx - zinc finger, B-box domain containing
Q8R173	Zdhhc3 - zinc finger, DHHC domain containing 3

Table 5.4.4 (A) & (B) Adult and Old Quadriceps and Redox Tables

Accession Number	Protein
Q8R0P4	Aamdc - RIKEN cDNA 1810020D17 gene
P51174	Acadl - acyl-Coenzyme A dehydrogenase, long-chain
P45952	Acadm - acyl-Coenzyme A dehydrogenase, medium chain
Q07417	Acads - acyl-Coenzyme A dehydrogenase, short chain
P50544	Acadvl - acyl-Coenzyme A dehydrogenase, very long chain
Q8QZT1	Acat1 - acetyl-Coenzyme A acetyltransferase 1
Q99KI0	Aco2 - aconitase 2, mitochondrial
Q9CQR4	Acot13 - acyl-CoA thioesterase 1
Q9QYR9	Acot2 - acyl-CoA thioesterase 2
P41216	Acsl1 - acyl-CoA synthetase long-chain family member 1
P68134	Acta1 - actin, α 1, skeletal muscle
Q8BFZ3	Actbl2 - actin, β-like 2
P56375	Acyp2 - acylphosphatase 2, muscle type
Q60936	Adck3 - aarF domain containing kinase 3
P28474	Adh5 - alcohol dehydrogenase 5 (class III), chi polypeptid
P28650	Adssl1 - adenylosuccinate synthetase like 1
P29699	Ahsg - α-2-HS-glycoprotein; Probably involved in differentiation
Q9R0Y5	Ak1 - adenylate kinase 1
P45376	Akr1b3 - aldo-keto reductase family 1, member B3 (aldose reductase)
P07724	Alb - albumi
P47738	Aldh2 - aldehyde dehydrogenase 2, mitochondrial
Q8CHT0	Aldh4a1 - aldehyde dehydrogenase 4 family, member A1
Q9EQ20	Aldh6a1 - aldehyde dehydrogenase family 6, subfamily A
P05064	Aldoa - aldolase A, fructose-bisphosphat
Q8C8R3	Ank2 - ankyrin 2, brain
Q9WV06	Ankrd2 - ankyrin repeat domain 2 (stretch responsive muscle)
P48036	Anxa5 - annexin A5
P14824	Anxa6 - annexin A6
Q00623	Apoa1 - apolipoprotein A-I
Q9WV35	Apobec2 - apolipoprotein B mRNA editing enzyme, catalytic polypeptide 2
Q02013	Aqp1 - aquaporin 1
Q69ZH9	Arhgap23 - Rho GTPase activating protein 23
Q99PT1	Arhgdia - Rho GDP dissociation inhibitor (GDI) α
Q3URY6	Armc2 - armadillo repeat containing 2
Q8C0M9	Asrgl1 - asparaginase like 1
Q9CWJ9	Atic - 5-aminoimidazole-4-carboxamide ribonucleotide formyltransferase/IMP cyclohydrolase
Q6PIE5	Atp1a2 - ATPase, Na+/K+ transporting, α 2 polypeptide
Q8R429	Atp2a1 - ATPase, Ca++ transporting, cardiac muscle, fast twitch 1
O55143	Atp2a2 - ATPase, Ca++ transporting, cardiac muscle, slow twitch 2
Q03265	Atp5a1 - ATP synthase, H+ transporting, mitochondrial F1 complex, α subunit 1

P56480	Atp5b - ATP synthase, H+ transporting mitochondrial F1 complex, β subunit
Q91VR2	Atp5c1 - ATP synthase, H+ transporting, mitochondrial F1 complex, γ polypeptide 1
Q9D3D9	Atp5d - ATP synthase, H+ transporting, mitochondrial F1 complex, δ subunit
P56382	Atp5e - ATP synthase, H+ transporting, mitochondrial F1 complex, ε subunit
Q9CQQ7	Atp5f1 - ATP synthase, H+ transporting, mitochondrial F0 complex, subunit B1
Q9CR84	Atp5g1 - ATP synthase, H+ transporting, mitochondrial F0 complex, subunit c1 (subunit 9)
Q9DCX2	Atp5h - ATP synthase, H+ transporting, mitochondrial F0 complex, subunit
P97450	Atp5j - ATP synthase, H+ transporting, mitochondrial F0 complex, subunit F
P56135	Atp5j2 - ATP synthase, H+ transporting, mitochondrial F0 complex, subunit F2
Q06185	Atp5k - ATP synthase, H+ transporting, mitochondrial F1F0 complex, subunit
Q9DB20	Atp5o - ATP synthase, H+ transporting, mitochondrial F1 complex, O subunit
Q9JLV1	Bag3 - BCL2-associated athanogene
Q80ZF8	Bai3 - brain-specific angiogenesis inhibitor 3
Q80VH0	Bank1 - B cell scaffold protein with ankyrin repeats 1
Q9Z277	Baz1b - bromodomain adjacent to zinc finger domain, 1B
Q80XN0	Bdh1 - 3-hydroxybutyrate dehydrogenase, type 1
P28653	Bgn - biglycan
O08539	Bin1 - bridging integrator 1
P18572	Bsg - basigin
O35658	C1qbp - complement component 1, q subcomponent binding protein
Q52KB6	C2cd3 - C2 calcium-dependent domain containing 3
P62204	Calm1 - calmodulin 1
P14211	Calr - calreticulin
O35887	Calu - calumeni
Q9CYT6	Cap2 - CAP, adenylate cyclase-associated protein, 2 (yeast)
P47754	Capza2 - capping protein (actin filament) muscle Z-line, α 2
P47757	Capzb - capping protein (actin filament) muscle Z-line, β
P16015	Car3 - carbonic anhydrase 3
O09165	Casq1 - calsequestrin 1
P24270	Cat - catalase
P49817	Cav1 - caveolin 1, caveolae protein
Q08857	Cd36 - CD36 antigen
Q9WTR5	Cdh13 - cadherin 13
P23953	Ces1c - carboxylesterase 1C
Q8VCT4	Ces1d - carboxylesterase 1D
P18760	Cfl1 - cofilin 1, non-muscle
P45591	Cfl2 - cofilin 2, muscle
Q9D1L0	Chchd2 - coiled-coil-helix-coiled-coil-helix domain containing 2
Q9CRB9	Chchd3 - coiled-coil-helix-coiled-coil-helix domain containing 3
Q04447	Ckb - creatine kinase, brain
P07310	Ckm - creatine kinase, muscle

Q6P8J7	Ckmt2 - creatine kinase, mitochondrial
Q8R1G2	Cmbl - carboxymethylenebutenolidase-like (Pseudomonas)
Q9QXT0	Cnpy2 - canopy 2 homolog (zebrafish)
P08122	Col4a2 - collagen, type IV, α 2
Q8K1Z0	Coq9 - coenzyme Q9 homolog (yeast)
P19783	Cox4i1 - cytochrome c oxidase subunit IV isoform 1
P12787	Cox5a - cytochrome c oxidase, subunit V
P19536	Cox5b - cytochrome c oxidase, subunit Vb
P56391	Cox6b1 - cytochrome c oxidase, subunit VIb polypeptide 1
Q9CPQ1	Cox6c - cytochrome c oxidase, subunit VIc
P56392	Cox7a1 - cytochrome c oxidase, subunit VIIa 1
P48771	Cox7a2 - cytochrome c oxidase, subunit VIIa 2
P52825	Cpt2 - carnitine palmitoyltransferase 2
P23927	Cryab - crystallin, α B
Q9CZU6	Cs - citrate synthase
Q9JKB3	Csda - cold shock domain protein A
P18242	Ctsd - cathepsin D
Q9D4H8	Cul2 - cullin 2
Q9CQ89	Cuta - cutA divalent cation tolerance homolog (E. coli)
Q9DCN2	Cyb5r3 - cytochrome b5 reductase 3
Q9D0M3	Cyc1 - cytochrome c-1
Q9D172	D10Jhu81e - DNA segment, Chr 10, Johns Hopkins University 81 expressed
P31786	Dbi - diazepam binding inhibitor
O35215	Ddt - D-dopachrome tautomerase
Q9CQ62	Decr1 - 2,4-dienoyl CoA reductase 1, mitochondrial
P31001	Des - desmin
Q8BMF4	Dlat - dihydrolipoamide S-acetyltransferase (E2 component of pyruvate dehydrogenase complex)
O08749	Dld - dihydrolipoamide dehydrogenase
Q9D2G2	Dlst - dihydrolipoamide S-succinyltransferase (E2 component of 2-oxo-glutarate complex)
Q9Z2W0	Dnpep - aspartyl aminopeptidase
Q9R0P5	Dstn - destrin
Q9D0M5	Dynll2 - dynein light chain LC8-type 2
O35459	Ech1 - enoyl coenzyme A hydratase 1, peroxisomal
Q8BH95	Echs1 - enoyl Coenzyme A hydratase, short chain, 1, mitochondrial
P42125	Eci1 - enoyl-Coenzyme A δ isomerase 1
P62631	Eef1a2 - eukaryotic translation elongation factor 1 α
O70251	Eef1b2 - eukaryotic translation elongation factor 1 β 2
P57776	Eef1d - eukaryotic translation elongation factor 1 δ (guanine nucleotide exchange protein
P58252	Eef2 - eukaryotic translation elongation factor 2
Q8BH64	Ehd2 - EH-domain containing 2
Q66JS6	Eif3j2 - eukaryotic translation initiation factor 3, subunit J2
Q9EST3	Eif4enif1 - eukaryotic translation initiation factor 4E nuclear import factor 1

P17182	Eno1 - enolase 1, α non-neuron
P17183	Eno2 - enolase 2, γ neurona
P21550	Eno3 - enolase 3, β muscle
Q6ZWR6	ENSMUSG00000096054 - Nesprin-1
Q99LC5	Etfa - electron transferring flavoprotein, α polypeptide
Q9DCW4	Etfb - electron transferring flavoprotein, β polypeptid
Q921G7	Etfdh - electron transferring flavoprotein, dehydrogenas
P11404	Fabp3 - fatty acid binding protein 3, muscle and heart
P04117	Fabp4 - fatty acid binding protein 4, adipocyte
Q61554	Fbn1 - fibrillin 1
Q8K0E8	Fgb - fibrinogen β chain
Q8VCM7	Fgg - fibrinogen γ chain
P97807	Fh1 - fumarate hydratase 1
P97447	Fhl1 - four and a half LIM domains 1
P26883	Fkbp1a - FK506 binding protein 1a
Q62446	Fkbp3 - FK506 binding protein 3
Q8VHX6	Flnc - filamin C, γ
P09528	Fth1 - ferritin heavy chain 1
P16858	GAPDH - glyceraldehyde-3-phosphate dehydrogenase
O55126	Gbas - glioblastoma amplified sequence
P21614	Gc - group specific component
Q61598	Gdi2 - guanosine diphosphate (GDP) dissociation inhibitor 2
Q9CPU0	Glo1 - glyoxalase 1
P26443	Glud1 - glutamate dehydrogenase 1
P62897	Gm10053 - predicted gene 10053
Q9CPQ8	Gm10221 - predicted gene 10221
P05201	Got1 - glutamate oxaloacetate transaminase 1, solub
P05202	Got2 - glutamate oxaloacetate transaminase 2, mitochondr
P06745	Gpi1 - glucose phosphate isomerase 1
Q8VHN7	Gpr98 - G protein-coupled receptor 98
P46412	Gpx3 - glutathione peroxidase 3
O70325	Gpx4 - glutathione peroxidase 4
Q99LP6	Grpel1 - GrpE-like 1, mitochondrial
P47791	Gsr - glutathione reductase
P10649	Gstm1 - glutathione S-transferase, μ 1
P19157	Gstp1 - glutathione S-transferase, π 1
Q9R062	Gyg - glycogenin
Q61425	Hadh - hydroxyacyl-Coenzyme A dehydrogenase
Q8BMS1	Hadha - hydroxyacyl-Coenzyme A dehydrogenase/3-ketoacyl-Coenzyme A thiolase/enoyl-Coenzyme A hydratase (trifunctional protein), α subunit
Q99JY0	Hadhb - hydroxyacyl-Coenzyme A dehydrogenase/3-ketoacyl-Coenzyme A thiolase/enoyl-Coenzyme A hydratase (trifunctional protein), β subunit
Q99KB8	Hagh - hydroxyacyl glutathione hydrolase
P01942	Hba-a1 - hemoglobin α, adult chain 1
P02088	Hbb-b2 - hemoglobin, β adult minor chain

P51859	Hdgf - hepatoma-derived growth factor
Q99L13	Hibadh - 3-hydroxyisobutyrate dehydrogenase
P70349	Hint1 - histidine triad nucleotide binding protein 1
P62806	Hist2h4 - histone cluster 2, H4
P49312	Hnrnpa1 - heterogeneous nuclear ribonucleoprotein A1
O88569	Hnrnpa2b1 - heterogeneous nuclear ribonucleoprotein A2/B1
Q8BG05	Hnrnpa3 - heterogeneous nuclear ribonucleoprotein A3
Q60668	Hnrnpd - heterogeneous nuclear ribonucleoprotein D
Q91X72	Hpx - hemopexin
P07901	Hsp90aa1 - heat shock protein 90, α (cytosolic), class A member 1
P11499	Hsp90ab1 - heat shock protein 90 α (cytosolic), class B member 1
P08113	Hsp90b1 - heat shock protein 90, β (Grp94), member 1
Q61696	Hspa1a - heat shock protein 1A
Q61316	Hspa4 - heat shock protein 4
P20029	Hspa5 - heat shock protein 5
P63017	Hspa8 - heat shock protein 8
P38647	Hspa9 - heat shock protein 9
P14602	Hspb1 - heat shock protein 1
Q99PR8	Hspb2 - heat shock protein 2
Q5EBG6	Hspb6 - heat shock protein, α-crystallin-related, B6
P35385	Hspb7 - heat shock protein family, member 7 (cardiovascular)
P63038	Hspd1 - heat shock protein 1 (chaperonin)
Q64433	Hspe1 - heat shock protein 1 (chaperonin 10)
P54071	IDH2 - isocitrate dehydrogenase 2 (NADP+), mitochondria
Q9D6R2	Idh3a - isocitrate dehydrogenase 3 (NAD+) α
P70404	Idh3g - isocitrate dehydrogenase 3 (NAD+), γ
P01837	Ig κ chain C region
P01649	Ig κ chain V-V regions
P01867	Igh-3 - Ig γ-2B chain C region
P01868	Ighg1 - Ig γ-1 chain C region secreted form
P01864	Ighg2c - immunoglobulin heavy constant γ 2C
P01872	Ighm - Ig μ chain C region
Q8CAQ8	Immt - inner membrane protein, mitochondrial
Q9JHI5	Ivd - isovaleryl coenzyme A dehydrogenase
Q8VCD7	Kdm4c - lysine (K)-specific demethylase 4C
O08677	Kng1 - kininogen 1
P04104	Krt1 - keratin 1
P02535	Krt10 - keratin 10
Q3TTY5	Krt2 - keratin 2
Q3UV17	Krt76 - keratin 76; Probably contributes to terminal cornification (By similarity)
Q9JKS4	Ldb3 - LIM domain binding 3
P06151	Ldha - lactate dehydrogenase A
P16125	Ldhb - lactate dehydrogenase B
P16045	Lgals1 - lectin, galactose binding, soluble 1

A2ARV4	Lrp2 - low density lipoprotein receptor-related protein 2
P51885	Lum - lumican
Q99JP0	Map4k3 - mitogen-activated protein kinase kinase kinase kinase 3
O08911	Mapk12 - mitogen-activated protein kinase 12
P04247	Mb - myoglobin
P14152	Mdh1 - malate dehydrogenase 1, NAD (soluble)
P08249	Mdh2 - malate dehydrogenase 2, NAD (mitochondrial)
P06801	Me1 - malic enzyme 1, NADP(+)-dependent, cytosolic
Q8CJ19	Mical3 - microtubule associated monoxygenase, calponin and LIM domain containing 3
P56379	Mp68 - RIKEN cDNA 2010107E04 gene
P63030	Mpc1 - mitochondrial pyruvate carrier 1
Q9D023	Mpc2 - mitochondrial pyruvate carrier 2
P26041	Msn - moesin
P27546	Mtap4 - microtubule-associated protein 4
P03930	mt-Atp8 - mitochondrially encoded ATP synthase
P00397	mt-Co1 - mitochondrially encoded cytochrome c oxidase I
P00405	mt-Co2 - mitochondrially encoded cytochrome c oxidase II
P03888	mt-Nd1 - mitochondrially encoded NADH dehydrogenase 1
P03893	mt-Nd2 - mitochondrially encoded NADH dehydrogenase 2
P03899	mt-Nd3 - mitochondrially encoded NADH dehydrogenase 3
P03911	mt-Nd4 - mitochondrially encoded NADH dehydrogenase 4
A2AMM0	Murc - muscle-related coiled-coil protein
P16332	Mut - methylmalonyl-Coenzyme A mutase
Q5XKE0	Mybpc2 - myosin binding protein C, fast-typ
P13541	Myh3 - myosin, heavy polypeptide 3, skeletal muscle, embryonic
Q5SX39	Myh4 - myosin, heavy polypeptide 4, skeletal muscle
A2AQP0	Myh7b - myosin, heavy chain 7B, cardiac muscle, β
P13542	Myh8 - myosin, heavy polypeptide 8, skeletal muscle, perinatal
P05977	Myl1 - myosin, light polypeptide 1
P09542	Myl3 - myosin, light polypeptide 3
Q60605	Myl6 - myosin, light polypeptide 6, alkali, smooth muscle and non-muscl
P97457	Mylpf - myosin light chain, phosphorylatable, fast skeletal muscle
Q9QZZ4	Myo15 - myosin XV
P97479	Myo7a - myosin VIIA
Q62234	Myom1 - myomesin 1
Q9JIF9	Myot - myotilin
P70670	Naca - nascent polypeptide-associated complex α polypeptide
P09405	Ncl - nucleoli
Q9QYG0	Ndrg2 - N-myc downstream regulated gene
Q99LC3	Ndufa10 - NADH dehydrogenase (ubiquinone) 1 α subcomplex 10
Q9D8B4	Ndufa11 - NADH dehydrogenase (ubiquinone) 1 α subcomplex 11
Q7TMF3	Ndufa12 - NADH dehydrogenase (ubiquinone) 1 α subcomplex, 12
Q9ERS2	Ndufa13 - NADH dehydrogenase (ubiquinone) 1 α subcomplex, 13

Q9CQ75	Ndufa2 - NADH dehydrogenase (ubiquinone) 1 α subcomplex, 2
Q9CQ91	Ndufa3 - NADH dehydrogenase (ubiquinone) 1 α subcomplex, 3
Q62425	Ndufa4 - NADH dehydrogenase (ubiquinone) 1 α subcomplex, 4
Q9CPP6	Ndufa5 - NADH dehydrogenase (ubiquinone) 1 α subcomplex, 5
Q9CQZ5	Ndufa6 - NADH dehydrogenase (ubiquinone) 1 α subcomplex, 6 (B14)
Q9Z1P6	Ndufa7 - NADH dehydrogenase (ubiquinone) 1 α subcomplex, 7 (B14.5a)
Q9DCJ5	Ndufa8 - NADH dehydrogenase (ubiquinone) 1 α subcomplex, 8
Q9DC69	Ndufa9 - NADH dehydrogenase (ubiquinone) 1 α subcomplex, 9
Q9CR21	Ndufab1 - NADH dehydrogenase (ubiquinone) 1, α/β subcomplex, 1
Q9DCS9	Ndufb10 - NADH dehydrogenase (ubiquinone) 1 β subcomplex, 10
O09111	Ndufb11 - NADH dehydrogenase (ubiquinone) 1 β subcomplex, 11
Q9CQZ6	Ndufb3 - NADH dehydrogenase (ubiquinone) 1 β subcomplex 3
Q9CQC7	Ndufb4 - NADH dehydrogenase (ubiquinone) 1 β subcomplex 4
Q9CQH3	Ndufb5 - NADH dehydrogenase (ubiquinone) 1 β subcomplex, 5
Q3UIU2	Ndufb6 - NADH dehydrogenase (ubiquinone) 1 β subcomplex, 6
Q9CR61	Ndufb7 - NADH dehydrogenase (ubiquinone) 1 β subcomplex, 7
Q9D6J5	Ndufb8 - NADH dehydrogenase (ubiquinone) 1 β subcomplex 8
Q9CQJ8	Ndufb9 - NADH dehydrogenase (ubiquinone) 1 β subcomplex, 9
Q9CQ54	Ndufc2 - NADH dehydrogenase (ubiquinone) 1, subcomplex unknown, 2
Q91VD9	Ndufs1 - NADH dehydrogenase (ubiquinone) Fe-S protein 1
Q91WD5	Ndufs2 - NADH dehydrogenase (ubiquinone) Fe-S protein 2
Q9DCT2	Ndufs3 - NADH dehydrogenase (ubiquinone) Fe-S protein 3
Q9CXZ1	Ndufs4 - NADH dehydrogenase (ubiquinone) Fe-S protein 4
Q8K3J1	Ndufs8 - NADH dehydrogenase (ubiquinone) Fe-S protein 8
Q91YT0	Ndufv1 - NADH dehydrogenase (ubiquinone) flavoprotein 1
Q9D6J6	Ndufv2 - NADH dehydrogenase (ubiquinone) flavoprotein 2
Q8BK30	Ndufv3 - NADH dehydrogenase (ubiquinone) flavoprotein 3
P29595	Nedd8 - neural precursor cell expressed, developmentally down-regulated gene 8
Q9JHW2	Nit2 - nitrilase family, member 2
P15532	Nme1 - NME/NM23 nucleoside diphosphate kinase 1
Q01768	Nme2 - NME/NM23 nucleoside diphosphate kinase 2
Q11011	Npepps - aminopeptidase puromycin sensitive
Q61937	Npm1 - nucleophosmin 1
Q9CZ44	Nsfl1c - NSFL1 (p97) cofactor (p47)
P29758	Oat - ornithine aminotransferase
Q60597	Ogdh - oxoglutarate dehydrogenase (lipoamide)
Q9D0K2	Oxct1 - 3-oxoacid CoA transferase 1
P09103	P4hb - prolyl 4-hydroxylase, β polypeptide
Q99LX0	Park7 - Parkinson disease (autosomal recessive, early onset) 7
P23506	Pcmt1 - protein-L-isoaspartate (D-aspartate) O-methyltransferase 1
P35486	Pdha1 - pyruvate dehydrogenase E1 α 1
Q9D051	Pdhb - pyruvate dehydrogenase (lipoamide) β
Q8BKZ9	Pdhx - pyruvate dehydrogenase complex, component
P27773	Pdia3 - protein disulfide isomerase associated 3

O70209	Pdlim3 - PDZ and LIM domain 3
Q8CI51	Pdlim5 - PDZ and LIM domain 5
P70296	Pebp1 - phosphatidylethanolamine binding protein 1
P47857	Pfkm - phosphofructokinase, muscle
P62962	Pfn1 - profilin 1
Q9JJV2	Pfn2 - profilin 2
Q9DBJ1	Pgam1 - phosphoglycerate mutase 1
O70250	Pgam2 - phosphoglycerate mutase 2
P09411	Pgk1-rs7 - phosphoglycerate kinase-1, related sequence-7
Q9D0F9	Pgm2 - phosphoglucomutase 2
P67778	Phb - prohibitin
Q9DAK9	Phpt1 - phosphohistidine phosphatase 1
P52480	Pkm - pyruvate kinase, muscle
O88492	Plin4 - perilipin 4;
Q9D819	Ppa1 - pyrophosphatase (inorganic) 1
Q91VM9	Ppa2 - pyrophosphatase (inorganic) 2
P17742	Ppia - peptidylprolyl isomerase A
P24369	Ppib - peptidylprolyl isomerase B
Q3UM45	Ppp1r7 - protein phosphatase 1, regulatory (inhibitor) subunit 7
P63330	Ppp2ca - protein phosphatase 2 (formerly 2A), catalytic subunit, α isoform
P35700	PRDX1 - peroxiredoxin 1
Q61171	PRDX2 - peroxiredoxin 2
P20108	PRDX3 - peroxiredoxin 3
P99029	PRDX5 - peroxiredoxin 5
O08709	PRDX6 - peroxiredoxin 6
Q9JK53	Prelp - proline arginine-rich end leucine-rich repeat
Q9QUR6	Prep - prolyl endopeptidase
P12367	Prkar2a - protein kinase, cAMP dependent regulatory, type II α
Q9Z2Y8	Prosc - proline synthetase co-transcribed
Q9R1P4	Psma1 - proteasome (prosome, macropain) subunit, α type 1
P49722	Psma2 - proteasome (prosome, macropain) subunit, α type 2
O70435	Psma3 - proteasome (prosome, macropain) subunit, α type 3
Q9R1P0	Psma4 - proteasome (prosome, macropain) subunit, α type 4
Q9Z2U1	Psma5 - proteasome (prosome, macropain) subunit, α type 5
Q9QUM9	Psma6 - proteasome (prosome, macropain) subunit, α type 6
Q9Z2U0	Psma7 - proteasome (prosome, macropain) subunit, α type 7
Q9R1P3	Psmb2 - proteasome (prosome, macropain) subunit, β type 2
Q9R1P1	Psmb3 - proteasome (prosome, macropain) subunit, β type 3
P99026	Psmb4 - proteasome (prosome, macropain) subunit, β type 4
O55234	Psmb5 - proteasome (prosome, macropain) subunit, β type 5
Q60692	Psmb6 - proteasome (prosome, macropain) subunit, β type 6
P70195	Psmb7 - proteasome (prosome, macropain) subunit, β type 7
Q60866	Pter - phosphotriesterase related
P26350	Ptma - prothymosin α

Q9D0J8	Ptms - parathymosin
O54724	Ptrf - polymerase I and transcript release factor
P32848	Pvalb - parvalbumin
Q9WUB3	Pygm - muscle glycogen phosphorylase
Q61838	Pzp - pregnancy zone protein
P51150	Rab7 - RAB7, member RAS oncogene family
P54728	Rad23b - RAD23b homolog (S. cerevisiae
P62827	Ran - RAN, member RAS oncogene family
Q8BP92	Rcn2 - reticulocalbin 2
P26043	Rdx - radixin
P47955	Rplp1 - ribosomal protein, large, P1
P99027	Rplp2 - ribosomal protein, large P2; Plays an important role in the elongation step of protein synthesis
Q9CQR2	Rps21 - ribosomal protein S21
P62858	Rps28 - ribosomal protein S28
P14206	Rpsa - ribosomal protein SA
P14069	S100a6 - S100 calcium binding protein A6 (calcyclin)
Q3TMH2	Scrn3 - secernin 3
Q8K2B3	Sdha - succinate dehydrogenase complex, subunit A, flavoprotein (Fp)
Q9CQA3	Sdhb - succinate dehydrogenase complex, subunit B, iron sulfur (Ip
Q9CZB0	Sdhc - succinate dehydrogenase complex, subunit C, integral membrane protein
Q9CXV1	Sdhd - succinate dehydrogenase complex, subunit D, integral membrane protei
Q63918	Sdpr - serum deprivation response
P17563	Selenbp1 - selenium binding protein 1
Q6P6M7	Sepsecs - Sep (O-phosphoserine) tRNA:Sec (selenocysteine) tRNA synthase
Q9CY58	Serbp1 - serpine1 mRNA binding protein 1
P22599	Serpina1b - serine (or cysteine) preptidase inhibitor, clade A, member 1B
Q00897	Serpina1d - serine (or cysteine) peptidase inhibitor, clade A, member 1D
Q00898	Serpina1e - serine (or cysteine) peptidase inhibitor, clade A, member 1E
P07759	Serpina3k - serine (or cysteine) peptidase inhibitor, clade A, member 3K
Q60854	Serpinb6a - serine (or cysteine) peptidase inhibitor, clade B, member 6a
P32261	Serpinc1 - serine (or cysteine) peptidase inhibitor, clade C (antithrombin), member 1
Q9WUZ7	Sh3bgr - SH3-binding domain glutamic acid-rich protein
Q9WTX5	Skp1a - S-phase kinase-associated protein 1A
Q9CR62	Slc25a11 - solute carrier family 25 (mitochondrial carrier oxoglutarate carrier), member 1
Q8BH59	Slc25a12 - solute carrier family 25 (mitochondrial carrier, Aralar), member 12
Q8VEM8	Slc25a3 - solute carrier family 25 (mitochondrial carrier, phosphate carrier), member 3
P48962	Slc25a4 - solute carrier family 25 (mitochondrial carrier, adenine nucleotide translocator), member 4
Q9DC77	Smpx - small muscle protein, X-linked
P08228	Sod1 - superoxide dismutase 1, soluble
P09671	Sod2 - superoxide dismutase 2, mitochondrial

Q7TQ48	Srl - sarcalumenin
Q99L47	St13 - suppression of tumorigenicity 13
Q8K031	Stard8 - START domain containing 8
Q60864	Stip1 - stress-induced phosphoprotein 1
Q9Z2I9	Sucla2 - succinate-Coenzyme A ligase, ADP-forming, β subunit
Q8R086	Suox - sulfite oxidase
P18419	Svs4 - seminal vesicle secretory protein 4
P30933	Svs5 - seminal vesicle secretory protein 5
Q5SV85	Synrg - synergin, γ
O89104	Sypl2 - synaptophysin-like 2
Q93092	Taldo1 - transaldolase 1
O70548	Tcap - titin-cap
P62869	Tceb2 - transcription elongation factor B (SIII), polypeptide
Q9Z1T2	Thbs4 - thrombospondin 4
P20801	Tnnc2 - troponin C2, fast
P13412	Tnni2 - troponin I, skeletal, fast 2
Q9QZ47	Tnnt3 - troponin T3, skeletal, fast
P17751	Tpi1 - triosephosphate isomerase 1
P58771	Tpm1 - tropomyosin 1, α
P58774	Tpm2 - tropomyosin 2, β
P21107	Tpm3 - tropomyosin 3, γ
P63028	Tpt1 - tumor protein, translationally-controlled
Q921I1	Trf - transferrin
A2ASS6	Ttn - titin
P07309	Ttr - transthyretin
P68372	Tubb4b - tubulin, β 4B class IVB
Q8BFR5	Tufm - Tu translation elongation factor, mitochondria
Q9Z0P5	Twf2 - twinfilin, actin-binding protein, homolog 2 (Drosophila)
P10639	Txn1 - thioredoxin 1
P68037	Ube2l3 - ubiquitin-conjugating enzyme E2L 3
P61089	Ube2n - ubiquitin-conjugating enzyme E2N
Q6P5E4	Uggt1 - UDP-glucose glycoprotein glucosyltransferase 1
Q91ZJ5	Ugp2 - UDP-glucose pyrophosphorylase 2
Q0KK59	Unc79 - unc-79 homolog (C. elegans)
Q8R1I1	Uqcr10 - ubiquinol-cytochrome c reductase, complex III subunit X
Q9D855	Uqcrb - ubiquinol-cytochrome c reductase binding protein
Q9CZ13	Uqcrc1 - ubiquinol-cytochrome c reductase core protein
Q9DB77	Uqcrc2 - ubiquinol cytochrome c reductase core protein
Q9CR68	Uqcrfs1 - ubiquinol-cytochrome c reductase, Rieske iron-sulfur polypeptide 1
P99028	Uqcrh - ubiquinol-cytochrome c reductase hinge protein
Q9CQ69	Uqcrq - ubiquinol-cytochrome c reductase, complex III subunit VII
Q78IK2	Usmg5 - upregulated during skeletal muscle growth 5
Q64727	Vcl - vinculin
Q01853	Vcp - valosin containing protein

Q60932	Vdac1 - voltage-dependent anion channel 1
Q60930	Vdac2 - voltage-dependent anion channel 2
Q60931	Vdac3 - voltage-dependent anion channel 3
P20152	Vim - vimentin
Q9CQV8	Ywhab - tyrosine 3-monooxygenase/tryptophan 5-monooxygenase activation protein, β polypeptide
P62259	Ywhae - tyrosine 3-monooxygenase/tryptophan 5-monooxygenase activation protein, ε polypeptide
P61982	Ywhag - tyrosine 3-monooxygenase/tryptophan 5-monooxygenase activation protein, γ polypeptide
P68510	Ywhah - tyrosine 3-monooxygenase/tryptophan 5-monooxygenase activation protein, η polypeptide
P63101	Ywhaz - tyrosine 3-monooxygenase/tryptophan 5-monooxygenase activation protein, ζ polypeptide